ÉCOLE POLYTECHNIQUE DE BRUXELLES
UNIVERSITÉ LIBRE DE BRUXELLES

POLITECNICO MILANO 1863

A detailed kinetic mechanism for combustion of natural gas in innovative, unconventional conditions

Thesis submitted by Ghobad BAGHERI
in fulfilment of the requirements of the Joint PhD Degree in

Aero-Thermo-Mechanics (ULB - “Docteur en Science de l’ingénieur et technologie”)
and Chemical Engineering (Polimi-DCMC "Giulio Natta")

Academic year 2018-2019

Supervisors: Professor Alessandro PARENTE (Université libre de Bruxelles)

Aero-Thermo-Mechanics Department

and Professor Tiziano FARAVELLI (Politecnico di Milano)

Department of Chemistry, Materials, and Chemical Engineering

European Commission | Horizon 2020 European Union funding for Research & Innovation

MARIE CURIE ACTIONS

CLEAN GAS

POLITECNICO DI MILANO
DEPARTMENT OF CHEMISTRY, MATERIALS AND CHEMICAL ENGINEERING
DOCTORAL PROGRAMME IN XXXI

A DETAILED KINETIC MECHANISM FOR COMBUSTION OF NATURAL GAS IN INNOVATIVE, UNCONVENTIONAL CONDITIONS.

Doctoral Dissertation of:
Ghobad Bagheri

Supervisors:
Prof. Tiziano Faravelli, Politecnico di Milano
Prof. Alessandro Parente, Université libre de Bruxelles

Tutor:
Prof. Giancarlo Terraneo

The Chair of the Doctoral Program:
Prof. Alessio Frassoldati

2019 – XXXI

This project has received funding from the European Union's Horizon 2020 research and innovation programme under the Marie Sklodowska-Curie grant agreement No. 643134.

For the boy that has never backed down
against nothing or nobody.

Acknowledgement

Firstly, I would like to thank my supervisor Prof. Tiziano Faravelli for the opportunity to complete my PhD at Polimi and introducing me to the world of combustion chemistry.

My sincere gratitude to all the past and present members of CRECK especially; Prof. Eliseo Ranzi whose door has always been open to me and never tiring of my "almost" endless questions, Isabella for truly helping me through the maze of bureaucracies. Thank you to Prof. Alessandro Parente for always being at the other end of the phone, and for explaining how things work.

Finally and most of all thank you to my incredible family, Mom, Dad and Amir. You have had faith in me from the beginning right through to today. You picked me up when I was at my lowest.

Summary

FORECASTING the global energy demand is remarkably important for future energy policy and security. Considering various scenarios for world energy production and demand, the role of natural gas in shaping future energy demand will be notable, derived by its environmental advantages and versatility relative to other combustible fuels. This work is in the context of Combustion for Low Emission Application of Natural Gas project (CLEAN-Gas) funded by European Union's Horizon 2020 research and innovation programme under Marie Sklodowska-Curie Innovative Training Network (ITN), aiming to propose an innovative approach to improve natural gas combustion in industrial processes including detailed chemistry and computational fluid dynamics. Towards the goal, this work aims to extend the knowledge on hidden aspects of natural gas in the low environmental impacts combustion technologies [1] through the development of comprehensive, detailed kinetic mechanism with predictive capabilities in a wide range of operating conditions of interest for real systems.

The kinetic mechanism of natural gas (C_1-C_3 fuels) describing the oxidation and combustion of natural gas is conceived and developed in a modular and hierarchical approach. This thesis is an effort to fill the pressing need of a reliable and widely validated kinetic mechanism, specially developed for modern combustion systems with near-zero emission. More than ~ 200 different experiments containing more than ~ 6000 data points of various apparatuses such as plug flow reactor (plug flow reactor (PFR)), Jet stirred reactor (jet stirred reactor (JSR)), shock tube, and 1-D laminar flame are collected from literature for the sake of extensive and critical model comparisons. This database is the most extensive set of experimental data available, which is beneficial for understanding the complex combustion processes of modern combustion technologies that have been hindered from successful integration into the industry.

A systematic study is performed on the combustion characteristics, less-known aspects and critical reaction pathways involved in MILD and oxy-fuel combustions. Diluent effects are evaluated in detail, and it is noteworthy to highlight that physical and chemical effects of diluent on the reactivity, laminar flame speed, ignition delay time,

[1] new industrial burners with near-zero emission technologies such as Moderate or intense low-oxygen dilution (MILD), flameless, and oxy-fuel combustions

and formation of products are strongly dependent on the operating conditions (temperature, pressure, and equivalence ratio). Therefore, the analysis of the dilution effects is very case sensitive, and the contribution of each characteristic may vary accordingly.

Both H_2O and CO_2 dilution reduces the system reactivity. The effect of H_2O is more notable due to chemical effects related to enhanced collisional efficiencies at the operating conditions of JSR experiments. On the contrary, CO_2 has a higher impact on inhibiting flame propagation at higher temperatures, mainly due to the thermal and radical scavenging effects. Moreover, the effect of CO_2 addition on methane ignition delay times is very marginal. The most likely explanation is that CO_2 is scarcely reactive during the ignition, because of its stability, and does not actively modify the pool of radicals.

Finally, despite the satisfactory model prediction and reasonable agreement shown, the underlying impact of rate parameters uncertainty on model prediction is still not negligible. It has been shown that even if the kinetic mechanism is complete and free of any missing reaction pathway, rate coefficient uncertainties generally precludes the possibility of predicting relevant combustion properties in some peculiar conditions. One of the primary reasons has been the lack of general agreement as to how to move forward in obtaining a comprehensive, unified and predictive model for fuels combustion.

Sommario

ESSERE in grado di predire il fabbisogno energetico globale è di cruciale importanza per la futura politica e sicurezza energetica. Dai diversi scenari derivanti da queste previsioni, riguardanti la produzione e la richiesta enegetica globale, emerge un crescente ruolo del gas naturale nella domanda energetica futura. Le ragioni sono da ritrovarsi nei benefici che comporta dal punto di vista ambientale, e nella maggiore versatilità rispetto ad altri combustibili. Questo lavoro mira a proporre un approccio innovativo per migliorare il processo di combustione del gas naturale in ambito industriale, includendo schemi cinetici dettagliati e fluidodinamica computazionale. Esso si inserisce nel contesto del progetto "Combustion for Low Emission Application of Natural Gas" (CLEAN-Gas), finanziato dal Marie Sklodowska-Curie Innovative Training Network (ITN). Relativamente a tale obiettivo, questo lavoro punta ad ampliare la conoscenza sugli aspetti meno noti della combustione del gas naturale nelle tecnologie a basso impatto ambientale, attraverso lo sviluppo di un meccanismo cinetico completo e dettagliato, con capacità predittive in una vasta gamma di condizioni operative di interesse per sistemi reali.

Il meccanismo cinetico del gas naturale (combustibili C_1-C_3), che descrive l'ossidazione e la combustione del gas naturale, è concepito e sviluppato in un approccio modulare e gerarchico. Questa tesi si impegna a soddisfare il bisogno incalzante di un meccanismo cinetico affidabile e ampiamente validato, sviluppato in particolare per i moderni sistemi di combustione con emissioni di inquinanti vicine allo zero. Più di 200 diversi esperimenti contenenti più di 6000 misure ottenute in diverse condizioni operative in diversi apparati, come il reattore a flusso a pistone (PFR), il reattore agitato (JSR), lo shock tube e la fiamma laminare monodimensionale, sono raccolti come risultato di una estesa analisi bibliografica, per un confronto esteso e critico dei modelli con i dati sperimentali. Questo database è la più ampia serie di dati sperimentali disponibili, utile per comprendere i complessi processi di combustione delle moderne tecnologie, la cui complessità ne ostacola la messa a punto in ambito industriale.

Viene effettuato uno studio sistematico sulle caratteristiche di combustione, sugli aspetti meno noti e sui percorsi reattivi coinvolti nei processi di combustione MILD e ossicombustione. Gli effetti del diluente sono valutati in dettaglio, ed è importante

sottolineare che gli effetti fisici e chimici del diluente sulla reattività, sulla velocità della fiamma laminare, sul ritardo di accensione e sulla formazione dei prodotti dipendono fortemente dalle condizioni operative (temperatura, pressione e rapporto di equivalenza). Pertanto, l'analisi degli effetti di diluizione è molto sensibile ai diversi casi considerati, e il contributo di ciascuna caratteristica può variare di conseguenza.

Sia la diluizione con H_2O che la diluizione con CO_2 riducono la reattività del sistema. L'effetto dell'H_2O è più pronunciato a causa di effetti chimici legati ad una maggiore efficienza di collisione nelle condizioni operative degli esperimenti JSR. Al contrario, la CO_2 ha un impatto maggiore sull'inibizione della propagazione della fiamma a temperature più elevate, principalmente a causa degli effetti di scavenging termico e radicale. Inoltre, l'effetto dell'aggiunta di CO_2 sui tempi di ritardo dell'accensione del metano è molto marginale. La spiegazione più probabile è che la CO_2 è scarsamente reattiva durante l'accensione, a causa della sua stabilità, e non modifica attivamente il pool di radicali.

Infine, nonostante la soddisfacente capacità di previsione del modello e il ragionevole accordo mostrato, l'impatto dell'incertezza dei parametri di velocità sulle previsioni del modello non è ancora trascurabile. È stato dimostrato che, anche se il meccanismo cinetico è completo e tutti i percorsi reattivi sono presi in considerazione, le incertezze del coefficiente di velocità generalmente precludono la possibilità di predire caratteristiche rilevanti del processo di combustione in particolari condizioni operative. Una delle ragioni principali è stata la mancanza di un accordo generale su come procedere per ottenere un modello completo, unificato e predittivo per la combustione dei combustibili.

Contents

List of Figures

List of Tables

CHAPTER 1

Introduction

1.1 The World Energy and Environmental Scenario

MODERN world depends heavily on energy generation in all of its forms. Determining the best energy source and generation technology is complicated, and some argues emphasis various criteria for what is 'best' such as reliability of production and cost-benefit analysis. However, undoubtedly, the most controversial and essential criteria are the impacts of the various energy production technologies on public health and environment [1]. Air pollutants arising from human activity overwhelmingly derive from energy production and use, mainly the combustion of fossil fuels and biomass. Some examples of air pollutants from human activity include [2]:

- **Sulphur oxides** (SO_X), in particular sulphur dioxide ($SO2$): Fossil fuels, coal and oil contain sulphur to differing degrees and, if not removed beforehand, SO_X are released at combustion such as in power generation or industrial processes. If not treated or captured, SO_X emissions are released to the atmosphere. Such emissions are linked to adverse health and environmental effects, as well as being a precursor to the formation of secondary particulate matter.

- **Nitrogen oxides** (NO_X), nitrogen oxide (NO) and nitrogen dioxide (NO_2): NO_X stem from high-temperature combustion, mainly in transport and power generation, or from the oxidation of NO to NO_2 in the atmosphere. NO_2 is a toxic gas and can lead to the formation of particulate matter and ozone.

  SO_2 and NOx released into the air are the biggest cause of acid rain. A chemical reaction happens when SO_2 and NOx mix with water, oxygen and other chemicals in the air. They then become sulphuric and nitric acids that mix with precipitation and fall to the ground.

- **Particulate matter (PM)** is a mix of solid/liquid organic and inorganic substances that may be a primary or secondary pollutant. PM is linked to major detrimental health impacts. Size is an important factor in determining these impacts: – "coarse particles" are between 2.5 and 10 micrometres (μm) in diameter and "fine particles" are smaller than $2.5\mu m$. The adverse health impacts of $PM10$ are less severe than those of the fine particles, however, there is a longer history of data on $PM10$ and even today many cities lack the equipment to monitor outdoor concentrations of $PM2.5$. Black carbon, a particular type of fine PM, is formed by the incomplete combustion of fossil fuels and bioenergy, and is a short-lived climate pollutant (SLCP).

- **Carbon monoxide (**CO**)** is a colourless, odourless, toxic gas that comes from the incomplete combustion of road transport fuels, natural gas, coal or wood.

- **Volatile organic compounds (VOCs)** are released from chemicals, solvents or fuels (as well as natural sources) as they evaporate or sublimate into the surrounding air; they are associated with a range of negative health effects. Methane (CH_4), the main component of natural gas (also a SLCP), is often considered separately from other VOCs as its characteristics differ.

- **Ammonia (**NH_3**)** is released in relation to agricultural and waste management activities; once in the atmosphere ammonia reacts with oxides of nitrogen and sulphur to form secondary particles.

Human daily activities require a mix of thermal, mechanical and chemical energies, and forecasting this global energy demand is critically important for energy policy and security. Indeed, a significant energy transition is underway, and many factors (i.e. climate change, government ambitions and policies) will shape the world's energy future [3]; therefore, various scenarios can be considered for future energy production and demand such as New Policies Scenario[1], the Current Policies Scenario[2] and the Sustainable Development Scenario[3] [4].

The overall share of fossil fuels in global primary energy demand has remained constant over the last 25 years (80%) [4]. Coal, oil and gas play a crucial role in today's global energy system, though energy efficiency has had a significant impact in modifying the growth in energy market. Figure 1.1 shows the world primary energy demand by fuel and energy-related CO_2 emissions by different scenarios.

[1]The New Policies Scenario is designed to show where existing policies as well as announced policy intentions might lead the energy sector.

[2]The Current Policies Scenario provides a point of comparison by considering only those policies and measures enacted into legislation.

[3]The Sustainable Development Scenario examines what it would take to achieve the main energy-related components of the "2030 Agenda for Sustainable Development" adopted in 2015 by member states of the United Nations.

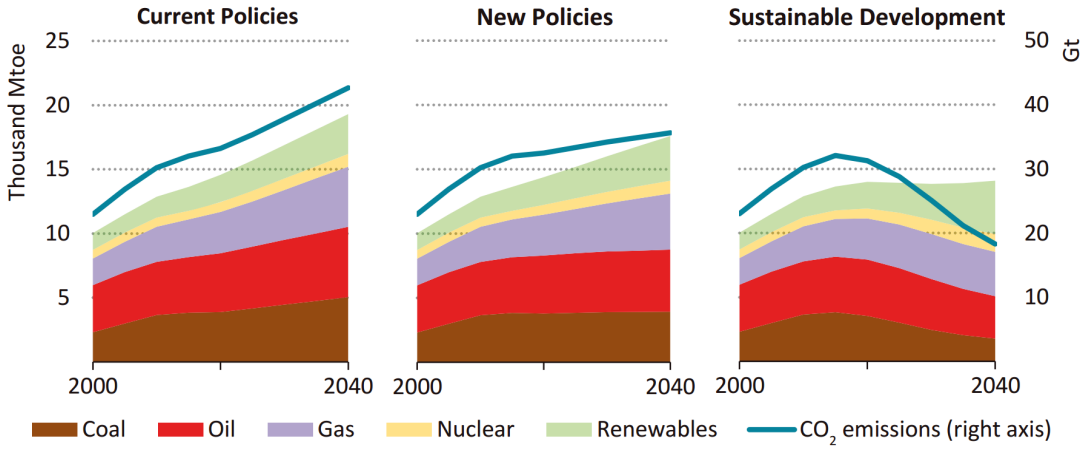

Figure 1.1: *World primary energy demand by fuel and energy-related CO_2 emissions by scenario. Mtoe is million tonnes of oil equivalent and Gt is gigatonnes. [4]*

In the Current Policies Scenario, continued strong growth among the necessary fuels leaves only a small room for renewables to step in and meet incremental demand. In fact, Coal use rises on the back of strong consumption in the developing world. In the absence of significant further commitments to enhance vehicle fuel efficiency, oil demand rises by 25% to 2040.

In the New Policies Scenario, global primary energy demand expands by 15 thousand Mote between today and 2040. The underlying structural trends that shape demand are population, economic and urbanisation. Energy policies also play a significant role, especially those relating to renewable resources, energy efficiency, measures to restrict air pollution.

In the Sustainable Development Scenario, demand is nearly flat out to 2040, reflecting in part the progressive potential of energy efficiency to reduce demand. After a peak, coal declines to the level equivalent of 1975 [3], when the global economy was hardly a quarter the size of today; moreover, Oil demand approaches a peak and starts to decline.

In practice, only the Sustainable Development Scenario (which works backwards from what is necessary to achieve global climate goals) of three main scenarios presents a decline in global energy-related CO_2 emissions over the period to 2040. Neither the fulfilment of current policies nor the additional consideration of "new policies", is adequate to obtain such a peak; however, the New Policies Scenario does detect a noteworthy slowdown in increase compared with the period $2000-2014$ [2]. More importantly, natural gas [4] consumption increases in every scenario, derived by its environmental advantages and versatility relative to other combustible fuels.

1.2 Natural gas

The energy sector is by far the largest source of air pollution emissions from human activity. They come primarily from the combustion of fossil fuels and bioenergy and

[4] it commonly consists of methane (CH_4), ethane C_2H_6) and propane (C_3H_8)

industrial activities. As shown in Figure 1.2 energy production and use not only accounts for most of the air pollution, it also accounts for a very high proportion of the human-related emissions of some key pollutants.

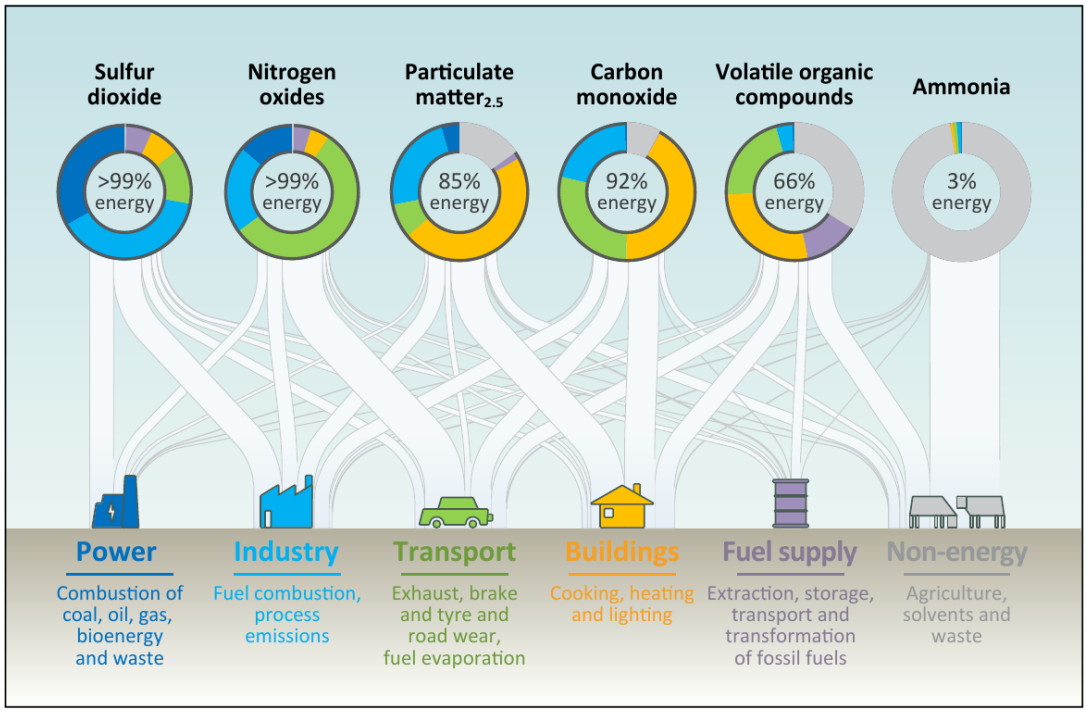

Figure 1.2: *Selected primary air pollutants and their sources, 2015 [2].*

The relationship between fuels, their use and the resulting emissions is not straightforward. These pollutants may be reduced or removed from these fuels at various stages before combustion, or the nature of the combustion process itself can influence emissions levels (e.g. the temperature of combustion), and post-combustion technologies may also be utilised to chemically alter or capture harmful emissions (e.g. carbon capture and sequestration). Thus, there is no single level of emissions per unit of a specific fuel but, instead, a range of emission factors depending on such variables.

Figure 1.3 indicates that the fuel type is strongly correlated with the type of air pollution, both in terms of emissions per unit of fuels and their share of total emissions. As can be seen, natural gas results in much lower emissions than other fossil fuels. It emitts the least carbon dioxide per unit of energy and has the lowest carbon density among fossil fuels.

As shown in Figure 1.1, natural gas is the fastest expanding fossil fuel in the New Policies Scenario, passing coal by 2030 to become the second-largest source of energy after oil. Gas consumption demand rising by 1.6% per year, where it will be almost 45% higher in 2040 than today [4]. Natural gas also plays a vital role in European's carbon-constrained power system. It provides reliability and flexibility with the share of 16% of gas-fired power in the European energy mix and increases to 20% by 2040 [2].

Widely utilisation of natural gas emphasises the importance of understanding its combustion and oxidation processes in order to fulfil the significant impact of energy efficiency in modifying the growth in the energy market.

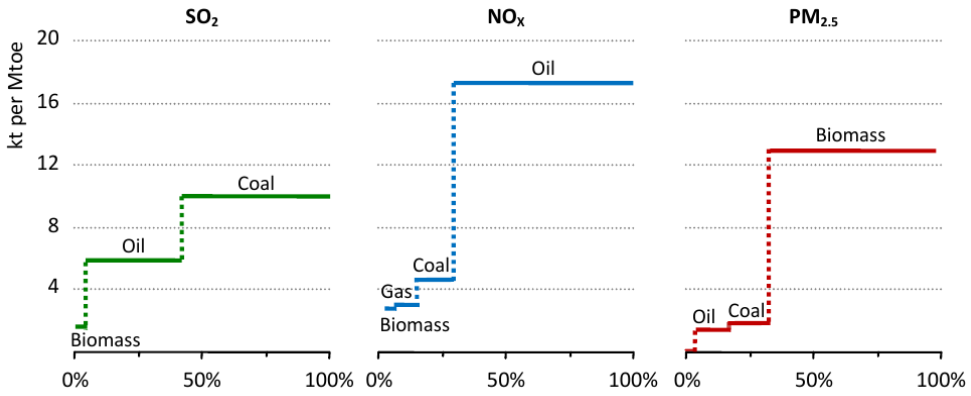

Figure 1.3: *Global average emissions factors and share of major pollutant emissions by fuel, 2015 [2] .*

1.3 Low Environmental Impact Combustion Technologies

Over the last decades, combustion technologies have been focused on the reduction of current emissions, including NOx, SOx, CO_2, CO, volatile organic components, and soot. Continuous advancements in control technologies have resulted in emissions reduction and successfully demonstrated that efficiency improvements are the most feasible and cost-effective approach. However, long-term solution for decreasing combustion-generated pollution would require a reduction at a level greater than that achieved only by efficiency improvements. For this reason, the development of new industrial burners with near-zero emission technologies such as Moderate or intense low-oxygen dilution (MILD), flameless, and oxy-fuel combustions are of great interest in the new energy scenario.

Moderate or intense low-oxygen dilution (MILD) combustion is well recognized as a very promising technique. MILD combustion takes place by preheating the reactants at a temperature higher than auto-ignition and by a very high dilution [5]. In fact, through the control of the maximum temperature by means of flue gas recirculation and the extension of the reaction zone [6, 7], it enhances combustion efficiency while remarkably reducing NOx emission. Similarly, flameless combustion is defined as a mode in which two conditions must be satisfied where the reaction is going to take place:

- the reactant temperature must exceed self-ignition temperature;
- the reactants must have entrained enough inert combustion products to reduce the final reaction temperature well below adiabatic flame temperature, to such an extent that a flame front cannot be stabilised [8].

Oxy-fuel combustion, which typically combines high purity oxygen ($> 95\%$) with recycled exhaust gases, always aiming to control the maximum flame temperature [9]. Burning fuel in oxygen and flue gas rather than air, of course, results in the elimination of NOx emissions and also favours the carbon dioxide sequestration from the exhausts.

Modern combustion systems are designed with the following goals: high combustion efficiency, high reliability, and minimum emission of the air pollutants. Numerical

prediction is a feasible and economical way to establish the criteria for designing the combustors under these conditions. Application of numerical simulation in the industry has multiplied during the last decades. It complements the theoretical investigations where non-linearity, a high number of degrees of freedom, or lack of symmetry are of importance. It also complements experiment where devices are expensive, data is inaccessible, or the phenomena very complex. For the study of combustion, numerical simulations improve our understanding of flame structure and dynamics. They are widely used in the design and optimisation of practical combustion systems because, compared to experimental testing and prototyping, the development costs of numerical simulation are very low. Today, no real progress in design or optimisation can be made without numerical simulations.

A large part of our understanding of the complex combustion processes comes from elementary chemical kinetic models. However, the lack of reliable and widely validate reaction mechanisms especially developed for modern combustion systems has hindered the development of these combustion techniques and prevented their integration into the industry.

Thus, this thesis is an effort to fill this pressing need by further validating a detailed reaction mechanism for combustion and oxidation of natural gas. An improved understanding of the reaction characterisation of natural gas in modern combustion systems is a potent tool in trying to:

- Reduce man's contribution to global warming[5]
- Improve industrial economic by optimising the efficiency of combustion process in flames, engines, and turbines.
- Help Socio-political aspects by minimising the fuels consumption.

1.4 Objectives

The main objective of this work is to further validate a detailed kinetic mechanism with a broad range of predictability. As the main constituents of natural gas are methane, ethane and propane, this study is limited to $C_1 - C_3$ fuels pyrolysis and oxidation in a broad range of conditions (temperature, pressure and equivalence ratio). Thus, the detailed objectives can be summarised in three folds:

- To collect and review a vast amount of experimental data on MILD and Oxy-fuel combustion that have been reported in recent years, analyse them by using a detailed kinetic mechanism and thereby identify aspects of the mechanism that requires further revision.
- To develop a detailed kinetic mechanism for $C_1 - C_3$ fuels combustion and oxidation based on the hierarchical approach.
- To provide a systematic discussion of the combustion characteristics, hidden aspects and critical reaction pathways involved in near-zero emissions combustion processes (MILD and OXY-fuel).

[5]Global warming, a long term rise in the average temperature of earth, is largely influenced by human activities through the emission of greenhouse gases such as carbon dioxide, methane, and nitrous oxide.

Moreover, it is noteworthy that the aim is not only the mechanism development and validation but also to extended that knowledge of the combustion characteristics and critical reaction pathways in unconventional conditions which differs from the traditional flames.

1.5 Scope and Organisation

The present study includes the development of the detailed kinetic mechanisms for natural gas ($C_1 - C_3$) for both conventional and unconventional combustions. The wide range of experimental data collected for the sake of mechanism assessment consists of species profile in JSR, PFR, one dimension flame (1-D flame) and shock tube, also laminar flame speed in 1-D flame, and the ignition delay time in the shock tube.

The kinetic mechanism will be conceived and developed in a modular and hierarchical approach. This mechanism can describe the oxidation and pyrolysis of any fuel from hydrogen and its mixture with carbon monoxide (syngas), followed by methane, methanol, formaldehyde, ethane, ethylene, acetylene, acetaldehyde, and ethanol. The mechanism will be built first by determining the most important reactions associated with fuel's oxidation and considering their rate constant based on the most recent accurate measurements and calculations, where possible, and otherwise on evaluated rate parameters, which can precisely reproduce a range of targets.

The mechanism development systemically requires accurate thermodynamic properties of species, which will be used to identify whether a reaction will proceed spontaneously. Thermodynamic properties are also utilised in the calculation of reverse rate constant, equilibrium constant, and the amount of heat release from a reaction.

In addition, this thesis frames the necessity of evaluating a vast amount of experimental data on MILD and oxy-fuel combustion for the sake of identifying hidden aspects of the mechanism requiring further revision.

Organisation

Chapter 2 contains literature information on previous studies and currently available detailed kinetic mechanism for combustion and oxidation of natural gas. The literature review is followed up by the theoretical background of thermodynamic, kinetic theory and detailed kinetic mechanism development approach.

Chapter 3 presents the thermochemical formulation and NASA polynomial format required for mechanism development. Then this section followed by introducing the thermochemical databases used for extracting important species thermochemical properties.

Chapter 4 critically reviews different reaction pathways, H-abstraction reaction classes and the reference kinetic parameters used to model pyrolysis and combustion. Then, it continues to review the controversy in some critical reactions of pyrolysis and oxidation channels by emphasising their role in unconventional combustion systems.

Chapter 5 starts with a description of the experimental database collected this study. The numerical tools and methodologies useful for mechanism assessment and development are explained. Then different experimental data targeting reactions or microscopic reactors are presented.

Chapter 6 covers the mechanism validation for MILD combustion and also characterises and highlights the peculiar aspects of this new and near-zero emission combustion technology. This chapter continues with analysing diluent effects on reactivity and ignition delay time of MILD regimes. In the last section of this chapter, thermochemical oscillations in MILD combustion and the mechanism triggering this behaviour are studied.

Chapter 7 comprises an overview of oxy-fuel combustion validation and its unique aspects. Laminar flame speed and ignition delay time will be thoroughly discussed and analysed.

Chapter 8 briefly evaluates the effect of collisional energy transfer and third-body efficiency. A few crucial third-body dependence reactions and their effects on combustion characteristics will be carefully analysed.

Chapter 9 aims to highlight that despite the satisfactory model prediction and reasonable agreement, the underlying impact of rate parameters uncertainty on the model prediction will still not negligible.

Chapter 10 summarises the results of this study, as well as recommendations for the future implementation of environmentally friendly combustion technologies.

CHAPTER 2

Theory and Background

2.1 Introduction

COMBUSTION science has a well-established role in the world energy policy today; improving the combustion quality and reducing pollution formation. Furthermore, combustion is a complex interdisciplinary field that requires knowledge from a molecular level to their uses and applications with a primary goal of emission mitigation and efficiency improvement.

Generally, there are four different activity level that combustion community contributes to [10]:

- Rate constant and thermochemical properties evaluation, mainly containing direct kinetic measurements or electronic structure (ab initio) methods combined with statistical theory.
- Fuel structure and Fundamental chemical reactions.
- Computational fluid dynamic (CFD) modelling and combustion interaction with fluid dynamic modellings.
- Industrial applications and large scale combustion.

Figure 2.1 illustrates a schematic of the underlying layers of required knowledge to understand the combustion process adequately. Level 1 primarily used to calculate accurate thermochemical and rate parameters of the species involved in the chemical reaction mechanisms by implementing statistical theory and ab-initio calculation.

Level 2 covers the amalgamation of the thermodynamic properties and reaction rate constants into the detailed reaction mechanisms. These mechanisms are further analysed and validated by direct comparison with experimental measurements starting with

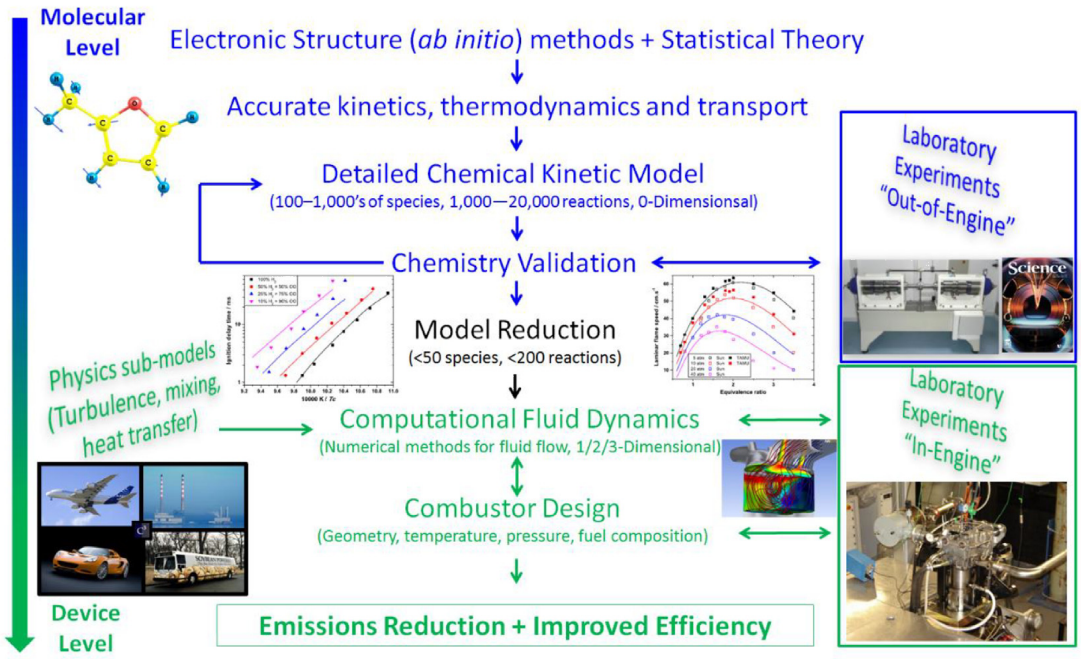

Figure 2.1: *Schematic diagram of the levels in the development of the understanding of combustion [10].*

canonical reactors to more complex systems. At level 3, chemical kinetic schemes are employed in combination with computational fluid dynamic codes or novel chemical reactor networks for cleaner and more efficient combustors. Level 4 faces the practical application such as jet engines, diesel engines, natural gas safety, etc [10].

This study will be devoted to level 2, the development, validation and analysis of a detailed kinetic mechanism which depends on fuel structure and fundamental kinetics.

2.2 Literature review

A chemical kinetic scheme consists of species with associated thermodynamic, transport properties and elementary reactions with corresponding rate constants. Over the past decades, the chemical reaction community has had considerable success in developing reliable chemical kinetic mechanisms for fuel oxidation and combustion with a wide range of predictability.

Improvements in chemical reaction modelling in term of the number of species and reactions that can be handled have considerably resembled the increase in the computational capabilities. Moor's law [11] predicts a doubling of computational power every 18-24 months [12], and this is well-correlated with enlargement of the chemical reaction mechanisms. This fact was well illustrated in the review by Curran [10] and is presented here again in Figure 2.2. This figure shows that the advancement in computational power with time is well correlated with growth in the size of the chemical reaction mechanisms.

Westbrook et al. [12] discussed the early progress of chemical reaction mechanisms, all facilitated by the development of stiff reaction solvers [14, 15]. The first modelled

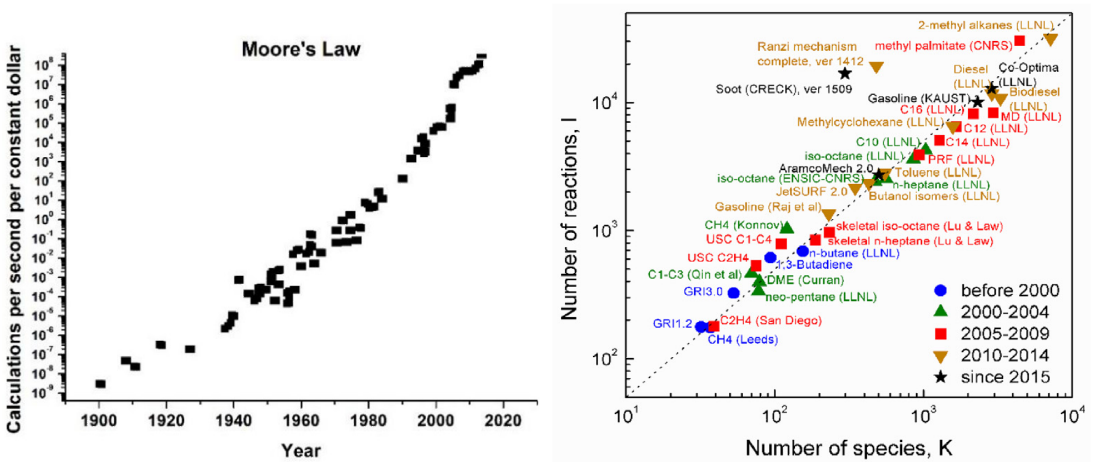

(a) (b)

Figure 2.2: *Illustration of the correlation between computer power and reaction mechanisms size. (a) Moor's law of computational capability growth. (b) Correlation between number of reactions and number of species for various published kinetic mechanisms for selected hydrocarbons and bio fuels. Update by H. Curran [10]; courtesy of T.F. Lu [13].*

chemical systems being those describing ozone [16] in 1953, and decomposition of the hydrazine [17] in 1956. After that, the development continued by the reaction system to model hydrogen combustion followed by methane [18–22] and methanol [23, 24] during the 60s and 70s. Then Westbrook and Dryer [25, 26] introduced the concept of hierarchical nature within chemical reaction mechanisms in which larger hydrocarbon kinetic mechanisms contain underlying species of the hydrogen/oxygen, hydrocarbon and oxygenated hydrocarbon species. Moreover, it was presented by Warnatz [27, 28] the complexity of the methane kinetic mechanisms due to methyl radicals (CH_3) recombination to form ethane with successive dehydrogenation forming ethylene and acetylene.

Many other kinetic reaction mechanisms for modelling combustion and oxidation of methane/ethane have been developed over the years including those for $C_2 - C_3$ from Ranzi and co-workers in Politecnico di Milano [29, 30], a natural gas from Dagaut and co-workers [31–33], the Leeds methane mechanism [34], a methane/ethane mechanism from Barbe et al. [35], The Miller-Bowman NO_x mechanism [36], and those for small oxygenated species from Dryer and co-workers [37–40]. Moreover, Frenklach et al. [41, 42] introduced the concept of optimal kinetic mechanism development through fitting rate constant parameters to a wide range of experimental data targets. This idea led up to the generation of GRI-Mech [43–45] which is an optimised mechanism for describing natural gas combustion. A wide range of experimental data was chosen as targets for fitting the rates and optimising GRI-Mech including ignition delay time, laminar flame speed and methane and ethane species profile in the shock tube.

Current progress in quantum chemistry and ab-initio calculation allowed to improved the new kinetic mechanisms with more precise thermochemical properties and less uncertain kinetic parameters. In the last few years, new generation of detailed kinetic mechanisms to describe oxidation and combustion of small hydrocarbon systems

have appeared. Williams et al. developed a version of San Diego Mech [46, 47], Wang et al. have developed USC Mech II [48] and JetSurf [49], the CRECK mechanism from Politecnico di Milano [50] has extensively been upgraded, AramcoMech [51–53] from NUI Galway has frequently been updated, and DTU Mech [54,55] were presented recently and all freely available on the internet.

All of these mechanisms have been evolved from somewhat different, but the very similar approach and pathways; for instance, the same mechanism implementing the same pathway and reaction set but with different rate constants. Thus, the current state of the art of mechanism development for $C_0 - C_4$ kinetics included more and more rate constants either measured or calculated from the quantum calculation, which have significantly improved the predictability of the detailed reaction mechanisms.

2.3 Thermodynamic and Kinetic Reaction Theory

Detailed kinetic mechanisms require accurate thermochemical and kinetic data in order to characterise the combustion process of hydrocarbons. While thermodynamic data are used to identify whether a reaction of the process will proceed spontaneously, kinetics of reactions demonstrate how fast the reaction or process will proceed.

A reaction can be considered spontaneous at constant pressure and temperature if the difference in Gibbs free energy (G) between reactants and products (ΔG) is negative. When the products of the reaction are more stable, they have a lower G then the reactants. Thus, the reaction has a negative (ΔG), and the reaction is thermodynamically feasible. Figure 2.3 shows the change in the G along the reaction progress from the reactants to products. The barrier of the energy that reactants need to overcome to proceed toward the reaction coordinate identifies the activation energy of the reaction. It is noted that when the change in G is negative, the reaction is exothermic [56].

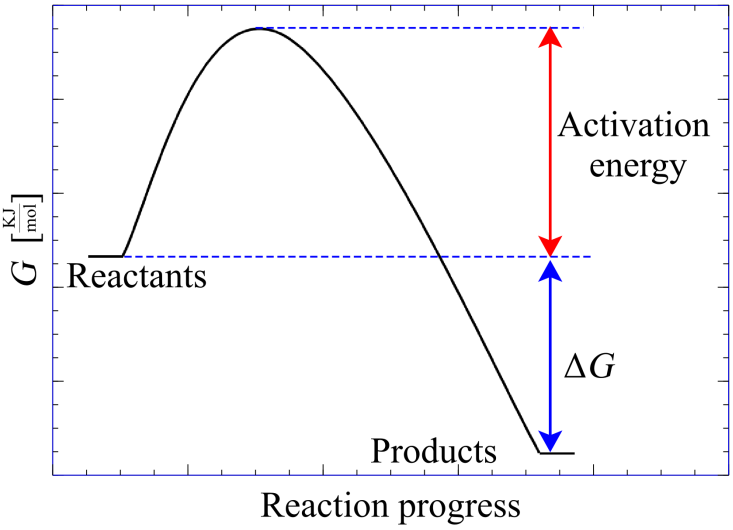

Figure 2.3: *Energy Diagram of the Gibbs free energy profile of a thermodynamically feasible reaction going from reactants to products.*

The change in the G of a reaction during a process is equal to change in the enthalpy

(H) of the system minus the change in the entroy (S) times the temperature (Eq. 2.1).

$$\Delta G = \Delta H - T\Delta S \tag{2.1}$$

In this equation the reaction is:

- Always spontaneous if $\Delta G < 0$
- In equilibrium if $\Delta G = 0$
- Non-spontaneous if $\Delta G > 0$

Fundamentally, chemical reaction mechanisms contain rate constants only in a single direction. Thermochemical properties are therefore used in the calculation of reverse rate constant, the amount of heat release rate, and equilibrium constant of a reaction. Implementing a reaction mechanism in combustion modelling of a system requires specific thermochemical properties of species such as standard enthalpy of formation ($\mathring{H}_f$), standard heat capacitiy ($\mathring{C}_p$) and standard entropy ($\mathring{S}$).

Conceivably, enthalpy of formation,$\mathring{H}_f$, is the most important thermochemical quantity of any given chemical species. If these pieces of information are available for all of the involved species in an arbitrary reaction, the enthalpy of that reaction (heat of formation) at a given temperature can be obtained by

$$\Delta\mathring{H}_{f,T} = \sum_{j}^{n} \mathring{H}_{f,T}\left(product_j\right) - \sum_{i}^{n} \mathring{H}_{f,T}\left(reactant_i\right) \tag{2.2}$$

Thus, enthalpy of a reaction simply obtained by subtracting the sum of the enthalpies of the reactants from the enthalpies of the products at the same temperature.

2.4 Detailed Kinetic Mechanism Theory

Detailed mechanisms are fundamentally developed to describe the transformation of the reactants into products at the molecular level [57]. For instance, the oxidation of methane has seemingly a simple overall reaction:

$$CH_4 + 2O_2 = CO_2 + 2H_2O \tag{R1}$$

However, as it is well-known, this process happens through a large number of elementary reactions and many species. Each reaction proceeds at a specific individual rate. Moreover, the reaction rate of a reversible reaction is a function of reactant and products concentration and the rate constant.

2.4.1 Rate Constant

The rate of reaction describes the rate of change of a given species. The general form of elementary reactions involving N chemical species can be introduced as Eq. 2.3.

$$\sum_{n=1}^{N} \upsilon'_{ni}\chi_n \Leftrightarrow \sum_{n=1}^{N} \upsilon''_{ni}\chi_n \qquad (i = 1, ..., I) \tag{2.3}$$

Where ${\upsilon'}_{ni}$ and ${\upsilon''}_{ni}$ are the forward and reverse stoichiometric coefficients for the chemical species χ_n of the nth species. Elementary reactions normally contain three or four species with unity stoichiometric coefficients.

The rate expression is expressed as the rate of destruction of a reactant or rate of formation of a product. Therefore, the formation rate ($\dot{\omega}_n$) of the nth species can be written as a summation of the rate of progress variables for all reactions involving the nth species.

$$\dot{\omega}_n = \sum_{i=1}^{I} \upsilon_{ni} q_i \qquad (n = 1, ..., n) \tag{2.4}$$

Where,

$$\upsilon_{ni} = {\upsilon''}_{ni} - {\upsilon'}_{ni} \tag{2.5}$$

The rate of progress variable (q_i) for the ith reaction can be calculated by the difference between forward and reverse rates.

$$q_i = k_{fi} \prod_{n=1}^{N} [X_n]^{{\upsilon'}_{ni}} - k_{ri} \prod_{n=1}^{N} [X_n]^{{\upsilon''}_{ni}} \tag{2.6}$$

Where k_f and k_r are the forward and reverse rate constant of the ith reaction. The rate of progress of a reaction is described using the concentration of each species in reactants or products in power of its stoichiometric coefficient. In the mechanism, the mass-action kinetics is valid, where the stoichiometric coefficient of species indicates the reaction order with respect to the concentration. In the detailed kinetic mechanism, the forward rate constants are specified and assumed to have the Arrhenius temperature dependence (Eq. 2.7).

$$k_f = AT^{\beta} exp\left(\frac{-E_a}{RT}\right) \tag{2.7}$$

where the pre-exponential factor A, the activation energy E_a, and temperature exponent β are specified in the kinetic mechanism as input. In Eq. 2.7, temperature [K] refers to the gas temperature. As mentioned earlier, the reverse rate constants k_r are related to the forward rate constant through equilibrium constant.

2.4.2 Pressure-dependent Reactions

Due to the complexity of the combustion processes, there are some reactions such as uni-molecular decomposition, radical-radical recombination, isomerisation, and chemically activated bimolecular reactions that are both pressure and temperature dependent [58]. Hence, it is necessary to incorporate this temperature and pressure dependence into reaction mechanisms in order to achieve precise predictions. Note that the pressure dependence of reaction rates is principally due to the collisional energy transfer. The mechanism proposed for uni-molecular decomposition reactions ($XY \Rightarrow products$) by Lindemann-Christiansen can be presented through the following steps:

- Collisional energy exchange between bath gases (M) to the reactants (XY)
  collisional activation $XY + M \Rightarrow XY^* + M$
  collisional deactivation $XY^* + M \Rightarrow XY + M$

- Intramolecular rearrangement

  molecular fragmentation $XY^* \Rightarrow products$

The typical timescales involved either in the collision processes or in the reaction process are 10^{-13} s and 10^{-9} s, respectively. A consequence of the separation of the collision and reaction timescales is that the rate coefficient for the overall reaction has a dependence on bath-gas pressure. This dependence is controlled by the competition between collisional energy transfer and intramolecular rearrangements processes [59] and as shown in figure 2.4 the dependency results in three domains of pressure (low-pressure, high-pressure and falloff region).

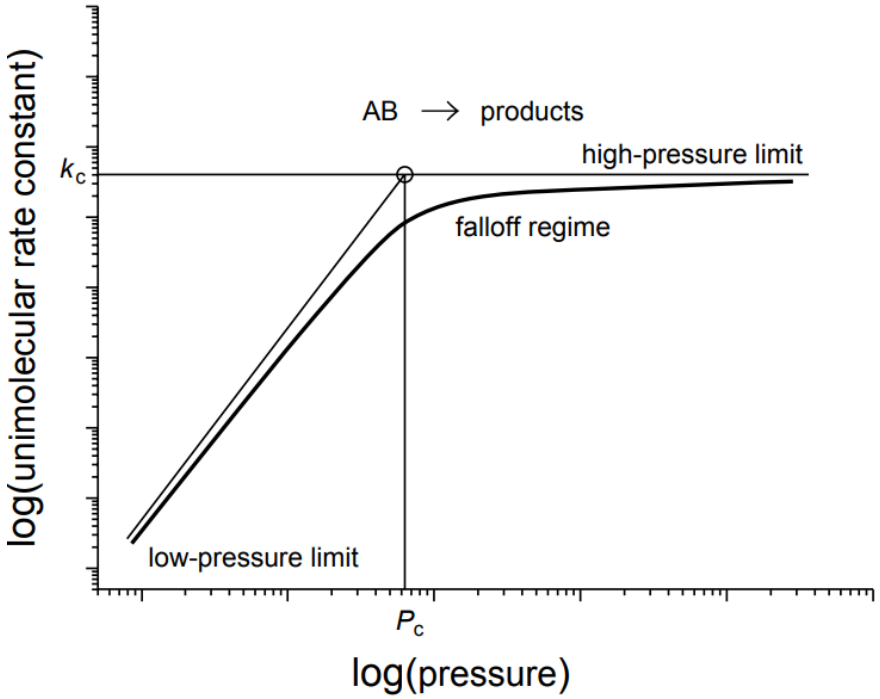

Figure 2.4: *Typical pressure dependence of uni-molecular.*

In high pressures, the exact high-pressure limit depends on the structure of the reactant, bath gas molecules, and temperature; moreover, the number of collisions between reactant and bath gas is so large that energy and angular momentum populations maintain equilibrium Boltzmann distribution. This high-pressure rate coefficient is pressure-independent and information about the collisional activation and deactivation are not required in this domain.

However, moving to the lower pressures, the bath gas collisions are no longer sufficiently frequent to maintain the Boltzmann distribution of energy and angular momentum. Below a specific pressure, collisional activation and deactivation processes become rate limiting, and the rate coefficient is proportionate to the bath-gas pressure.

However, for the pressures that fall in between high and low pressures, the rate constant is expressed with a more complex expression, and rate constant is no longer linear (in log scale plot). For more detail information the reader can refer to the discussion on the pressure dependence reactions by Carstensen and Dean [58].

In kinetic mechanism development, several different methods can be used describing the rate constant in the fall-off region. However, two commonly used expressions are TROE formalism [60] with high and low-pressure limits and the PLOG format [61].

TROE Formalism

Generally, in TROE formalism [60] two different rate expressions are specified for very low and very high pressures so-called low-pressure (k_0) and high-pressure (k_∞) limits, respectively. In the low-pressure limit, the third-body efficiency is also required to provide the necessary energy transfer for the reaction. This formalism is build upon Lindmann [62] description of fall-off reactions (Eq. 2.8).

$$k = k_\infty \left(\frac{P_r}{1 + P_r} \right) F \tag{2.8}$$

where P_r, the reduced pressure, is defined as:

$$P_r = \frac{k_0 \left[M \right]}{k_\infty} \tag{2.9}$$

here $[M]$ represents the concentration of the mixture, and possibly including third-body efficiencies.

In the Lindemann form, F in Eq. 2.8 is unity, while in the TROE description involves a more complex expression:

$$\log F = \left[1 + \left[\frac{\log P_r + c}{n - d \left(\log P_r + c \right)} \right]^2 \right]^{-1} \log F_{cent} \tag{2.10}$$

The constants in Eq. 2.10 are given by

$$c = -0.4 - 0.67 \log F_{cent} \tag{2.11}$$

$$n = 0.75 - 1.27 \log F_{cent} \tag{2.12}$$

$$d = 0.14 \tag{2.13}$$

and

$$F_{cent} = (1 - \alpha)\, exp \left(\frac{-T}{T^{***}} \right) + \alpha exp \left(\frac{-T}{T^{*}} \right) + exp \left(\frac{-T^{**}}{T} \right) \tag{2.14}$$

The four parameters α, T^{***}, T^{*} and T^{**} of the Eq. 2.14 are introduced as auxiliary inputs to the kinetic mechanism.

PLOG Format

Besides TROE formalism, Miller and Lutz [61] developed a generalised method for specifying pressure dependent rate constants. This method is based on the direct logarithmic interpolation of the reaction rate specified at individual pressures. In this formulation, the standard modified Arrhenius rate parameters are given for discrete pressures

```
2CH3=H+C2H5              4.740000e+12    0.105           10664.30
 PLOG /  1.000000e-02    4.740000e+12    1.050000e-01    1.066430e+04    /
 PLOG /  1.000000e-01    2.570000e+13    -9.600000e-02   1.140610e+04    /
 PLOG /  1.000000e+00    3.100000e+14    -3.620000e-01   1.337250e+04    /
 PLOG /  1.000000e+01    2.150000e+10    8.850000e-01    1.353250e+04    /
 PLOG /  1.000000e+02    1.032000e+02    3.230000e+00    1.123610e+04    /
```

Figure 2.5: *Example of PLOG format to describe the pressure dependent reactions.*

within the pressure range of interest. When the actual region of a specific pressure is computed, the rate parameters are determined through logarithmic interpolation between discrete pressures. For example, the PLOG format specified for a reaction is shown in Figure 2.5. Arrhenius parameters are specified at different pressures.

This strategy provides a very straight-forward way to incorporate rate data for more than one pressure. The first line introduces an elementary reaction and a set of dummy rate parameters, where the following lines express the real rate parameters. The set of pressure points for which rate parameters are assigned must include at least two different pressures. In such cases during simulation, if the current pressure is within 1% of one of the pressures for which rate constants are given, then that set of rate parameters will be used directly. However, If the current pressure is in between the pressure points provided, then the rate will be obtained by a linear interpolation of $\ln k$ as a function of $\ln P$. For P between P_i and $P_i + 1$, rate constant of k is obtained using:

$$\ln k = \ln k_i + (\ln k_{i+1} - \ln k_i) \frac{\ln P - \ln P_i}{\ln P_{i+1} - \ln P_i} \tag{2.15}$$

If the rate of the reaction is demanded at pressures lower than any of those PLOG provided, the rate parameters proposed for the lowest pressure will be used. Likewise, if the rate of the reaction is needed for a pressure higher than any of those proposed, the rate parameters of the highest pressure will be used. Furthermore, if the reaction rate at a given pressure cannot be expressed by only a single set of Arrhenius parameters, more than one set can be provided in the duplicated form.

This PLOG reaction format can be adopted as an alternative approach to defining any pressure dependence, and this concept is advantageous due to the straightforward implementation. However, the resolution or accuracy of the pressure dependence will depend on the number of pressure points included for each reaction. Besides these advantages, the PLOG generalism does not account for any third body efficiency of various level of energy transfer by different diluent.

2.4.3 Third-body

Third-body Reactions

Rate constant Eq. 2.7 is always temperature dependent; however, there are some reactions that a third-body is needed for the reaction to proceed. These reactions are often dissociation or recombination reactions, and the concentration of the effective third body also appears in the reaction expression, such as

$$H + O_2 + [M] \Leftrightarrow HO_2 + [M] \tag{R2}$$

It should be noted that the third-body neither consumed nor formed, and it just presented in the expression of the rate of the progress. Thus, the rate of progress differs from Eq. 2.6 by an extra term

$$q_i = \left(\sum_{n=1}^{N} (a_{ni})\,[X_n]\right)\left(k_{fi}\prod_{n=1}^{N}[X_n]^{\upsilon'_{ni}} - k_{ri}\prod_{n=1}^{N}[X_n]^{\upsilon''_{ni}}\right) \tag{2.16}$$

Where a_{ni} is the contribution of the species, and it is equal to 1 when all the species contribute equally. Then the first term of the Eq. 2.16 is the total concentration of the mixture. However, it often happens that some species act more effectively as third-bodies than others. The different third-body efficiencies must be assigned by an auxiliary input in the detailed kinetic mechanism.

Multiple Bath-gas Reactions

The common application of the multiple bath-gas reactions in pressure dependent reactions is when a specific species present as the bath gas. Most of the times the reactions for different bath-gas species are all defined in the same mechanism. Thereafter, the reaction rate computed at the fall off region or low-pressure limit will theoretically be identical regardless of the type of the species which acts as the bath gas. However, if multiple forms of the same reaction with different bath-gas species are proposed in a given mechanism, then the net of reaction rate is determined by summing up the different rates. Considering, k_i defines the rate expression of the reaction at the limiting pressure for i^{th} bath gas, then the total rate is calculated as:

$$k = \sum_{i}^{N} X_i k_i \qquad (N = number\ of\ bath\ gases) \tag{2.17}$$

To implement such cases, an advanced way of specifying the reaction with multiple bath-gas species is required. In principle, the rate expressions of different bath-gas species can be presented all together in the same reaction. The following figure 2.6 shows the extended format for TROE formalism pressure dependence proposed by Professor Stephen J. Klippenstein (Argonne National Laboratory).

```
H+O2(+M)=HO2+(M)                  4.650e+012   0.440   0.0
LowMX/                            1.737e+019  -1.230   0.0/
TroeMX/         6.700e-001 1.000e-030 1.000e+030 1.000e+030/
LowSP/AR                          6.810e+018  -1.200   0.0/
TroeSP/AR       7.000e-001 1.000e-030 1.000e+030 1.000e+030/
LowSP/HE                          9.192e+018  -1.200   0.0/
TroeSP/HE       5.900e-001 1.000e-030 1.000e+030 1.000e+030/
HE / 1.0 / AR / 1.0 / H2/ 1.30/ H2O/ 10.00/
```

Figure 2.6: *An example of extended TROE formalism.*

Where the keywords Low and TROE are the standard keywords of TROE formalism (see section 2.4.2), but here these keywords are expanded by SP and MX; which symbolise the rate constants for a given species (for instance Helium (HE) and Argon

(AR). MX indicates the rate expression for the rest of the mixture. For reactions presented in this style, the net reaction rate is calculated by summing up the different rates multiplied by the mole fraction of corresponding bath-gas species (2.17).

This formulation is also available for general PLOG pressure dependence reaction by introducing PLOGMX and PLOGSP keywords for mixture and different third-bodies, respectively. Figure 2.7 shows an example of extended PLOG pressure dependence proposed by Professor Stephen J. Klippenstein (Argonne National Laboratory).

```
H+O2=HO2                  1.0              0.0     0.0
PLOGMX/1.                 2.48E+17        -2.226   36.  /
PLOGMX/10.                1.90E+18        -2.194   6.0  /
PLOGMX/100.               6.05E+19        -2.330   635. /
PLOGSP/HE 1.              2.48E+17        -2.226   36.  /
PLOGSP/HE 10.             1.90E+18        -2.194   6.0  /
PLOGSP/HE 100.            6.05E+19        -2.330   635. /
```

Figure 2.7: *An example of extended PLOG* pressure dependence reaction.

As discussed for PLOG reactions in the section 2.4.2, third-body efficiencies are not allowed to be specified in the input. However, in the extended version shown in Figure 2.7, the rate expression for specific species and the remaining mixture can be characterised. The reaction rate of different species will be first calculated through appropriate interpolation at the given pressure. Consequently, the net rate of reaction will be determined as shown in Eq 2.17.

2.5 CRECK Detailed Kinetic Mechanism

The oxidation of large hydrocarbons and oxygenated hydrocarbon fuels are strongly built based on the detailed understanding of the pyrolysis and oxidation kinetics of simple fuels as well as small hydrocarbon fuels. Figure 2.8 presents the typical structure of detailed chemical mechanisms. A necessary implication of this figure is the hierarchical nature of hydrocarbons mechanisms as discussed by Westbrook and Dryer [26]. Similarly, the mechanism of the oxygenated fuels also from some parts of sub-mechanisms of the small hydrocarbons.

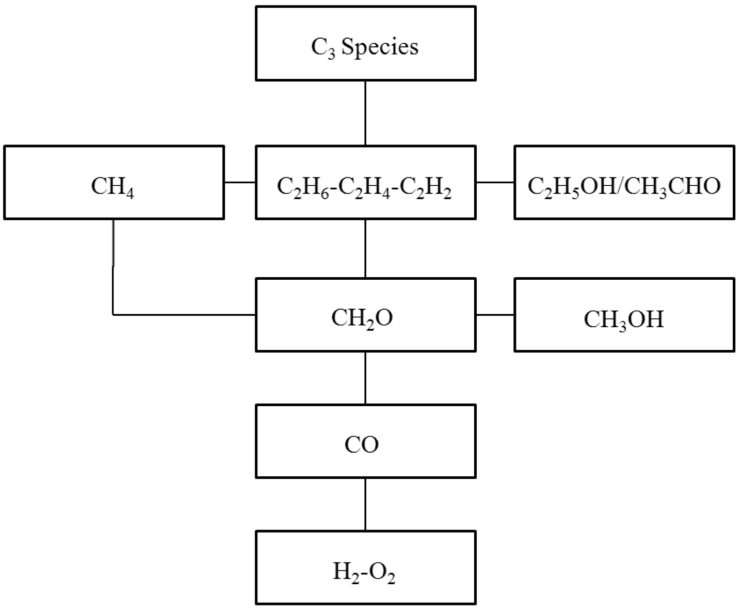

Figure 2.8: *Hierarchical structure of combustion mechanism of simple hydrocarbons [26]*

The mechanism (Figure 2.9) has been conceived and developed in a modular, hierarchical and general approach of the Chemical Reaction Engineering and Chemical Kinetics group (CRECK). It can describe the oxidation and pyrolysis of any fuels from hydrogen to heavy biodiesels, including biofuels such as alcohols. Such mechanism modules constructed hierarchically, including mechanisms to explain the combustion of hydrogen and its mixtures with carbon monoxide (syngas), followed by methane, methanol, formaldehyde, ethane, ethylene, acetylene, acetaldehyde, and ethanol.

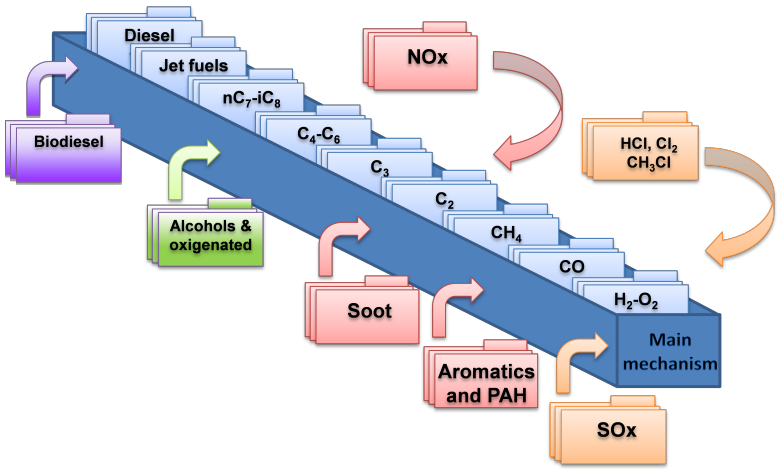

Figure 2.9: *Schematic representation of CRECK mechanism of pyrolysis and oxidation.*

The mechanism is created by first determining the most important reactions associated with a fuel's oxidation and considering their rate constants based on the most recent accurate measurements and calculations, where possible, and otherwise on evaluated rate parameters, which can accurately reproduce a range of targets including global targets such as ignition delay times and flame speeds, but also speciation data in flow- and jet-stirred reactors and in burner-stabilized flames. Schematically, this C_0-C_3 mechanism is obtained by coupling the H_2-O_2 and C_1-C_2 from Metcalfe et al. [51], the C_3 from Burke et al. [56, 63], and the mechanisms of heavier species from Ranzi et al. [29, 30].

2.6 Summary

This Chapter reviewed some theoretical and fundamental principles of chemical kinetics and thermodynamics, the core of any chemical kinetic models. Summarising the standard procedure for developing a kinetic model it is necessary to:

- Determine the thermodynamic functions for any species involved in the kinetic mechanism and fit them into NASA polynomials.
- Estimate rate constants parameters for each reaction in the most accurate way. Theory, experimental measurements and analogy can guide the formulation of rules as discussed in Chapter 3.
- Implement the pressure dependent reactions. Various expressions (*TROE* and *PLOG*) have been proposed while estimating correct rate constants and third-body efficiencies for these reactions are still controversial.

The mechanism will be conceived and developed in a modular, hierarchical and general approach of the Chemical Reaction Engineering and Chemical Kinetics group (CRECK). The description of these features is the main topic of the next Chapters.

CHAPTER 3

Thermochemical Properties

3.1 Introduction

THERMOCHEMISTRY is a branch of thermodynamics that mainly focuses on the changes occurring during chemical reactions. During thermochemical processes, chemical reactions are understood to explain not only reactions in which the initial reactants transfer to the different products but also those reactions that result in a physical transformation of the state. The availability of reliable thermochemical properties often fosters the abstraction of patterns or generalities that can reveal new insight into the details of reactivity and chemical bonding.

Thermochemistry and kinetics have a strong dependency. To better understand, consider a simplified elementary reversible reaction involving chemical species that can be presented in the general form:

$$aA + bB \Leftrightarrow cC + dD \tag{3.1}$$

Where A, B, C and D show the chemical symbols of the species, and a, b, c and d are the stoichiometric coefficients. In this chemical reaction in Eq. 3.1 the equilibrium constant (K_c) may be expressed in terms of concentration of the species, [X] (concentration of given species X):

$$K_c = \frac{[C]^c[D]^d}{[A]^a[B]^b} \tag{3.2}$$

or equilibrium constant (K_p) in term of partial pressure, p_X (partial presseure of given species X) :

$$K_p = \frac{{p_C}^c.{p_D}^d}{{p_A}^a.{p_B}^b} \tag{3.3}$$

A correlation between K_c and K_p can be defined using the equation of state for ideal gas Eq. 3.4 ,where T is temperature, R is the gas constant and n is amount of gas in moles.

$$pV = nRT \qquad or \qquad \frac{p}{RT} = \frac{n}{V} \tag{3.4}$$

thus, the correlation between partial pressure and concentration can be presented in Eq. 3.5.

$$p = [X]RT \tag{3.5}$$

where the concentration is calculated by $n/V = [X]$. Then pressure is equal to the concentration multiplied by the gas constant and temperature. Consequently, the correlation between the equilibrium constants can be rewritten as:

$$K_p = K_c \, (RT)^{\Delta n} \tag{3.6}$$

where Δn is the change in the number of moles from reactant to products, and is defined as follow:

$$\Delta n = (c + d) - (a + b) \tag{3.7}$$

K_p can also be expressed in terms of thermodynamics properties by using Gibbs free energy.

$$K_p = exp\left(\frac{-\Delta G}{RT}\right) \tag{3.8}$$

which also can be rearranged as

$$\Delta G = -RT \ln K_p \tag{3.9}$$

Substituting Eq. 2.1 into Eq. 3.9, it can be concluded that

$$\ln K_p = \frac{\Delta S}{R} - \frac{\Delta H}{RT} \tag{3.10}$$

which can be further rewritten in the form of Arrhenius expression:

$$\ln K = \ln\left(\frac{A_f}{A_r}\right) - \frac{(E_f - E_r)}{RT} \tag{3.11}$$

$\Delta S/R$ in Eq. 3.10 can be identified with pre-exponential factor (lnA) in Eq. 3.11, and also the enthalpy term $\Delta H/RT$ can be assign to the change in the energy barriers $(E_f - E_r)$ in the Arrhenius equation. Here the indexes f and r refer to forward and reverse reactions, respectively.

More importantly, in reaction systems, the reverse rate constants k_r are related to the forward rate constants through the equilibrium constants by

$$k_r = \frac{k_f}{K_c} \tag{3.12}$$

Thermodynamic properties dictate the reverse rate constants of reactions and reliable thermochemical properties are demanded in order to predict rates of the chemical reactions accurately.

3.2 Representation of Thermochemical Parameters

Detailed kinetic mechanisms essentially require thermochemical data to be provided in NASA polynomial format [64]. These polynomial coefficient are used to calculate various thermodynamic properties as a function of temperature. This NASA polynomial provides two correlations for high and low temperature ranges. Figure 3.1 presents an example of a typical way of defining thermodynamic polynomial input CHEMKIN format [65] to be used together with the kinetic mechanism in modelling.

```
CH4                     C   1H   4          G    300.00   4000.00 1000.00      1
 .165326226E+01 .100263099E-01-.331661238E-05 .536483138E-09-.314696758E-13    2
-.100095936E+05 .990506283E+01 .514911468E+01-.136622009E-01 .491453921E-04    3
-.484246767E-07 .166603441E-10-.102465983E+05-.463848842E+01                   4
CH3OH                   C   1H   4O   1     G    300.00   4000.00 1000.00      1
 .352726795E+01 .103178783E-01-.362892944E-05 .577448016E-09-.342182632E-13    2
-.260028834E+05 .516758693E+01 .565851051E+01-.162983419E-01 .691938156E-04    3
-.758372926E-07 .280427550E-10-.256119736E+05-.897330508E+00                   4
CH3O2H                  C   1H   4O   2     G    300.00   4000.00 1000.00      1
 .776538058E+01 .861499712E-02-.298006935E-05 .468638071E-09-.275339255E-13    2
-.182979984E+05-.143992663E+02 .290540897E+01 .174994735E-01 .528243630E-05    3
-.252827275E-07 .134368212E-10-.168894632E+05 .113741987E+02                   4
C2H2                    C   2H   2          G    300.00   4000.00 1000.00      1
 .465878489E+01 .488396667E-02-.160828888E-05 .246974544E-09-.138605959E-13    2
 .257594042E+05-.399838194E+01 .808679682E+00 .233615762E-01-.355172234E-04    3
 .280152958E-07-.850075165E-11 .264289808E+05 .139396761E+02                   4
```

Figure 3.1: *Example pf thermodynamic database file for use with detailed kinetic mechanism*

Figure 3.2 outlines the specific location of the value in Figure 3.1. There are four lines devoted for each species. The first line contains the species name, data, reference of the species, the elements that species contains, the phase the molecule is in and temperatures denoted for high and low-temperature coefficients. $Tlow$ refers to the low-temperature limit, $Thigh$ refers to high-temperature limit and Tbk refers to the break-point temperature between low and high. The second line consists of coefficients $a1 - a5$, the third line contains coefficients $a6 - a10$ and the fourth line includes coefficients $a11 - a14$.

```
                    column numbers:
1         10        20        30        40        50        60        70        80
|23456789|123456789|123456789|123456789|123456789|123456789|123456789|123456789|

|<-name>||<-date->|<ref>|<---- elements --->G|<- Tlow >|<- Thi->|<- Tbk->|    21
|<--- a1 ---->|<---- a2 ---->|<---- a3 ---->|<---- a4 ---->|<---- a5 ---->|    2
|<--- a6 ---->|<---- a7 ---->|<---- a8 ---->|<---- a9 ---->|<---- a10 --->|    3
|<--- a11 --->|<---- a12 --->|<---- a13 --->|<---- a14 --->|                   4
```

Figure 3.2: *Description of specified data in NASA polynomial format[ref 20].*

The fourteen coefficients presented in the polynomial are then used to determine thermodynamic properties as follow:

3.2.1 Heat Capacity

The heat capacity of a Species presents the amount of heat required for that species to raise the temperature. Heat capacity can be defined in two different terms; heat capacity

at constant pressure (C_p) and heat capacity at constant volume (C_v). These terms are correlated to each other through the gas constant of the given species (Eq. 3.13).

$$C_p - C_v = R \tag{3.13}$$

the standard C_p in terms of polynomial can be defined through:

$$\frac{\mathring{C}_p}{R} = \sum_{n=1}^{N} a_n T^{(n-1)} \tag{3.14}$$

By substituting the polynomial coefficients, it takes the following form:

$$\frac{\mathring{C}_p}{R} = a_1 + a_2 T + a_3 T^2 + a_4 T^3 + a_5 T^4 \qquad T > Tbk \tag{3.15}$$

$$\frac{\mathring{C}_p}{R} = a_8 + a_9 T + a_{10} T^2 + a_{11} T^3 + a_{12} T^4 \qquad T < Tbk \tag{3.16}$$

3.2.2 Enthalpy of Formation

Standard enthalpy of formation is the change in the enthalpy of one mole pure substance when formed from its elements in standard states. Enthalpies of formation can be given in terms of polynomial fit:

$$\mathring{H} = \int_0^T \mathring{C}_p dT \tag{3.17}$$

Consequently:

$$\frac{\mathring{H}}{RT} = \sum_{n=1}^{N} \frac{a_n T^{(n-1)}}{n} + \frac{a_{N+1}}{T} \tag{3.18}$$

Enthalpy of formation can be calculated at a given temperature using NASA polynomial format through Eq. 3.19 and Eq. 3.20. Equation 3.19 is used for the temperature higher than break-point temperature while Eq. 3.20 is for temperature below it.

$$\frac{\mathring{H}}{RT} = a_1 + \frac{a_2}{2} T + \frac{a_3}{3} T^2 + \frac{a_4}{4} T^3 + \frac{a_5}{5} T^4 + \frac{a_6}{T} \qquad T > Tbk \tag{3.19}$$

$$\frac{\mathring{H}}{RT} = a_8 + \frac{a_9}{2} T + \frac{a_{10}}{3} T^2 + \frac{a_{11}}{4} T^3 + \frac{a_{12}}{5} T^4 + \frac{a_{13}}{T} \qquad T < Tbk \tag{3.20}$$

3.2.3 Entropy

The standard entropy of species in molar basis is the entropy of the substance in its standard state at a given temperature. Standard entropy can be calculated from NASA polynomial coefficients. Entropies of formation are given by:

$$\mathring{S} = \int_0^T \frac{\mathring{C}_p}{T} dT \tag{3.21}$$

Therefore, in terms of Polynomial fit:

$$\frac{\mathring{S}}{R} = a_1 \ln T + \sum_{n=2}^{N} \frac{a_n T^{(n-1)}}{n-1} + a_{N+2} \tag{3.22}$$

At temperatures higher than break point Eq. 3.23 can be implemented while below this temperature Eq. 3.24 can be used with the coefficients in the CHEMKIN format.

$$\frac{\mathring{S}}{R} = a_1 \ln T + a_2 T + \frac{a_3}{2} T^2 + \frac{a_4}{3} T^3 + \frac{a_5}{4} T^4 + a_7 \qquad T > Tbk \tag{3.23}$$

$$\frac{\mathring{S}}{R} = a_8 \ln T + a_9 T + \frac{a_{10}}{2} T^2 + \frac{a_{11}}{3} T^3 + \frac{a_{12}}{4} T^4 + a_{14} \qquad T < Tbk \tag{3.24}$$

3.3 Thermochemical Databases

Thermochemical tables are tabulations of thermochemical properties sorted by chemical species. The thermochemical properties of chemical species can be obtained form two basic categories of determination: species-specific and species-interrelating [66]. Species-specific information (such as spectroscopic measurements, electronic structure computation, and direct measurements) can be directly used to derive certain properties such as heat capacity, entropy and enthalpy increment. Where, species-interrelating can be used to quantify information relative to other chemical species such as bond dissociation energies, enthalpies of chemical reactions, kinetic equilibrium, and etc ...

Various thermodynamic databases are available in the literature. The widely used databases are NIST [67], Active Thermochemical Tables (ATcT) [68] and Burcat's thermodynamic database [69]. Additionally, there are still species for which there are no published thermodynamic data available. For these species, group additivity method developed by Benson [70] can be employed.

3.3.1 Hydrogen and Syngas Core)

Active Thermochemical Tables (ATcT) [68] is a new criterion of how to obtain accurate, reliable, and internally consistent thermochemistry and overcome the limitations that are intrinsic to the traditional approach to thermochemistry. This paradigm provides high-quality, consistent thermochemical values which are critical in many areas of chemistry, including the development of realistic predictive models of complex combustion systems. ATcT utilises the Thermochemical Network (TN) approach to expose the maze of inherent inter-dependencies explicitly, and allow a statistical analysis of the individual measurements that define the TN.

The result affords the best possible thermochemistry, based on optimal use of all the currently available knowledge. Furthermore, ATcT proposes several further features that are neither present nor possible in the traditional thermochemistry approach. The solutions and their adjunct uncertainties are guaranteed to be consistent both internally and with all the knowledge stored in the thermochemical network, thus producing thermochemical values that are superior to those obtained from a sequential approach.

In spite of the new knowledge that can be delivered through ATcT and all affected thermochemical values, for the bigger TNs the computation cost is very high and to the

best of our knowledge, it is not yet fully implemented for the methane or bigger networks. Moreover, in the published ATcT database [68] only a list of $0\,K$ and $298.15\,K$ enthalpies of formation are provided. Thus, thermochemical properties of the species involved in hydrogen and syngas cores were obtained through personal communication.

Table 3.1 lists the thermodynamic properties (formation enthalpy at $298\,K$, entropy at $298\,K$, and heat capacity at various temperatures) for eleven species of the hydrogen and syngas sub-modules considered in the current model. NASA polynomial fits are also provided in the kinetic mechanism.

The thermodynamic properties of species involved in the hydrogen core are expected to be well known in the combustion community. However, in order to better understand the level of accuracy of new calculated values, ATcT data are compared with the thermodynamic properties presented in Aramco.2 [63] as a newly updated and widely validated kinetic mechanism. It should be noted that Aramco.2 thermodynamic parameters for the enthalpy and entropy of formation and heat capacities were adopted from the Burcat database [69] when possible, in the absence of data from the Burcat database thermodynamic parameters were estimated using the group additivity method employed by Benson [70] utilised.

Table 3.1: *Thermodynamic properties of hydrogen and syngas sub-module species form ATcT database [68]. Units are* $cal\,mol^{-1}\,K^{-1}$ *for* C_p *and* $\mathring{S}$*, and* $kcal\,mol^{-1}$ *for* $\mathring{H}_f$*. The temperatures for* C_p *and* $\mathring{S}$ *are in* K*.*

Species	$\mathring{H}_{f298}$	$\mathring{S}_{298}$	C_{p600}	C_{p800}	C_{p1000}	C_{p1200}	C_{p1400}	C_{p1600}	C_{p1800}	C_{p2000}
H	52.0966	27.3989	4.9676	4.9675	4.9675	4.9675	4.9675	4.9675	4.9675	4.9675
H_2	-0.001	31.2107	6.9938	7.0787	7.1996	7.4256	7.6348	7.8286	8.0084	8.1753
O	59.5602	38.4682	5.0512	5.0151	5.0027	4.9932	4.9854	4.9798	4.9762	4.975
O_2	-0.0011	48.9984	7.6666	8.0642	8.3367	8.501	8.6529	8.7935	8.9244	9.0464
OH	8.9583	43.8852	7.0572	7.1485	7.3371	7.5746	7.7863	7.9751	8.1435	8.2939
HO_2	2.9279	54.7321	10.0445	10.8583	11.5233	12.0422	12.5144	12.9417	13.3263	13.6702
H_2O_2	-32.3732	56.0151	12.8153	14.0564	15.0622	15.8369	16.5026	17.0726	17.5595	17.975
H_2O	-57.7947	45.1004	8.6799	9.2556	9.8652	10.4722	11.007	11.4773	11.8906	12.2532
HCO	9.9889	53.5723	9.8372	10.8498	11.6621	12.2205	12.7189	13.1646	13.5644	13.9242
CO	-26.4139	47.2097	7.2693	7.6228	7.9221	8.1407	8.32	8.4654	8.5819	8.6739
CO_2	-94.0343	51.0598	11.3147	12.2914	12.984	13.4156	13.7679	14.0517	14.2771	14.4535

Then, except H_2O and H_2O_2, the comparison of the thermodynamic data proves no significant difference. Figure 3.3 presents the relative difference comparison of C_p and $\mathring{H}$ between ATcT and Aramco.2 [63] for H_2O and H_2O_2. As can be seen from these figures, the deviation increases with temperature where for the water reaches 1.5% and 3% of relative difference in $2600\,K$ for C_p and $\mathring{H}$, respectively. In figure 3.3b, the relative difference in enthalpy of H_2O_2 drastically increases after $T = 2000\,K$ because the values of enthalpy goes to zero at 2400 and the quantities close to this temperature are very small; thus a very small difference between quantities results in a high relative difference.

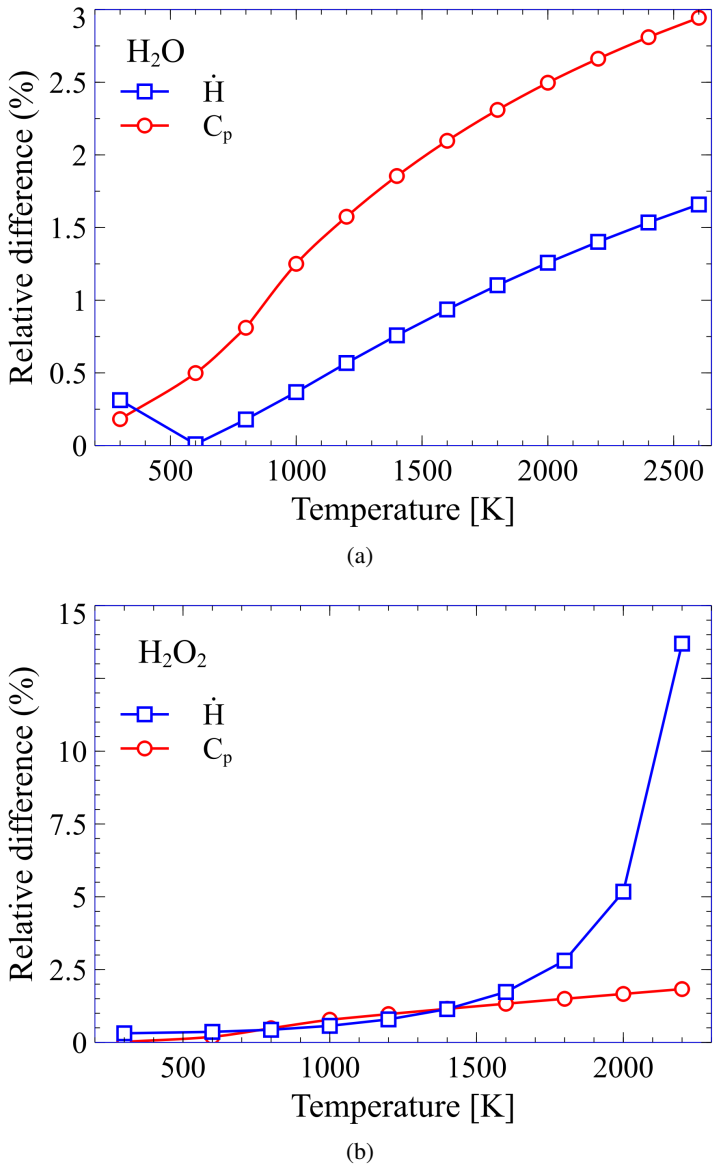

Figure 3.3: *Relative difference of $\mathring{H}$ and C_p values, compared between ATcT data and Aramco.2 thermodynamic data for H_2O and H_2O_2.*

3.3.2 C_1 and C_2 Sub-mechanisms

Accurate thermodynamic parameters are very important when modelling combustion systems. Values for the enthalpy and entropy of formation and heat capacities $C_1 - C_2$ hydrocarbon species considered in the current model, with a few exceptions, have been extracted from the thermochemical Database of Burcat [69]. In the absence of data from the Burcat database thermodynamic parameters have been adapted from Aramco.2 [56, 63], where the group additivity method employed by Benson [70] and utilized in the Therm program developed by Ritter and Bozzelli [71].

3.3.3 CH_3OO and CH_3OOH

In the literature, thermodynamic properties of alkyl peroxide species and their radical derivatives often vary considerably [72]. The thermodynamic properties for CH_3OO and CH_3OOH, which are of particular interest for modelling CH_4 oxidation at high pressure and low to intermediate temperatures have been adapted from Hashemi et al. [55]. The thermodynamic data for the two species are shown in Table 3.2. Polynomial fits for thermodynamic properties of CH_3OO and CH_3OOH can be found in the Kinetic mechanism.

Table 3.2: *Thermodynamic properties of CH_3OO and CH_3OOH [55]. Units are $cal\,mol^{-1}\,K^{-1}$ for C_p and $\mathring{S}$, and $kcal\,mol^{-1}$ for $\mathring{H}_f$. The temperatures for C_p and $\mathring{S}$ are in K.*

Species	$\mathring{H}_{f298}$	$\mathring{S}_{298}$	C_{p300}	C_{p400}	C_{p500}	C_{p600}	C_{p800}	C_{p1000}	C_{p1500}
CH_3OO	3.06	65.45	11.91	14.01	15.98	17.78	20.72	22.83	26.15
CH_3OOH	-30.51	67.31	14.49	16.98	19.22	21.18	24.31	26.58	30.27

The heats of formation for CH_3OO and CH_3OOH at $T = 0\,K$ are reported to be 5.39 and $-27.45\,kcal/mol$, respectively [55]. As can be seen from Table 3.2, these values correspond to $\mathring{H}_{f298}(CH_3OO) = 3.06$ and $\mathring{H}_{f298}(CH_3OOH) = -30.51kcal/mol$. The enthalpy of formation for CH_3OO shows a slightly lower value than other recent theoretical values of $3.4\,kcal/mol$ from Janoschek and Rossi [73] and $3.3kcal/mol$ from Goldsmith et al. [74]; however it is in good agreement with the experimental value of $3.0 \pm 1.2kcal/mol$ from Meloni et al. [75]. For CH_3OOH, the enthalpy of formation at $T = 298\,K$ is in an excellent agreement with theoretical values of$-30.4 \pm 1\,kcal/mol$ [76] and $-30.7 \pm 0.9kcal/mol$ [74].

3.4 Summary

Consequently, the thermochemical properties of species available in the mechanism are extracted from the most accurate databases in the literature. Hydrogen and Syngas cores were implemented from Active Thermochemical Tables (ATcT) (personal communication) [68]. Other important species thermochemical properties are extracted from Burcat's thermodynamic database [69]. For the rest of species in the mechanism, which are not presented in databases, thermochemistry properties suggested in the CRECK mechanism [50] are used.

CHAPTER 4

Kinetic Mechanism

4.1 Introduction

METHANE is the smallest hydrocarbon with the highest H/C ratio of all carbonaceous fuels. Thus, this large H/C ratio enables reduced overall CO_2 emissions from combustion compared to other hydrocarbon fuels. It is, therefore, no surprise that a detailed understanding of the combustion chemistry of methane over a wide range of conditions is desirable to design efficient combustion devices using CH_4 as the main fuel component.

The widespread use of methane; the importance of its intermediate species and radicals to the chemistry of larger hydrocarbon fuels; the fact that it is the smallest hydrocarbon; and its ease of use in the laboratory have made methane a widely studied molecule [77]. Despite this large volume of studies, research on methane combustion is still ongoing to explore conditions that have been less investigated or to refine specific parts of the detailed kinetics mechanism or reactions for unconventional combustion.

The reaction path analysis of carbon atoms formed from one mole of methane shows two major pathways. In the premixed stoichiometric mixture of methane for temperature from 1000 up to $3000\,K$ these two major paths are as follow [78]:

$$Oxidation : CH_4 \longrightarrow CH_3 \longrightarrow CH_3O \longrightarrow CH_2O \longrightarrow HCO \longrightarrow CO \longrightarrow CO_2$$

$$Pyrolysis : CH_4 \longrightarrow CH_3 \longrightarrow C_2H_6 \longrightarrow C_2H_5 \longrightarrow C_2H_4 \longrightarrow C_2H_3 \longrightarrow C_2H_2$$

The importance of the pyrolysis mechanism as the main alternative reaction pathway is well documented int the literature [5, 79, 80], and on the fuel-rich mixture, the formation of C_2 species is the main reaction pathway. CH_3O, CH_2O and HCO are

the important intermediate species in methane oxidation pathway; moreover, in certain conditions, methanol (CH_3OH) and hydroxymethyl (CH_2OH) become the main path leading to formaldehyde (CH_2O) formation [81].

The $C_0 - C_3$ CRECK detailed kinetic mechanism has been obtained by coupling the H_2/O_2 and $C_1 - C_2$ from Metcalfe et al. [51], C_3 from Burke et al. [63] and heavier species from Ranzi et al. [30, 82]. Several reactions, as listed in Table 1, are also updated for the sake of performance improvement. In the current mechanism, further improvements were achieved by updating the acetaldehyde sub-mechanism, according to Pelucchi et al. [83].

Moreover, the rate rule for H-abstraction reactions of Ranzi et al. [84] was implemented and the rate parameters extracted in the absence of data from the literature. Indeed, the rate rule approach is more useful for the higher molecules. It is implemented because the $C_0 - C_3$ mechanism is not only a natural gas reaction mechanism but also a core mechanism for heavier fuel sub-mechanisms in CRECK mechanism. Including H-abstraction rate rule will facilitate linking this core mechanism to other sub-mechanisms.

The aim of this Section is not to discuss the reaction rate adopted in the kinetic but to review the controversy in some critical reactions of pyrolysis and oxidation channels. These reactions are chosen by emphasising their role in unconventional combustion systems.

Table 4.1: *Modified reactions in the chemical kinetic model. The rate constants are in the form of* $k = AT^n exp(-E_a/RT)$. *Units are mol, cm, K, s, and cal.*

Reactions	A	n	E_a	Reference
$C_2H_3 + H = C_2H_2 + H_2$	9.64E+13	0	0	[85]
$C_3H_4 - P + OH = C_3H_3 + H_2O$	2.00E+07	2	5000	[86]
$C_3H_4 - A + OH = C_3H_3 + H_2O$	2.00E+07	2	5000	[86]
$H + C_2H(+M) = C_2H_2(+M)$	1.00E+17	-1	0	[44]
$CH_3O + HCO = CH_3OH + CO$	1.00E+13	0	0	[85]
$H + O_2 = O + OH$ *	1.14E+14	0	15286	[87]
$CH_3CO + O_2 = CH_3CO_3$				
Logarithmic Pressure: 0.1	3.41E+69	-18.9	14400	
Logarithmic Pressure: 1.0	5.79E+61	-16.07	13400	[88]
Logarithmic Pressure: 10.0	5.07E+52	-12.96	11560	
$C_3H_4 - P = C_3H_4 - A$				
Logarithmic Pressure: 0.100	6.4E+61	-14.59	88200	
Logarithmic Pressure: 1.000	5.2E+60	-13.93	91100	[89]
Logarithmic Pressure: 10.00	1.9E+57	-12.62	93300	
Logarithmic Pressure: 100.0	1.4E+52	-10.86	95400	
$CH_3 + C_2H_6 = CH_4 + C_2H_5$	2.72E+00	3.767	9096	[90]
$H + C_3H_3 = C_3H_4 - A$				
Logarithmic Pressure: 0.04	3.39E+36	-7.41	6337	
Logarithmic Pressure: 1.00	3.16E+29	-5.00	4711	[91, 92]
Logarithmic Pressure: 10.0	8.71E+23	-3.20	3255	
Logarithmic Pressure: 100.0	2.05E+13	0.206	-173	
$H + C_3H_3 = C_3H_4 - P$				
Logarithmic Pressure: 0.04	3.63E+36	-7.36	6039	
Logarithmic Pressure: 1.00	7.94E+29	-5.06	4861	[91, 92]
Logarithmic Pressure: 10.0	1.07E+24	-3.15	3261	
Logarithmic Pressure: 100.0	6.40E+13	0.102	-31.2	
$H + C_3H_4 - A = C_3H_5 - S$				
Logarithmic Pressure: 0.04	3.38E+49	-12.75	14072	
Logarithmic Pressure: 1.00	1.37E+51	-12.55	15428	
Logarithmic Pressure: 10.0	3.88E+50	-11.90	16915	
Logarithmic Pressure: 100.0	2.17E+49	-11.10	18746	
DUPLIICATE				[93]
Logarithmic Pressure: 0.04	2.98E+43	-11.43	8046	
Logarithmic Pressure: 1.00	5.75E+39	-9.51	7458	
Logarithmic Pressure: 10.0	4.33E+40	-9.60	6722	
Logarithmic Pressure: 100.0	3.44E+34	-7.36	6150	

* Within the uncertainty the rate increased by 10%

4.2 Pyrolysis Pathway

Pyrolysis, thermal decomposition, of methane is at the heart of our understanding of kinetic and mechanistic research regarding hydrocarbons. It is also the starting point and the underlying kernel for oxidation reactions of higher hydrocarbons through the

regular path of pure decomposition [29]. Additionally, it contains the main reaction steps of chemically activated addition and isomerisation reactions [94]. These reactions are propellant for the formation of resonantly stabilised propargyl (C_3H_3) radical which is the precursors to the polycyclic aromatic hydrocarbons (PAH) and soot [56]. These show that methane pyrolysis sub-mechanism plays a crucial role, and it is frequently implemented in combustion modelling [95,96]. Consequently, a kinetic review is necessary to describe the most critical reactions associated with methane pyrolysis and to establish the new-found status of this model.

Methane is severally stable at the lower temperatures compared to other hydrocarbons, due to the presence of strong aliphatic $C-H$ bonds. Thus, methane thermal-decomposition is an endothermic process and requiring $\sim\ 105kcal/mol$ energy to break down the $C-H$ bond. It is well known that several difficulties associated with this high-temperature pyrolytic condition appear owing to soot and non-gaseous carbonaceous products formation [97]. Therefore, comparing to methane oxidation, the amount of experimental literature on methane pyrolysis are more scarce and only limited to low and atmospheric pressures to prevent carbon formation. This limited experimental information has built the core of understanding about pyrolysed products and widely used for mechanism developments.

The initiation and also rate-determining step in methane pyrolysis is through reaction 4.1; moreover, this reaction is considered as the primary source of radicals. More importantly, it works as a radical sink affecting flame speed and ignition delay time in the combustion of various hydrocarbons. When methane conversion increases, hydrogen atom abstraction by reaction 4.2 becomes the dominant path in methyl (CH_3) formation.

$$CH_3 + H(+M) = CH_4(+M) \tag{4.1}$$

$$CH_4 + H = CH_3 + H_2 \tag{4.2}$$

This recombination reaction 4.1 has been widely studied both experimentally and numerically. However, the low-pressure limit of this pressure dependent reaction is less characterised, owing to differences in the extraction of extrapolated data from experimental fall of curves and also the theoretical calculation of the energy transfer parameters [98]. Golden [99] discussed that in the calculation of energy transfer, the centrifugal corrections were not precisely implemented which made the collisions less competitive and as a result, the less effective collisions influence the low-pressure limits.

Figure 4.1 examines some of the widely used rate constants for Reaction 4.1. The rate proposed in GRI.3 [45] is considered because this rate with small modifications have been implemented in other kinetic mechanisms such as Aramco [51] and Jetsurf [100]. Recent theoretical study on this reaction by Troe and Ushakov [98] was carried out by considering the correction for energy transfer parameters. This rate was later re-evaluated by Golden [99], where he concluded that the rate calculated by Troe and Ushakov [98] more precisely predicts the data compared to other older rates . Troe and Ushakov rate is presented in the simple power law as this curve perfectly fit their calculation; thus, this curve need to be refitted to the Arrhenius form for the sake of mechanistic implementation.

In figure 4.1, the fitted rate to the simple power law proposed by Troe and UShakov [98] is presented in the dot-dash line, which reasonably reproduces the curve. However,

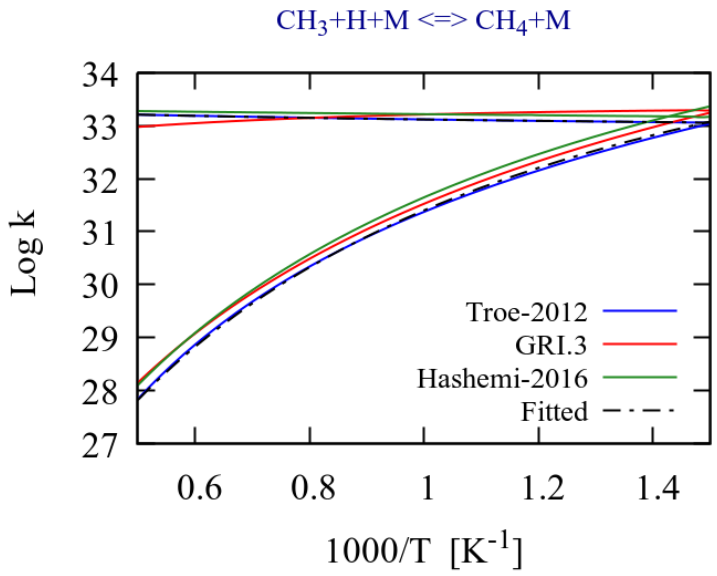

Figure 4.1: *High and low pressure reaction rates of the $CH_3 + H + M = CH_4 + M$. Troe-2012 refers to [98], GRI.3 to [45], and Hashemi-2016 to [55]. Fitted is the Arrhenius form of [98].*

it should be noted that the maximum error in this fitting is $\sim 9\%$ in $T = 500\ K$, and this error could not be reduced due to the limitation of Arrhenius curve in following up the power law curve. The fall off centre broadening factors F_c is also presented in a somewhat complicated formulation, but Golden [99] suggested a modified formulation in the traditional form of F_c with a little difference from full implementation of Troe and Ushakov. Table 4.2 contains these rates with their associated centre broadening factors.

Table 4.2: *Rate constants of the dissociation/recombination reaction* $CH_3 + H(+M) = CH_4(+M)$.

No	Rate parameters [mole.cm.s]	Ref
1.	$k_0 = 2.34E+21 \times exp(-(T/21.22)^{0.5})$	[98]
	$k_\infty = 2.01E+14 \times (T/300)^{0.186} \times exp(-T/25200)$	[98]
	$F_C = 0.262 + [(T-2950)/6100]^2$	[98]
2.	$k_0 = 1.222E+36 \times T^{-5.607} \times exp(-2000/T)$	Fitted
	$k_\infty = 1.055E+14 \times T^{0.122} \times exp(-15.6/T)$	Fitted
	$F_C = 0.63exp(-T/3315) + 0.37exp(-T/61)$	[99]

Low-pressure limit of reaction 4.1 has a strong collision dependency. In fact, in the combustion community, the collision efficiencies of different colliders are not well characterised, and they are usually treated empirically as the dependency of the collisional energy transfer on temperature, bath gas, and chemical structure of reactant are not fully understood. Jasper et al. [101] extended a theoretical characterisation of the collisional energy transfer of methane dissociation in combustion applications. They pointed out that collision efficiencies vary with temperature; however, the trend of these variations depends on the chemical structure of bath gases.

This temperature dependency is stronger for lighter bath gases (He and H_2) while polyatomic gases have the weakest temperature dependence (H_2O and CH_4). Based on this research [101] and our mechanistic analysis, the relative collision efficiencies ($k_0[M]/k_0[Ar]$) for Reaction4.1 are adopted as presented in table 4.3. It should be noted that the fitted rate in table 4.2 is also devoted to the system with Ar as bath gas; thus it is consistent with the relative collision efficiencies in Table4.3.

Table 4.3: *Relative collision efficiencies* ($k_0[M]/k_0[Ar]$) *for Reaction* $CH_3 + H(+M) = CH_4(+M)$

Collider	CH_4	H_2O	H_2	CO	CO_2	C_2H_6	N_2	He
Collision efficiency	4.5	8	4	1.4	4.5	4	1.5	2

It is well known that methane decomposition in pyrolysis is followed by the formation of ethane (C_2H_6) which is described by trimolecular recombination of methyl (CH_3) radical 4.3. In the past, considerable attention has been paid to this reaction. The Tore like rate expression adapted in the current mechanism is based on the theoretical and experimental study of Wang et al. [102], and the reason behind this implementation was well-discussed in detail in [51].

$$CH_3 + CH_3 + M = C_2H_6 + M \tag{4.3}$$

$$C_2H_6 + CH_3 = C_2H_5 + CH_4 \tag{4.4}$$

Figure 4.2 depicts a sensitivity analysis on ethane during methane pyrolysis (an initial condition similar to Ref [103]). Methane decomposition reaction 4.1 is the most sensitive reaction while H-atom abstraction by a methyl radical through reaction 4.4 has a relatively large negative sensitivity coefficient to ethane formation. Indeed, this reaction consumes methyl radical (main path to ethane formation) and reforms methane and actively reduces the conversion rate.

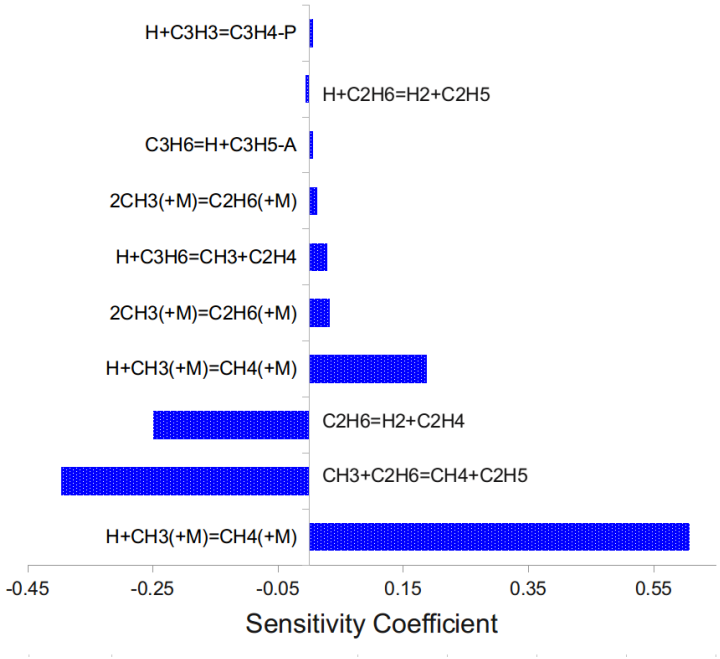

Figure 4.2: *Sensitivity analysis of* C_2H_6 *during methane pyrolysis in* $P = 1[atm]$, $T = 1273[K]$, *and* $31\%CH_4/He$.

Theoretically and experimentally calculated rate constants for 4.4 H-abstraction are compared in Figure 4.3. The available rate constants at lower temperatures are old, and as can be seen the most discrepancy between different rates is observed in this region. Recent experimental evaluation of Peukert et al. [104] shows that the values reported by Moller et al. [105] at high temperatures are a factor of ~ 4 higher. Baulch et al. (1992) [106] evaluation of existing data suggested values pretty similar to Tsang and Hampson [85], but in the newer evaluation of Baulch et al. (2005) [107] more statistical weight was given to Moller et al. [105] data resulting in a larger deviation. Referring to Peukert et al. [104] over the temperature range of $1153 - 1297\ K$ experimental rate constant can be described by $3.26 \times 10^{12} exp(-6043/T)\ [cm^3 mole^{-1} s^{-1}]$. However, their theoretical calculated rate has a discrepancy about $\pm 20\%$ of the measured values.

On the contrary rate constants used by Aramco mechanism [51] and Polimi1412 [30] are two stand-alone rates. The rate constant of Aramco is relatively high in the low temperatures whereas Polimi1412 is lower at higher temperatures compared to Peukert et al. [104]. In order to show the importance of this reaction in combustion, a set of experiments with high sensitivity to this reaction were selected from literature and modelling carried out by replacing different rate constants; Aramco [51], Polimi [30], Peukert 2013 experimental and theoretical evaluation [104] into the scheme.

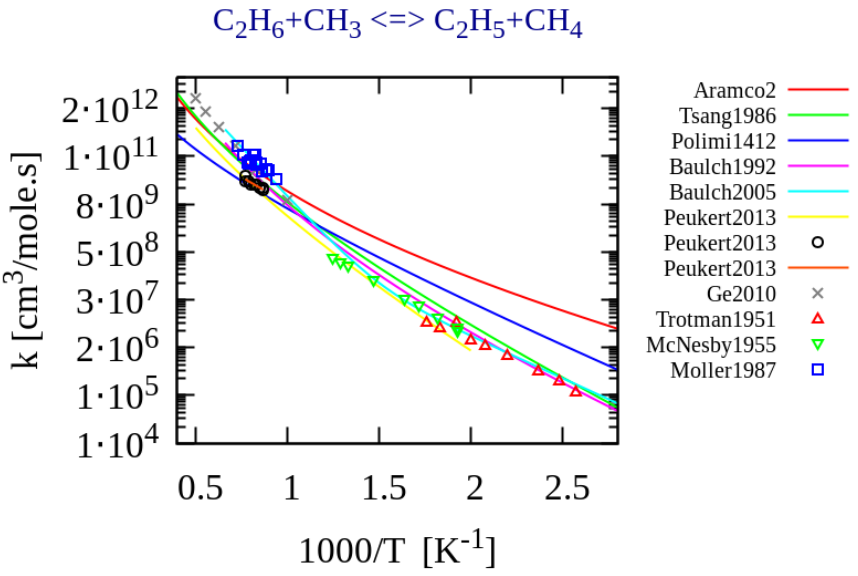

Figure 4.3: *Comparison of experimental and theoretical rate constants for the reaction of* $C_2H_6 + CH_3 = C_2H_5 + CH_4$.

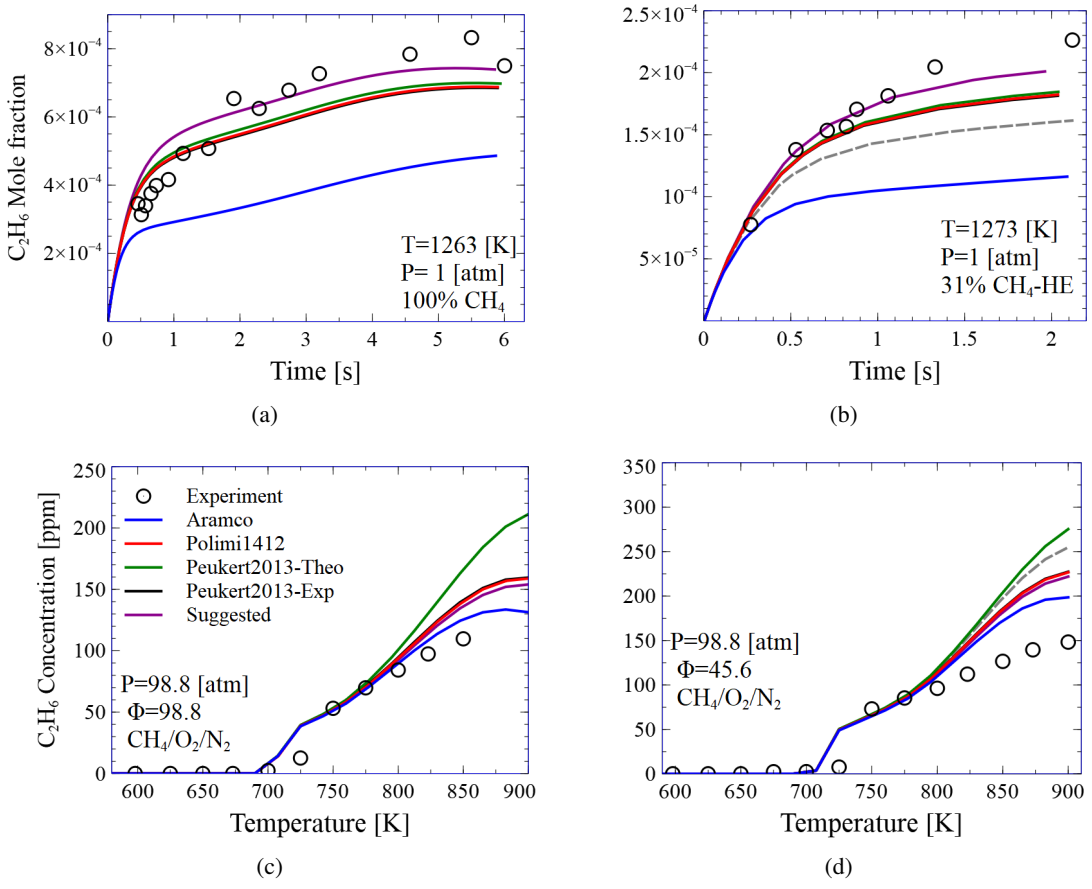

Figure 4.4: *Evaluation of the mechanism prediction with different rate constants for the reaction of* $C_2H_6 + CH_3 = C_2H_5 + CH_4$.

Figure 4.4 resembles the prediction of the kinetic scheme with only replacing different rate constants for the reaction 4.4. These experimental data present ethane formation during methane pyrolysis and also partial oxidation. Figure 4.4 (a) and (b) show ethane time-dependent profiles at temperatures 1263 and $1273K$. As can be seen from Figure 4.3 the rate constant of Aramco [51] has a higher H-abstraction rate leading to under-prediction of ethane. Though, the rest of the rate constants predict a higher amount of ethane. The lower panel of this figure presents the ethane profile in high pressure and low-temperature methane oxidation. Peukert et al. [104] theoretical rate considerably over predicts the experimental data, while the Aramco rate fairly models ethane profiles.

To sum up this reaction, none of the available rates was capable of reproducing experimental data; accordingly. Qualitative observation of these figures proves that the rate parameters of this reaction require further critical evaluation. The critical evaluation can help us to understand that the source of error is from rate parameters or rather than that the experimental uncertainty in the measurement.

Figure 4.5 shows a simplified pyrolysis pathway analysis of methane, highlighting the key reaction steps. As can be seen, another critical reaction is ethyl radical (C_2H_5) decomposition, owing to relatively weak bond energies and it rapidly decomposes to a stable molecule (C_2H_4) and a H atom. The rate expression for this reaction adapted from the theoretical evaluation of Miller and Klippenstein [108].

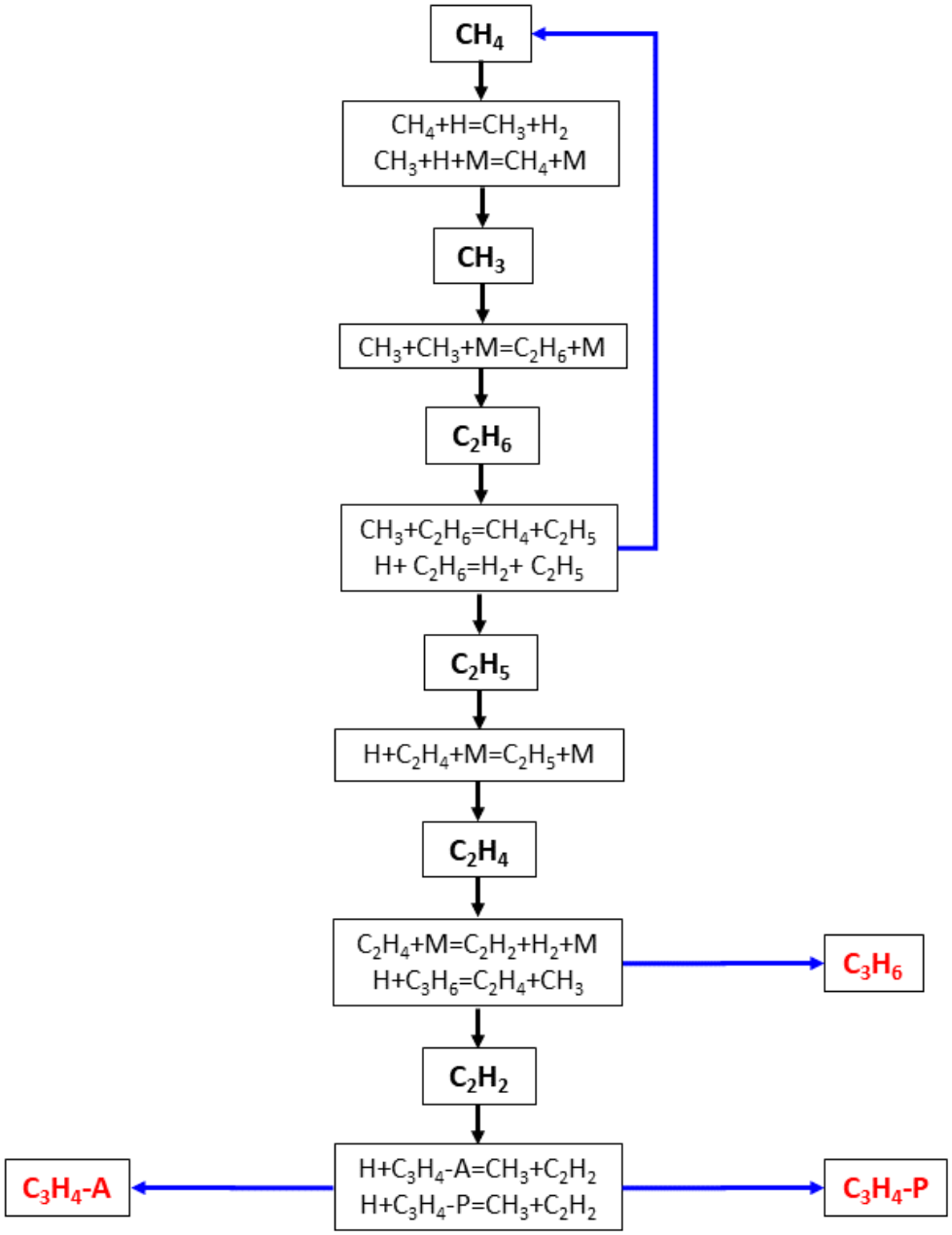

Figure 4.5: *Methane pyrolysis pathway, highlighting the key reaction steps based on the rate of production analysis.*

4.3 Oxidation pathway

The reaction of methyl radical and oxygen is important in the prediction of methane ignition delay times. This reaction leads to three main channels as:

$$\begin{aligned} CH_3 + O_2(+M) &= CH_3O_2(+M) \\ &= CH_3O + O \\ &= CH_2O + OH \end{aligned} \tag{4.5}$$

Zhu and Lin [109] discussed that the association reaction occurs at intermediate to low temperatures and its rate is enhanced at elevated pressures. Furthermore, the other two reaction channels become competitive with stabilization of the hot peroxy radical as the temperature increases. At these conditions, methane is a relatively unreactive fuel due to the presence of strong aliphatic bonds; therefore, the stabilization reaction is necessary for defining the autoignition.

The pressure-dependent expression of methyl proxy channel was adopted from Fernandes and Luther [110], where they studied this reaction in a high-pressure between 2 and $1000\,bar$ and at temperatures of $300 - 700\,K$. The other two channels of methyl radical and molecular oxygen reaction have been the cause of some controversy, which directed to recent investigations [111–114]. This discussion and earlier work are well documented by Metcalfe et al. [51] and will not be discussed in detail here. In current work, the rate constants adopted for $CH_3O + O$ channel is from Srinivasan et al. [114], and for reaction $CH_2O + OH$ from Klippenstein presented in [51]. A thorough discussion supporting the choice of these rate constants is presented in [115]. There is some uncertainty as to whether reactions $CH_3O + O$ and $CH_2O + OH$ are pressure dependent under most combustion conditions ($\leq 100atm$) [51].

From this, we can conclude that the rate constants of three main channels of methyl and oxygen reaction 4.5 have been implemented from different investigations, which can make this reaction even more uncertain. In fact, the branching ratio between various channels plays a significant role in the transition from low to intermediate temperature chemistry. This circumstance can be justified through the following discussion.

The correct prediction of the temperature where the conversion starts is essential for the mechanism. The reaction 4.6 plays a vital role in the methane conversion at lean conditions. Table 4.4 presents the rate constants for this reaction from literature and also a modified rate.

$$O_2 + CH_3 = CH_2O + OH \tag{4.6}$$

Figure 4.6 shows an Arrhenius plot for reaction 4.6, comparing the modified rate constant with other values. The rate constants are plotted from Srinivasan et al. 2005 [114] (green line), Aramco Mech [51] (red line), and modified rate (Modified). As can be seen from this figure, there is a substantial deviation between the rate calculated by [114] and the rate suggested by Klippenstein in [51] especially at the lower temperatures. The modified rate is used for the sake of uncertainty analysis.

A set of experimental data of ultra-lean methane oxidation with high sensitivity to reaction 4.6 was chosen to examine the effect of this reaction. In the kinetic scheme, this single reaction was substituted with different rates presented in Table 4.4 and the

Table 4.4: *Rate constants of the reaction 4.6 in* $cm^3/mol.s$

Reaction	A	n	Ea	Reference
R(1)	1.87E+11	0.00	9842	[114]
R(2)	2.611E+00	3.283	8105	[51]
R(3)	1.611E+00	3.283	8105	[51] reduced by $\sim 40\%$

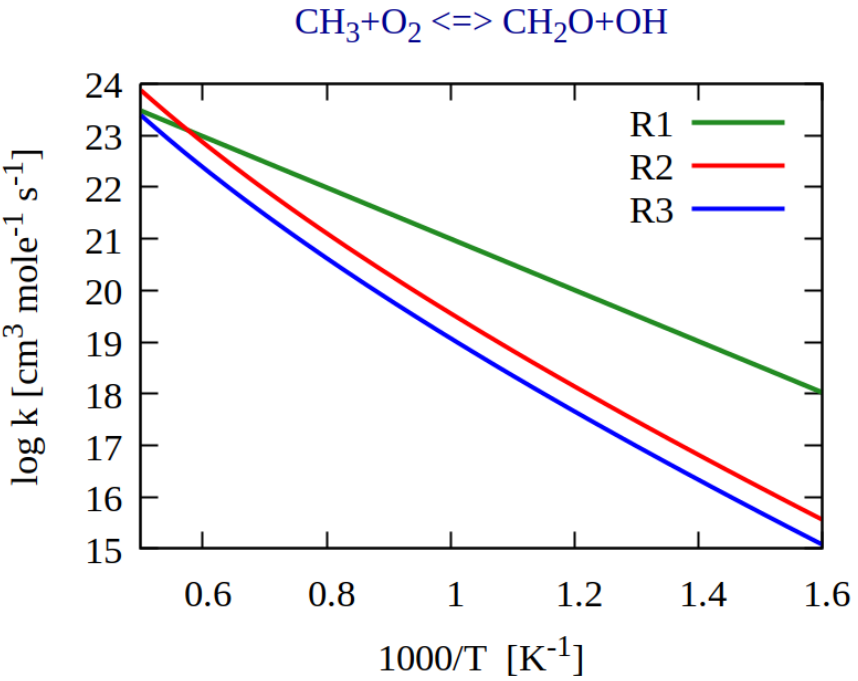

Figure 4.6: *Arrhenius plot comparison of presented reaction rates in Table 4.4.*

results are plotted in Figure 4.7. It is evident that the prediction with the modified rate constant is in a satisfactory agreement with the experimental results. Moreover, while the rate suggested by [51] can fairly capture the trend but $20\ K$ earlier, the rate of [114] is too reactive, and the result is inappropriate. It can be concluded that the uncertainty of reaction 4.6 is likely to be more than 40% (as a 40% reduction is needed to capture the experimental data). Although, the modified rate improves the kinetic scheme prediction, it results in a discrepancy of ignition delay time [5] in other conditions. Thus, the rate suggested by [51] is implemented in this study.

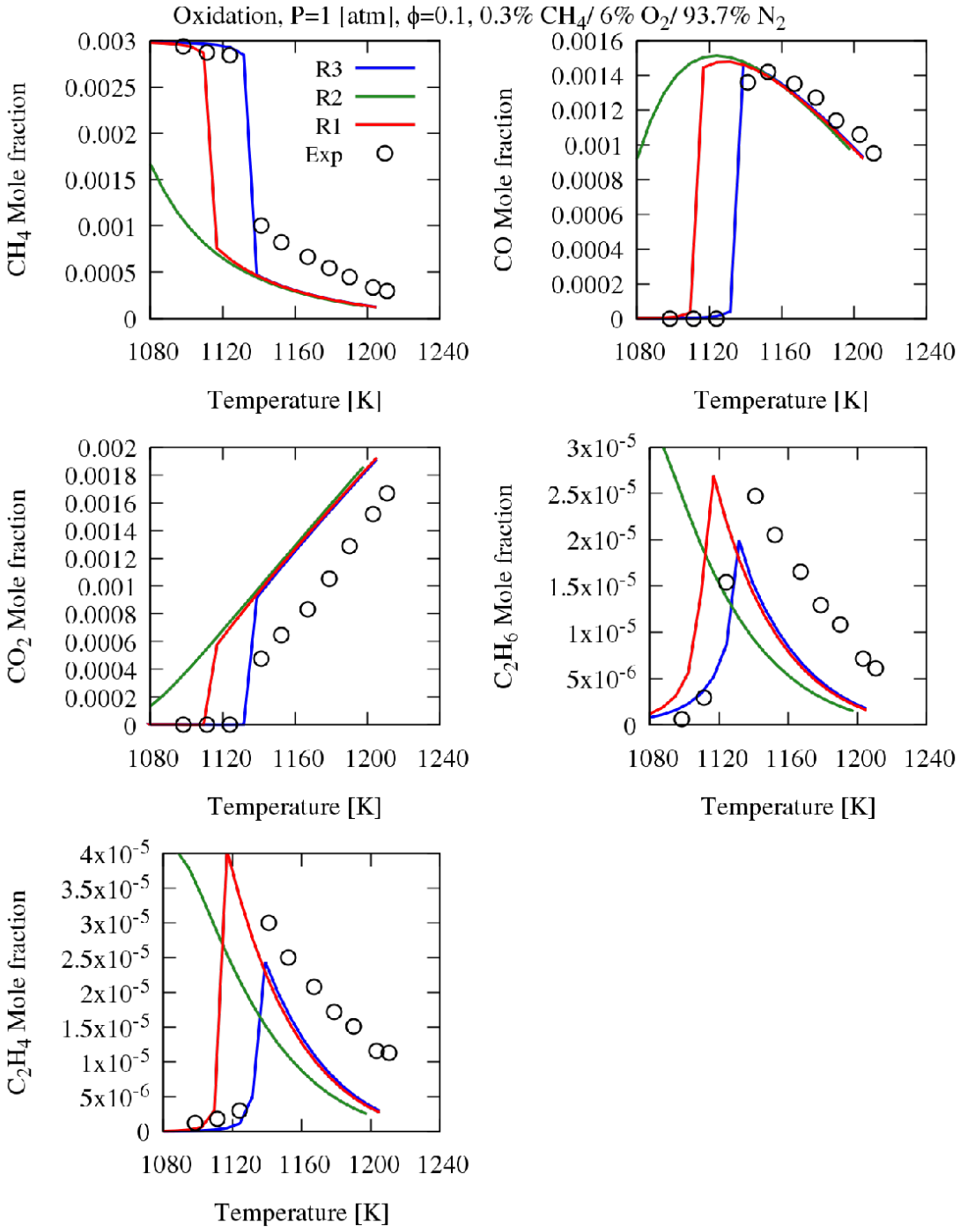

Figure 4.7: *Comparison of different rate constants for R5 in the atmospheric Jet-stirred reactor of methane oxidation. Exp refers to [32].*

4.4 H-Abstraction

The development of detailed kinetic mechanisms requires not only the knowledge of the multiple reaction pathways but also the assignment of consistent rate constants for these pathways. The good news is that the vast majority of radical reactions in combustion systems belong to only a limited number of reaction classes [116]. Moreover, most of the rate constant within a given reaction class can be pretty well-approximated by implementing rate rules. Through a systematic electronic structure calculation for smaller members of a reaction class, the rules can be developed that may then be employed to the class including the larger members that calculation might be time-consuming.

It is known that the rate constants for a specific reactions class are correlated with the reaction thermodynamics [117]. Based on the Transition State Theory (TST), it is feasible to estimate rate constants for a reaction within a particular reaction class on the basis of the known information about other reactions associated with that class [70]. For instance, if in a reaction class, the transition states are similar, one can expect that the pre-exponential factors of the rate constants are similar due to the similar entropy change between the reactants and transition states [116].

The potential to generate consistent reaction class rate rules relies on the assumption that inside the same reaction class, the geometries and energetics of the transition states are supposed to be similar, leading to similar rate coefficients. One example that represents where this assumption is relevant is shown in Figure 4.8. Carstensen and Dean [118] explained that the calculated rate coefficients for H-atom abstraction from alkanes group very tightly for the three types of abstractions (generating primary, secondary, and tertiary radicals).

As can be seen from Figure 4.8, the near convergence of the plots at high temperatures, indicating that all of these reactions have a similar pre-exponential factor or similar entropies of activation. The deviations in the calculated rate constants at lower temperatures indicate the different enthalpies associated with breaking the various bond types, thereby leading to different activation energies. Thus, the overall rate constant for a H-atom abstraction from an alkane can be assigned by simply counting the number of primary, secondary, and tertiary $-H$ bonds and multiplying those numbers by the appropriate rate rule for that particular bond type.

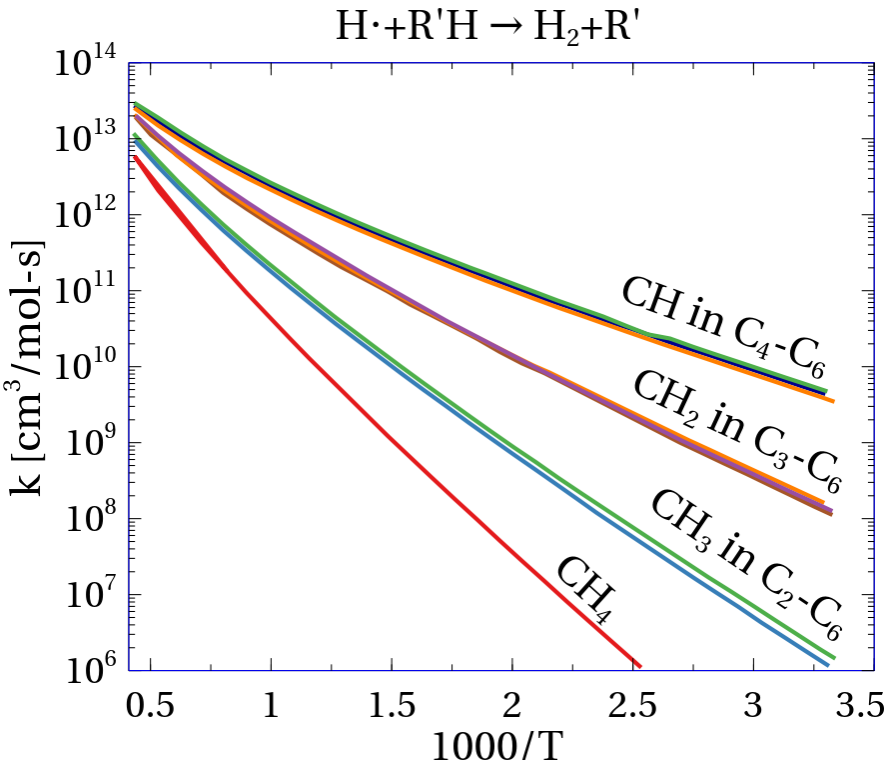

Figure 4.8: *Predicted rate constant for H-abstraction from alkanes grouped by the type of $C-H$ bond that is broken.*

Various investigators have used TST approaches to demonstrate the feasibility of assigning rate rules. For example, Sumathi et al. [119–121] showed that the rate constants predicted by group additivity for H-abstraction reactions by H and CH; are typically within about a factor of 2 for all the reactions inside an identical reaction family. Similar studies by Saeys et al. [122, 123] and Sabbe et al. [124–126] determined rate rules for a variety of H-abstraction and radical addition reactions. In general, the resulting rate rules were found to agree fairly well with accessible experimental data [116].

4.4.1 H-Abstraction Reactions

The rate coefficients for the generic H-abstraction reactions according to the approach proposed by Ranzi et al. [84] can be formulated as:

$$R\cdot + R'H \rightarrow RH + R'\cdot \tag{4.7}$$

This rate rule defined based on the group contribution method of Benson et al. [70]. The rate constant for the forward reaction is only a function of the abstracting radical and the type of hydrogen abstracted in the molecule. Thus, It is acceptable to write the rate constant as

$$k_f = {k^\circ}_{ref,R\cdot} C_{R'H} \tag{4.8}$$

Where ${k^\circ}_{ref,R\cdot}$ is the reference rate parameter describing the reactivity of $R\cdot$ radical , and $C_{R'H}$ describes the reactivity of the transferred H-atom. Both of the terms can be expressed in the Arrhenius form, thus, the 4.8 can be rewritten as

$$k_f = \left({A^\circ}_{ref,R\cdot} T^{n^\circ} exp\left(\frac{{E^\circ}_{ref,R\cdot}}{RT}\right)\right)\left(A_C exp\left(\frac{E_C}{RT}\right)\right) \tag{4.9}$$

moreover, by combining the two Arrhenius expressions, the following equation can be obtained for forward rate constants.

$$k_f = \left({A^\circ}_{ref,R\cdot} A_C\right) T^{n^\circ}\left(exp\left(\frac{{E^\circ}_{ref,R\cdot} + E_C}{RT}\right)\right) \tag{4.10}$$

The equation 4.10 explicitly expresses the correction factor of the frequency factor (A_C) and activation energy (E_C) which directly depends on the H-atom being abstracted.

Based on this formulation, the values presented in Table 4.5 for H-abstraction reactions provide guidance to the determination of the rate values. It is worth mentioning that the values provided as reference rates correspond to the secondary H-abstractions (see Figure 4.8). Since the secondary H-abstractions rate locates in between primary and secondary H-abstraction, a smaller correction for dissociation energies will be therefore required. As an example, a methyl radical (CH_3) removing a primary H-atom according to the reaction 4.4 $CH_3 + C_2H_6 = CH_4 + C_2H_5$ the reference rate constant, on a per H-atom basis, is $3.00E+04\, T^2\, exp(5000/RT)$.

Table 4.6 oulines the bond dissociation energy corrections ($C_{R'H}$) for various type of abstractions, highlighting the different bond strengths of primary, secondary and tertiary $C-H$ bonds. It explicates that comparing to the secondary bond, breaking a primary $C-H$ bond requires about $2.8\, kcal/mol$ more energy while tertiary $C-H$ bonds are respectively 1.4 kcal/mol weaker. Moreover, The same activation energy correction for the type of H-atom is implemented for any abstracting radical. Now we go back to the example proposed in the previous paragraph by considering corrections of Table 4.6. As CH_3 radical abstracts the primary type of a H-atom from C_2H_6, the corrected parameters for the reference parameters is

$$(3.00E+04\times 1)T^2 \exp(\frac{5000+2800}{RT}) \tag{4.11}$$

H-abstraction reactions are chain propagation reactions. In principle, a radical can abstract an H-atom from a stable molecule forming another stable molecule and another radical, thus propagating the reactivity. Accurate H-abstraction rate parameters are critical in combustion modelling. Values for H-abstraction reactions in the current mechanism have been extracted from. In the absence of data from Aramco.2, rate rule parameters described in this section have been adapted. Indeed, the rate rule approach is more useful for the higher molecules. It is implemented because the C_0-C_3 mechanism is not only a natural gas reaction mechanism but also a core mechanism for heavier fuel sub-mechanisms in CRECK mechanism. Including H-abstraction rate rule will facilitate linking this core mechanism to other sub-mechanisms.

Table 4.5: *Reference kinetic parameters ($k^{\circ}{}_{ref,R\cdot}$) for the H-abstraction reactions used for the Rate Rules.*

$R\cdot$	RH	$A^{\circ}{}_{ref,R\cdot}$	n°	$E^{\circ}{}_{ref,R\cdot}[cal/mol]$
H	H_2	3.00E+06	2	4000
CH_3	CH_4	3.00E+04	2	5000
C_2H_3	C_2H_4	6.78E+04	2	3900
C_2H_5	C_2H_6	2.30E+04	2	7000
NC_3H_7	C_3H_8	1.35E+04	2	6700
IC_3H_7	C_3H_8	1.35E+04	2	9900
C_3H_5-S	C_3H_6	2.70E+04	2	4500
C_3H_5-T	C_3H_6	2.70E+04	2	4500
C_3H_5-A	C_3H_6	5.39E+04	2	12800
C_4H_5	C_4H_6	2.70E+04	2	4500
C_4H_71-4	$C4H8-1$	1.35E+04	2	6600
C_4H_71-3	C_4H_8-2	3.40E+04	2	13700
IC_4H_7	IC_4H_8	2.70E+04	2	13700
C_4H_3	C_4H_4	4.09E+04	2	5200
C_6H_5	C_6H_6	3.70E+07	1	2000
O	OH	2.35E+06	2	2500
O_2	HO_2	1.70E+06	2	44000
OH	H_2O	1.50E+09	1	50
HO_2	H_2O_2	8.00E+05	2	11000
CH_3O	CH_3OH	4.28E+04	2	1500
CH_2OH	CH_3OH	2.83E+04	2	10400
HCO	CH_2O	1.26E+05	2	12300
CH_3CO	CH_3CHO	1.35E+05	2	14000
CH_2CHO	CH_3CHO	2.30E+04	2	11500
C_3H_3	C_3H_4-A	2.70E+04	2	14000
$HCCO$	CH_2CO	4.28E+04	2	5200

Table 4.6: *Correction factors of bond dissociation energies $C_{R'H}$ in different abstraction type of $C-H$.*

Type of Abstraction	A_C	$E_C[cal/mol]$	Description
Type 1	1	2800	Primary H-abstraction
Type 2	1	0	Secondary H-abstraction
Type 3	1	-1400	Tertiary H-abstraction
Type 4	7	4150	H of H_2
Type 5	1.75	6800	H of CH_4
Type 6	5	12600	H of H_2O
Type 7	0.4	-4850	H of H_2O_2
Type 8	4	-1700	Acylic
Type 9	0.5	1800	H in OH of Alcohol

4.5 Summary

This Chapter critically reviewed different reaction pathways, H-abstraction reaction classes and the reference kinetic parameters used to model pyrolysis and combustion. The aim of this Section is not to discuss the reaction rate adopted in the kinetic but to review the controversy in some critical reactions of pyrolysis and oxidation channels. These reactions are chosen by emphasising their role in unconventional combustion systems.

The rate parameters of the reactions discussed in this section are fairly acceptable for conventional flame modelling; however, moving to unconventional conditions (high dilution level, distributed ignition, low-temperature oxidation), better rate parameters are required. An important implication of these findings is that the critical reactions in unconventional conditions differ from the traditional flame; hence, a systematic evaluation aimed at reducing the uncertainty or advising parameters from more accurate calculations or measurements is of prominent concern for new combustion technologies. This necessity frames one of the outcomes of this work and motivates the discussion carried out in Chapter 4, 6 and 7.

Moreover, it has to be stressed that the values for H-abstraction reactions in the current mechanism have been extracted when possible from literature. In the absence of data from lierature, rate rule parameters described in this section have been adapted. Indeed, the rate rule approach is more useful for the higher molecules. It is implemented because the $C_0 - C_3$ mechanism is not only a natural gas reaction mechanism but also a core mechanism for heavier fuel sub-mechanisms in CRECK mechanism. Including H-abstraction rate rule will facilitate linking this core mechanism to other sub-mechanisms.

CHAPTER 5

Experimental Database and Validation

CRAFTING kinetic reaction mechanisms for combustion strongly rely on experimental data over a wide range of operating conditions. It is well confirmed that combustion is a complex process, due to the underlying chemical and physical phenomena. Therefore, to more precisely assess kinetic mechanisms, it is necessary to design and implement experiments with minimised physical processes. In this context, ideal reactors such as PFR, JSR, and Shock tube play crucial roles. These experiments performed under controlled operating conditions; thus, kinetic mechanisms can be validated and improved through extensive comparison of modelling predictions and experimental data. In this chapter, the experimental database collected in this study for mechanism assessment and numerical tools used for model prediction and analysis are presented.

The methodology implemented for systematic comparison and mechanism development is outlined in Figure 5.1. Three main working areas of this study including data collection, mechanism development, and model prediction are highlighted. This figure also depicts the workflow and how different parts of the research are connected. These sections are discussed in detail in the following paragraphs of this chapter.

5.1 Experimental Database

A wide range of experimental data obtained from several different techniques and conditions can be used to check the data consistency and constrain kinetic mechanisms. These experimental data can be commonly classified as global and detailed.

- Global data contain ignition delay time and laminar flame speed.

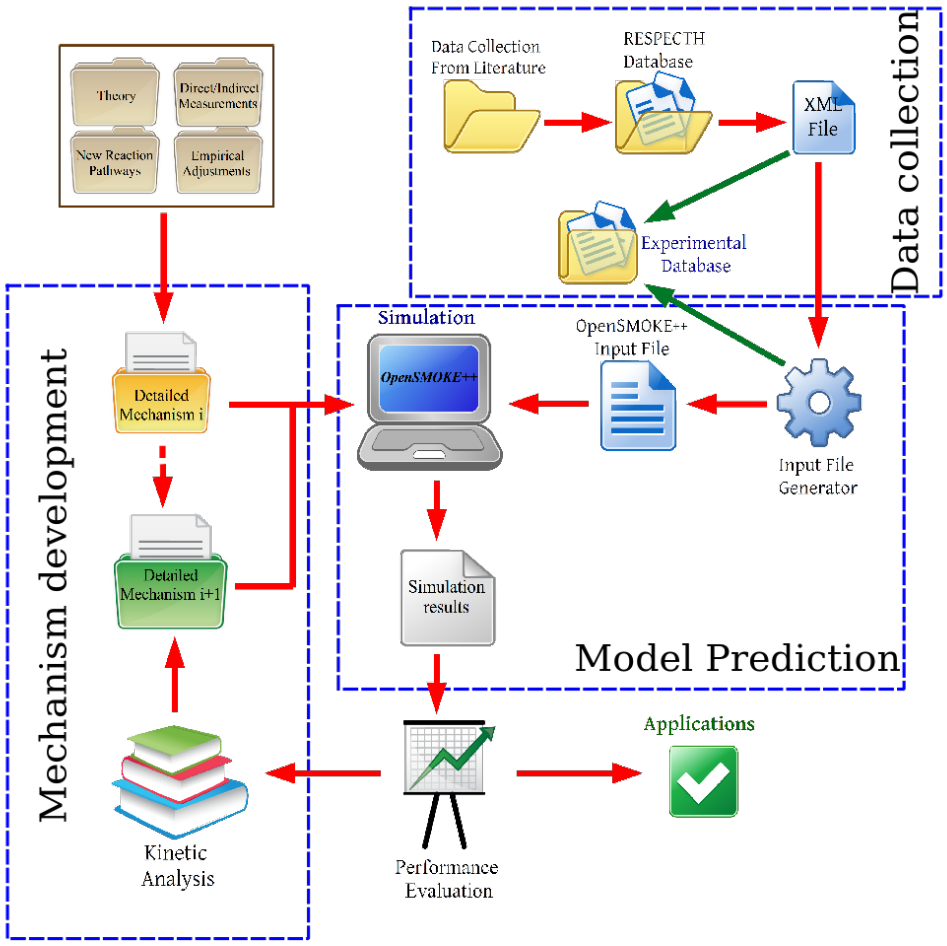

Figure 5.1: *General methodology implemented for mechanism development.*

- Detailed data include concentration profile of stable and unstable chemical species.

In global data, ignition delay times can be obtained using shock tubes, rapid compression machines or plug flow reactors. Ignition times are remarkably important for probing initiation and termination reactions as well as the reaction of radicals with molecular oxygen. In contrast, global experiments are less useful for probing atoms and radicals propagation reactions. General forms of these reactions can be expressed as:

$$Initiation\ reactions \quad \begin{cases} RH(+M) \leftrightharpoons R + H(+M) \\ RH(+M) \leftrightharpoons R' + R"(+M) \\ RH + O_2 \leftrightharpoons R + HO_2 \end{cases}$$

$$Termination\ reactions \quad \begin{cases} R + H(+M) \leftrightharpoons RH(+M) \\ R' + R"(+M) \leftrightharpoons RH(+M) \end{cases}$$

Flame speeds or burning velocities can be determined using various experimental

facilities such as Bunsen burners, spherical flames in the combustion bomb, stagnation flow flames, heat flux burners and counterflow flames. Flame speeds are extremely useful for probing H-atom reactions, for example, the main chain branching reaction.

As far as detailed data concerned, mostly stable and unstable species profiles are acquired from several reactors together with sampling methods and analytical techniques. For this purpose, the gas sampling performed using the appropriate type of probes or traps, and after that analytical techniques are used to analyse compositions.

The most popular experimental facilities currently used are shock tubes, flow reactors (JSR and PFR) and burner stabilised flames (premix flames and opposed flames). Combining the data of these experimental facilities are valuable since they can cover a broader range of operating conditions (pressure, temperature, residence time, equivalence ratio and concentration) providing complex information of the conventional combustion systems (internal combustion engines, gas turbines and burners).

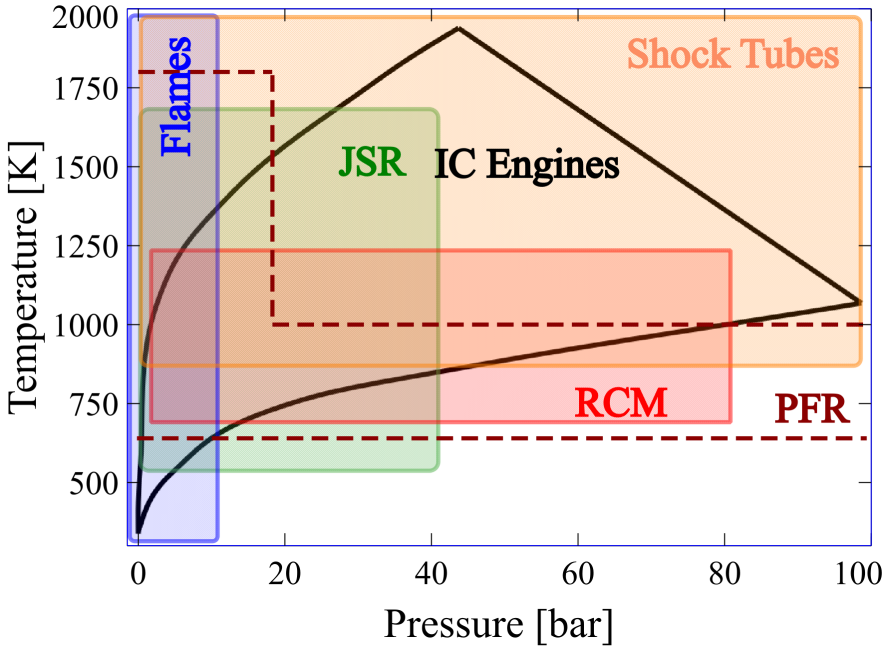

Figure 5.2: *Layout comparison of engines conditions and achievable operating conditions in various experimental facilities.*

Thus, to better illustrate the complexity of the combustion systems, Figure 5.2 outlines the entire range of pressures and temperatures pertinent to internal combustion engines and gas turbines. It is obvious that by combining an extensive range of experimental facilities one can obtain detailed data over the entire operating condition. An important implication of this figure is that individual experimental facilities have a limited operating range. Therefore, a wide range of experimental data target is of great interest for comprehensive validate predictability of the detailed kinetic mechanism.

In order to establish the database, a comprehensive range of experimental data for pyrolysis, oxidation and combustion has been collected. This database covers a wide range of pressures, temperatures, and equivalence ratios. More than $\sim$ 200 different experiments containing more than $\sim$ 6000 data points were collected from literature for various canonical reactors and 1-D flames. As examples, Tables 5.1 and 5.2 list the

range of experimental data collected for oxidation of methane (CH_4) in JSR and PFR.

The predictive power of the detailed kinetic mechanism is examined against not only experimental data of methane, but also database collected for C_2 species including ethane, ethylene and acetylene. Validation of C_2 species can be used to investigate various combustion characteristics of natural gas. It is noteworthy to mention that a full set of experimental database and model prediction are outlined in the Appendix.

Table 5.1: *List of collect experimental data in jet stirred reactors.*

Fuel	Φ	P [atm]	τ [s]	T [K]	Ref
1%CH_4	0.1-1.5	1	0.12	1000-1450	[127]
1%CH_4+20%CO_2	0.1-1.5	1	0.12	1000-1450	[127]
0.8%CH_4+0.8%H_2	0.1-1.5	1	0.12	925-1400	[127]
0.9%CH_4+0.4%H_2	0.3-1	1	0.12	950-1277	[127]
0.8%CH_4+0.8%H_2+20%CO_2	0.1-1.5	1	0.12	926-1450	[127]
0.8%CH_4+0.4%H_2+0.4%CO	0.1-1.5	1	0.12	950-1400	[127, 128]
1%CH_4+10%H_2O	0.1-1.5	1	0.15	1026-1452	[129]
1%CH_4	0.1-1.5	10	0.25	902-1300	[127, 128]
0.8%CH_4+0.8%H_2	0.1-1.5	10	0.25	900-1251	[128]
0.8%CH_4+0.8%H_2+20%CO_2	0.1-1.5	10	0.25	900-1200	[128]
CH_4+H_2 (H_2=0-2%)	0.3	1	0.12	1025-1050	[130]
CH_4+H_2+20%CO_2 (H_2=0-2%)	0.3	1	0.12	1025-1050	[130]
CH_4+H_2 (H_2=0-2%)	0.3	10	0.25	1025-1050	[130]
CH_4+H_2+20%CO_2 (H_2=0-2%)	0.3	10	0.25	1025-1050	[130]
0.3%CH_4+0.03%C_2H_6	0.75	1	0.14	1170-1230	[131]
0.727%CH_4+0.0727%C_2H_6	1-1.5	10	0.14	1100-1500	[131]
3%CH_4	0.1	1	0.1	1100-1200	[31]
3%CH_4	0.5-1	10	0.15	930-1200	[31]
0.9132%CH_4+0.0868%C_2H_6	0.3-1	10	0.25	900-1200	[132]
0.5479%CH_4+0.0521%C_2H_6+0.4%H_2	0.3-1	10	0.25	900-1200	[132]
0.5479%CH_4+0.0521%C_2H_6+1.75%H_2	0.3-1	10	0.25	900-1200	[132]
CH_4+90%N2	0.5-1.5	1.1	0.5	1000-1250	[133, 134]
CH_4+90%CO_2	0.5-1.5	1.1	0.5	1000-1250	[133, 134]
CH_4+40.5%H_2O+49.5%N2	0.5-1.5	1.1	0.5	1000-1250	[133, 134]

Table 5.2: *List of collect experimental data in plug flow reactors.*

Fuel	Φ	P [atm]	τ [s]	T [K]	Ref
$1\%CH_4$+$0.35\%H_2O$	3.3	1.1	0.25	1050-1850	[135]
$1\%CH_4$+$2.5\%H_2O$	3.3	1.1	0.25	1050-1850	[135]
$1\%CH_4$+$4.8\%H_2O$	3.3	1.1	0.25	1050-1850	[135]
$1\%CH_4$+$6.9\%H_2O$	3.3	1.1	0.25	1050-1850	[135]
$1\%CH_4$+$9.3\%H_2O$	3.3	1.1	0.25	1050-1850	[135]
$7.14\%CH_4$	2	6	4.5-8.4	532-922	[136]
$4.63\%CH_4$	98.8	100	12070/T	598-900	[72]
$4.42\%CH_4$	45.6	100	11690/T	598-900	[72]
$1.12\%CH_4$	25.2	90	10450/T	598-900	[72]
$4.66\%CH_4$	95.5	50	5870/T	598-900	[72]
$0.159\%CH_4$	1.09	100	11870/T	673-900	[72]
$0.149\%CH_4$	1.03	90	10430/T	598-900	[72]
$0.0964\%CH_4$	0.042	100	12020/T	648-900	[72]
$0.0993\%CH_4$	0.04	90	10740/T	598-900	[72]
$0.0963\%CH_4$	0.042	50	6030/T	648-900	[72]

5.2 Numerical methodologies

The detailed kinetic mechanisms including rate constants, thermodynamic and transport properties are used by numerical models to simulate practical devices. The commonly used numerical codes to simulate chemically reacting systems include *CHEMKIN* suit [61], *OPENSMOKE++* [137], *Cantera* [138] and *FlameMaster* [139].

OPENSMOKE++ [137] is a framework conceived to perform numerical modelling of combustion employing large kinetic mechanisms. In order to preprocess a kinetic scheme, the *OPENSMOKE++* Suite provides a *CHEMKIN* preprocessor utility. The user has to supply the files containing the thermodynamic data, the kinetic mechanism, and (optionally) the transport data. For the simulation of ideal reactors, usually the transport data are not needed and therefore the user could choose to preprocess only the thermodynamic and the kinetic data. This framework can handle simulation of ideal reactors (Batch reactor, JSR and PFR), rapid compression machines, shock tubes and 1-D flames Premixed laminar flame, diffusion opposed flame. *OPENSMOKE++* also provides numerical tools useful for analysis and interpret modelling results from a kinetic point of view, which are briefly reported in the next paragraphs. However, the full detail of the equations and implemented solvers can be found in [137].

5.2.1 Sensitivity Analysis

Sensitivity analysis is very important for kinetic studies in order to quantitatively determine the important reactions controlling reactivity under specific operating condition. For this purpose *OPENSMOKE++* provides first-order sensitivity coefficient concerning reaction rate constants such as pre-exponential factor or activation energy. The sensitivity coefficient exploits the quantitative understanding of the contribution of individual reactions to how governing equations depends on the various parameters in-

troduced inside the model. The equation for the first order sensitivity coefficients can be defined as:

$$S_{ij} = \frac{\partial y_i}{\partial \alpha_j} \tag{5.1}$$

Where in this equation (5.1), indexes i and j refer to the target variable and the parameters of the model, respectively. In order to make these sensitivity coefficients more valuable for analysis and comparison, they are normalised in the logarithmic derivatives.

$$\tilde{S}_{ij} = \frac{\partial \ln y_i}{\partial \ln \alpha_j} = \frac{y_i}{\alpha_j} S_{ij} \tag{5.2}$$

The sensitivity coefficients can occasionally be more valuable when they are normalised by the maximum value of each dependent variable.

$$\widehat{S}_{ij} = \frac{\alpha_j}{\max y_i} S_{ij} \tag{5.3}$$

This sort of normalisation can be particularly more useful when the independent variable (y_i) is a mass fraction, because of avoiding artificial high sensitivity coefficients where mass fraction approaching zero and affected by numerical errors [137]. If the sensitivity coefficient for a specific species is negative, this means that the reaction directly or indirectly increases the consumption of the target species and vice versa for the positive coefficient.

5.3 Validation of Experimental Data

The kinetic mechanism is validated against all collected experimental data, and these comparisons confirm a good agreement with experimental data. The results presented afterwards in this section are only a small part of the comprehensive validation of the mechanism. However, the full set of these validations is attached as appendix of this thesis.

5.3.1 Ignition Delay Time

Ignition mainly occurs through two different mechanism:

- Induced ignition; this is when an external source ignites the fuel mixture (spark in internal combustion engines).
- Auto-ignition; the fuel mixture spontaneously ignites without an external source of energy (diesel engine).

The induction period before the ignition, known as the ignition delay time characterises the auto-ignition. During this period there is no detectable increase in temperature, pressure or energy release. However, chemical reactions are taking place resulting in the growth of the radical pool [56]. These invisible chemical reactions, pyrolysis reactions, are faster and precede oxidation reactions, mainly for heavier hydrocarbons (fuel fragmentation) [29]. When the radical pool increased to a critical concentration,

reactions of the fuel rapidly increase. This consequently results in a significant heat release and changes in temperature, pressure and concentrations of intermediate species. Thus, auto-ignition can be characterised as the time between heating the mixture to the desired temperature and the onset/maximum rate of rising of temperature/pressure/light emission.

Chemical kinetic mechanisms are mostly verified against ignition delay times; thus, when the mechanism is tested against ignition delay time data it can be then used to predict the ignition conditions of a fuel. There are two experimental facilities commonly used to measure ignition delay times;

- Shock tubes
- Rapid compression machines

These two facilities cover two distinct ranges of operating conditions referring to Figure 5.2. While Shock tube characterises the high-temperature region, rapid compression machine describes intermediate and low temperatures chemistry. It is important to highlight that shock tube simulations are performed as zero-dimensional calculations and begin at the onset of the reflected shock period. Homogeneous, constant volume and adiabatic conditions can reasonably be assumed behind the reflected shock wave. The reflected shock temperature and pressure can, therefore, be used as the initial temperature and pressure, respectively. In *OPENSMOKE++* suit, this simulation can be carried out by using simple batch reactor solver. To have a more effective comparison, the target of simulated ignition delay time (CH, OH, T or P) is defined in order to be consistent with the particular diagnostic used in the experiment being simulated.

In order to show the prediction power of the mechanism, Figures 5.3 and 5.4 present various sets of ignition delay times of methane in different pressures and equivalence ratios. In these Figures, the results are also compared with the results of Aramco.2 mechanism [63]. There is a satisfactory agreement with the experiment, and both the mechanisms practically give the same results.

The experiment of Seery et al. [18], consisting of methane/oxygen/argon mixtures between ~ 1.8 to $\sim 4[atm]$ and $\Phi = 0.2 - 5$, and Petersen et al. [140] consisting of methane/oxygen argon at high pressure ($p = 15 - 85[atm]$) and $\phi = 0.4 - 6$ are compared with the mechanism prediction in Figures 5.3 and 5.4, respectively. As reported in the literature [55] and also can be observed here, the ignition delay time diminishes with increasing both pressure and temperature; with a greater sensitivity to the temperature. Moreover, The ignition delay becomes faster for lean mixtures despite that the lean mixtures had higher dilution level compared to rich mixtures.

In order to better understand the characteristics of ignition time, a sensitivity analysis of the ignition delay time of stoichiometric methane at $P = 2atm$ and $1600K$ was carried out (see Figure 5.5). The chain branching reaction R3 is the most sensitive one in reducing ignition delay and promoting the ignition.

$$H + O_2 = O + OH \tag{R3}$$

Any reaction that competes with the main chain branching reaction R3 subtracting H radical inhibits the ignition. Therefore, the excess CH_4 can inhibit the ignition by

promoting R4.

$$H + CH_4 = H_2 + CH3 \tag{R4}$$

As already stated in the literature [141] and also confirmed by Figure 5.5, excess oxygen accelerates the ignition by promoting two chain branching sequences of CH_3 and O_2.

$$O_2 + CH_3 = CH_2O + OH \tag{R5}$$

$$O_2 + CH_3 = CH_3O + O \tag{R6}$$

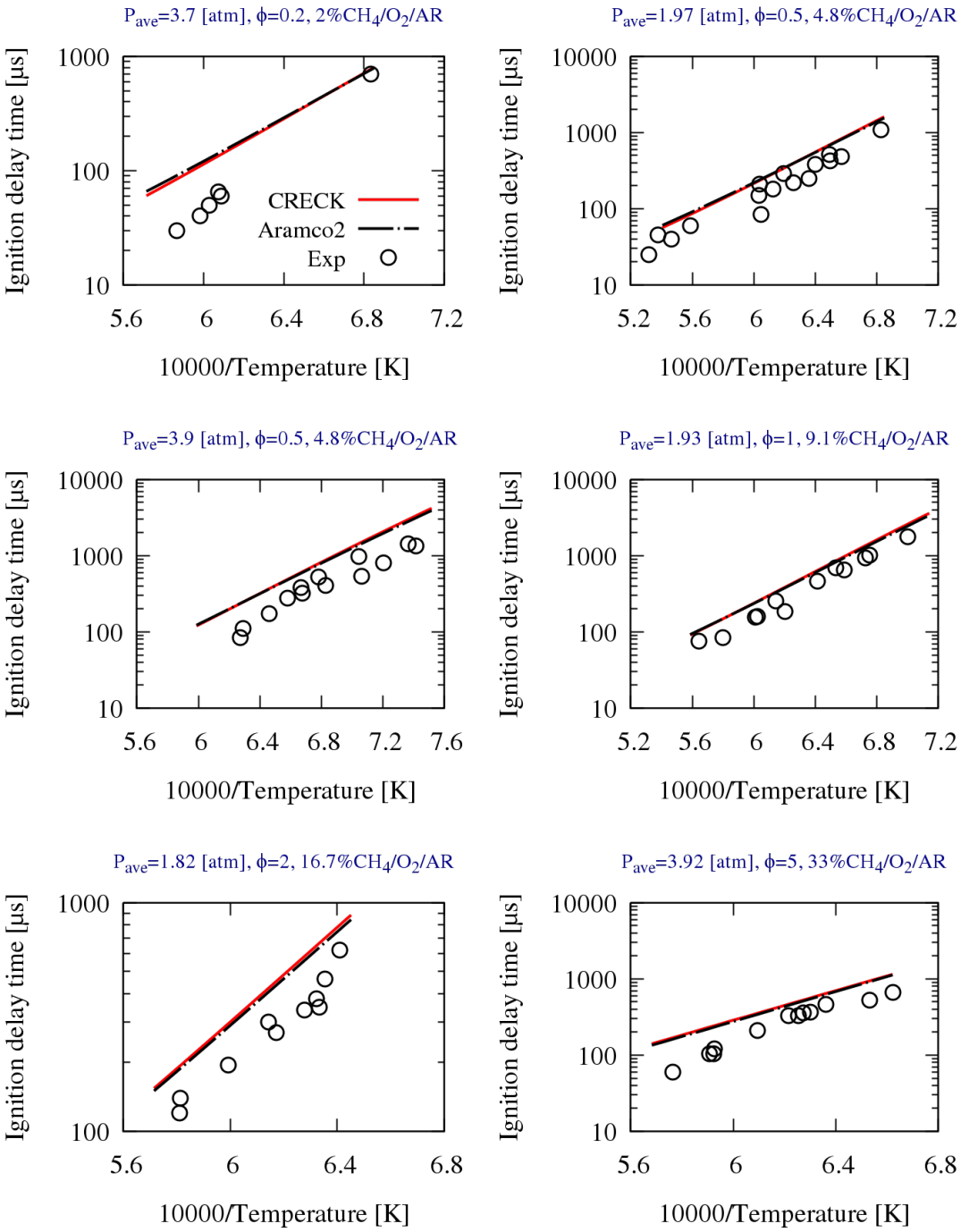

Figure 5.3: *Ignition delay time of methane at various equivalence ratios and pressures* $P = 1.82 - 4[atm]$ *and* $\Phi = 0.2 - 5$. *Exp refers to the experimental data of [18]*

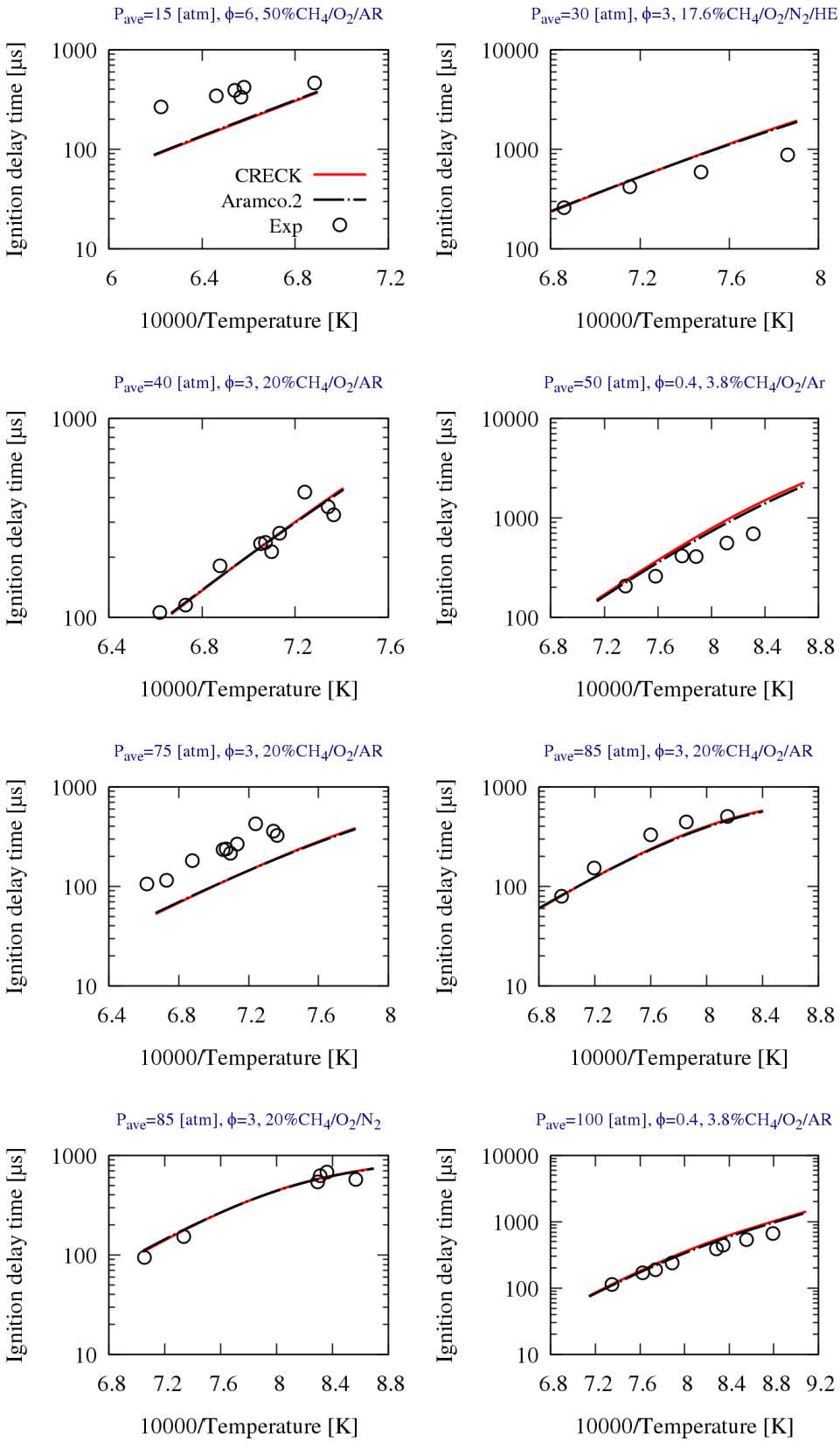

Figure 5.4: *Ignition delay time of methane at various equivalence ratios and pressures* $P = 15 - 85[atm]$ *and* $\Phi = 0.4 - 6$. *Exp refers to [140]*

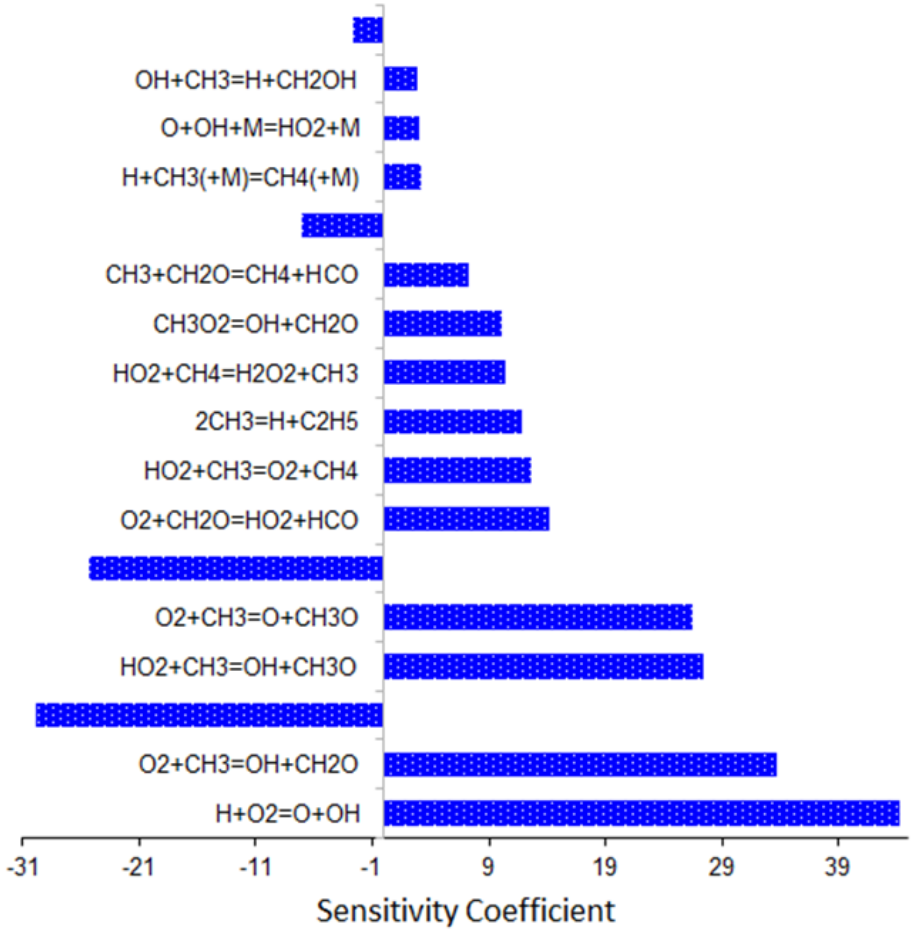

Figure 5.5: *Sensitivity of ignition delay time of methane (shock tube) for stoichiometric mixture at* $P = 2atm$ *and* $T = 1600K$.

5.3.2 Laminar Flame Speed

The flame speed of a fuel is the rate at which the combustion wave will propagate through a gaseous mixture [30]. Flame speed studies provide an insight into the global reactivity of a fuel. For example, in spark engines, the duration of combustion can be determined by flame speed [142]. Several experimental methods can be used to determine the flame speed such as;

- Heat flux method
- Flat flame burner
- Spherical bomb technique
- Counter flow burner

Flame speed simulations are performed in *OPENSMOKE++* by using Premixed laminar flame solver. For this simulation, the code uses an automatic algorithm to check the grid independent and converges to the final solution.

Figure 5.6 shows examples of validation of the laminar flame speed of methane. In this Figure, the results are also compared with one of the newly developed mechanism *Aramco.2* [51]. The predicted laminar flame speeds agree well with the measurements at pressures of 1, 2, 5, 10 and $20atm$. The established mechanism presents a slightly better prediction at higher pressure (due to the improvement in acetylene formation) comparing to *Aramco.2*; however, in the atmospheric pressure both of the mechanism perform similarly.

The set of laminar flame speeds [143, 144] shown in Figure 5.6 have been widely used for the sake of flame speed analysis as well as mechanism development [30,51,55]. Laminar flame speed decreases at elevated pressure, but as discussed by Ranzi et al. [30] laminar burning velocity increases as it is a product of upstream density and laminar flame speed. As reported in the literature [25, 145], R3 is the key chain branching reaction in any hydrogen-containing system. Consequently, any reaction or process consumes H radical and competing with R3 will diminish the overall oxidation rate and therefore inhibit the combustion.

$$H + O_2 = O + OH \qquad \text{(R3 revisited)}$$

For example, the following third-body pressure dependence reactions directly compete with R3. Their rates notably intensify at higher pressures and thereby become dominant and reduce the flame speed. On the contrary, these reactions do not compete effectively with R3 at atmospheric or below atmospheric pressures, so their effect is compensated by temperature rise.

$$H + O_2 + [M] = HO_2 + [M] \qquad \text{(R8)}$$

$$H + CH_3 + [M] = CH_4 + [M] \qquad \text{(R9)}$$

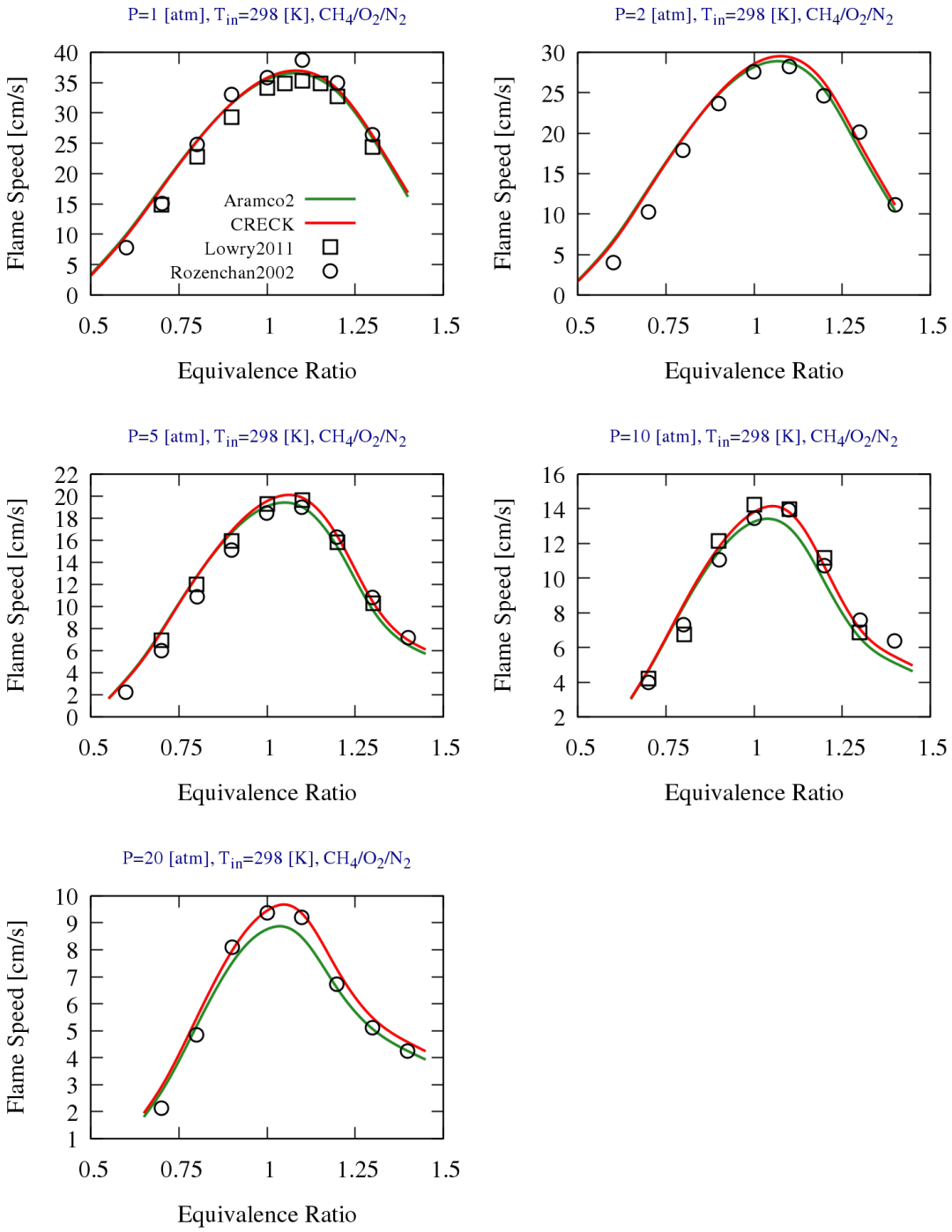

Figure 5.6: *Methane laminar flame speed in various pressures* $(1 - 20atm)$*. Rozenchan2002 refers to [143] and Lowry2011 refers to [144].*

5.3.3 Jet Stirred Reactor

The jet stirred reactor (JSR) is the conventional continuously stirred reactor used for gas-phase kinetics studies. It generally uses nozzles or jets to rapidly mix fuel and oxidizer at a given temperature and pressure. The reactants flow into the reactor at a given flow rate. Species concentration profiles are obtained by probing the outlet gas. Studying the evolution of a species as a function of time or temperature offers an insight into the chemistry occurring inside the reactor under a particular set of conditions (T, p, Φ etc.). This information is essential in the validation of chemical kinetic models.

The transient perfectly stirred reactor solver of *OPENSMOKE++* is used for the simulation of the isothermal and non-isothermal experiments. A proper end times are chosen, wherein these are only arbitrary numbers to run the simulation long enough to reach the steady-state solution (usually 100 times of the residence time in the reactor).

JSR data can be used to identify intermediate products formed during pyrolysis and oxidation.

Figure 5.7 presents an example of methane oxidation in a highly diluted condition. The developed mechanism shows a good agreement with experimental data. In this condition, formaldehyde concentration at lower temperatures is well captured despite its small formation rate.

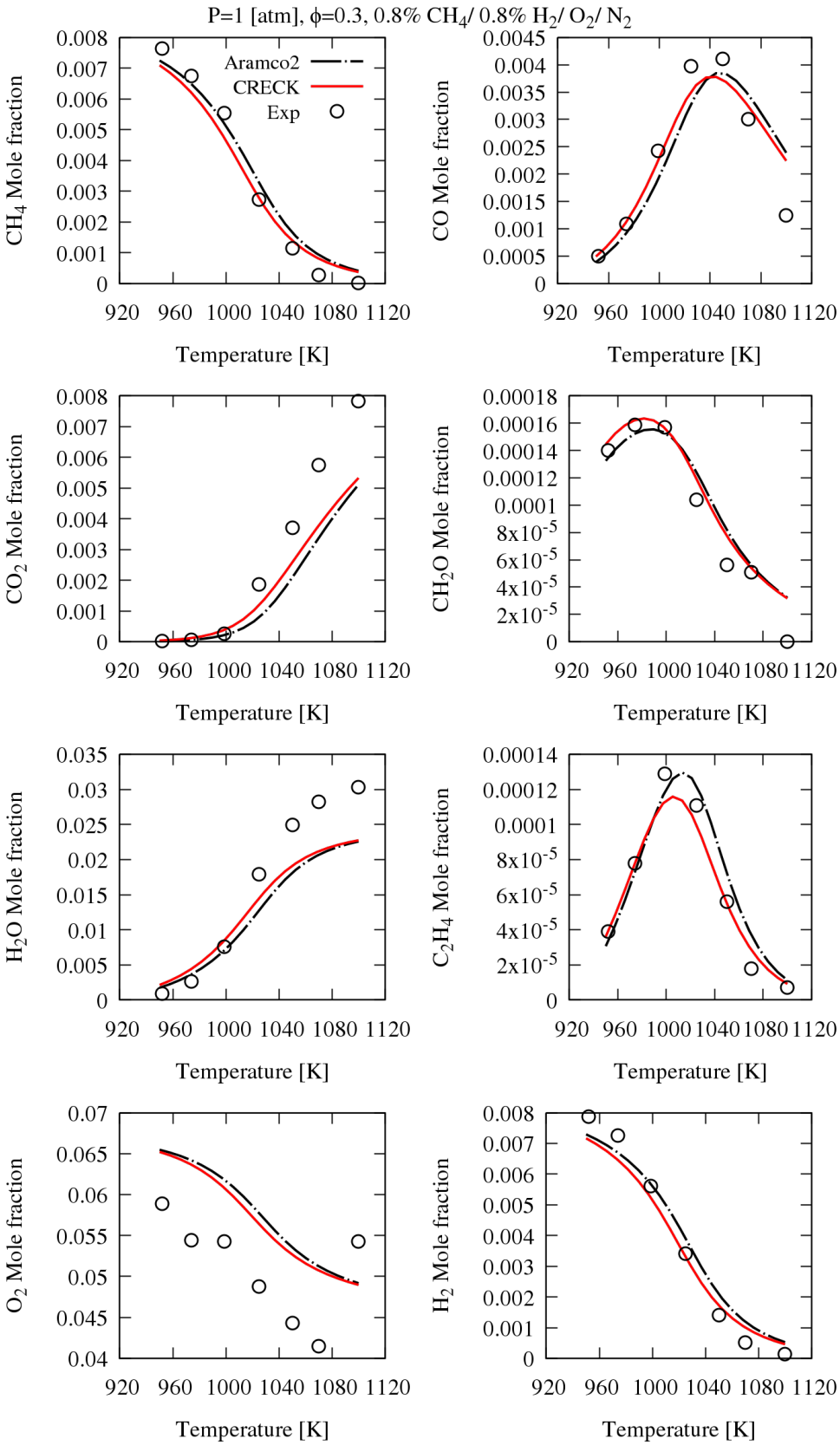

Figure 5.7: *Jet-stirred reactor species profiles of methane oxidation. Exp refers to [128].*

5.3.4 Plug Flow Reactor

A flow reactor or plug flow reactor (PFR) is used to determine the evolution of reactant, intermediate, and product species as a function of time or temperature. The data obtained can be used to identify intermediate products formed during pyrolysis or oxidation. The reactants flow through the reactor at a constant flow rate, pressure and temperature. In this reactor, the nominal residence time of the mixture inside the reactor can be calculated as

$$\tau = \frac{\rho V}{\dot{m}} \tag{5.3}$$

Where V is the volume of the reactor, ρ is the density and $\dot{m}$ is the mass flow rate of the mixture.

In this section, the result of a laminar plug flow reactor at high pressure ($P = 100atm$) and low temperature (T=600-900K) is presented. As shown in Figure 5.8, under this very fuel rich condition ($\Phi = 98.8$), the fuel conversion starts at $\sim 700\,K$. The major products at this peculiar condition are C_2H_6, C_2H_4 and CO, while the maximum methane conversion predicted by mechanism is $\sim 2.6\%$. The model predicts well the onset of reaction and the methane consumption due to ignition.

This particular experiment is useful to analyse the path for oxidation methane at high pressure and low temperature. It is well known that at this condition the formation of peroxide radicals is an important step to predict the early stage of the ignition [72]. Moreover, the formation of peroxide radicals is considered as the main characteristic of the low-temperature path of combustion [55]. Then it is necessary to validate the mechanism in such conditions to confirm a wide range of reliability.

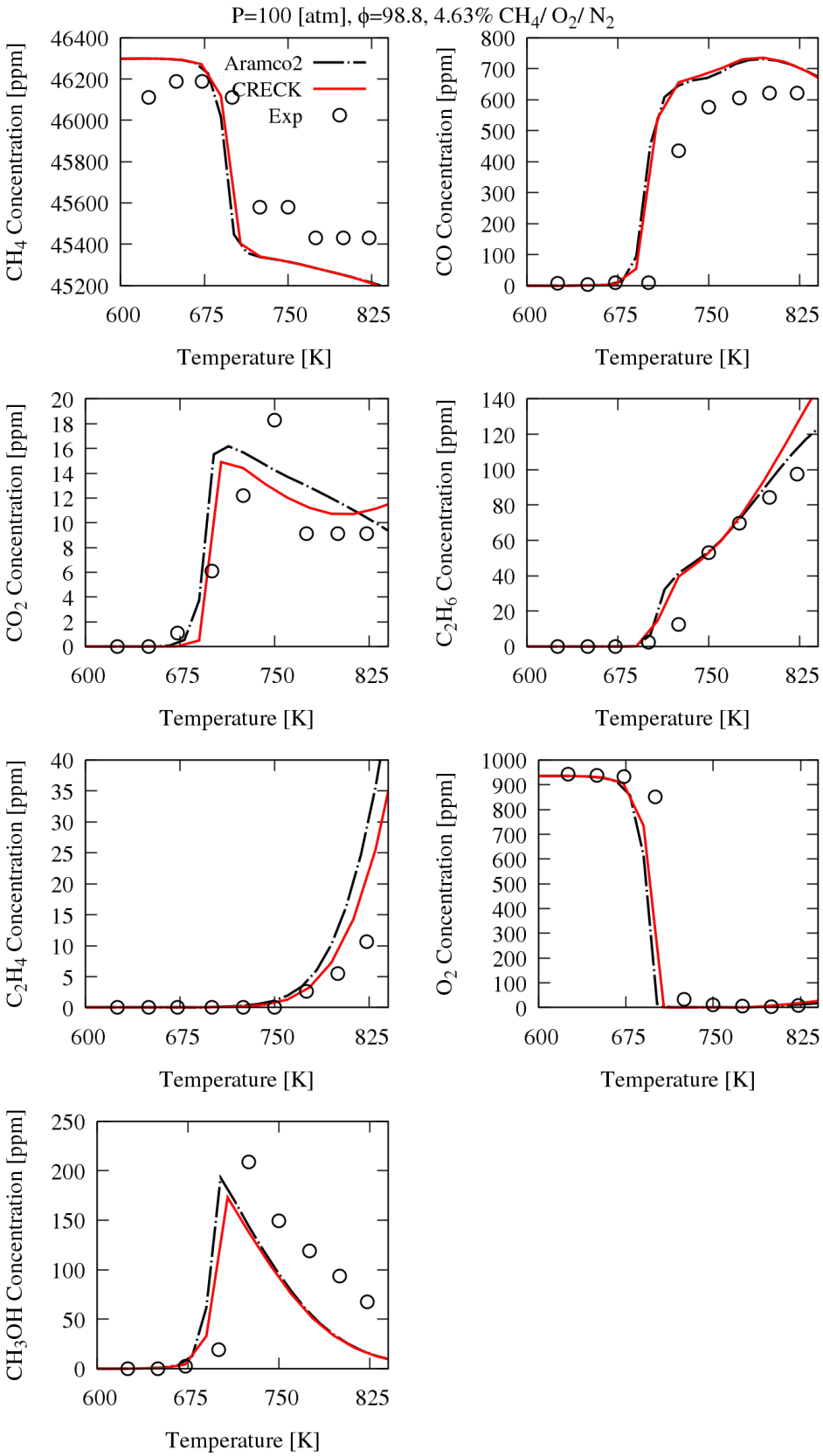

Figure 5.8: *Methane partial oxidation in PFR at high pressure. Exp refers to [72].*

5.4 Mechanism Validation for low Environmental Impacts Combustion Technologies

Although emission of sulphur and metal components depends strictly on fuel properties, CO, unburned hydrocarbons, NOx, polycyclic-aromatics, and soot particles can be reduced by adopting an appropriate combustion technology. High temperatures promote NOx formation, whereas low temperature does not guarantee complete combustion and CO and volatile components can be released.

Moreover, incomplete mixing between fuel and oxygen at the molecular level occurring in diffusion flames causes rich local conditions thus favouring polycyclic aromatic hydrocarbons (PAH) and soot formation. For these reasons, new combustion technologies mainly move towards an improved mixing, also trying to reduce the maximum combustion temperature and its turbulent fluctuations. In this direction, the MILD combustion is well recognised as a very promising technique. MILD combustion takes place by preheating the reactants at a temperature higher than auto-ignition and by a very high dilution [146]. In fact, through the control of the maximum temperature using a large flue gas recirculation and by the volumetric extension of the reaction zone, it enhances combustion stability while remarkably reducing NOx emission [6, 7].

Similarly, flameless combustion [8] is defined as a mode in which two conditions must be satisfied where the reaction is going to take place:

- Reactants temperature must exceed self-ignition temperature.
- Reactants must have entrained enough inert combustion products to reduce the final reaction temperature well below adiabatic flame temperature, to such an extent that a flame front cannot be stabilised.

The high-temperature air combustions (HiTAC) discussed by Hasegawa et al. [147] is an additional technology mainly based on the preheating of air and control of the oxygen concentration in the reacting system.

Another advantageous technique is the OXY-fuel combustion, which typically combines high purity oxygen (>95%) with recycled exhaust gases, always aiming to control the maximum flame temperature. Burning fuel in oxygen and flue gas rather than air, of course, results in the elimination of NOx emissions and also favours the carbon dioxide sequestration from the exhausts.

The different combustion regimes and dominant elementary chemical pathways of fuel oxidation depend on operating temperatures and pressures [148]. As discussed earlier, MILD combustion differs from conventional combustion. It lowers the operating temperatures while the radical pool and mainly the OH concentration is homogeneously distributed in a relatively larger region compared to conventional combustion [149,150]. Although MILD combustion has been widely investigated [5,133,151–154], only minor attention has been devoted to the validation of detailed kinetic mechanisms in these conditions, mostly underlining shortcomings of existing kinetic models.

5.4.1 Methane Pyrolysis

Hierarchically, the thermal decomposition or pyrolysis of methane, together with the H_2/O_2 sub-mechanism, is the core of kinetic mechanisms of oxidation and combus-

tion of any hydrocarbon. The competition between oxidation and pyrolysis channels plays a crucial role in these new combustion processes and in the intermediate temperature chemistry [80, 134, 155], which significantly impacts the triggering of ignition in the MILD regime. At high temperatures, pyrolysis reactions are faster and precede oxidation reactions, mainly for heavier hydrocarbons (fuel fragmentation) [29]. Additionally, pyrolysis paths also involve chemically activated addition and isomerisation reactions [97]. These reactions explain the formation of the resonantly stabilised propargyl (C_3H_3) radical, which is a key precursor of PAH and soot [156]. For these reasons, it is evident that methane pyrolysis sub-mechanism needs to be implemented and carefully validated in combustion kinetic models.

At low temperatures, methane is more stable compared to other hydrocarbons, due to the lack of $C-C$ bonds and the only presence of stronger aliphatic $C-H$ bonds. Thus, methane thermal-decomposition is strongly endothermic and requires $\sim 105 kcal/mol$ energy for the breaking the $C-H$ bond. Moreover, there are fundamental difficulties associated with the high-temperature pyrolytic conditions because of the formation of PAHs and soot [103, 157]. Thus, compared to oxidation experiments, the experimental data on methane pyrolysis are scarce and are mainly limited to low and atmospheric pressures to prevent or limit carbon formation. Moreover, further experimental data refer to the carbon vapour deposition (CVD) [158], but they are out of the scope of this work because they associate with very low pressure ($< 0.1 atm$). Therefore, the development and validation of the kinetic mechanisms are based only on these limited experiments. As already discussed in the literature [96], the detailed kinetic mechanism of methane pyrolysis and oxidation limited to C_1 and C_2 species can present discrepancies in H_2 and C_2H_2 formation, because of the possible growth of PAH and unsaturated species.

In order to guarantee the model accuracy in pyrolytic conditions, the heavier species and their successive reactions to form butadiene, PAH and aromatic species need to be accounted for. To further emphasise this feature, Figure 5.9 shows the temporal profile of methane mole fraction for the pyrolysis in a plug flow reactor at constant temperature $1263K$ and atmospheric conditions. The experiments of Billaud et al. [159] are compared with the predictions of two detailed kinetic schemes (CRECK and Aramco [51, 63]), both applied with and without the extension to the sub-mechanism of heavier species (C_4-C_6).

In this figure, Aramco 1.3 [51] is a detailed mechanism developed to characterise C_0-C_2 hydrocarbons and oxygenated fuels, while Aramco 2.0, based on Aramco 1.3, is able to characterise also C_3 and C_4 hydrocarbons and oxygenated fuels. Similarly, CRECK+PAH is a detailed kinetic model containing the C_0-C_3 core mechanism as, together with C_4-C_6 and PAH sub-mechanisms. Aramco and CRECK models consistently show a higher reactivity when are extended to higher molecular weight species. It is possible also to notice an improved agreement with experimental data, suggesting the need for considering also heavier species in the development and validation of the kinetic mechanism, mainly for severe pyrolysis conditions.

5.4.2 Unconventional Combustion Experimental Database

At fixed fuel concentration, fuel reactivity increases as the equivalence ratio decreases. In fact, oxidation channels with the formation of formaldehyde prevail over pyrolysis

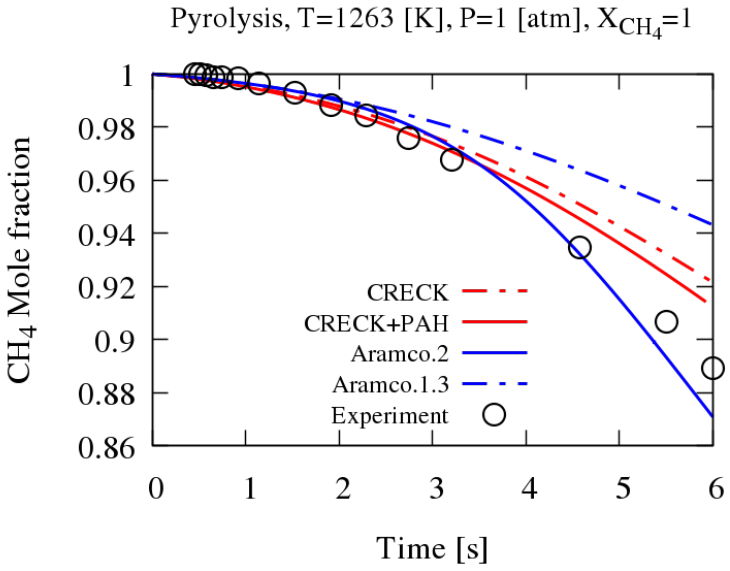

Figure 5.9: *Comparison of CH_4 profile in pyrolysis with and without sub-mechanism of higher species. Experimental data refers to Billaud et al. [159].*

channels in lean fuel mixtures, whereas, in rich conditions, the reactivity decreases because of the pyrolytic pathways favoured by the recombination of methyl radicals and the successive dehydrogenation steps. Moreover, pyrolysis is an endothermic process, thus decreasing the reactivity not only by forming more stable radicals but also through temperature reduction [127].

Although the extended and complete set of experimental conditions and their validations are reported in the Supplementary Material, Table 5.3 summarizes the conditions of a selected set of experimental data useful for the validation of the mechanism and discussed with better detail in this study. These experiments of MILD and OXY-fuel combustion are divided into four different categories including JSR, PFR, flame speeds and ignition delay times. For the complete validation of the CRECK kinetic mechanism, readers can refer to the Supplementary Material.

Notably, the following aspects of unconventional combustion and the effect of CO_2 and H_2O dilution will be analysed and discussed:

- System reactivity in ideal reactors
- Laminar flame speed (oxy-fuel systems)
- The ignition delay time in shock tubes and plug flow reactors
- Thermo-chemical oscillation in Jet stirred reactors

Table 5.3: *List of experimental measurements for unconventional combustion validation and analysis*

Experiment	Mixture	Temperature [K]	Φ	Pressure [atm]	Reference
Jet Stirred Reactors	$1\%CH_4/O_2/N_2$	1000-1175	0.1	1	[127]
	$1\%CH_4/O_2/20\%CO_2/N_2$	1000-1175	0.1	1	[127]
	$1\%CH_4/O_2/10\%H_2O/N_2$	1000-1175	0.1	1	[127]
	$CH_4/H_2/O_2/N_2$ (H_2=0-2%)	1025	0.3	1-10	[130]
	$CH_4/H_2/O_2/20\%CO_2/N_2$ (H_2=0-2%)	1025	0.3	1-10	[130]
Plug Flow reactors	$CH_4/O_2/H_2O/N_2$ (H_2O =0.35-9.3%)	1075-1800	1.6	1.1	[135]
	$CH_4/O_2/85\%N_2$	1200-1400	0.1-0.8	1	[5]
	$CH_4/O_2/85\%N_2$	1250	0.1-0.4	1	[5]
	$CH_4/O_2/85\%N_2$	1300	0.1-0.7	1	[5]
Laminar Flame Speeds	CH_4/O_2 (H_2O=0-0.5)	Tin=373	0.5-1	1	[160]
	CH_4/O_2 (CO_2=0-0.5)	Tin=373	0.5-1	1	[160]
	CH_4 (O_2/N_2=1/1) (0-10%-20%H_2O)	Tin=373	0.6-1.5	1	[160]
	$CH_4/O_2/CO_2$ (XCO_2/(XCO_2+XO_2)=0.4-0.7)	Tin=300	0.4-1.6	1-3	[161]
Ignition Delay Times	$CH_4/O_2/30\%CO_2/AR$	1660-2000	1	0.76-3.77	[162]
	$CH_4/O_2/30\%CO_2/AR$	1730-2000	0.5	0.77-3.92	[162]
	$CH_4/O_2/CO_2/N_2$ (CO_2=0-75%)	1350-1900	0.5	1.75	[163]

5.5 Summary

This Chapter covered the description of the experimental database, numerical methodologies and mechanism validations. More than ~ 200 different experiments containing more than ~ 6000 data points were collected from literature for various devices such as plug flow reactor (PFR), Jet stirred reactor (JSR), shock tube, and 1-D laminar flame were collected for mechanism validation and development.

The OpenSMOKE++ framework [137], was applied for the numerical simulations of reacting systems. This package can handle simulation of ideal chemical reactors (plug flow, batch, jet stirred reactors), shock tube and 1-D laminar flame. It also provides useful numerical tools such as the sensitivity and rate production analysis, which are applied to analyse and improve the whole kinetic mechanism.

Although the extended and complete set of experimental conditions and their validations are reported in the Appendix, a selected set of experimental data in a diverse range of conditions were modelled and analysed in this section. The experimental values well captured by the model, but small discrepancies can be seen in some conditions where the analysis also provided accordingly. Moreover, a list of summarised conditions of experimental data useful for the validation and critical analysis of the unconventional conditions presented to be discussed with better detail in Chapters 6 and 7.

CHAPTER 6

MILD combustion

THE MILD combustion is well recognized as a very promising technique. MILD combustion takes place by preheating the reactants at a temperature higher than auto-ignition and by a very high dilution [5]. In fact, through the control of the maximum temperature by means of flue gas recirculation and the extension of the reaction zone [6, 7], it enhances combustion efficiency while remarkably reducing NOx emission. Similarly, flameless combustion is defined as a mode in which two conditions must be satisfied where the reaction is going to take place:

- the reactant temperature must exceed self-ignition temperature;
- the reactants must have entrained enough inert combustion products to reduce the final reaction temperature well below adiabatic flame temperature, to such an extent that a flame front cannot be stabilised [8].

6.1 MILD Definition

The determination of the MILD regime confinement is still ambiguous, despite numerous studies that have been devoted to the characterisation of this regime. The classification and characterisation of the MILD operating conditions were studied, including the Jet Stirred Reactors (JSR) [155, 164, 165], Plug Flow Reactors (PFR) [5, 80], jet-in-hot-coflow burners [166–168], and entrained flow jet flames [7, 169, 170]. One of the well-known definitions is based on the initial temperature (T_{in}) and temperature increase during combustion (ΔT), delimited with self-autoignition temperature (T_{auto}). Moreover, a combustion regime considers as MILD, If it suffices the following condition [146]:

$$T_{in} > T_{auto} > \Delta T \tag{6.1}$$

According to this criterion, (T_{auto}) is evaluated as a temperature that any small temperature rise dislocate the system to the upper branch of the S-shape curve and the system reaches self-sustain reactivity [146].

It is evident that the S-shape curve has implied an influential role in the classification of MILD combustion. Another critical definition of the premixed MILD regime has been characterised without regard to (T_{auto}), as the MILD condition can be obtained when the S-shape curve shows a monotonic behaviour, also without ignition and extinction turning points. By assuming global step irreversible reaction, constant thermochemistry properties, and steady-state mass and heat conservation, MILD regime most satisfies the condition of Eq.6.2 [151, 171].

$$\frac{E_{Global}}{T_{in}R_u} < 4\left(1 + \frac{c_p W_f T_{in}}{QY_f}\right) \tag{6.2}$$

Where E_{Global} is the effective activation energy of the global step reaction, R_u the universal gas constant, c_p the constant pressure specific heat, Q the heat of combustion, W_f molecular weight of the fuel, and Y_f the mass fraction of the fuel at the inlet. The term of $c_p W_f T_{in}/QY_f$ can be therefore estimated by $T_{in}/\Delta T$, where ΔT is the temperature rise during combustion [146]. According to this correlation, MILD combustion occurs where the temperature increase (ΔT) always maintains smaller than inlet temperature.

However, in diffusion-controlled, MILD combustion regime features distinct characteristics by significantly broadening reactive structure and vanishing the typical pyrolytic region. Additionally, the location of the oxidative structure in mixture fraction shift towards the hot side, and it is not correlated to the position of the stoichiometric mixture fraction [153]. Evans et al. [168] developed a unidimensional analysis of non-premixed MILD combustion regime by including fuel-specific global activation energy (E_{Global}) without any needs of the composition-dependent reference temperature. The results obtained through counter-flow flamelet analysis suggests a new classification for non-premixed MILD combustion regime. This analysis proposed a condition for the existence of ignition and extension turning points; therefore, the corresponding monotonic S-shape curve indicating MILD combustion given by:

$$\zeta = (\beta^2 + 6\beta + 1)\alpha^2 - (6\beta - 2)\alpha + 1 < 0 \tag{6.3}$$

Where β is the ratio of activation temperature ($E_{Global}/(R_u T_{st,b})$), α refers to the heat release parameter ($\Delta T_{st}/T_{st,b}$), and stoichiometric and fully burnt conditions are indicated by st and b, respectively. These boundaries determine that non-premixed MILD regime take place by augmentation of initial temperatures, or minimisation of the overall temperature rise and may be obtained following forced ignition [168].

The classification maps of the MILD combustion regimes according to the three definitions mentioned above, autoignitive [146], premixed flamelet [151], and non-premixed flamelet [168] are depicted in Fig 6.1. The values of this figure are obtained by assuming $T_{auto} = 800K$ and $E_{Global} = 40000[cal/mol]$ [146]. The region held in common between different criteria (denoted as B and C) satisfies both autoignitive and gradual ignition definitions, and in this intersection, the feasibility of establishing a MILD regime is higher than other areas. There are two regions (A and D) that only covered by premixed and non-premixed flamelet models. Region A exposes a combustion regime requiring a forced ignition to propagation. This forced ignition occurs

by providing a local source of energy, but this energy addition must be higher than the lowest temperature of a combustible gas mixture [166]. An important implication of this figure is that in the region (A) a flammable mixture is needed to establish a forced ignition; however, MILD combustion in the region (B and C) mainly occurs for the non-flammable mixtures (Lower oxygen concentration).

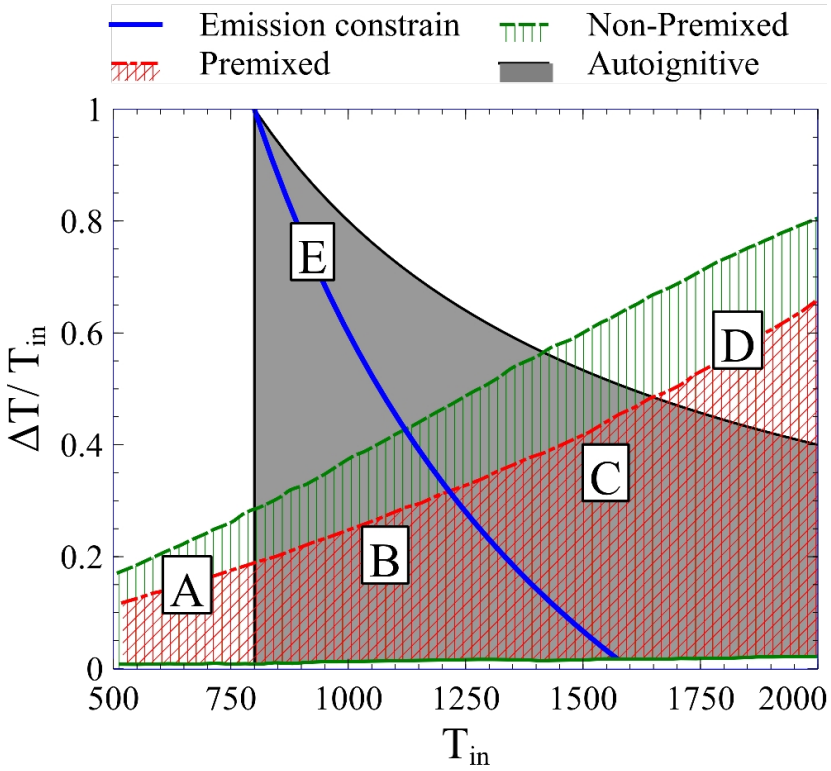

Figure 6.1: *Comparative map of MILD combustion regimes based on the different definitions: autoignitive [146] (grey shaded), premixed [151] (red filled pattern) and non-premixed flamelet [168] (green filled pattern). Blue line shows emission constrain of Mild combustion in presence of N_2. Region (A) shows forced ignition, (B) Clean-MILD, (C) Oxy-MILD, and (D) HiTAC. (adapted from [168])*

Another area that does not coincide, (D), lays in high temperatures region. Non-premixed and premixed definitions allow higher temperature rise compared to the autoignitive definition. For instance, according to these two definitions ΔT may reach $1300 - 1600K$, when T_{in} is around $2000K$. It is obvious that the higher the temperature gradient lowers the possibility of establishing a uniform temperature distribution. The main feature of MILD combustion regime cannot be attained; thus, the feasibility of establishing a MILD regime will be strongly attenuated. The maximum allowable temperature increase during the combustion process is higher than self auto-ignition temperature; hence, this region is classified as high-Temperature Air Combustion (HiTAC). HiTAC refers to the combustion technologies which utilise preheated reactants, and this class of combustion is not limited to the temperature rise [147].

The main feature of MILD combustion processes is driven by its operating condition that can significantly reduce the pollutants formation (NO_x and Soot) [79]. Pre-

vious studies [172–174] indicate that MILD combustion strongly influences NO_x formation through different reaction pathways; however, the considerable reduction principally takes place by the elimination of thermal NO_x or Zel'dovich mechanism [146]. For the polluted combustion processes dominated by thermal NO_x, the temperature is dominant parameter comparing to oxygen content and residence time. According to Zel'dovich mechanism, NO_x formation increases rapidly at temperatures about $1800K$, because of high activation energy ($76110\, cal/mole$ [175]) associated with the rate limiting step reaction $O + N_2 = NO + N$ [145].

Subsequently, it is necessary to define an emission constraint to the operating condition of MILD systems diluted with nitrogen. Figure 6.1 outlines an emission constraint (solid blue line) by considering that the maximum temperature of the system is limited to $1800\ K$. This line divides the MILD region into two different categories (B and C). The left-hand side (B) which will be called Clean-MILD afterwards, shows the concerning area for Nitrogen diluted and limited maximum temperatures. Whereas the right-hand side (C) that can be named by Oxy-MILD combustion, presents the combustion system diluted with different bath gases (except N_2) with the admissibility of higher operating temperatures.

Summing up the map-classification of the MILD regime and extended discussion, it can be highlighted that the available definitions partly assess the boundaries of MILD combustion. Two interpretations of Premixed and non-Premixed flamelet relay on activation energy of global step reaction (E_{Global}) which is an artificial number with active dependency on pressure, temperature, and bath gases. As E_{Global} is fuel dependent determining E_{Global} could be very challenging especially when surrogate fuels or different bath gases are used. In contrast, autoignitive criterion exploits T_{auto} temperature, where it reasonably confines the lower limits of MILD by $T_{in} > T_{auto}$ which fairly excludes forced ignition. However, this criterion does not suitably limit maximum temperatures ($\Delta T < T_{auto}$).

6.2 Mechanism Validation and MILD Combustion Characteristics

Based on different experimental data, this section analyses sequentially the effect of CO_2 and H_2O dilution in lean methane mixtures [127, 129], then the effect of CO_2 dilution in a lean CH_4/H_2 system [128], and, the effect of H_2O addition in rich methane mixtures at high-temperatures [135]. thereafter, the ignition delay time phenomenon of MILD will be studied inside a PFR [5].

6.2.1 Diluent Effects on Reactivity

Figure 6.2 shows methane oxidation profiles in three different diluted mixtures N_2, ($N_2 + 20\%CO_2$) and ($N_2 + 10\%H_2O$) versus reactor temperatures. Ultra-lean fuel mixtures ($\Phi = 0.1$) were experimentally studied in a JSR at atmospheric pressure and steady-state conditions [127, 129]. High dilution and preheating before injection minimised temperature gradients inside the reactor, accordingly, near isothermal conditions were obtained.

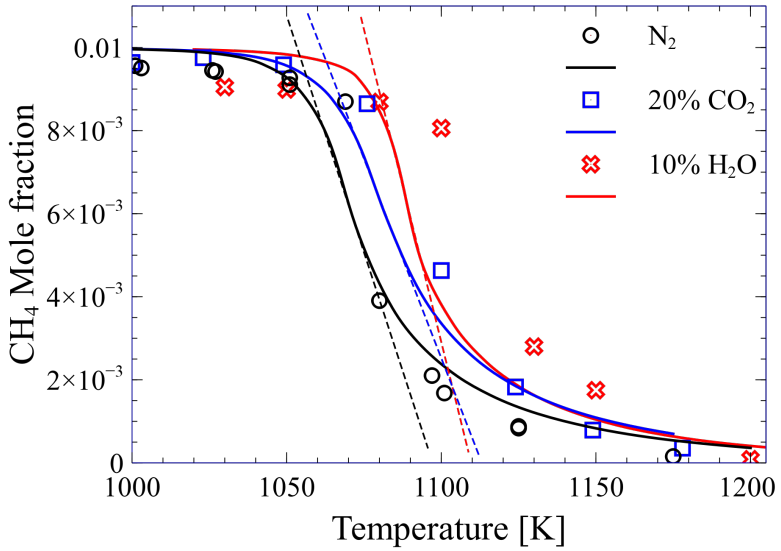

Figure 6.2: *Methane concentration profiles vs temperature in three diluted systems at atmospheric pressure and ultra-lean conditions ($\Phi = 0.1$). Reactants are diluted with $79\%N_2$, ($59\%N_2 + 20\%CO_2$), and ($69\%N_2 + 10\%H_2O$).*

It is evident that CO_2 and H_2O dilutions cause a delay in the system reactivity, which slightly shifts CH_4 conversion toward higher temperatures, compared to the N_2 diluted system. Simulations reasonably agree with experimental data even if the dilution effect is underestimated, mainly in the H_2O diluted system. At temperatures higher than $1200K$, all the systems converge toward a complete CH_4 conversion. Comparing the dashed lines of Figure 6.2, one can first observe a temperature delay of about 10 to $20K$, when adding CO_2 or H_2O respectively. Moreover, it is possible to observe that, after a delay in CH_4 conversion, the H_2O diluted system shows a somehow higher increase of reactivity with respect to the other systems.

In these isothermal conditions, the CO_2 and H_2O dilution change the system reactivity, because of chemical reactions and/or collisional efficiencies. It is noteworthy that the competition between the two pathways of $H + O_2$ plays a crucial role in defining the system reactivity in this intermediate temperature range.

$$H + O_2 = O + OH \qquad \text{(R3 revisited)}$$

$$H + O_2 + [M] = HO_2 + [M] \qquad \text{(R8 revisited)}$$

Third-body efficiencies influence the HO_2 formation and can explain the different delays in the start of methane conversion. The third-body efficiency of H_2O and CO_2 in reaction R8 are 10 and 3.8, respectively. By merely considering the mole fraction of the bath gases as a representative of their concentrations and also accounting for their collision efficiencies, the different delay times (τ_i) are then justified:

$$\tau_{N_2} < \tau_{N_2+CO_2} < \tau_{N_2+H_2O} \qquad (6.2)$$

This fact is well confirmed by the sensitivity analysis shown in the Figure 6.3, where the sensitivity coefficient of reaction R8 is the highest in the water-diluted system and the lowest in the N_2 system. As shown in Figure 6.3, the system reactivity is dominated by the chain branching reaction R3, and the ignition happens when it prevails over R8. When the chain branching reaction takes place, the concentration of O and OH radicals increase in the system, which will, in turn, activate the second chain branching reaction R12 in the water diluted system.

$$O + H_2O = OH + OH \tag{R12}$$

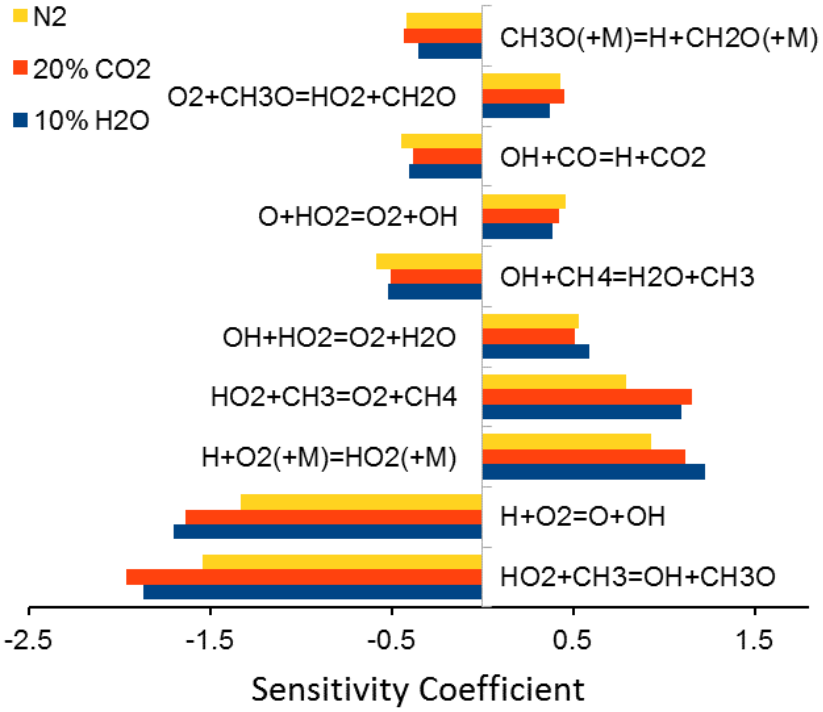

Figure 6.3: *Sensitivity analysis of CH_4 concentration in the three diluted systems presented in Figure 6.2 at $T = 1100[K]$.*

Cong and Dagaut [130] likewise investigated the effect of hydrogen addition to the oxidation of methane in a JSR at different pressures (1 and $10atm$) first with neat N_2 dilution, then with a $20\%CO_2$ addition. Together with the fuel (CH_4/H_2), a fixed amount of O_2 ($6.67\%mol$) was fed to the system at a constant equivalence ratio of $\Phi = 0.3$. As expected, their results confirmed that H_2 addition promotes methane conversion. Indeed, the hydrogen addition enhances H and OH radical concentrations, through the $H_2 - O_2$ sub-mechanism. At lean conditions, hydrogen promotes H radical concentration through the H abstraction reactions (R13 and R14) by OH and O radicals, more effectively than CH_3 radical.

$$H_2 + O = OH + H \tag{R13}$$

$$H_2 + OH = H_2O + H \tag{R14}$$

Higher H concentrations, in turn, increase OH radical formation via R3 and R15 reactions.

$$HO_2 + H = OH + OH \tag{R15}$$

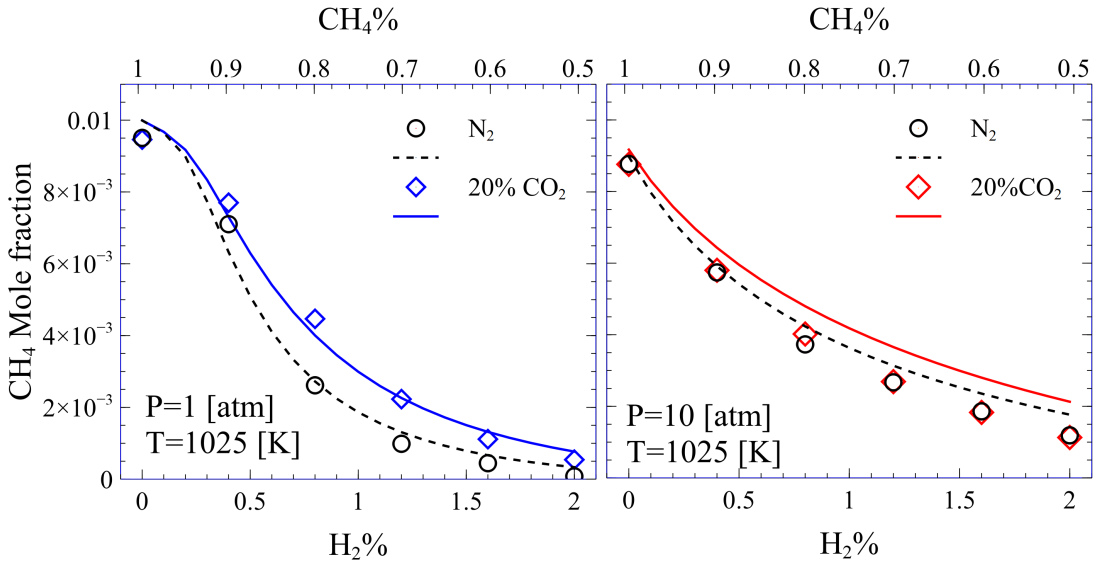

Figure 6.4: *Effect of H_2 addition on CH_4 conversion in a JSR at 1 and $10atm$, with and without $20\%CO_2$ addition. Conditions: 6.67% oxygen, $\Phi = 0.3$, $T = 1025K$. Experiments refer to [130].*

In contrast, the $20\%CO_2$ addition partially reduces the reactivity because of the higher collision efficiency in R8. Figure 6.4 shows the satisfactory comparison of experimental data and model predictions at a constant temperature ($T = 1025K$) at two different pressures (1 and $10atm$), both for the neat N_2 and the $20\%CO_2$ cases. Due to the pressure dependency of the unimolecular decomposition reaction of CH_4, there is a small conversion (5%) of pure CH_4 at $10atm$, whereas it does not show any reactivity at atmospheric pressure. Hydrogen addition favours methane oxidation by promoting H radical formation, and this effect is more evident at atmospheric pressure. When comparing the methane concentrations profiles versus H_2 additions at 1 and $10atm$ it is possible to highlight the different behaviour. There is an initial higher reactivity at higher pressure, but only with low hydrogen additions. On the contrary, at atmospheric pressure, after a sort of small induction, H_2 additions favour a higher reactivity, and the system becomes more reactive, after $1 - 1.3\%$ H_2.

Figure 6.5 presents the sensitivity analysis of methane reactivity for the cases shown in Figure 6.4 with 1% hydrogen. The different sensitivity coefficients of reactions R3 and R8 highlight that their competition is more effective at $1atm$, and mainly in the N_2 diluted systems. The CO_2 addition, as well as the higher pressure favour the HO_2

formation, and this competition becomes less effective. Thus, the CO_2 diluted system at $10atm$ shows the lowest sensitivity coefficients to R8

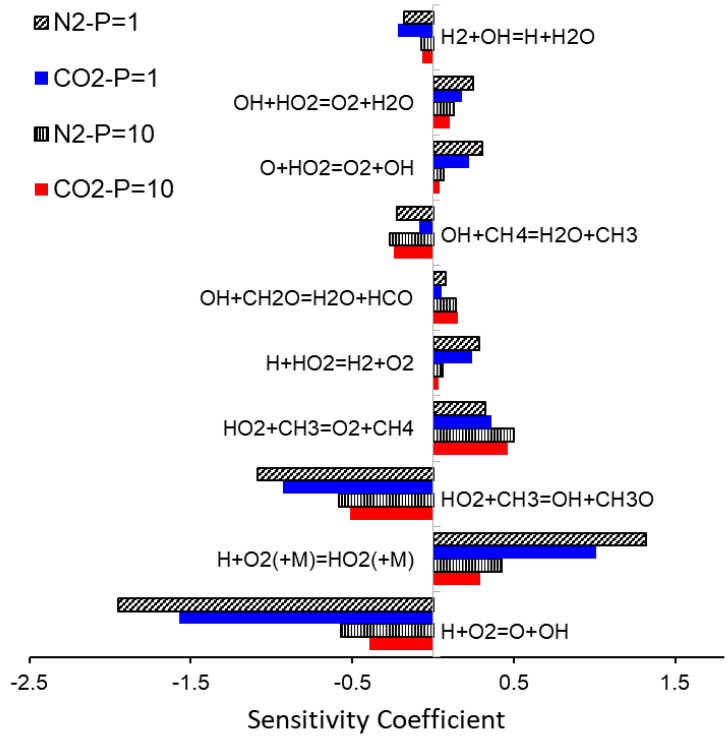

Figure 6.5: *Sensitivity analysis of methane concentrations for the four cases presented in Figure 6.4.* CH_4 *doped with* $1\%H_2$*, at* $1025K$ *and* $\Phi = 0.3$*.*

As the HO_2 formation is preferential at higher pressure, the competition between two chain propagation R16 and termination R17 reactions of $HO_2 + CH_3$ becomes more intense.

$$HO_2 + CH_3 = OH + CH_3O \tag{R16}$$

$$HO_2 + CH_3 = O_2 + CH_4 \tag{R17}$$

A complete mechanism validation and analysis of these experimental data of Cong and Dagaut [130] on the effect of hydrogen additions on methane conversion is presented in the appendix.

Rasmussen et al. [135] studied the H_2O addition effect on rich CH_4 oxidation ($\Phi = 1.6$) in an isothermal PFR at high temperatures (1073-$1823K$), and atmospheric pressure. To further improve the assessment, five cases with different water additions (from 0.35% to 9.28%) are selected. Figure 8 confirms that the kinetic mechanism is able to capture CH_4 conversion profiles versus temperature with different extent of water addition. This effect on CH_4 reactivity is indeed quite marginal in these high-temperature conditions, where a possible increase of HO_2/H_2O_2 formation (because of R8) cannot influence the system reactivity.

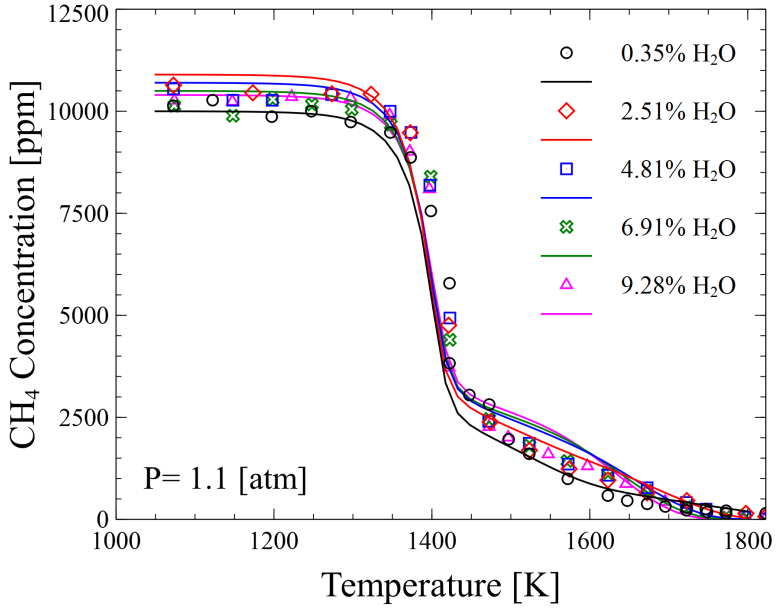

(a)

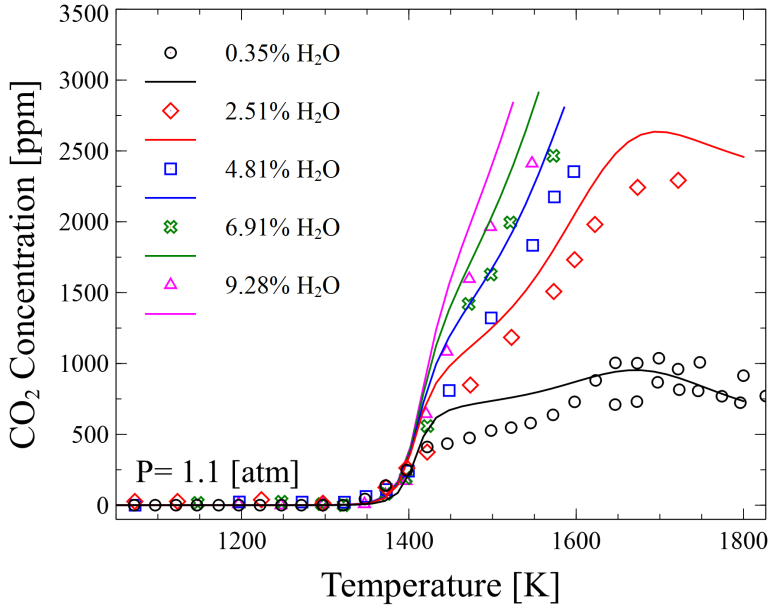

(b)

Figure 6.6: *Comparison of methane and CO_2 profiles between experimental data (points) and model simulations (lines) in a PFR for five H_2O diluted system. Conditions: $P = 1.1$, $\Phi = 1.6$, and $CH_4/O_2/N_2$ diluted with 0.35, 2.5, 4.8, 6.9, 9.3% H_2O. Experiments refer to [135].*

Although all the methane conversion profiles are similar, the CO_2 formation is affected mainly by H_2O addition. In particular, Figure 6.6b shows that CO_2 formation grows by increasing water dilution in the system. The water-gas shift reaction

$$CO + H_2O = CO_2 + H_2 \tag{R18}$$

explains this behaviour. The increased concentration of OH radicals and the reaction R19 support this path.

$$CO + OH = CO_2 + H \tag{R19}$$

As highlighted by Rasmussen et al. [135], the H_2O addition favours OH and H_2 formation and inhibits also soot formation owing to its chemical effects on the chemistry of C_2H_2 (oxidation of C_2H_2). Promoting OH and H_2 formation from H_2O justifies the changes in C_2H_2 chemistry, which reduces or eliminates soot formation in temperatures higher than $1500K$.

6.2.2 Ignition Delay Time

Preheated and highly diluted mixtures in MILD combustion lead to a relatively slow reaction time scale compared to the conventional combustion systems [5]. Despite the considerable practical applications developed in the last decades, the lack of a fundamental understanding of MILD combustion in a wide range of operating conditions somehow further limits its extensive applications at an industrial level.

Recently, Sabia et al. [5] studied ignition delay times of lean $CH_4/O_2/N_2$ mixtures in typical MILD-like operating conditions. These experiments extend the current database on auto-ignition times adding useful data for lean mixtures at atmospheric pressure and moderate temperature. Methane combustion was investigated in a non-isothermal PFR at intermediate and high temperatures. Ignition delay time was defined as the contact time required by the system to obtain a temperature increase of $10K$ with respect to the inlet temperature [5, 80]. The ignition delay time in this reactor is practically independent on inlet flow velocity. This fact was primarily verified by varying the inlet flow velocities in the range of $30 - 50m/s$.

Figure 12 shows the ignition delay times at various lean C/O ratios (0.025-0.2) with a fixed $85\%N_2$ dilution [5]. Two sets of ignition time relative to inflow velocity of 30 and $35m/s$ for each mixture are reported and compared with model predictions. The results demonstrate a negligible effect of the different inflow velocity on the measurements and predictions of ignition delay time. Considering the uncertainty of temperature measurements and the overall heat transfer coefficient, here assumed as $h = 100W/K/m2$ [5], the model predictions agree satisfactorily with the experimental data.

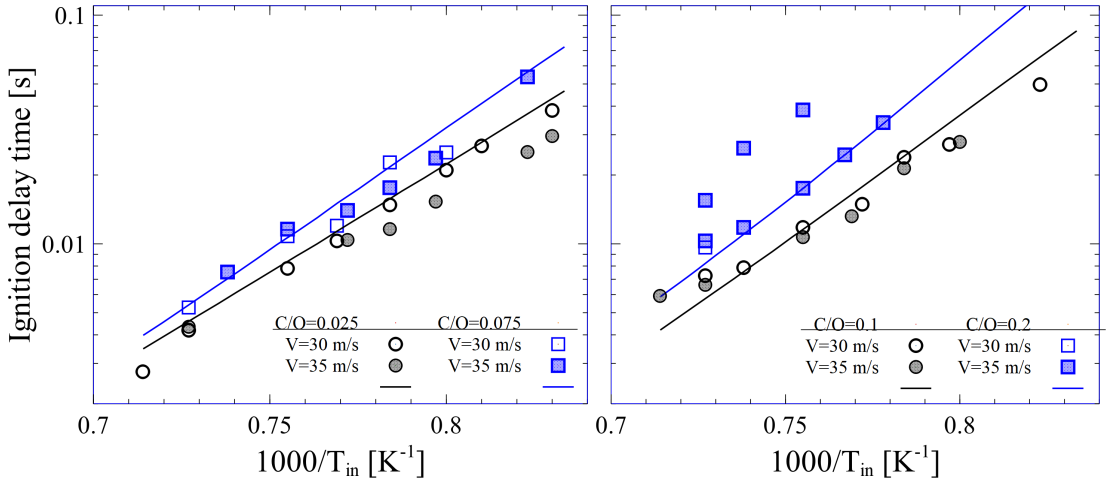

Figure 6.7: *Ignition delay times of four lean mixture diluted with* $85\%N_2$ *and two different inlet velocity (*30 *and* $35m/s$*). Symbols refer to experiments [5] and lines show the model predictions.*

The auto-ignition time of the ultra-lean mixture ($C/O = 0.025$) is shorter than the one of other mixtures because the lower methane content reduces the extent of methyl recombination, thus promoting the oxidation pathways. This feature is entirely consistent with the empirical expression of methane ignition delay times, which depends typically on methane concentration to a power $0.3 - 0.5$, usually derived at higher equivalence ratios [176, 177].

The model accurately predicts also the apparent activation energy, which spans between 35000 and $42000cal/mol$, depending on the different cases. As clearly discussed by Sabia et al. [5], a transitional regime with two auto-ignition times was detected in the experiments for the near stoichiometric mixture ($C/O = 0.2$). This fact can explain the more substantial discrepancies observed in Figure 6.7. It is clear that at high temperatures and higher methane concentration the assumption of an ideal plug flow reactor, without significant material and thermal axial diffusion terms is no longer correct. Thus, the observed presence of hysteresis effects and multiple steady-state solutions [178] are due to the reaction heat and the relevant interactions between the thermal feedback and the overall heat transfer. In these conditions, the accurate description of the reactor becomes more critical than the identification and validation of the kinetic mechanism, and this aspect goes beyond the scope of this work.

The facility effects on the ignition delay time for these data is further analysed in Figure 16 where the ignition delay times versus C/O ratio are reported at 1250 and 1300 K. Three sets of simulations are presented for different global heat transfer coefficient. Together with the model prediction obtained by $h = 100W/m2K$ (as reported in the paper), a nearly-adiabatic ($0.01W/m2K$) and nearly-isothermal ($500W/m2K$) simulation are also reported. It is worth highlighting that the variation of the heat transfer coefficient, significantly affects the ignition delay time, mainly at high C/O values. On the contrary, this effect is negligible for the ultra-lean system ($C/O = 0.025$), where the total reaction heat is very limited. The most striking observation emerging herein is that the heat exchange largely influences these experimental data.

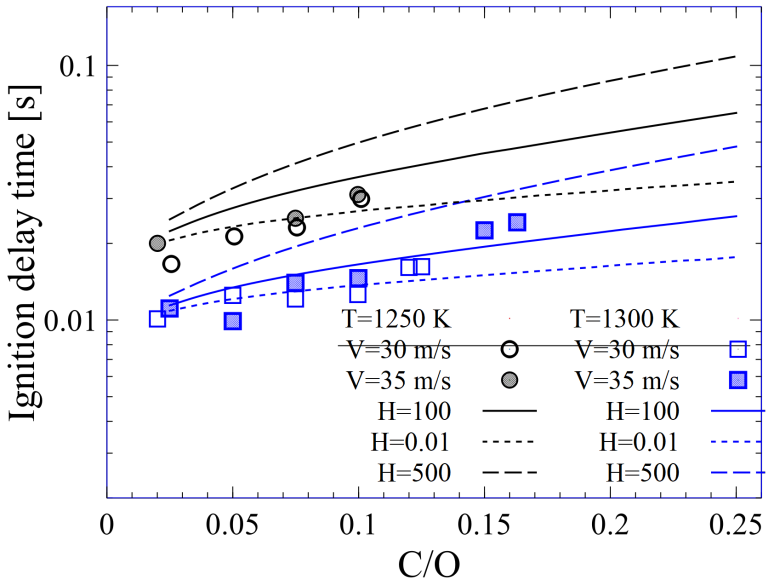

Figure 6.8: *Ignition delay time versus C/O ratio at 1250 and $1300K$ diluted in 85% nitrogen and two different inlet velocity (30 and $35m/s$). Symbols refer to experiments [5] and the lines show the model predictions. $h = 100(w/K/m2)$ refers to predictions with the expected global heat transfer coefficient, whereas $h = 0.01$ and $h = 500(w/K/m2)$ refer to near adiabatic and near isothermal conditions, respectively.*

6.3 Thermochemical Oscillation in MILD Combustion

Despite many advantages, thermochemical instability may occur under operating conditions typical of MILD combustion. This instability mainly derives from thermo-kinetic interactions, experimentally and numerically investigated in the previous literature for different fuels such as hydrogen (H_2) [179, 180], syngas (CO/H_2) [181–183], methane (CH_4) [154, 155, 184, 185], ethane (C_2H_6) [179], and acetaldehyde (CH_3CHO) [83, 186, 187].

Hopf bifurcation analysis of methane oxidation has demonstrated the actuality of purely kinetically driven oscillation, and multiple extinctions and ignitions [185]. de Joannon et al. [155] studied methane oxidation in a jet-stirred reactor experimentally, and they identified several oscillatory behaviours. These oscillations were then classified in different typologies referring to different amplitudes and frequencies. Successive studies [154, 188] focused on the effect of heat transfer, residence time, and diluent on such oscillations. In [155], de Joannon et al. associated oscillations to the role of CH_3 recombination channel and pyrolysis pathways. However, this study was later extended to discuss the competition between oxidation and recombination channels that causes a modulation of heat release [154].

Dally and Peters [189] claimed that for stoichiometric and lean mixtures, radical scavenging effects from the fuel is the initiation mechanism of the oscillations, followed by heat losses to the environment. However, they did not find any evidence to verify the recombination channel proposed by others. In contrast to previous studies, Sabia et al. [190] found such dynamic behaviours under adiabatic conditions, where oscillatory behaviours are exclusively related to chemical kinetics. It was observed that temperature oscillations for lean conditions are strongly related to chemical interaction in the H_2/O_2 core mechanism. For rich conditions, oscillatory behaviours were fundamentally associated with CO_2 reactions.

Even though methane oscillation in MILD regime has been documented experimentally and numerically, the literature lacks a general consensus concerning the origin of such oscillatory phenomena. Moving from recently published experimental data [133, 134], this section presents a thorough kinetic discussion useful to interpret the observed instability in methane MILD combustion.

6.3.1 Thermo-kinetic oscillation

In JSR, ignition and extinction phenomena are accompanied by oscillatory behaviour, where the steady state becomes unstable. During these oscillations variables of the system, such as temperature and concentrations, vary significantly. Previous studies [133, 134] indicate that the experimental temperature measurement is the main criterion to detect oscillations as the experimental facilities are not able to resolve fluctuations in species concentrations. Thus, experimental measurements only represent time- averaged values for concentrations [133, 134]. Moreover, these temperature measurements could be also very challenging due to the presence of regular and irregular oscillation, limited temperature fluctuations, and very high oscillation frequencies.

During the 80's, several studies investigating kinetically driven oscillation of H_2/O_2 system appeared, and the phenomenon triggering this oscillation was addressed. The origin of this phenomenon can be traced to the kinetic interaction involving radi-

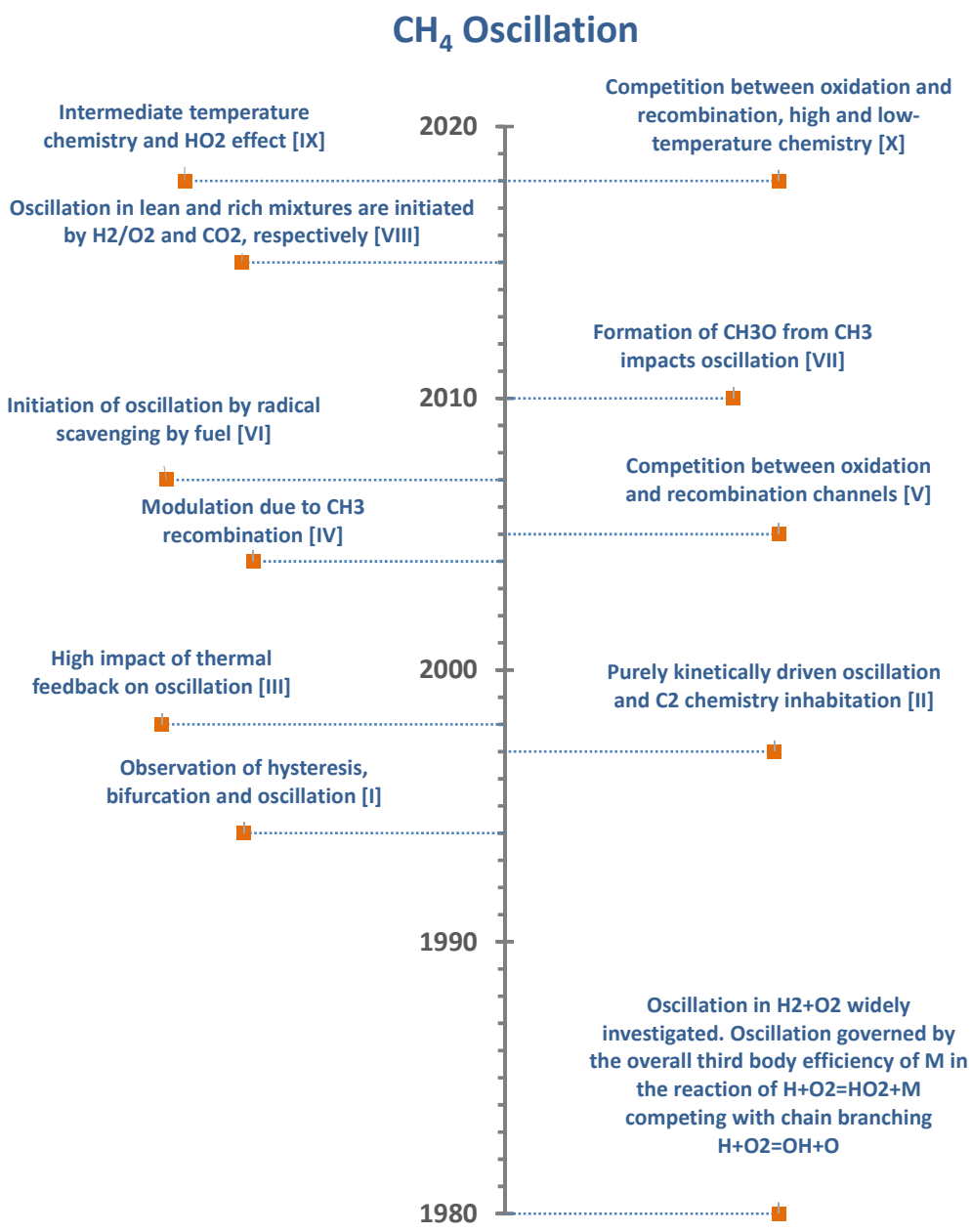

Figure 6.9: *Time line of oscillation in MILD methane mixture. [I] refers to Gray et al. [184], [II] Park et al. [185], [III] Park et al. [191], [IV] de Joannon et al. [155], [V] de Joannon et al. [154], [VI] Dally et al. [189], [VII] Wada et al. [188], [VIII] Sabia et al. [190], [XI] Bagheri et al. [133], and [X] Lubrano Lavadera et al. [134]*

cal chain branching coupled to the inhibition caused by the third-body efficiency of the complete combustion product (H_2O) formed during ignition, through the non-branching reaction of

$$H + O_2 + [M] = HO_2 + [M] \qquad \text{(R8 revisited)}$$

Then the displacement of the products with incoming reactants diminishes the third-

body efficiency and shifts the system from this predominantly recombination reaction back to the chain branching reaction via

$$H + O_2 = O + OH \qquad \text{(R3 revisited)}$$

Figure 6.9 provides a timeline survey at previous studies on methane oscillation. As mentioned earlier, oscillation of hydrogen was successfully investigated during the 80's. As indicated in this figure starting from the mid of 90's until very recently many studies have addressed the reasons behind methane oscillations, however each study proposed a different mechanism. Most of these studies focused on the effects of various parameters such as residence time, heat transfer, initial mixture, and temperature on the oscillation characteristics. Despite the outstanding value of these previous investigations in unveiling the influence of many different parameters, the lack of a deep kinetic understanding of the initiation mechanism (triggering oscillation) led to quite controversial conclusion, preventing the possibility of generalization.

In the recent paper by Lubrano et al. [134], a comprehensive set of experimental data was presented which bringing new insights as well as the opportunity to redefine the complex oscillatory behaviour in methane MILD combustion. This set of experimental data accompanied by the data presented in [133] are considered and discussed in this study. Table 6.1 summaries the nine different mixtures considered in the present discussion.

Table 6.1: *Investigated experimental mixture compositions.*

Case	Φ	CH_4	O_2	Diluent	Reference
A	1.5	0.0429	0.0571	N_2	[134]
B	1.5	0.0429	0.0571	CO_2	[134]
C	1.5	0.0429	0.0571	N_2/H_2O	[134]
D	1.0	0.0333	0.0667	N_2	[133]
E	1.0	0.0333	0.0667	CO_2	[133]
F	1.0	0.0333	0.0667	N_2/H_2O	[133]
G	0.5	0.02	0.08	N_2	[134]
H	0.5	0.02	0.08	CO_2	[134]
I	0.5	0.02	0.08	N_2/H_2O	[134]

6.3.2 Model predictions and comparison

Figure 6.10 compares experimental and predicted methane profiles for the nine different mixtures. Although at low temperatures ($T \lesssim 1100\ K$) and higher temperatures ($T \gtrsim 1250\ K$) the system reaches and maintains steady state solutions, regular and irregular temperature oscillations are observed at intermediate temperatures. Lower and upper temperature limit defining the range of experimental oscillations are indicated as dashed lines in Figure 6.10 where the grey areas represents region of oscillation from kinetic simulations. The range of temperature where a system oscillates depends on both, stoichiometry and diluent. It is worth mentioning that, while all systems at lean and stoichiometric conditions exhibit oscillations, rich systems with N_2 and N_2/H_2O dilution do not show such behaviours.

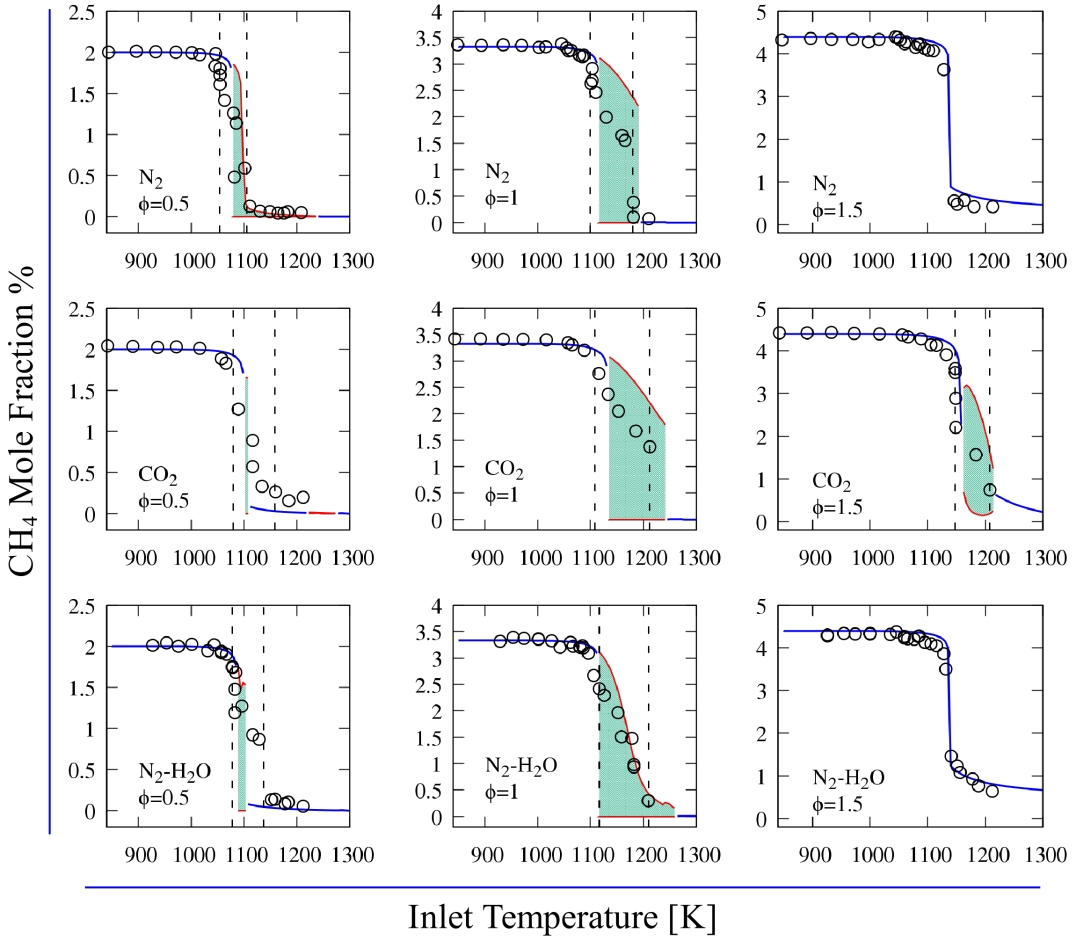

Figure 6.10: *Methane profile in different diluted systems (N_2, CO_2, and N_2/H_2O) and for equivalence ratios (0.5, 1, and 1.5). Shadow areas indicate the predicted range and extent of oscillations, whereas vertical dashed lines show lower and upper oscillation experimental limits.Experiments refer to [133, 134]*

Although the main parameter determining oscillations is temperature, also equivalence ratios and dilutions strongly affect the reactivity of the system. Steady-state solutions in the whole temperature range are correctly replicated by the model for the rich condition of N_2 and N_2/H_2O. Stoichiometric conditions enhance oscillating phenomena. These conditions have been partly discussed in a previous paper [133]. Oscillations occur where the system reactivity is sufficient to promote ignition, but not high enough to sustain complete fuel conversion. Thus, in JSR, such instabilities are the result of a continuous competition between fuel conversion and accumulation along the time, because of the continuous feeding of reactants. In this former work, the competition between two possible recombination/dismutation channels of CH_3 and HO_2 radicals was highlighted where the termination reaction to form CH_4 and O_2 reduces the reactivity and the propagation reaction to form CH_3O and OH evidently increases the conversion.

For several conditions, dynamic simulations of JSR confirm the oscillating be-

haviour in the intermediate range of temperatures, between the slow and the very high reactivity conditions. The comparison between experimental and predicted range of oscillations indicates a systematic shift of about 10-20 K. Anyhow, taking into account the complexity of such measurements due to the presence of regular and irregular oscillation, the observed agreement is considered satisfactory. Moreover, it is convenient to distinguish between oscillations of different nature. Indeed, two different behaviours can be mainly observed at lean conditions ($\phi = 0.5$): primary oscillations, characterized by significant variations of methane conversion ($10 - 95\%$), and secondary oscillations, with very limited variations approaching complete methane conversion ($95 - 100\%$). The moderate temperature fluctuations, together with the very short oscillation period (lower than $0.05s$), make the experimental detection of this behaviour very challenging. Nevertheless, primary oscillations are of main concern because they can cause critical instabilities in MILD combustion regimes.

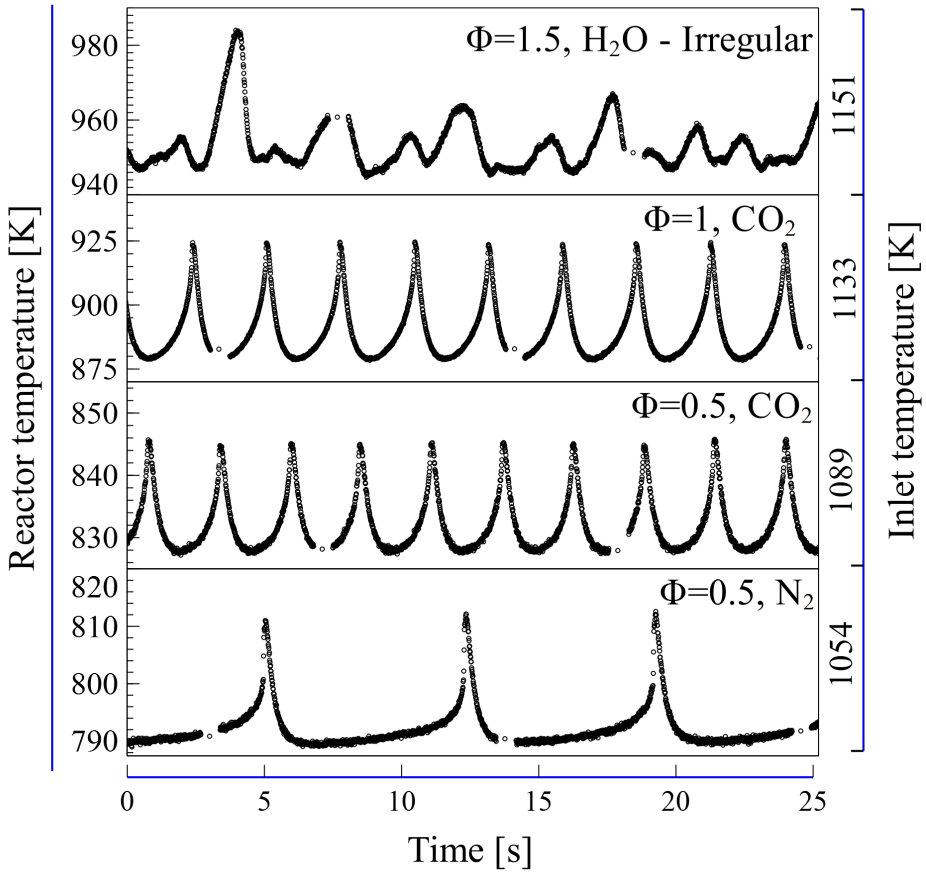

Figure 6.11: *Representative examples of experimental temperature [K] oscillations in different methane MILD combustion systems. The right axis shows inlet temperatures, while the left axis indicates temperature inside the reactors [133, 134].*

Figure 6.11 shows examples of measured temperature oscillations along time. Regular and irregular temperature time profiles captured by the thermocouple allow identifying the range of inlet temperatures leading to instabilities for the different systems. The time to reach steady conditions is usually less than a minute, and a typical run lasts 5 to 10 minutes. The time scale refers to conditions where the system already

approaches permanent oscillations. The detection of these oscillations from numerical simulations defines the range of inlet temperatures leading to instabilities for the different systems. Experimental facilities are not able to resolve fluctuations in species concentrations; therefore, experimental measurements represent time- averaged values.

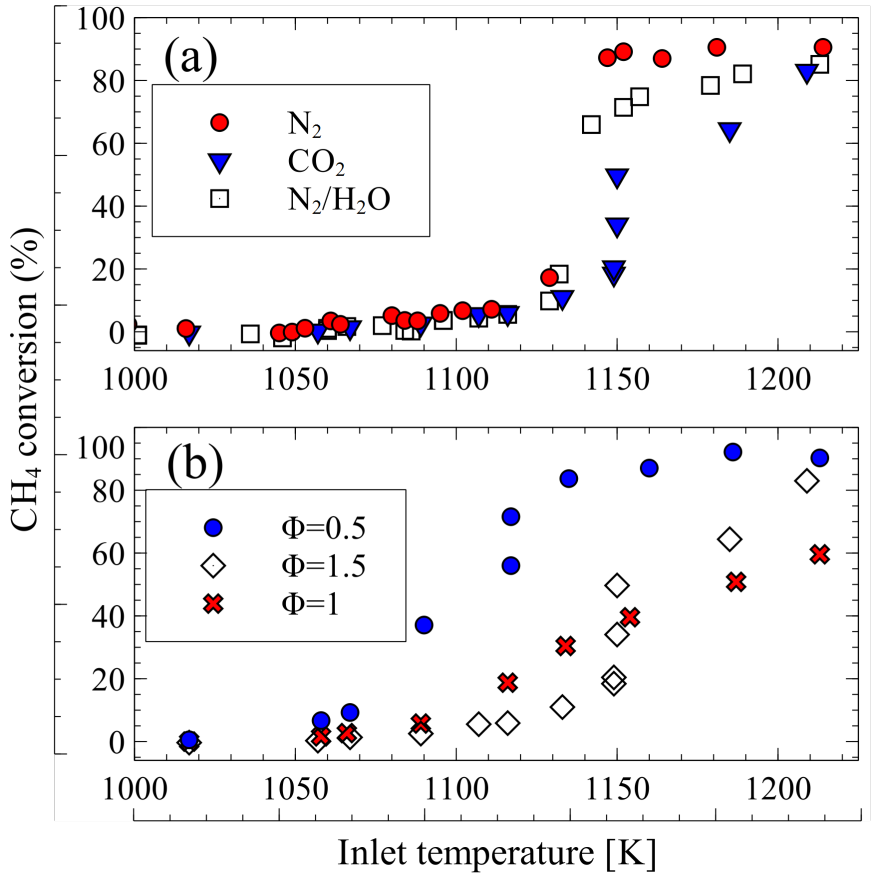

Figure 6.12: *Methane conversion profiles in different diluted systems of $\phi = 1.5$ (a) and for equivalence ratios in in CO_2 diluted system (b).*

In order to better compare these experiments and to highlight the effect of different dilutions and equivalence ratios, Figure 6.12a compares methane conversion for different dilutions for the cases at $\phi = 1.5$, and Figure 6.12b shows the effect of different equivalence ratios ($\phi = 0.5$, 1.0, and1.5) for CO_2 diluted cases. Experimental measurements highlight that the system diluted in CO_2 is the least reactive. The N_2 diluted mixture is slightly more reactive than the N_2/H_2O, mainly at high temperatures. Lean conditions exhibit higher reactivity, whereas the stoichiometric and rich cases systems present a more similar reactivity, with the stoichiometric case being more reactive at lower temperatures and less reactive at higher temperatures.

With a better detail, Figure 6.13 compares predicted temperature oscillations for varying dilutions (a), inlet temperatures (b), and equivalence ratios (c). Due to the high dilution, the mixture heat capacity (C_p) plays a dominant role in determining the amplitude of temperature oscillations. Figure 6.13a shows the effect of different diluent. The maximum rise of temperature (first peak) is inversely proportional to specific heat;

therefore, the CO_2 diluted system presents the lowest temperature oscillation range ($\sim 300K$), whereas the oscillation range of N_2/H_2O and N_2 systems are slightly lower and higher, respectively, than $\sim 500K$. It has to be underlined that predicted oscillation amplitudes are significantly higher than the measured ones (usually within $100K$). This fact can be explained considering that the predicted temperature oscillations are characterized by spike variations in less than $10^{-2}s$, which is below the response time of the thermocouple ($\sim 0.03s$). For this reason, the comparisons between experimental and predicted oscillations has to mostly rely on the characteristic periods of oscillations. Figure 6.13b highlights the effect of inlet temperatures on oscillation period. For temperatures increasing from 1140 to $1180K$, the period decreases from more than 2 to less than $1s$. This behaviour is associated with the increasing reactivity of the system . Finally, Figure 6.13c shows the effect of the equivalence ratio at $T = 1180\ K$, reflecting the relative reactivity already observed in Figure 6.12. In particular, in the lean case the reactivity is high enough to allow for a stable solution.

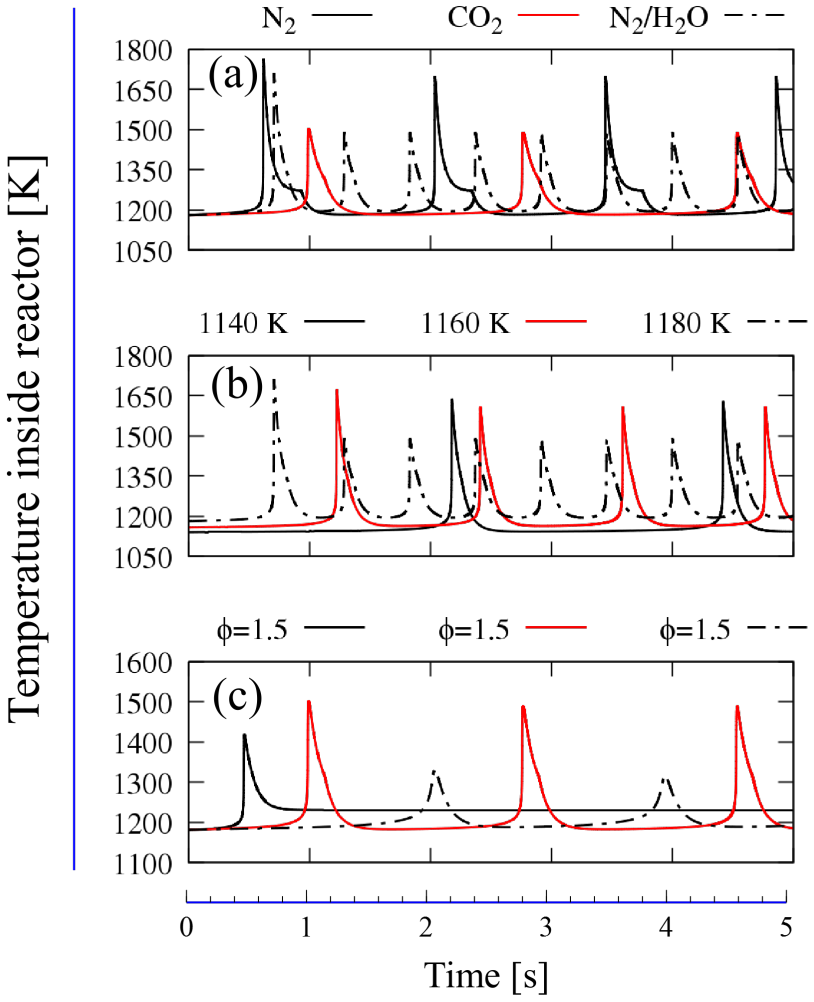

Figure 6.13: *Predicted temperature oscillations; (a) Effect of different dilutions on stoichiometric oxidation at* $1180K$*; (b) Effect of inlet temperature in stoichiometric mixtures diluted in* N_2/H_2O*; (c) Effect of equivalence ratios in the case of* CO_2 *dilution,* $T = 1180K$

Figure 6.14 compares the average oscillation periods versus the inlet reactor temperature, for the stoichiometric cases with three different dilutions. For increasing temperature, the increasing reactivity results in a reduction of the oscillation period from $\sim 9s$ at $\sim 1100K$ to less than $\sim 1s$ for $T \gtrsim 1150K$. No significant differences are observed between the three dilutions, exception made for a very slight delay in the onset of oscillations for the CO_2 system, at a given temperature. As already observed, the decrease of the oscillation period with rising temperatures is due to the increased reactivity. The simulation results demonstrate the feasibility of predicting lower and upper oscillation temperature limits with an accuracy of $\sim 20K$; thus, the overall comparisons with experiments seem to be satisfactory. The reactivity in the case of CO_2 dilution is slightly slower compared to other cases, as also experimentally observed. At temperatures, higher than $1150K$, oscillation periods become slightly lower for the N_2/H_2O mixture with respect to the N_2 one. At lower temperatures an opposite trend is observed, with the N_2 system showing the shorter characteristic periods. Both these trends are captured by the model.

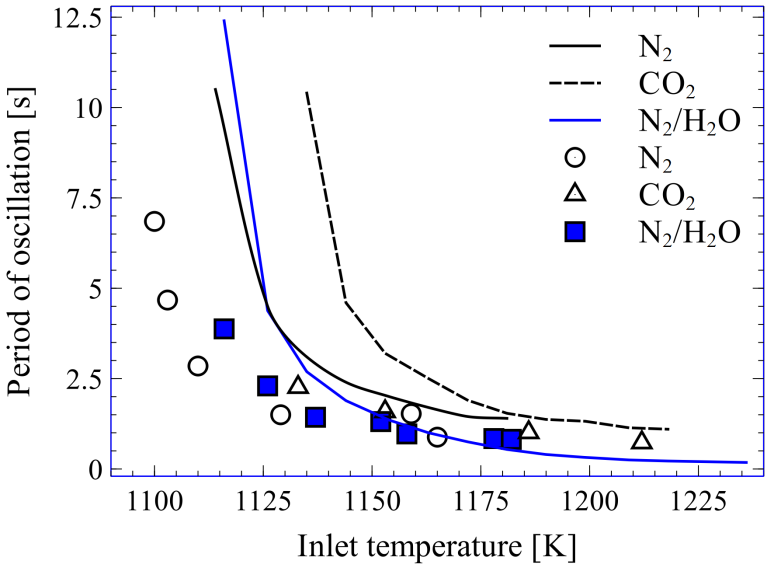

Figure 6.14: *Comparison of predicted (lines) and experimental (symbols) oscillation periods [s] as a function of inlet temperature for stoichiometric methane oxidation with a residence time of* $\tau = 0.5s$.

To better discuss these differences in reactivity and characteristic periods, it is convenient to analyse and discuss the following aspects:

- N_2 dilution effect on third body efficiency.
- Scavenging effect of CO_2.
- Water promotion of OH radical formation.
- Starting and damping of oscillations.
- Intermediate to high temperature chemistry shift.

N_2 dilution effect on third body efficiency

As already mentioned, the competition between initiation and termination reactions justifies the oscillating behaviours. Similarly, the recombination and dismutation channels

$$HO_2 + CH_3 = OH + CH_3O \quad \text{(R16 revisited)}$$

$$HO_2 + CH_3 = O_2 + CH_4 \quad \text{(R17 revisited)}$$

of CH_3 and HO_2 radicals explain the accumulation and ignition phases during permanent oscillations. The competition between

$$H + O_2 = O + OH \quad \text{(R3 revisited)}$$

$$H + O_2 + [M] = HO_2 + [M] \quad \text{(R8 revisited)}$$

is particularly important at intermediate temperatures ($950 < T < 1200$). Collisional efficiencies of different diluent strongly affect the relative ratio of these reactions. Indeed, compared to other bath gases, N_2 has a negligible effect on recombination and termination reactions due to its lower third body efficiency. Moreover, the formation of methane complete combustion products (H_2O and CO_2) increasingly impacts the importance of termination reactions.

Scavenging effect of CO_2

The conventional approach to determine the chemical and physical effects of diluents on the reactivity of the system is through defining imaginary species [192]. These species have the thermochemical properties of the contemplated species; however, they do not take apart in any reaction. In this analysis, physical effect is identified by the difference between the result of N_2 dilution and the result of imaginary diluent (iCO_2), whereas the chemical effect is highlighted by comparing the result of real and imaginary diluent [192]. Figure 6.15 presents methane depletion versus time, highlighting prevalence of chemical effect (i.e chemical reactions and collisional efficiencies) over physical effect (i.e diluent heat capacities).

The lower reactivity of the CO_2 system is mainly due to the scavenging effect of CO_2 on H_2 and H with a promotion of CO formation through the reactions of

$$CO + OH = CO_2 + H \quad \text{(R19 revisited)}$$

$$CO + H_2O = CO_2 + H_2 \quad \text{(R18 revisited)}$$

proceeding in the reverse direction. Reaction R22 consumes H_2 and competes with the reaction of $H_2 + O = H + OH$. Moreover, R2 subtracts H atoms to the degenerate branching channel ($H + O_2 = O + OH$) significantly impacting the overall system reactivity. As highlighted in Figure 6.16, lower and higher yields of H and CO, respectively, are a clear result of this scavenging effects. The lower concentration peaks in H and OH profiles explain the lower reactivity of the CO_2 diluted system.

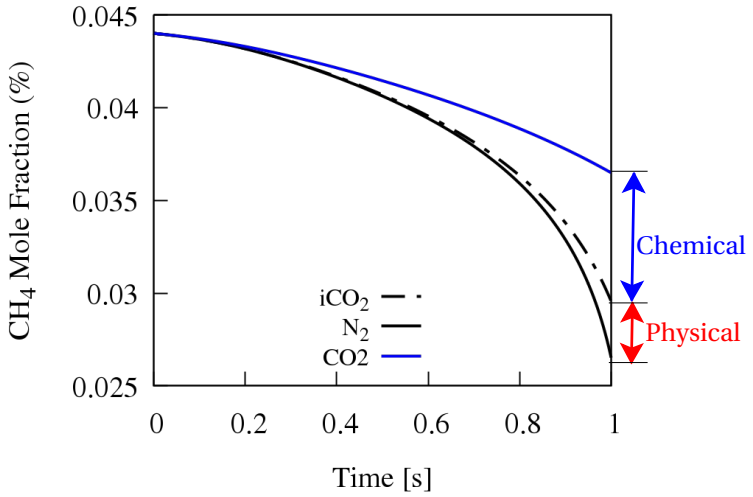

Figure 6.15: *Quantification of chemical and physical effects of CO_2 on CH_4 mole fraction profile versus time at inlet temperature of* $1180K$ *and* $\phi = 1.5$.

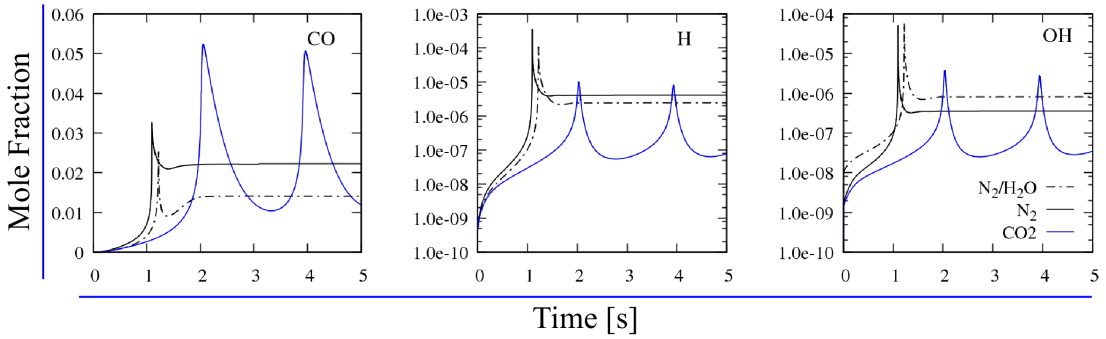

Figure 6.16: *CO, H, and OH mole fraction profiles versus time for different diluted systems at inlet temperature of* $1180K$ *and* $\phi = 1.5$.

Water promotion of OH radical formation

A lower concentration of H radical as well as higher OH radical yields can be seen comparing the N_2 and N_2/H_2O in figure 6.16. The presence of water promotes reactivity through the reaction

$$O + H_2O = OH + OH \qquad \text{(R12 revisited)}$$

producing OH radical. On the other hand, the higher collisional efficiency of water also enhances recombination and termination reactions. The transition between low reactivity and near complete methane conversion, is firmly ruled by the competition between radical formation and termination reactions. Therefore, the different bath gases influence the relative importance of OH and HO_2 radicals.

Although the relative formation of these radicals is mainly governed by the two competing $H + O_2$ reactions, on the fly rate of production analysis depicts that also many other reactions are involved in OH formation, as well as in the shift between

intermediate and high-temperature chemistry. Figure 6.17 shows the relative contributions of key reactions to OH formation at intermediate temperatures for stoichiometric mixtures. Whereas at low temperatures OH radical is mainly formed through CH_3 radical interaction with O_2, between 1050 and $1150K$, the decomposition reaction of

$$H_2O_2 + [M] = OH + OH + [M] \tag{R20}$$

is the dominant path to OH. Indeed, HO_2 radicals attack methane and produce H_2O_2, together with

$$HO_2 + CH_3 = OH + CH_3O \tag{R16 revisited}$$

The large availability of HO_2 radicals from the third body reaction, increases the importance of H-abstractions on methane, forming H_2O_2. Obviously, the same channel produces CH_3, which also interacts with HO_2 forming OH. At temperatures above $1150K$, the chain branching reaction

$$H + O_2 + [M] = HO_2 + [M] \tag{R8 revisited}$$

becomes the dominant one and OH concentration drastically increases. The above reasons justify the switch in reactivity observed in Figure 6.14, where the addition of water increases oscillation periods at $T < 1150K$.

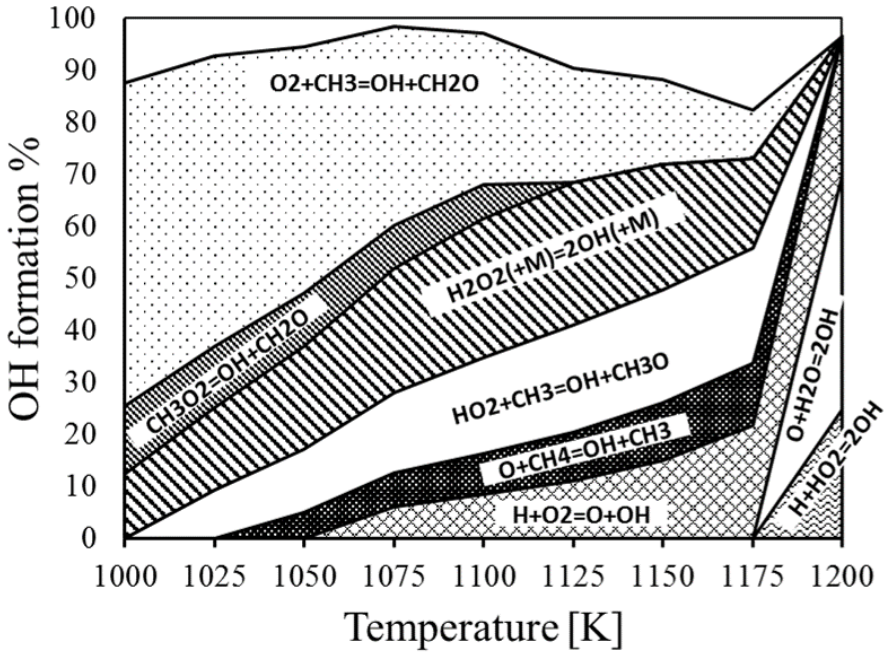

Figure 6.17: *Cumulative contribution of key reactions for OH formation at stoichiometric CO_2 diluted and intermediate temperatures ($T = 1000 - 1200K$).*

6.3.3 Starting and damping of oscillations

Rate of production analysis (ROPA) was carried out for both starting and damping points of oscillation in all the cases. Figure 6.18a and 6.18b outline two specific pathways for starting and damping temperature of oscillation in stoichiometric condition, respectively. In the lower limit of oscillation (starting), the key step is methoxy (CH_3O) formation through reaction

$$HO_2 + CH_3 = OH + CH_3O \qquad \text{(R16 revisited)}$$

This propagation reaction converts two stable radicals (HO_2 and CH_3) into two more reactive radicals (OH and CH_3O) and promotes the reactivity. The methoxy radical lifetime is very short, and as it forms, it decomposes rapidly to formaldehyde (CH_2O). Moreover, CH_2O mainly converts to HCO through H-abstraction by methyl radical, yielding methane.

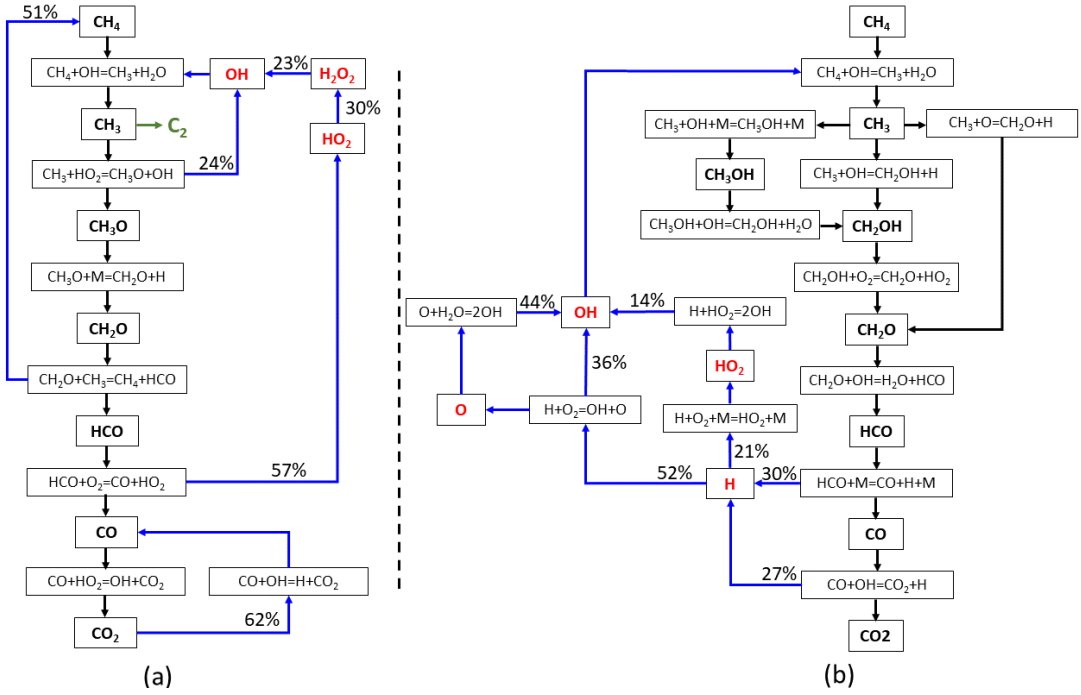

Figure 6.18: *Pathway analysis of stoichiometric conditions. (a). Starting point of oscillation; (b). damping point of oscillation.*

This sudden conversion of HO_2 to OH by reaction with CH_3 causes fast increase in OH concentration. Moreover, HCO interact with O_2, to form CO and HO_2. During oscillations, two different reactivities related to the short interval of the conversion from HO_2 to OH can be observed. In the upper oscillation limit (Figure 6.18b) methyl radical does not form methoxy (CH_3O), yielding formaldehyde directly or via hydroxymethyl (CH_2OH) decomposition. At higher temperatures HCO decomposes to H and CO, and CO therefore converts to CO_2 through

$$CO + OH = CO_2 + H \qquad \text{(R19 revisited)}$$

These two steps sustain H radical yields in the upper oscillation limit, leading to a stable solution. From figure 6.18 it is possible to observe that, the lower oscillation limit does not primarily involve in the competition between

$$H + O_2 = O + OH \quad \text{(R3 revisited)}$$

$$H + O_2 + [M] = HO_2 + [M] \quad \text{(R8 revisited)}$$

to form OH or HO_2, but as the temperature rises, the competition between these two channels becomes more important. The third-body reaction produces HO_2, which later through reaction of

$$HO_2 + H = OH + OH \quad \text{(R15 revisited)}$$

forms two OH radicals. This conversion affects the upper oscillation limit considering that HO_2 concentration is strongly third body dependent. Nevertheless, it was seen that the lower oscillation limit presents different reaction pathways for converting HO_2 to OH. These two pathologies for lower and upper oscillation limits are also valid for other stoichiometric conditions (N_2 and N_2/H_2O) for which the same analyses were carried out highlighting similar kinetic steps.

An implication of these results is that HO_2 plays a dominant role in MILD combustion, and transformation of this radical to OH causes a sort of instability. In contrast, pathway analysis (ROPA) of lean conditions shows that the main channel leading to OH in primary oscillation is $CH_3 + O_2$. These findings lead to a more generalized hypothesis to describe the oscillation phenomenon. It is clear that OH starts to be formed when the temperature is higher than $\sim$ 1100 K. At these temperatures the formation rate of OH is low; however, its consumption rate is high enough to completely consume OH radicals in a period shorter than its formation. Consequently,it can be concluded that transition from intermediate temperature to high-temperature region relates to OH formation, and this transition may endure for a specific range of temperature ($50 - 150$ K). As long as the transition lasts, the system is unable to shift to the high-temperature region, thus facing two competing regimes (intermediate and high temperature chemistry).

6.3.4 Intermediate to high temperature chemistry shift

In order to justify the interchangeable reactivity, a schematic of methane profile is shown in Figure 6.19. As can be seen from this figure, the system exhibits two conversion level ,high and low, with respect to the initial mixture during each period. The high conversion corresponds to high-temperature chemistry governed by OH radical, while low conversion is driven by intermediate chemistry specifically HO_2. The modulation between these two fast and slow chemistries is replicated over time, and this oscillatory behaviour is the unique solution of the system.

In order to better understand the effect of the shift between OH and HO_2 on oscillations, the reactivity factor (R_f) has been defined as the following ratio,

$$R_f = \frac{OH}{HO_2} \tag{6.3}$$

Following the above discussion, OH and HO_2 indicate high and intermediate temperature chemistry, respectively. The concentration of HO_2 is higher than OH at intermediate temperature chemistry ($R_f < 1$), and vice verse at high temperature ($R_f > 1$).

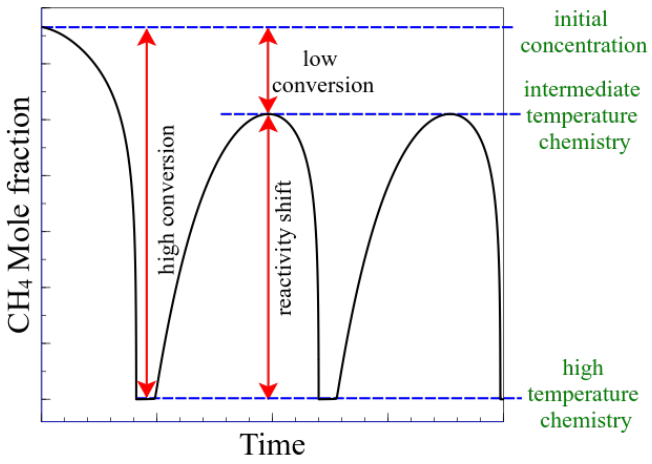

Figure 6.19: *Schematic of methane profile during oscillation indicating low and high conversion regions.*

Figure 6.20 plots both CH_4 profile and R_f versus time at three stoichiometric conditions and different diluent. Left axes show CH_4 concentration while the right axes present the value of R_f. A horizontal dashed line is added at $R_f = 1$ as a baseline to exemplify OH shift. From this figure, it is clear that when R_f is higher than unity, the system is more reactive. When the reactivity factor is higher than ~ 1, methane consumption is accelerated and the systems faces a complete conversion. Consumption of OH radical by the fuel is very fast and its formation requires building up of HO_2. Reducing R_f results in a less reactive system driven by HO_2 radical.

It should be highlighted that the R_f ratio is slightly higher in $N_2 + H_2O$ system and this due to a higher anOH formation. Thus, periods of oscillation are shorter, and accumulation of methane reaches a smaller peak. The reaction of

$$O + H_2O = OH + OH \qquad \text{(R12 revisited)}$$

works as a secondary chain branching reaction owing to the concentration of H_2O. This reaction together with the primary chain branching reaction,

$$H + O_2 = O + OH \qquad \text{(R3 revisited)}$$

work like an auto-catalytic step by forming of 3 OH radicals as follow

$$\begin{array}{c} H + O_2 = O + OH \\ H_2O + O = 2OH \\ \hline H + O_2 + H_2O = 3OH \end{array}$$

These figures confirms that oscillation has a strong dependency to high and intermediate temperature chemistry. Provided that the systems that here discussed are non-isothermal and the temperature of the reaction raises due to exothermicity with fuel conversion, it is not easy to decouple the two distinct effects. To clarify the association between intrinsic shift and oscillation, isothermal conditions with oscillatory behaviour from [128, 131] were also investigated. It is important to note that in these

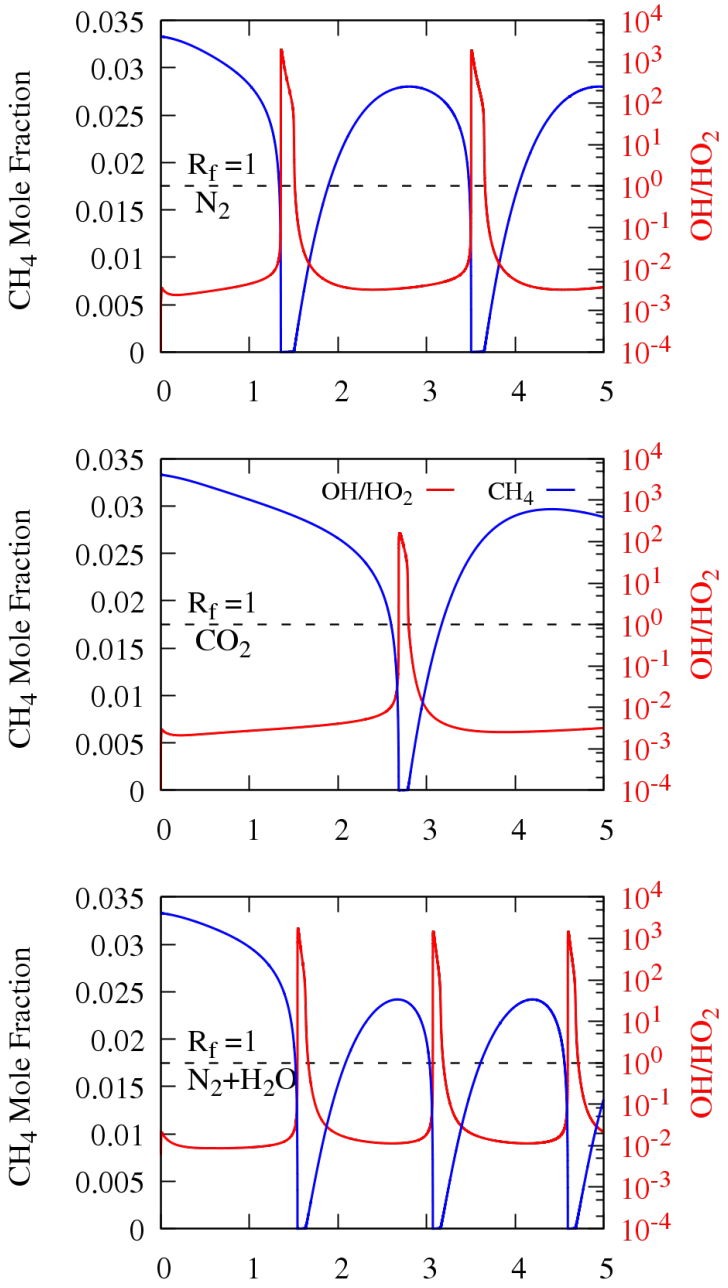

Figure 6.20: *Reactivity factor (red line) and CH_4 profiles (dashed blue line) of the stoichiometric cases versus time in the intermediate temperature $T = 1150K$.*

isothermal studies oscillation was not recorded; however, as shown in [133] an attempt at modelling these cases reveals the existence of the cyclic oscillatory behaviour.

Upper panel of Figure 6.21 presents CH_4, OH and HO_2 profiles of stoichiometric methane doped with ethane at isothermal an elevated pressure (P=10 atm) as in Ref [131]. Moreover, the lower panel shows the same profile in a distinct condition with neat methane at atmospheric pressure and lean condition ($\Phi = 0.3$). Despite the different initial conditions, these two figures presenting the similar competition be-

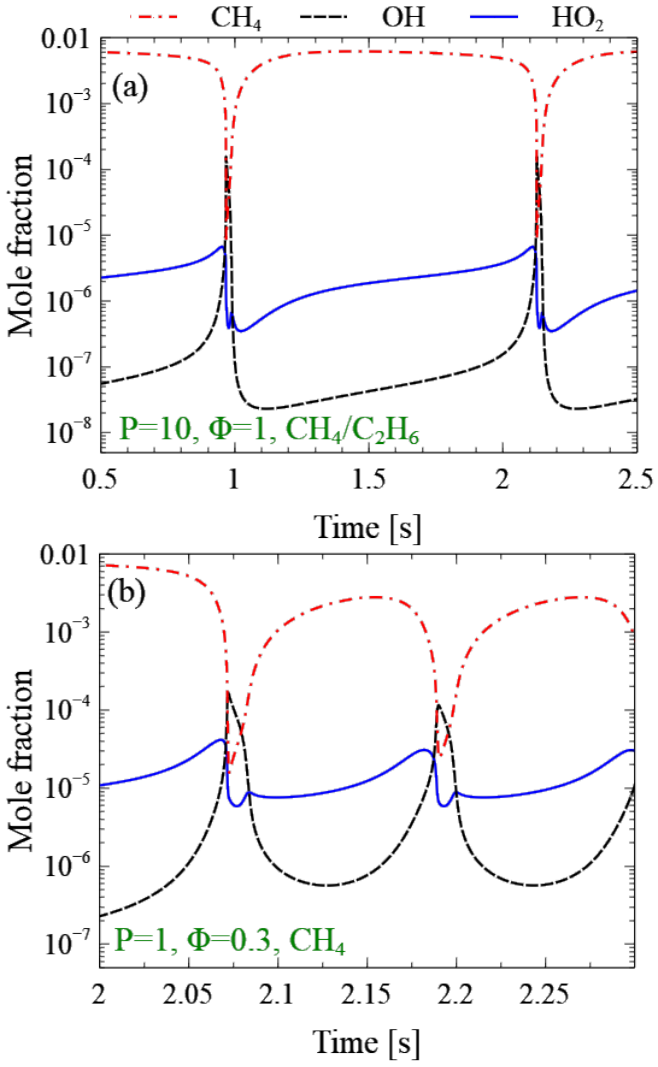

Figure 6.21: *Profile of Species in isothermal condition. Upper figure presents stoichiometric methane doped with ethane at elevated pressure (P=10 atm) and $T = 1200K$ [131]. Lower figure shows the neat methane at atmospheric pressure, lean condition ($\Phi = 0.3$) and $T = 1165K$*

tween OH and HO_2 as mentioned earlier. During slow conversion HO_2 concentration is higher than OH, HO_2 builds up in the system through reactions such as R8 and

$$O_2 + HCO = HO_2 + CO \qquad \text{(R21)}$$

As reported in figure 6.21 HO_2 concentration builds up the fast process forming OH radical. The direct transformation HO_2 to OH takes place faster than build up, through following reactions (figure 6.18);

$$HO_2 + H = OH + OH \qquad \text{(R15 revisited)}$$

$$O + HO_2 = OH + O2 \quad \text{(R22)}$$

$$HO_2 + CH_3 = OH + CH_3O \quad \text{(R16 revisited)}$$

Or depending on the condition HO_2 first forms H_2O_2 , and then H_2O_2 rapidly decomposes and accelerate the reactivity.

It is obvious that OH concentration increases, the system is dominated by high-temperature chemistry which consequently leads to the immediate consumption of the fuel. It should be noted that the significant amount of OH is consumed in this phase; however, its reformation through HO_2 requires another successive build up. These two regimes with interchangeable reactivity embrace all the above considerations referring to MILD combustion oscillatory behaviours.

6.4 Summary

This Chapter profoundly assessed MILD combustion from definition down to the kinetic reaction points of view. The map-classification of the MILD regime and extended discussion highlighted that the available definitions partly assess the boundaries of MILD combustion. Two interpretations of Premixed and non-Premixed flamelet relay on the apparent activation energy of global step reaction (E_{Global}) which is an artificial number with active dependency on pressure, temperature, and bath gases. As E_{Global} is fuel dependent determining E_{Global} could be very challenging especially when surrogate fuels or different bath gases are used. In contrast, autoignitive criterion exploits T_{auto} temperature, where it reasonably confines the lower limits of MILD by $T_{in} > T_{auto}$ which fairly excludes forced ignition. However, this criterion does not suitably limit maximum temperatures ($\Delta T < T_{auto}$).

One of the primary objectives of this study presented in this chapter; to evaluate a vast amount of experimental data on MILD combustion of methane that have been reported in recent years, to analyse them by using a detailed kinetic mechanism and thereby to identify aspects of the mechanism requiring further revision. Moreover, the validation targets of the CRECK core mechanism, which is developed upon Aramco 2.0 [63] proving its reliability also for unconventional combustion conditions, which were not included in the extensive validation reported by Metcalfe et al. [51]. However, the aim is not only the mechanism validation but also a better understanding of the combustion characteristics and critical reaction pathways.

- The kinetic analysis presented in this Chapter allows summarising the following major peculiarities. At low and intermediate temperature, H_2O and CO_2 dilution reduce the system reactivity. The effect of H_2O is more relevant. This is mostly due to chemical effects related to enhanced third body collisional efficiencies that favour chain termination over branching pathways, at the operating conditions of JSR experiments. Additionally, it is highlighted that the inhibition effect vanishes for increasing pressure, as expected because of the rate constant is gradually approaching the high-pressure limit.

- The chemical effect of water gradually vanishes at high temperatures ($1300 - 1400\,K$) in the flow reactor. This behaviour is due to the transition to the hot

ignition regime, occurring according to the sequence $HO2 \rightarrow H2O2 \rightarrow OH + OH$.

- Oscillations in MILD combustion occur where the system reactivity is sufficient to promote ignition, but not high enough to sustain complete fuel conversion. The transition from intermediate to the high-temperature region is dominated by OH formation, typically lasting for specific $50 - 150\,K$ temperature windows.

Finally, Despite the satisfactory agreement, model predictions in the case of water dilution could benefit from a more fundamental evaluation of collisional efficiency compared to the current value usually ranging between 6 and 12. However, recent research efforts are devoted to better a priori assessment of energy-transferring collisions and pressure dependent kinetics based on master equation simulations. A better description of relevant reactions proceeding through the formation of rovibrationally excited complexes will also benefit from the implementation of non-linear mixture rules.

CHAPTER 7

Oxy-fuel Combustion

ANOTHER advantageous technique is the Oxy-fuel combustion, which typically combines high purity oxygen ($> 95\%$) [9] with recycled exhaust gases, always aiming to control the maximum flame temperature. Burning fuel in oxygen and flue gas rather than air, of course, results in the elimination of NOx emissions and also favours the carbon dioxide sequestration from the exhausts.

7.1 Oxy-fuel definition

Oxy-fuel combustion is one of the leading technologies and is of interest for CO_2 capture and storage in power generation plants. Oxy-fuel is implemented by burning the fuel with nearly pure oxygen diluted with a large amount of recycled flue gas [193]. Various forms of Oxy-fuel combustion have been used in different applications even before the concern over CO_2 sequestration raised in the world energy scenario. Figure 7.1 (adapted from Chen et al. [9]) schematises various Oxy-fuel combustion conditions concerning the oxygen concentration and the preheating temperature of the reactants.

Zone I of this figure is the so-called air combustion and the air-like Oxy-fuel combustion zone, which involves a flue gas recirculation of $60 - 80\%$. In this way, the oxidizer usually contains less than 21% oxygen, and the flame temperature is controlled [9].

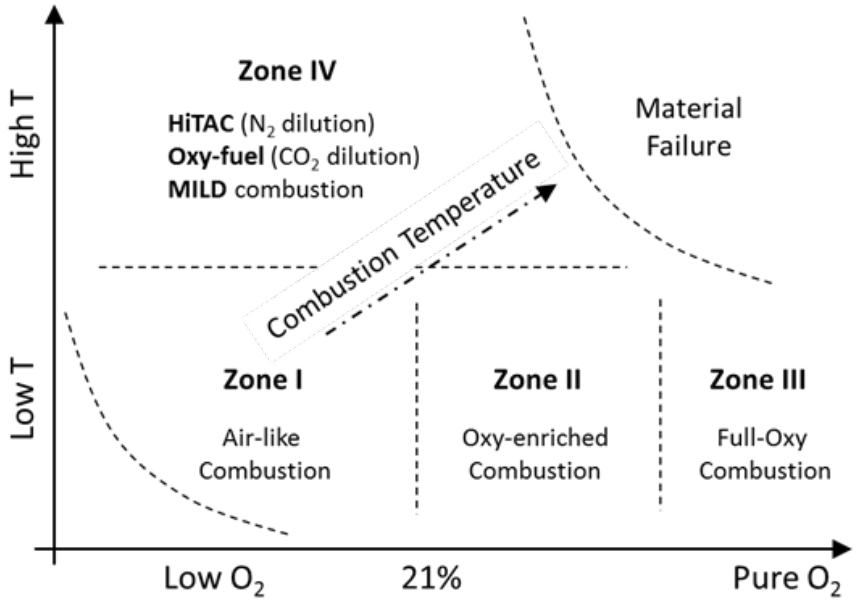

Figure 7.1: *Oxy-fuel, HiTAC, and MILD combustion regimes as a function of the oxygen mole fraction and the preheat temperature of the reactants (after [9]).*

Zone II is the oxygen-enriched combustion area, where the oxygen concentration is significantly higher than 21%. Thus, the oxygen-enriched combustion features a higher sensible enthalpy and a higher flame temperature.

Zone III is the full Oxy-fuel combustion, where pure oxygen is used as the oxidizer. In this regime, the dilution is reduced to zero, and the pure oxygen highly intensifies the flame structure and the maximum temperature [194].

Finally, the Zone IV depicts high-temperature Oxy-fuel combustion and HiTAC that can be achieved by using highly preheated oxidizer. It should be noted that MILD combustion is also embedded in this zone where stable combustion is still attainable with oxygen mole fraction significantly lower than 21%.

Both Figure 6.1 and 7.1 indicate the typical operating conditions of the new combustion technologies. Temperatures and oxygen concentrations can vary in a wide range, and particular attention is required for the effect of the high dilutions, not only N_2 but mainly CO_2 and H_2O. Truthfully, both water and carbon dioxide can have significant chemical effects, in addition to those related to their thermal properties.

7.2 Mechanism Validation and Oxy-fuel Combustion Characteristic

7.2.1 Flame Speed

The laminar flame speed is one of the most critical combustion properties of a fuel. It is a function of the thermodynamic state of the fuel/oxidizer mixture (pressure, temperature, and composition). The composition rigorously defines the net fundamental properties effects on diffusivity, reactivity, and exothermicity [30]. Mainly, the flame characteristics of Oxy-fuel combustion are different from the ones of the conventional combustion. The effect of H_2O and CO_2 addition on premixed Oxy-fuel combustion

was systematically investigated by Mazas et al. [160]. They examined the effect of the oxygen enrichment ratio, equivalence ratio, and H_2O addition on N_2 and CO_2 diluted mixtures. Mazas et al. [160] highlighted a quasi-linear decrease in the laminar flame speed of $CH_4/O_2/N_2/H_2O$ and $CH_4/O_2/CO_2/H_2O$ by increasing the water addition. These experimental data are useful for the mechanism validation at high flame temperatures. A selected set of data is here discussed, whereas more information can be found in the supplementary material.

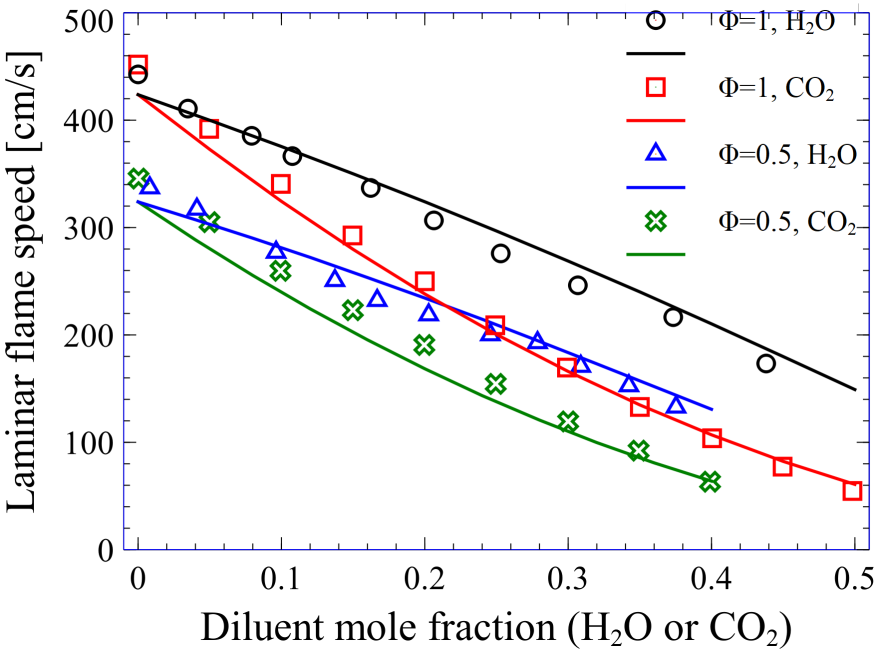

Figure 7.2: *Laminar flame speed of $CH_4/O_2/H_2O$ and $CH_4/O_2/CO_2$ mixtures, for $\Phi = 0.5$ and $\Phi = 1$ at $T_{in} = 373K$ and atmospheric pressure. Symbols refer to experimental data [160] and lines to model predictions.*

Figure 7.2 compares the experimental and predicted effect of H_2O and CO_2 dilution in full Oxy-fuel combustion (CH_4/O_2) for lean ($\Phi = 0.5$) and stoichiometric ($\Phi = 1$) mixtures. It is apparent from this figure that CO_2 has a more distinguishable effect on laminar flame speed reduction comparing to H_2O. The more substantial effect of CO_2 dilution is well captured by the model and is mainly due to the lower flame temperature, because of the higher heat capacity of CO_2.

Thermochemical properties of CO_2 and H_2O are different from those of N_2, and their involvement in the reaction system can change the flame temperature, the laminar flame speed, and other characteristics of high-temperature combustion. Thus, CO_2 and H_2O dilution can change the system reactivity not only because of chemical effects, but also due to their thermal properties. Indeed, the physical effect of the diluent occurs by altering heat capacity, transport properties, and thermal diffusion of the reacting system, whereas the chemical effect is the result of the intrinsic reactivity of CO_2 and H_2O in the system. In order to distinguish between chemical and physical effects on system reactivity, it can be convenient to repeat the simulations of the CO_2* and H_2O* diluted systems by using dummy inert species with the same thermal properties of the real species (CO_2 or H_2O), but not involved in the reaction mechanism [127, 192] [50,58].

The simulation results obtained by using the dummy diluents (CO_2* and H_2O*) will permit to highlight the physical effect.

Mazas et al. [160] also reported experimental data of premixed laminar flame speeds of $CH_4/O_2/N_2/H_2O$ systems with three different H_2O addition ($XH_2O = 0.0, 0.1$ and 0.2) in the range of equivalence ratio $0.6 - 1.6$. Figure 7.3(a) shows the good agreement between model predictions and experimental data. The water addition reduces the flame speed over the entire equivalence ratio range. Dashed lines in Figure 7.3(a) indicate the predictions obtained by using the dummy species (H_2O*) to distinguish the physical from the chemical effects. The superimposed profiles highlight that the physical effects of water are here prevailing over a very weak chemical effect.

Despite the very limited chemical effect, Figure 7.3(b) provides the sensitivity analysis of the laminar flame speed at $\Phi = 1$ for the various H_2O dilutions. As discussed by Ranzi et al. [30], the chain branching reaction R3 is the key step in all the combustion systems, and any active channel that competes with R3 and reduces H radical concentration results in diminishing overall oxidation rate. Namely, the third body reactions R8 and R9 directly compete with reaction R3, inhibiting the reactivity, and suppressing the flame speed.

$$H + CH_3 + [M] = CH_4 + [M] \qquad \text{(R9 revisited)}$$

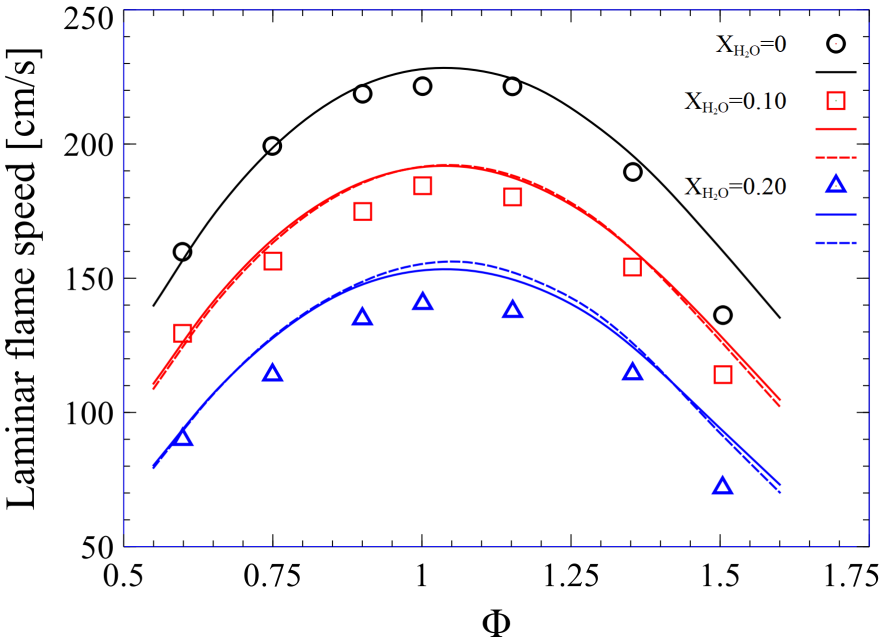

(a)

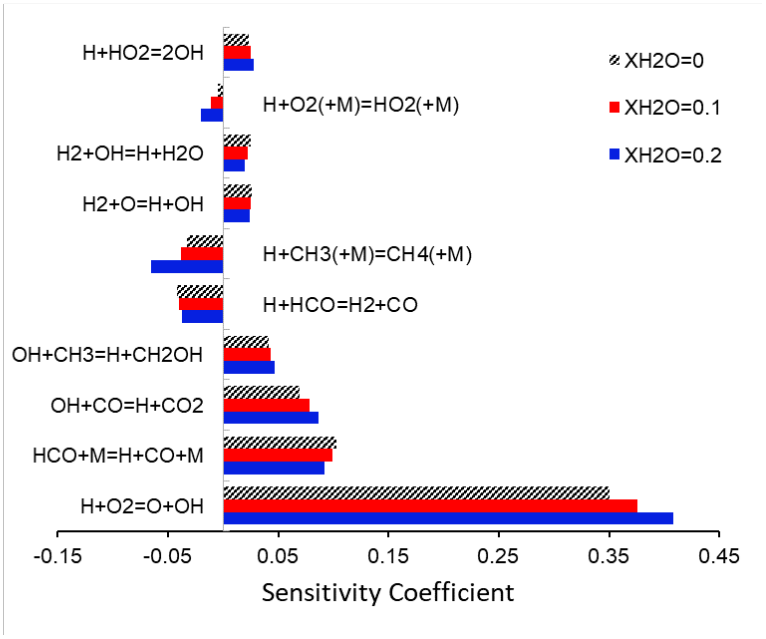

(b)

Figure 7.3: *(a) Enriched laminar flame speed of CH_4 ($O_2/N_2 = 1$) diluted with $0, 10$ and $20\%H_2O$ at $T_{in} = 373K$ and atmospheric pressure. Symbols refer to experimental data [160], solid and dashed lines refer to model predictions with H_2O and dummy H_2O*. (b) Sensitivity analysis of the laminar flame speed at the stoichiometric condition.*

This recombination reaction works as radical sinks affecting flame speed and the ignition delay time of practically all the hydrocarbons and oxygenated fuels. As earlier discussed, a higher H_2O collision efficiency possibly could slightly reduce the model

deviations as water addition increases. Both R8 and R9 have been widely studied, both experimentally and theoretically; however, uncertainties still exist in the first principle assessment of collisional efficiencies [98, 99, 101, 195].

Recently, laminar flame characteristics of methane Oxy-fuel combustion highly diluted with CO_2 were experimentally analysed by Xie et al. [161] inside a constant volume chamber. They measured the laminar flame speed of various CO_2 dilution systems at three different pressures (1, 2 and $3[atm]$). Figure 7.4(a) satisfactorily compares experimental data with model predictions and highlights the strong effect of CO_2 additions. The dashed lines show the predictions obtained by using the dummy species (CO_2*). Although the physical effect of CO_2 dilution results in a substantial reduction of the flame temperature, it is relevant to observe that there is also a critical inhibiting effect of CO_2, mainly in stoichiometric conditions, due to the reaction R19.

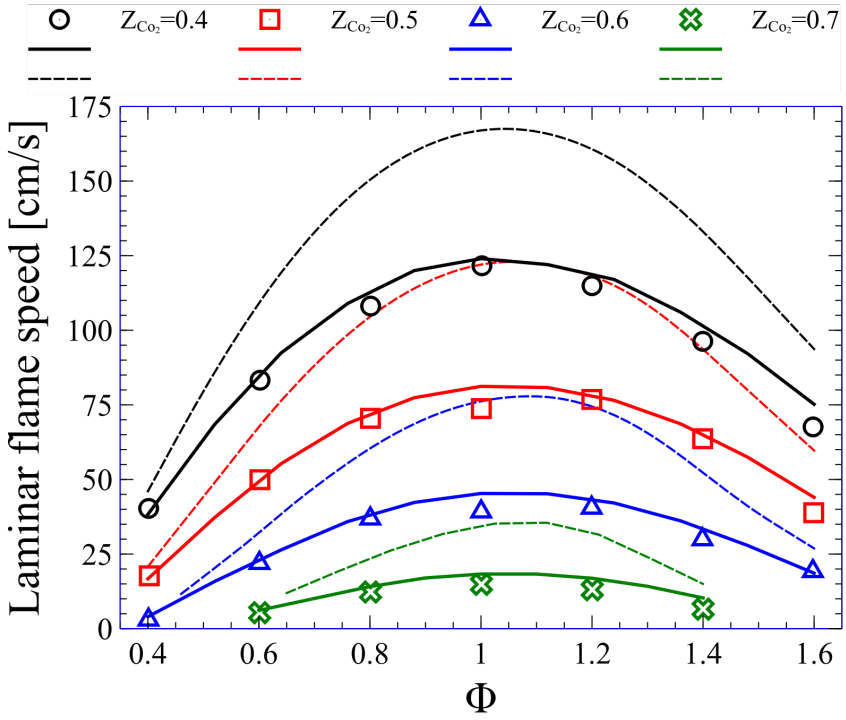

(a)

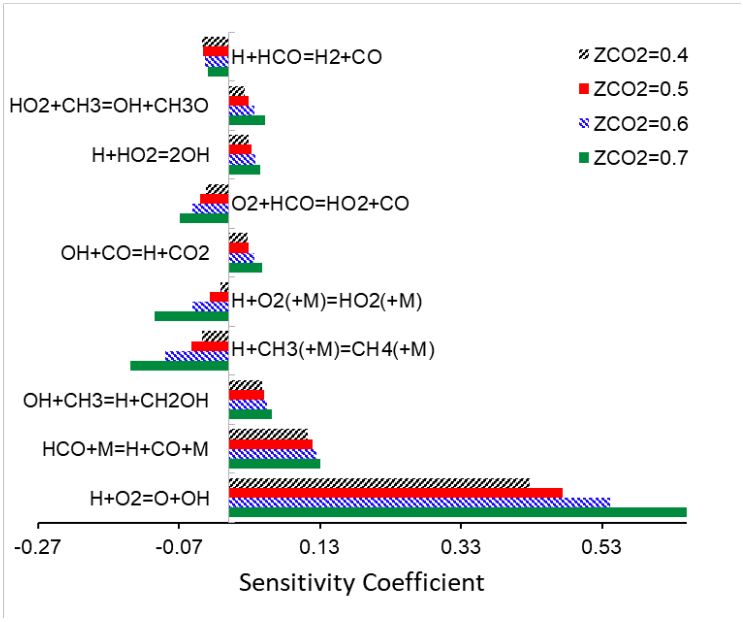

(b)

Figure 7.4: *(a) Laminar flame speed of $CH_4/O_2/CO_2$ mixtures at $T_{in} = 300K$ and atmospheric pressure. CO_2 mole fraction is defined by $Z_{CO_2} = X_{CO_2}/(X_{CO_2} + X_{O_2})$ Symbols refer to experimental data [161], solid and dashed lines are model predictions with reactive and non-reactive CO_2. (b) Sensitivity analysis on the laminar flame speed of the different cases of the panel (a) at $\Phi = 1$.*

To better assess the effect of CO_2 dilution on the flame speed, Figure 7.4(b) presents the sensitivity analysis to laminar flame speed for the four different dilutions at $\Phi = 1.0$. Similar to the previous analysis, the chain branching reaction R9 has the highest sensitivity coefficient, and CO_2 addition further increases its importance. The sensitivity coefficients of third body reactions R8 and R9), at different CO_2 dilutions, shows the increasing importance of these reactions in the reduction of the flame speed. Higher third body efficiency of the R8 favours HO_2 formation and the propagation reactions:

$$HO_2 + H = OH + OH \qquad \text{(R15 revisited)}$$

$$HO_2 + CH_3 = CH_3O + OH \qquad \text{(R16 revisited)}$$

become more sensitive at higher CO_2 dilution.

Another example of the chemical effect of CO_2 dilution on the laminar flame speed, a $CH_4/O_2/CO_2$ system is analysed in the whole range of equivalence ratios, at different pressures (1, 2 and $3atm$) and $T_{in} = 300K$. The CO_2 fraction inside the $CH_4/O_2/CO_2$ mixture, defined as $X_{CO_2}/(XCO_2 + XO_2)$, is equal to 0.5. Figure 7.5(a) presents the comparison between experimental measurements of laminar flame speeds [161] and model predictions. Solid and dashed lines indicate the model predictions with reactive CO_2 and non-reactive CO_2* dilution, respectively. At higher pressures, the flame speed diminishes, mainly because of a more substantial influence of the third body recombination reactions.

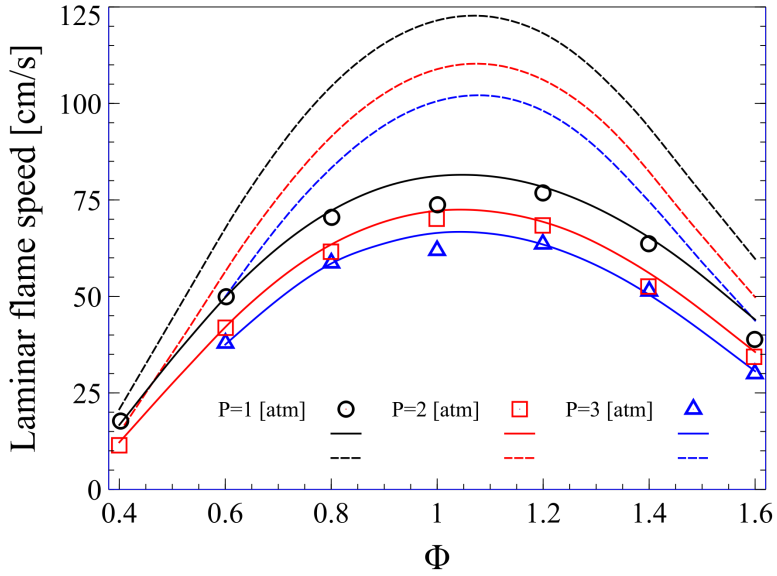

(a)

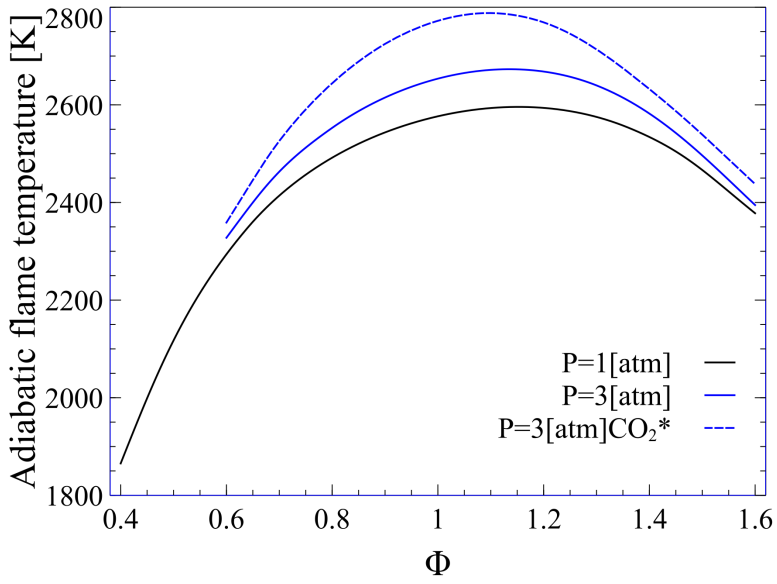

(b)

Figure 7.5: *(a) Laminar flame speed of $CH_4/O_2/CO_2$ mixtures at 1,2 and $3atm$ and $T_{in} = 300K$. CO_2 mole fraction is defined by $ZCO_2 = XCO_2/(XCO_2 + XO_2)$. Symbols refer to experimental data [161], solid and dashed lines are model predictions with reactive and unreactive CO_2*. (b) Adiabatic flame temperatures at 1 and 3 atm. Lines are model predictions with reactive (solid) and unreactive CO_2 (dashed).*

Figure 7.5(b) presents the predicted adiabatic flame temperature at 1 and $3[atm]$. As expected, because of the lower importance of the endothermic dissociation reactions, the adiabatic flame temperature increases, when pressure increases. Correspondingly, despite the decrement in laminar flame speed at higher pressures, the burning velocity of the mixture increases [27]. Moreover, from Figure 12(b) it is possible to see

a significant temperature rise, when working with the non-reactive (CO_2*) dilution. Besides the considerable importance of recombination reactions, model predictions indeed show that CO_2 dilution globally promotes the endothermic reverse of the water gas shift reaction:

$$CO + H_2O = CO_2 + H_2 \qquad \text{(R18 revisited)}$$

This feature additionally reveals the explanation of the predicted higher flame temperatures within the unreactive (CO_2*) dilution.

7.2.2 Ignition Delay Time

Optimal operating conditions to design industrial burners and devices require a thorough assessment of chemical time scales (typically the ignition delay time) and autoignition temperatures. Thus, industrial applications of new combustion technologies ask for the identification of optimal operating conditions to obtain high efficiency and to lower pollutant emissions. The ignition delay time is an intrinsic characteristic ruled by fuel chemistry, driving the assessment of optimal operating conditions and the definition of key parameters such as the times scales needed to establish combustion within the mixing layer or the length limitation in combustor design [176].

7.2.3 Ignition Delay Time in Shock Tube

Shock tube reactors are a nearly ideal device, which has been and is an integral part of the ignition delay time measurement in combustion researches. Exhaust gas recirculation (EGR) in Oxy-fuel combustion involves a large amount of CO_2 and H_2O. Thus it strongly modifies the reacting system regarding kinetic and thermal effects. Shock tubes may encounter many flows field non-idealities in the presence of polyatomic molecules (CO_2 and H_2O); however, this behaviour is not exclusive to specific bath gases, and different gases can similarly cause bifurcation in shock tubes [162]. As a result, a limited number of shock tube studies considering CO_2 as bath gas can be found in the literature [162, 163, 196–198].

Figure 7.6 shows the ignition delay times of different $CH4/O2/CO2$ mixtures ($\Phi = 0.5$ and 1) at 1 and $4atm$ measured in a shock tube [162]. Mixtures are diluted with $30\%CO_2$. At a given pressure, the ignition delay times of the lean mixtures are shorter than those of stoichiometric concentrations. The pressure rise also shortens the ignition time by a factor of $\sim 3-5$; furthermore, this behaviour is also more noticeable at lower temperatures. The difference between the lean and the stoichiometric mixture increases from ~ 10 to $sim20\%$ moving to higher pressures. The kinetic mechanism accurately captures both of these trends, as well as the variations of the apparent activation energy of these data. In fact, by raising the pressure from 0.77 to $3.85atm$, the apparent activation energy moves from $52000cal/mol$ to $47000cal/mol$, with limited dependence on the stoichiometry.

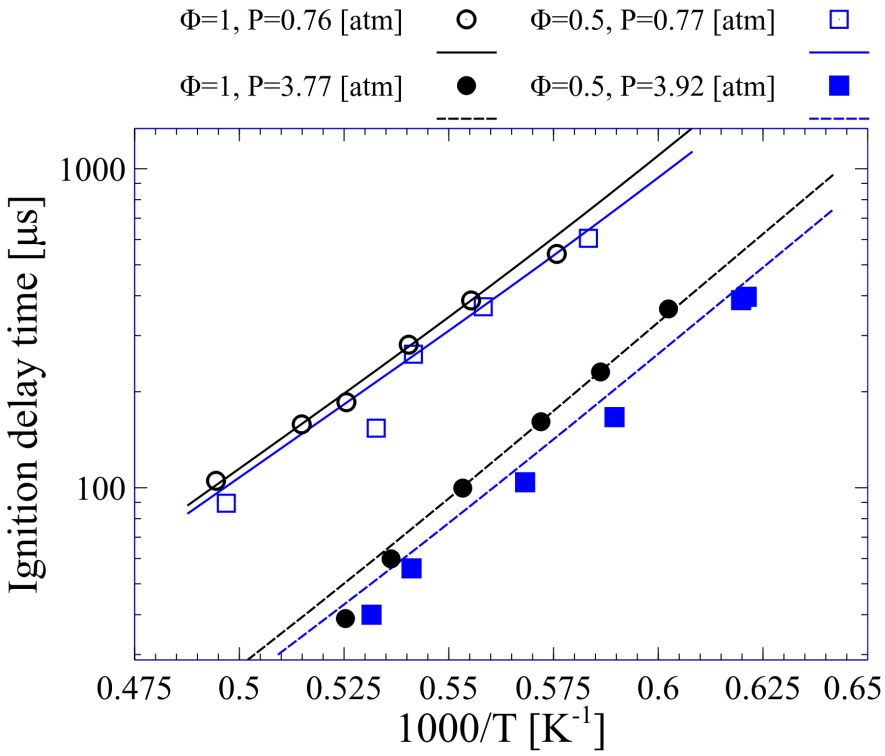

Figure 7.6: *Comparison of ignition delay times at two different pressure* 0.77 *and* $3.85[atm]$ *and stoichiometric and lean mixtures (*$\Phi = 0.5$ *and 1) diluted with* $30\%CO_2$*. Experimental data refers to [162].*

Hargis et al. [163] performed experimental measurements of methane ignition delay in the presence of CO_2 in a shock tube. Figure 14 compares experimental ignition delay times with model predictions alongside with the effect of CO_2 addition (0, 25, 50 and 75%), at $1.75atm$. These results demonstrate that the CO_2 dilution plays only a negligible role in the ignition delay times, under the investigated conditions. Moreover, the differences of the ignition delay time of all the mixtures seem very marginal, within the uncertainty of the measurement. This similarity in the ignition delay times highlights that CO_2 is scarcely reactive during the ignition, because of its stability, and does not actively modify the pool of radicals. In contrast, a minimal increase in predicted ignition delay times can be observed at low temperatures. These small variations seem to indicate a limited effect of the third-body efficiency of CO_2 on the ignition mechanism.

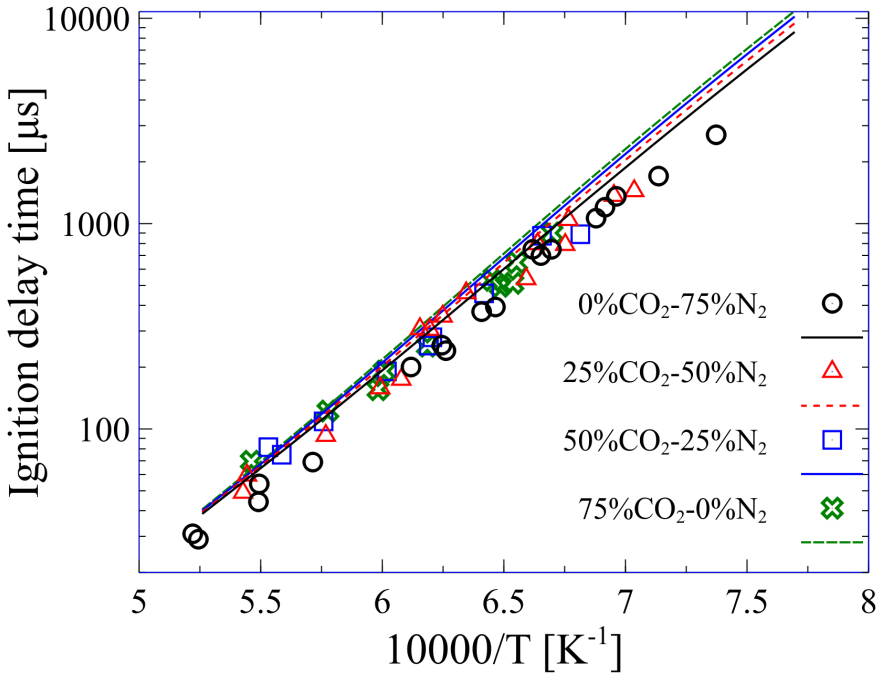

Figure 7.7: *Ignition delay times for a lean mixture ($\Phi = 0.5$) in various CO_2 dilution levels at $1.75atm$. Experimental data refers to [163].*

In this regard, it is important to underline that the collisional efficiencies of different colliders are not always well characterised, and they are often treated empirically as the dependency of the collisional energy transfer on temperature, bath gas, and chemical structure of reactant are not fully understood. Jasper et al. [101] extended a theoretical characterisation of the collisional energy transfer in master equation simulations of methane dissociation for combustion applications. They pointed out that collision efficiencies can vary with the temperature; however, the trend of these variations depends on the chemical structure of bath gases. This temperature dependency is stronger for lighter bath gases (He and H_2), while polyatomic gases have the weakest temperature dependence (H_2O and CH_4).

7.3 Summary

Oxy-fuel combustion is one of the leading technologies and is of interest for CO_2 capture and storage in power generation plants. it is implemented by burning the fuel with nearly pure oxygen diluted with a large amount of recycled flue gas ($60 - 80\%$). Mainly, the flame characteristics of oxy-fuel combustion are different from the ones of the conventional combustion. Oxy-flame is a function of the thermodynamic state of the fuel/oxidizer mixture and diluent (pressure, temperature, and composition). The composition rigorously defines the net fundamental properties effects on diffusivity, reactivity, and exothermicity.

it is important to highlight that physical or chemical effect of diluent on the reactivity, laminar flame speed, ignition delay time, and formation of products are strongly dependent on the operating conditions (temperature, pressure, and equivalence ratios). Therefore, the analysis of the dilution effects is very case sensitive, and the contribution of each characteristic may vary accordingly.

The kinetic analysis presented in this Chapter allows summarising following major features.

- H_2O and CO_2 additions greatly reduce laminar flame speeds, and here the CO_2 effect is more relevant. This effect is mostly related to thermal effects in the case of water, and a combination of thermal and radical scavenging effects in the case of CO_2. For these reasons, CO_2 has the highest impact in inhibiting flame propagation.

- At high-temperature conditions, the effect of CO_2 addition on methane ignition delay times is very marginal as its stability does not allow to affect ignition chemistry. This is justified by the broader temperature range involved in the propagation of a laminar flame, concerning shock tubes ignition measurements, where the reactivity is mainly sensitive to the reflected shock conditions.

An important implication of this section is that at the current state of mechanism development, the level of accuracy is limited by the uncertainty in third body efficiencies; thus, there can be more rooms for improving third body efficiencies in the future study of combustion kinetic mechanisms.

CHAPTER 8

Third-body Efficiency

8.1 Introduction

DETAILED Kinetic mechanisms characterising the combustion of hydrocarbons generally contain only three classes of reactions:

- Unimolecular reactions
- Bimolecular reactions
- Termolecular association reactions

where in termolecular reactions, the third molecule is an unreactive collider that allows energy transfer through collisions to/from the reactive bimolecular complex [199]. The reverse form of any radical-radical recombination is a unimolecular decomposition reaction. In a unimolecular decomposition the third body provides activation energy, while in the reverse reaction, it absorbs excess energy. When the unimolecular reaction is in the second order region, the recombination is third order with energy transfer being rate determining for both. The collisional activation (see Section 2.4.2) is rate determining step more likely at lower temperatures, low pressures and for small radicals, corresponding to the requirements for a third body in the decomposition reaction.

It is well grasped that low-pressure limit of pressure dependence reactions has a strong collision dependency. However, in most of the kinetic mechanisms, the collision efficiencies of different colliders are not well characterised, and they are usually treated empirically. Due to the fact that the dependency of the collisional energy transfer on temperature, bath gas, and chemical structure of reactant are not fully understood.

- **Pressure effect:** On a physical basis, it is more likely that collisional activation is faster than the reaction at high pressures due to a higher probability of collisions and more molecules around. However, at the low-pressure chance of occurring collision is lower due to having less molecules around, and then collisional activation is now slower than reaction step (see Section 2.4.2).

- **Complexity of the the reactants structure:** The number of atoms in the molecules determines the number of normal modes of vibration available for the molecule. The critical energy will be accumulated in the normal modes of vibration, thus, the more complex the structure of the molecule the higher the number of modes over which this energy can be spread. It is well-known that the reaction is a consequence of a bond breaking where only specific modes will contribute vibration to this bond. The reactants with a more complex structure and a more significant number of normal modes face difficulties in energy flowing into the critical coordinate, and the time lag between reaction and collisional step will be longer. Therefore, for the complex molecule, the reaction step is more likely to be the rate-determining step [200].

  On the contrary, small molecules have a fewer normal mode where the critical energy can be spread, and it is more presumable that the required critical energy flows into to the critical coordinate. Hence, it is likely that in smaller molecules collisional activation will be rate determining step.

- **Temperature effect:** The temperature effect is associated with the increase in the fraction of high energy molecule at higher temperatures. At higher temperatures, the activation is more likely to be faster than reaction . Thus, the higher the temperature, the more likely it is that the reaction will be rate determining step [200].

- **Bath gas:** The collisional energy transfer of the polyatomic bath gases is likely to be higher than atomic or diatomic colliders. Moreover, collision efficiencies vary with temperature; however, the trend of these variations depends on the chemical structure of bath gases. This temperature dependency is stronger for lighter bath gases (He and H_2) while polyatomic gases have the weakest temperature dependence (H_2O and CH_4) [101].

Despite the satisfactory model prediction and good agreement shown in Chapter 5, 6 and 7, this chapter presents an in-depth discussion regarding the role of third-body efficiency in the future improvements of the kinetic mechanism. By implementing the Brute-Force approach, more fundamental evaluation of collisional efficiency will be carried out. Moreover, it will be revealed how the Kinetic mechanism could benefit from more accurate third-body coefficients, especially in the case of different bath gases (H_2O and CO_2).

8.2 Effect of Third-body Efficiency

In the low-pressure limit of a unimolecular reaction, the reaction rate is proportional to the collision activation of the bath gas and is consequently proportional to the pressure

of the bath gas. Formally, the relative collision efficiency with which different bath gases promote a unimolecular reaction can be expressed as the ratio of the low-pressure limit rate k_0 ($k_{0,M}/k_{0,R}$ where R is the chosen reference bath gas, and it is usually N_2 or Ar) [201].

8.2.1 $H + O_2(+M) = HO_2(+M)$

The competition between chain branching reaction

$$H + O_2 = O + OH \tag{8.1}$$

and collisional stabilisation to H_2O in

$$H + O_2(+M) = HO_2(+M) \tag{8.2}$$

is of primary importance to combustion, with these reactions showing up prominently in sensitivity plots for all fuels [202]. Recently, the effect of the collider on the pressure dependence of reaction 8.2 has been revisited Burke and Song [203]. This collider dependence is usually important, though particularly in modelling exhaust gas recirculation (EGR) [204, 205], Oxy-fuel [206], and MILD combustion [146] schemes, where the mole fraction of multiple colliders other than N_2 are raised.

Several systematic studies concerning the chemical and physical effects of bath gases on promoting or inhibiting reactivity as well as the concentration of the products are available in the literature [129, 207–212]. However, the evaluation of third-bodies effects on combustion and oxidation, which can also be considered as a physical effect is limited [80, 213]. Thus, in the following paragraphs, a few cases from the collected database will be analysed, in order to extend the knowledge and also highlight the necessity of defining more accurate third-body efficiencies.

Figure 8.1 presents a comparison of different methane profiles predicted by the model with and without third-body modification. More information about the experiment and initial conditions can be found in section 6.2.1. In this figure, solid lines show the model prediction without any third-body adjustment, where the dashed lines show the model prediction with modified third-body efficiencies for CO_2 and H_2O in the reaction of 8.2. The default third-body coefficients of CO_2 and H_2O in the Kinetic mechanism are 3.8 and 10, respectively, which adopted from Aramco.2 [51]. These values are increased by a factor of two ($\times 2$) to evaluate their effects in reactivity, and dashed lines in Figure 8.1 present the predictions. As it was expected, as well as explained in Section 6.2.1, increasing the third body efficiencies of reaction 8.1, strongly reduces the reactivity in intermediate temperatures. Doubling the coefficients results in $\sim 20\,K$ delay in the methane concentration profiles in this specific condition.

In a detailed analysis for the stabilization reaction 8.2, Klippenstein and coworkers [202] highlighted the effect of different colliders (Ar, N_2, and He) on the predicted pressure dependence. The collisional energy transfer parameters were obtained from trajectory calculations employing analytic potentials based on fits to high-level ab initio data. As shown in Figure 8.2, their predictions of the $H + O_2(+Ar)$ recombination reaction illustrates a good agreement at a wide range of temperatures compared to the accessible experimental data [214–217] relevance to combustion.

As stated by the authors, these prior predictions for N_2 and He colliders also exhibit similar levels of agreement with the slightly more limited experimental data. Moreover,

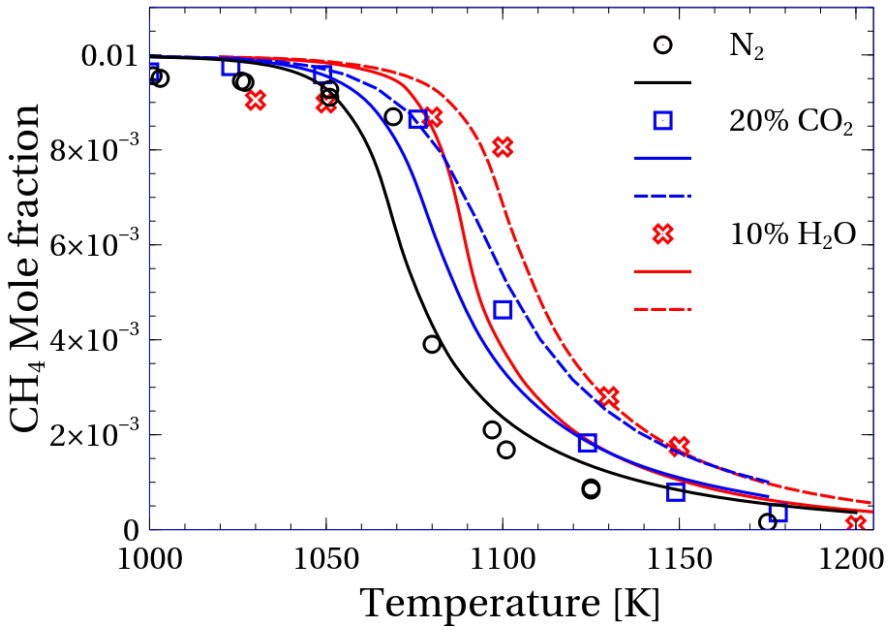

Figure 8.1: *Comparison of the methane conversion profiles at atmospheric pressure and ultra-lean conditions ($\Phi = 0.1$). Symbols refer to [127, 129], solid line is the model prediction with original third-body coefficients, and the dashed lines represent the prediction with modified third-body efficiencies of CO_2 and H_2O in reaction of $H + O_2(+M) = HO_2(+M)$.*

they are in the process of continuing this analysis to study H_2O as a collider, which is of practical importance since the high concentrations of H_2O in some combustion environments, linked with its enhanced efficiency, makes it a key contributor to the stabilization of HO_2. Their Preliminary results suggest that H_2O has a substantially enhanced collision efficiency, but apparently not as enhanced as is commonly ranged in the kinetic mechanisms (6 to 16). To sum up, there is still a lack of systematic study of CO_2 collisional energy transfer and further work should also consider the collision efficiency of CO_2.

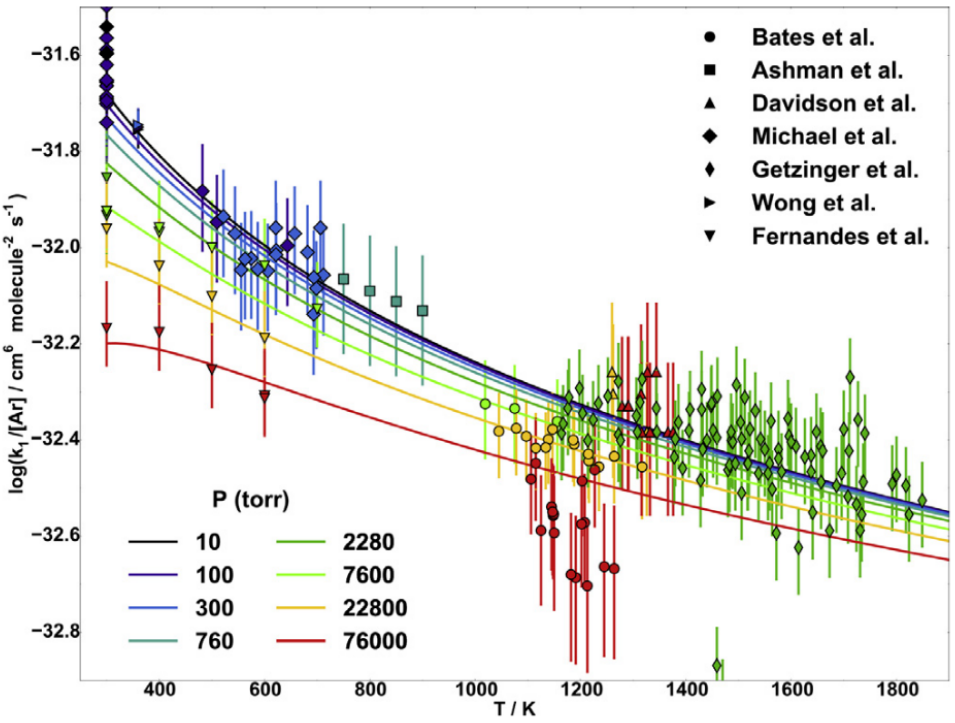

Figure 8.2: *Temperature and pressure dependence of predicted and observed rate constants for $H + O_2(+Ar) = HO_2(+Ar)$. The different colored lines denotes the Klippenstein and coworkers [202] priori trajectory energy transfer based 2DME predictions for the pressures denoted in the label. The experimental data points [214–220] are color coded according to the closest corresponding pressure from the theoretical analysis. Adopted from [202]*

8.2.2 $HCO(+M) = H + CO(+M)$

Formyl radical, HCO, is an important species that plays an abundant role in the oxidation of hydrocarbons. The combustion mechanism for the oxidation of simple hydrocarbon fuels to CO/CO_2 proceeds through formaldehyde, CH_2O. In turn, CH_2O primarily reacts through exothermic reactions [221],

$$H + CH_2O = H_2 + HCO \qquad (\Delta_{0K} = -16.6 kcal/mol) \tag{8.3}$$

$$OH + CH_2O = H_2O + HCO \qquad (\Delta_{0K} = -30.9 kcal/mol) \tag{8.4}$$

resulting in HCO formation. Flame simulations by [222, 223], have highlighted the particular importance of these two $CH2O$ destruction reactions, observing that the main product, HCO, had strong correlations with local heat release rates in CH_4 flames. HCO, in turn, is often consumed through three major competing pathways,

$$HCO(+M) = H + CO(+M) \tag{8.5}$$

$$HCO + O_2 = HO_2 + CO \tag{8.6}$$

$$H + HCO = H_2 + CO \tag{8.7}$$

Reaction 8.5 is a chain propagating reaction, producing an H radical, which feeds possibly the most critical reaction in combustion, the chain branching reaction 8.1. The competition between the propagation reaction 8.5, and termination reactions 8.6 and 8.7, defines the net rate of production of H-radical and therefore affects predictions of hydrocarbon laminar flame speeds [30]. While the rate constant for reaction 8.5 has considerable uncertainty due to the significant prompt dissociation at $T > 1000$ as well as limited data on the third-body collisional energy transfer [221].

Table 8.1 outlines a list of H_2O and CO_2 third-body coefficients in various kinetic mechanisms for reaction 8.5. As can be seen, the CO_2 third-body differs from 2 to 5, while most of the mechanisms implement value in the range of $2 - 3$. However, the value of third-body coefficients are more diverse for H_2O, and it varies between 0 to 15. Large variation in third-body efficiencies of H_2O clearly states the high level of uncertainty associated with H_2O collision efficiency, simply due to the lack of knowledge required for the assessment. Moreover, in the following paragraphs, it will be shown that how the change in third-body efficiencies by a factor of 2 (in the range of deviation presented in Table 8.1) can affect the laminar flame speed predictions.

Table 8.1: *List of H_2O and CO_2 Third body efficiencies in various kinetic mechanisms for reaction 8.5.*

Mechanism	H_2O	CO_2	Reference
GRI3.0	0	2	[44]
Polimi-1412	5	3	[30]
JetSurf2.0	0	3.6	[49]
DTU	15	5	[55]
LLNL	5	3	[224]
San Diego	12	2.5	[225]
Aramco	6	2	[51]
ELTE optimised	12	2	[226]
Blanquart	0	3.6	[227]

In order to better clarify the effect of third-body efficiency in the HCO decomposition reaction, Figure 8.3 present the laminar flame speed predictions with and without modified third-body efficiencies. More information about these laminar flame speed of Oxy-fuel combustion can be found in section 7.2.1. In this figure, solid line presents the laminar flames predicted with third-body efficiency of 6 and 2 for H_2O and CO_2, respectively, while the dashed lines show the $\times 2$ third-body coefficients ($M_{H2O} = 12$ and $M_{CO2} = 4$). In the first place, It may not be observed that the effect is not significant; however, it is not true, and the increase of flame speeds is in the range of 7 to $15\,cm/s$. The relative deviation of the flame speeds without dilution is $\sim 3.3\%$, while by increasing the level of dilution to 50% the relative deviation increases to $\sim 4\%$. It is important to highlight that in this specific condition due to burning methane with pure oxygen in the condition zero dilution, the formation of product is very high impacting the third body efficiencies. To sum up, the considerable effect of collisional energy transfer to HCO dissociation reaction indicates great potential in third-body for future mechanism optimisations and improvements.

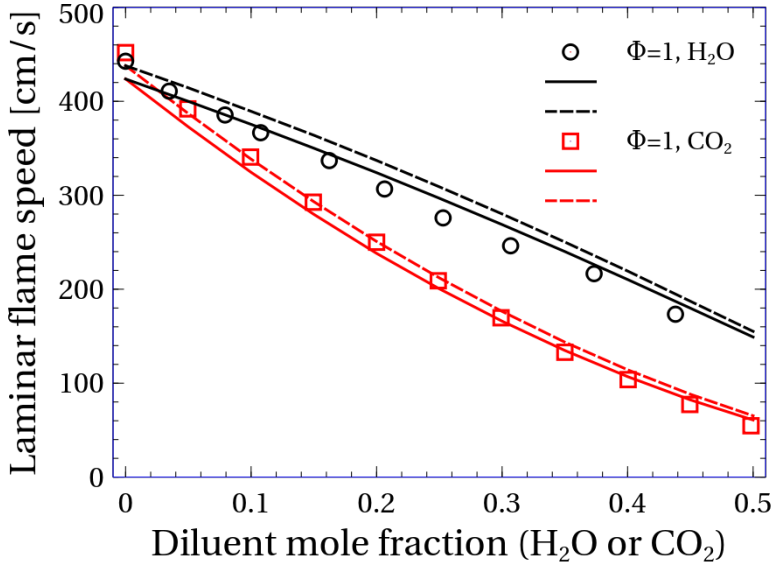

Figure 8.3: *Laminar flame speed of $CH_4/O_2/H_2O$ and $CH_4/O_2/CO_2$ mixtures, for $\Phi = 1$ at $T_{in} = 373K$ and atmospheric pressure. Symbols refer to experimental data [160], Solid lines to model predictions, and dashed lines to the model predictions ($M_{H2O} = 6$ and $M_{CO2} = 2$) with modified third-body efficiencies ($M_{H2O} = 12$ and $M_{CO2} = 4$).*

8.3 Multiple Bath gases Third-body

Attempts to implement the data from high accuracy theoretical predictions of the pressure dependence indicate a variety of weaknesses in current chemical kinetic modelling codes [202].

First, the TROE formalisms (see the section 2.4.2) are not the same for different colliders. A single TROE expression including temperature-and pressure-independent third-body efficiencies for single-component pressure dependence [228] is only accurate within $\sim 10-20\%$ [98,228], third-body discrepancies in the pressure and temperature dependence of Ar and H_2O equal $\sim 20\%$ and $\sim 40\%$ respectively [217,219,220].

In addition, the mixture rule disregards nonlinearities in the low-pressure limit of $\sim 10\%$ [203], and therefore, the form of representation just could account for ~ 50 to 90% errors.

Second, another method can be introduced by a reaction as n separate expressions each with different temperature and pressure dependence for each collider. The form of implementation that essentially handles each of the n separate expressions as different reactions, adding errors in the fall-off regime leading a factor of n in the high-pressure limit [203].

Third, The PLOG format (see the section 2.4.2), which employs logarithmic interpolations of tabulated data [229], could bypass the limitations in the TROE formalism, but the current adopted format does not allow for the specification of any collider specific information in the PLOG format. A recent study of Burke and Song [203] demonstrated the need to pay more attention to converting the fall-off data for single colliders to rate coefficients for a mixture of colliders. This conversion is regularly conducted through linear mixture rules, which may include errors as large as 70%.

Finally, in the author opinion, to overcome the challenge of third-body collision not only more accurate date (theoretical and experimental) on collisional energy transfer but also improved procedures for representing pressure dependent rate coefficients in modelling codes are extremely needed. Therefore, The implementation of the recently introduced modified TROE and PLOG expressions by Professor Stephen J. Klippenstein (Argonne National Laboratory) for multiple bath gases is of great interest to overcome the current limitations that severely hamper efforts to properly explore the kinetics of EGR, MILD, and Oxy-fuel combustion.

8.4 Summary

This chapter briefly evaluated the effect of collisional energy transfer and third-body efficiency. A few crucial third-body dependence reactions and their effects on combustion characteristics were selected through the analysis carried out in the previous chapters, then these cases carefully analysed. Despite two important reactions of $H + O_2(+M) = HO_2(+M)$ and $H + CH_3(+M) = CH_4(+M)$ that a right amount experimental and theoretical studies are available, the rest of third-body dependence reactions strongly require more information regarding third-body efficiencies. Thus, there are critical needs for a systematic evaluation for these type of reactions. Finally, an Important implication of this chapter is that the uncertainty of third-body coefficients is possibly higher than the devoted rate parameters of the reaction. Moreover, the expressions for multiple bath gases are of great interest to overcome the current limitations that severely hamper efforts to properly explore the kinetics of EGR, MILD, and Oxy-fuel combustion.

CHAPTER 9

Mechanism Evaluation

9.1 Introduction

THE aphorism of George Box, " all models are wrong; some models are useful", is considered to be applicable to not only statistical models, but to scientific models. However, the most practical question is how wrong do they have to be to not be useful" [230].

In complex problems of combustion, coupled with high nonlinearity and dimensionality, many aspects of the system are not precisely known. As discussed before, developing detailed kinetic mechanisms involves compiling set of elementary reactions whose rate parameters may be determined form individual reaction-rate theory, rate measurements, or a combination of both. All these methods have uncertainties; whether in the determined rate parameters, thermodynamic properties, or incomplete physics and missing reaction pathways [231].

Considering the rate coefficient of the most important reaction combustion systems (see section 8.2.1)

$$H + O_2 = O + OH \tag{9.1}$$

with the rate constant k_1 which has been experimentally evaluated at least 77 in forward and reverse directions. Besides, k_1 rate has been reviewed and revisited at least 31 times [67]. Figure represents Wang and Sheen [231] historical review of uncertainty in k_1 in terms of the past achievements and future challenges. The progress in shock tube techniques and laser diagnostics in the late 80s and 90s brought notable improvements to the accuracy of k_1 [232]. To the extent that the best experimental evaluations provide uncertainty of better than 15% for k_1 over the temperature range of $1100-3370\,K$ [87]. It is noteworthy to highlight that among all of the elementary reactions in combustion,

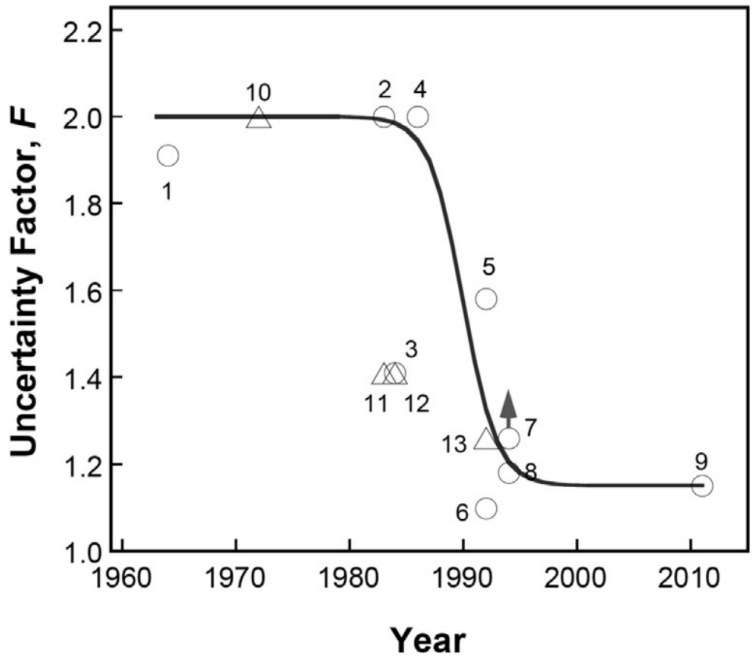

Figure 9.1: *Selected uncertainty factors quoted in experimental studies of the rate coefficient of $H + O_2 = O + OH$. Circles: forward reaction; triangles: reverse reaction. The plot is adapted from Wang and Sheen [231].*

this can be considered as the best-achieved precision. Although this is truly astonishing, such precision may still not be sufficient for the combustion modelling and prediction. For instance, if the logarithmic sensitivity coefficient of a combustion prediction is 0.2 concerning k_1, it alone causes $\pm 3\%$ uncertainty in the combustion prediction. In general, other reactions rate coefficients are less accurate than k_1. The currently known uncertainty factors for a $C_1 - C_3$ mechanism can be exhibited as [231]

- 8% of reactions range from 1.15 for k_1, 1.2 to 2.
- 66% of reactions 2 to 3.
- 20% of reactions 5 to 10.

Thus, even if the kinetic mechanism is complete and free of any missing reaction pathway, the underlying impact of rate parameters uncertainty on model prediction is still not negligible. Besides the overall satisfactory predictions for flame speeds, ignition delay times as well as major species, the kinetic mechanism may not provide accurate predictions in some peculiar conditions. This section aims to provide a brief analysis of the conditions that the kinetic mechanism may fail or may not provide adequate predictions due to a higher degree of uncertainty in controlling parameters.

9.2 Flame Speed

As discussed earlier, flame speed is an important combustion property which provides an insight into the global reactivity of the fuel. Detailed kinetic mechanisms are usually validated against experimental measurements at various pressures or temperatures; although, the effect of different mixtures and dilution is less studied.

Figure 9.2 presents the laminar flame speed of rich methane and oxygen mixture diluted with 0 to 40% of water. In this figure, an endeavour has been made to highlight the model deficiency by comparing several detailed kinetic mechanisms (CRECK, Aramco2.0, DTU-2016, GRI3.0) with the experimental observation of Maze et al. [160]. As can be seen, all the models except GRI3.0 over-predict the experimental data by $\sim 10\%$ or even higher. However, moving to Figure 9.3, which shows the laminar flame speed of methane and oxygen mixture diluted with 20% of CO_2, all the models under-predict the measurement with the maximum of $\sim 20\%$ under-prediction for GRI3.0 at Phi=1. As it is clear form Figure 9.3, the CRECk model of this study exhibits a better performance in terms of the shape of profile and deviation. However, notable discrepancies still exist in all models.

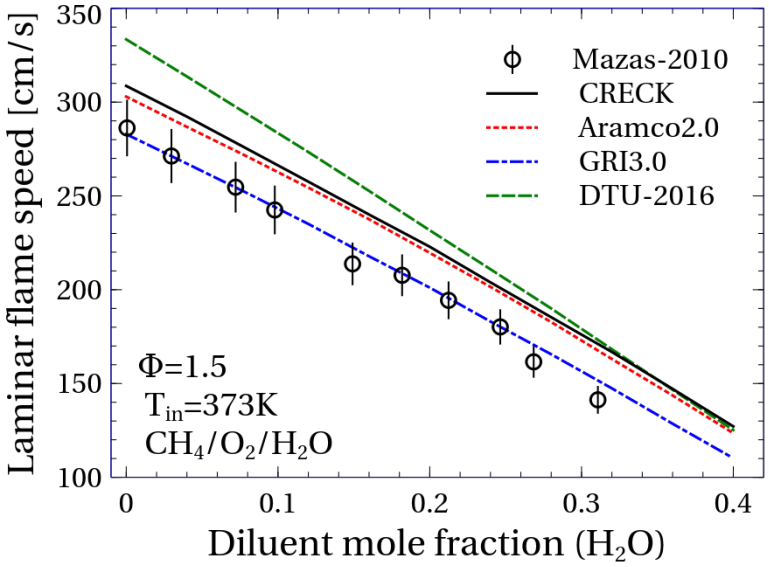

Figure 9.2: *Experimental (symbols) and computed (lines) laminar flame speeds of $CH_4/O_2/H_2O$ mixture, for $\Phi = 1.50$, at $T_{in} = 373K$ and atmospheric pressure. Mazas-2010 refers to [160], Aramco2.0 to [63], GRI3.0 to [44], and DTU-2016 to [55].*

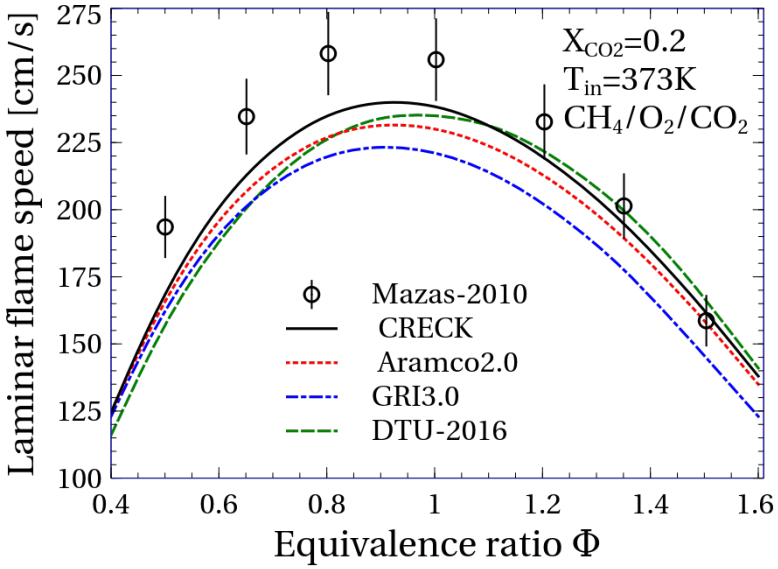

Figure 9.3: *Experimental (symbols) and computed (lines) laminar flame speeds of $CH_4/O_2/CO2$ mixtures as a function of the equivalence ratio for $X_{CO2} = CO_2/(CO_2 + O_2) = 0.20$, at $T_{in} = 373K$ and atmospheric pressure. Mazas-2010 refers to [160], Aramco2.0 to [63], GRI3.0 to [44], and DTU-2016 to [55].*

The lack of adequate predication in Figures 9.2 and 9.3 can be explain through following points:

- One of the major sources of the discrepancy is the model input uncertainty. Experimental observations, as a source of input data, always contain measurement uncertainty of fundamental combustion properties that are used to evaluate and constrain the model. Despite the uncertainties in the measurements reported by the authors, these uncertainties can be best quantified by examining similar errors in different apparatus and by replicating measurements in various experimental apparatus in on or more laboratories. Thus, as these data are the only one from its kind in these extreme conditions, the repetition of the experiments is of great interest to assess the uncertainty precision and whether the model meets accuracy requirements in the intended domain.

- As shown in Figure 9.4, the chain branching reaction ($H + O_2 = O + OH$) is the most sensitive in determining the laminar flame speed. k_1 discussed previously to be the most precise rate parameters among all elementary reactions with 15% uncertainty. To assess the effect of this uncertainty on the laminar flame speed, Figure 9.5 shows the upper and lower band of flame speed defined according to the uncertainty of k_1. It is apparent that the k_1 uncertainty alone can cause $\pm 10 - 15\%$ variation in laminar flame speed, and eventually, the experimental measurements fall in between the bands. Thus, even if the kinetic mechanism is complete and free of any missing reaction pathway, rate coefficient uncertainties generally preclude the possibility of predicting relevant combustion properties in some peculiar conditions.

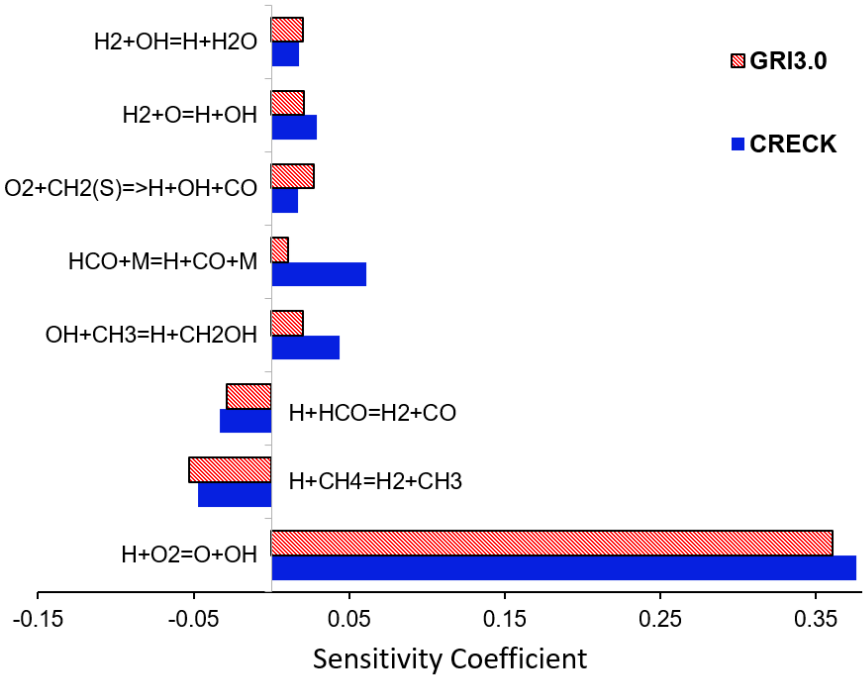

Figure 9.4: *Sensitivity analysis of laminar flame speed of CH_4/O_2 mixture, for $\Phi = 1.50$, at $T_{in} = 373K$ and atmospheric pressure.*

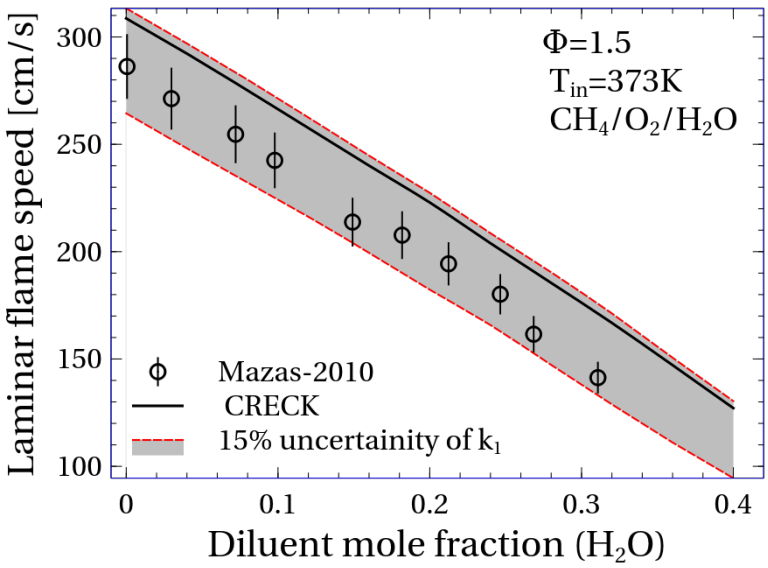

Figure 9.5: *Laminar flame speeds of $CH_4/O_2/H_2O$ mixture, for $\Phi = 1.50$, at $T_{in} = 373K$ and atmospheric pressure. The shaded area indices 15% uncertainty in k_1. Mazas-2010 refers to [160].*

9.3 Intermediate Temperature Chemistry

Further examples that adequate predictions can not be achieved are highlighted in Figures 9.6 to 9.8. These figures depict that available mechanisms are unable to capture the slow reactivity region after ignition in atmospheric pressure. Detail information about these conditions are shown in Table 9.1. As can be seen from this table, all of the conditions refer to methane combustion in stoichiometric condition and various mixtures.

Table 9.1: *List of initial conditions presented in Figure 9.6 to 9.8. All the experiments refer to JSR.*

Figure No.	Fuels	Diluents	Φ
Figure 9.6	$1\%CH_4$	N_2	1
Figure 9.7	$1\%CH_4$	$N_2 + 20\%CO_2$	1
Figure 9.8	$0.9\%CH_4 + 0.4\%H_2$	N_2	1

In these MILD conditions, the slower reactivity after fast depletion of fuel is more likely to be the consequence of increasing the combustion products concentration (H_2O and CO_2). As discussed earlier, these products inhibit the reactivity of the system through their physical and chemical effects. For example, the kinetic interaction involves radical chain branching coupled to the inhibition caused by the third-body efficiency of the complete combustion product (H_2O and), through the non-branching reaction of HO_2.

Moreover, as mentioned earlier, HO_2 plays a dominant role in intermediate temperature chemistry, in particular, conditions regarding JSR experiments. In the case of methane, OH starts to be formed when the temperature is higher than $\sim 1100\ K$. At these temperatures, the formation rate of OH through HO_2 is slow; however, its consumption rate is high enough to completely consume OH radicals in a period shorter than its formation. At temperatures above $1150K$, the chain branching reaction k_1 becomes the dominant one, and OH concentration drastically increases.

To sum up, kinetic schemes are mainly able to predict the evolution of the oxidation process in traditional combustion systems, namely, for high-temperature conditions, because of high adiabatic flame temperatures, and where H_2O and CO_2 are present as oxidation process products (in the post-combustion region), with a relatively low concentration. In MILD/oxyfuel systems, temperature gradients are modest, so kinetic routes are slowly passing from intermediate to well-known high-temperature kinetics. Such operative conditions stress the competition between kinetic routes inducing peculiar oxidation behaviours [80]. In such reference systems, the H_2O and CO_2 concentrations are very high, and thus, the uncertainty of kinetic reaction parameters is elaborated.

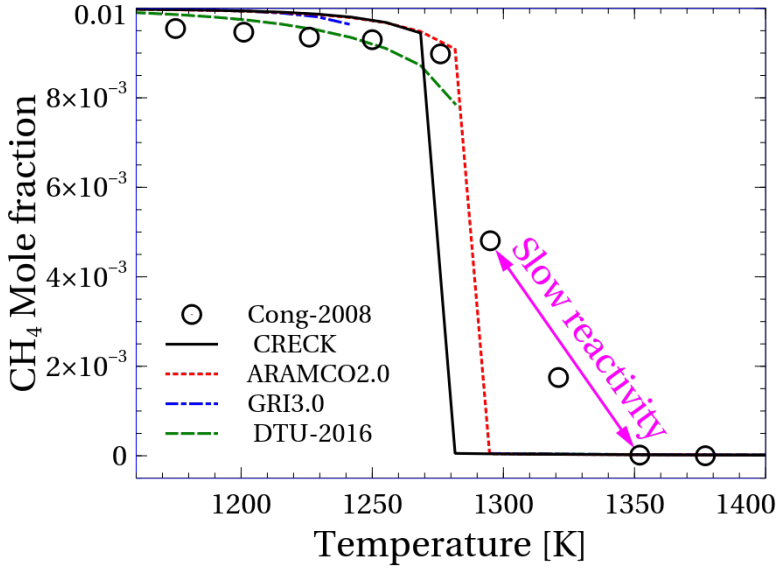

Figure 9.6: *Methane profile of a atmospheric Jet-stirred reactor with stoichiometric* $1\%CH_4 + O_2$ *mixture and* N_2 *dilution. Cong-2008 refers to [127], Aramco2.0 to [63], GRI3.0 to [44], and DTU-2016 to [55].*

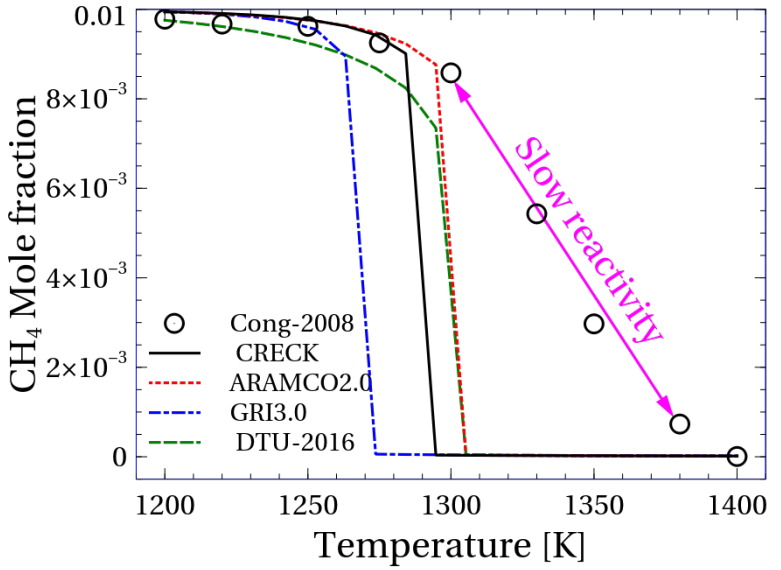

Figure 9.7: *Methane profile of a atmospheric Jet-stirred reactor with stoichiometric* $1\%CH_4 + O_2$ *mixture and* $N_2 + 20\%CO_2$ *dilution . Cong-2008 refers to [127], Aramco2.0 to [63], GRI3.0 to [44], and DTU-2016 to [55].*

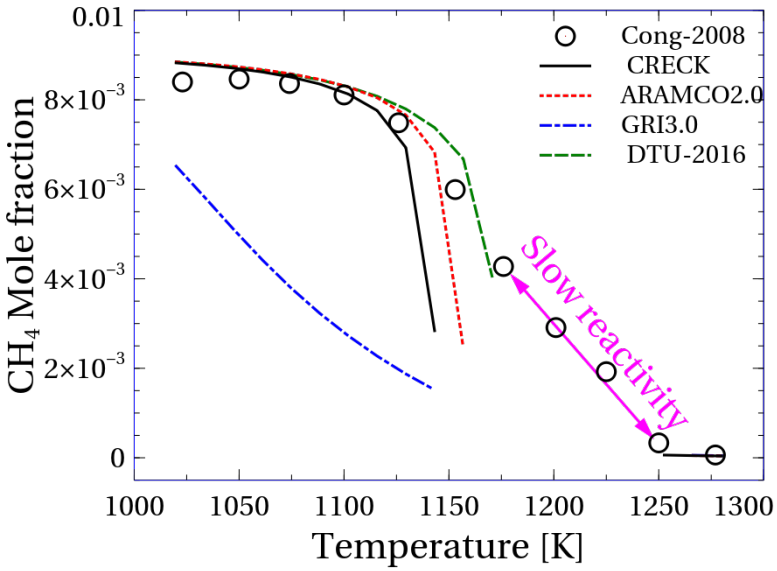

Figure 9.8: *Methane profile of a atmospheric Jet-stirred reactor with stoichiometric* $0.9\%CH_4 + 0.4\%H_2 + O_2$ *mixture and* N_2 *dilution . Cong-2008 refers to [127], Aramco2.0 to [63], GRI3.0 to [44], and DTU-2016 to [55]. The region that the model predictions are not presented indicates the oscillation regime and the steady-state solution can not be found.*

9.4 Summary

This chapter aimed to highlight that despite the satisfactory model prediction and reasonable agreement shown in previous chapters, the underlying impact of rate parameters uncertainty on model prediction is still not negligible. It has been revealed that even if the kinetic mechanism is complete and free of any missing reaction pathway, rate coefficient uncertainties generally precludes the possibility of predicting relevant combustion properties in some peculiar conditions.

CHAPTER 10

Conclusions and Recommendations

10.1 Summary and conclusion

THIS project was undertaken in the context of Combustion for Low Emission Application of Natural Gas (CLEAN-Gas) project, European Union's Horizon 2020 research and innovation programme under Marie Sklodowska-Curie Innovative Training Network (ITN), carried out at Politecnico di Milano and Université Libre de Bruxelles. As a large part of our understanding of the complex combustion processes comes from elementary chemical kinetic models, this study set out to develop a detailed kinetic mechanism for natural gas ($C_1 - C_3$ fuels) combustion and oxidation based on the hierarchical approach. The objective of the current study was to provide a systematic discussion on the combustion characteristics, hidden aspects and critical reaction pathways involved in near-zero-emissions combustion processes (MILD and OXY-fuel) by comparing the model predictions with the most extensive set of experimental data available. This database covers a wide range of pressure, temperature, and equivalence ratio receiving more than ~ 6000 data points.

This detailed kinetic mechanism was built with an emphasis on low-environmental impacts combustion technologies such as MILD and oxy-fuel combustion. The detailed kinetic mechanism successfully captures the effect of various bath gases in MILD and oxy-fuel combustion over a broad range of conditions. Sensitivity and reactive path analyses clearly highlight the dominant kinetics. Moreover, a particular focus has been given to assessing the relative contributions of the physical and chemical effect of the diluents on the reactivity. Laminar flame speed, ignition delay time, and formation of products are strongly dependent on the operating conditions (temperature, pressure, and equivalence ratios), making the role of bath gases principally case sensitive. For example, at high temperature or low pressures, third body reactions

are of lower importance. However, third body reactions may correspond to propagation steps forming radicals with lower reactivity (e.g. $H + O_2(+M) = HO_2(+M)$) building up in the system enhancing recombination reactions, to termination reactions. An additional example can be the removal of reactive H radicals from flames (e.g. $H + CH_3(+M) = CH_4(+M)$), or initiation reactions triggering reactivity in the transition from intermediate ($1000 < T < 1200\,K$) to high temperatures ($T > 1200\,K$), such as $H_2O_2(+M) = OH + OH(+M)$.

From the outcome of our investigation, it is possible to conclude thatH_2O and CO_2 dilution reduces the system reactivity. The effect of H_2O is more pronounced due to chemical effects related to enhanced collisional efficiencies at the operating conditions of JSR experiments. Whereas CO_2 has a higher impact in inhibiting flame propagation at higher temperatures, mainly due to the thermal and radical scavenging effects. Moreover, the effect of CO_2 addition on methane ignition delay times is very marginal. The most likely explanation is that CO_2 is scarcely reactive during the ignition, because of its stability, and does not actively modify the pool of radicals.

Finally, despite the satisfactory model prediction and reasonable agreement shown, the underlying impact of rate parameters uncertainty on model prediction is still not negligible. It has been shown that even if the kinetic mechanism is complete and free of any missing reaction pathway, rate coefficient uncertainties generally precludes the possibility of predicting relevant combustion properties in some peculiar conditions.

10.2 Recommendations

1. An important implication of this study is that the critical reactions concerning modern combustions differ from more conventional flames. Several reaction rates might be reasonably acceptable for conventional flames modelling; however, moving to modern combustions (high dilution level, distributed ignition, low-temperature oxidation), problem arise, and more accurate rate parameters are required. Consequently, a systematic evaluation aimed at reducing the uncertainty or advising parameters from more accurate calculations or measurements is of prominent concern for new combustion technologies.

2. Despite the satisfactory agreement, model predictions in the case of water dilution could benefit from a more fundamental evaluation of collisional efficiency compared to the current value, usually ranging between 6 and 12. However, recent research efforts are devoted to better a priori assessment of energy-transferring collisions and pressure-dependent kinetics based on master equation simulations. A better description of relevant reactions proceeding through the formation of rovibrationally excited complexes will also benefit from the implementation of non-linear mixture rules.

3. Low-pressure limit of pressure dependence reactions has a strong collision dependency. It is well grasped that PLOG reactions are becoming increasingly popular in kinetic mechanisms due to the more accurate fitting compared to TROE formalism. However, we lose details related to third-body efficiencies in the standard format of PLOG. An extended version of PLOG reaction capable of considering multiple bath-gas species has been recently proposed by Professor Stephen J.

Klippenstein (Argonne National Laboratory). This formulation has not yet been implemented in any reaction mechanism, but its integration into the detailed combustion kinetics will enhance the accuracy of the pressure-dependent reactions as well as third-body efficiencies.

4. Significant progress in combustion chemistry has been made over the last decades, but in comparison to a broad portfolio of hydrocarbon fuels, one may have to consider, the pace of the progress has been slow. One of the primary reasons has been the lack of consensus as to how to move forward in obtaining a comprehensive, unified and predictive model of fuel combustion.

Bibliography

[1] D. A. Vallero, "Environmental Impacts of Energy Production, Distribution and Transport," in *Future Energy (Second Edition)*, p. 551–581, Elsevier, 2014.

[2] I. OECD *et al.*, "Energy and Air Pollution: World Energy Outlook Special Report 2016," 2016.

[3] ExxonMobil, "2018 Outlook for Energy: A View to 2040." `https://corporate.exxonmobil.com/-/media/Global/Files/outlook-for-energy/2018-Outlook-for-Energy.pdf`, 2019. (Accessed on 05/04/2019).

[4] I. E. Agency, "World Energy Outlook 2018." `https://www.iea.org/weo2018/`, 2019. (Accessed on 05/04/2019).

[5] P. Sabia, M. de Joannon, A. Picarelli, and R. Ragucci, "Methane auto-ignition delay times and oxidation regimes in MILD combustion at atmospheric pressure," *Combustion and Flame*, vol. 160, no. 1, p. 47–55, 2013.

[6] R. Weber, J. P. Smart, and W. vd Kamp, "On the (MILD) combustion of gaseous, liquid, and solid fuels in high temperature preheated air," *Proceedings of the Combustion Institute*, vol. 30, no. 2, p. 2623–2629, 2005.

[7] P. Li, B. B. Dally, J. Mi, and F. Wang, "MILD oxy-combustion of gaseous fuels in a laboratory-scale furnace," *Combustion and Flame*, vol. 160, no. 5, p. 933–946, 2013.

[8] J. Wünning and J. Wünning, "Flameless oxidation to reduce thermal NO-formation," *Progress in energy and combustion science*, vol. 23, no. 1, p. 81–94, 1997.

[9] L. Chen, S. Z. Yong, and A. F. Ghoniem, "Oxy-fuel combustion of pulverized coal: Characterization, fundamentals, stabilization and CFD modeling," *Progress in energy and combustion science*, vol. 38, no. 2, p. 156–214, 2012.

[10] H. J. Curran, "Developing detailed chemical kinetic mechanisms for fuel combustion," *Proceedings of the Combustion Institute*, 2018.

[11] D. C. Brock and G. E. Moore, *Understanding Moore's law: four decades of innovation*. Chemical Heritage Foundation, 2006.

[12] C. K. Westbrook, Y. Mizobuchi, T. J. Poinsot, P. J. Smith, and J. Warnatz, "Computational combustion," *Proceedings of the Combustion Institute*, vol. 30, no. 1, p. 125–157, 2005.

[13] T. Lu and C. K. Law, "Toward accommodating realistic fuel chemistry in large-scale computations," *Progress in Energy and Combustion Science*, vol. 35, no. 2, p. 192–215, 2009.

[14] C. W. Gear, *Numerical initial value problems in ordinary differential equations*. Prentice Hall PTR, 1971.

[15] C. W. Gear, "The automatic integration of ordinary differential equations," *Communications of the ACM*, vol. 14, no. 3, p. 176–179, 1971.

[16] J. Hirschfelder, C. Curtiss, and D. E. Campbell, "The theory of flame propagation. IV," *The Journal of Physical Chemistry*, vol. 57, no. 4, p. 403–414, 1953.

[17] D. B. Spalding, "The theory of flame phenomena with a chain reaction," *Phil. Trans. R. Soc. Lond. A*, vol. 249, no. 957, p. 1–25, 1956.

[18] D. J. Seery and C. T. Bowman, "An experimental and analytical study of methane oxidation behind shock waves," *Combustion and Flame*, vol. 14, no. 1, p. 37–47, 1970.

[19] C. T. Bowman, "An experimental and analytical investigation of the high-temperature oxidation mechanisms of hydrocarbon fuels," *Combustion Science and Technology*, vol. 2, no. 2-3, p. 161–172, 1970.

[20] P. J. Marteney, "Analytical study of the kinetics of formation of nitrogen oxide in hydrocarbon-Air Combustion," *Combustion Science and Technology*, vol. 1, no. 6, p. 461–469, 1970.

[21] L. D. Smoot, W. C. Hecker, and G. A. Williams, "Prediction of propagating methane-air flames," *Combustion and flame*, vol. 26, p. 323–342, 1976.

[22] G. Tsatsaronis, "Prediction of propagating laminar flames in methane, oxygen, nitrogen mixtures," *Combustion and Flame*, vol. 33, p. 217–239, 1978.

[23] C. T. Bowman, "A shock-tube investigation of the high-temperature oxidation of methanol," *Combustion and Flame*, vol. 25, p. 343–354, 1975.

[24] C. K. Westbrook and F. L. Dryer, "Comprehensive mechanism for methanol oxidation," *Combustion Science and Technology*, vol. 20, no. 3-4, p. 125–140, 1979.

[25] C. K. Westbrook and F. L. Dryer, "Chemical kinetics and modeling of combustion processes," in *Symposium (International) on Combustion*, vol. 18, p. 749–767, Elsevier, 1981.

[26] C. K. Westbrook and F. L. Dryer, "Chemical kinetic modeling of hydrocarbon combustion," *Progress in Energy and Combustion Science*, vol. 10, no. 1, p. 1–57, 1984.

[27] J. Warnatz, "The structure of laminar alkane-, alkene-, and acetylene flames," in *Symposium (International) on Combustion*, vol. 18, p. 369–384, Elsevier, 1981.

[28] J. Warnatz, "The mechanism of high temperature combustion of propane and butane," *Combustion Science and Technology*, vol. 34, no. 1-6, p. 177–200, 1983.

[29] E. Ranzi, A. Sogaro, P. Gaffuri, G. Pennati, and T. Faravelli, "A wide range modeling study of methane oxidation," *Combustion science and technology*, vol. 96, no. 4-6, p. 279–325, 1994.

[30] E. Ranzi, A. Frassoldati, R. Grana, A. Cuoci, T. Faravelli, A. Kelley, and C. Law, "Hierarchical and comparative kinetic modeling of laminar flame speeds of hydrocarbon and oxygenated fuels," *Progress in Energy and Combustion Science*, vol. 38, no. 4, p. 468–501, 2012.

[31] P. DAGAUT, J.-C. BOETTNER, and M. CATHONNET, "Methane oxidation: experimental and kinetic modeling study," *Combustion science and technology*, vol. 77, no. 1-3, p. 127–148, 1991.

[32] P. Dagaut, M. Cathonnet, and J.-c. Boettner, "Kinetics of ethane oxidation," *International Journal of Chemical Kinetics*, vol. 23, no. 5, p. 437–455, 1991.

[33] Y. Tan, P. Dagaut, M. Cathonnet, J. C. Boettner, J. S. Bachman, and P. Carlier, "Natural gas and blends oxidation and ignition: Experiments and modeling," in *Symposium (International) on Combustion*, vol. 25, p. 1563–1569, Elsevier, 1994.

[34] K. Hughes, T. Turányi, A. Clague, and M. Pilling, "Development and testing of a comprehensive chemical mechanism for the oxidation of methane," *International Journal of Chemical Kinetics*, vol. 33, no. 9, p. 513–538, 2001.

[35] P. Barbé, F. Battin-Leclerc, and G. Côme, "Experimental and modelling study of methane and ethane oxidation between 773 and 1573 K," *Journal de chimie physique*, vol. 92, p. 1666–1692, 1995.

[36] J. A. Miller and C. T. Bowman, "Mechanism and modeling of nitrogen chemistry in combustion," *Progress in energy and combustion science*, vol. 15, no. 4, p. 287–338, 1989.

[37] R. Yetter, F. Dryer, and H. Rabitz, "A comprehensive reaction mechanism for carbon monoxide/hydrogen/oxygen kinetics," *Combustion Science and Technology*, vol. 79, no. 1-3, p. 97–128, 1991.

[38] S. Hochgreb and F. Dryer, "A comprehensive study on CH2O oxidation kinetics," *Combustion and flame*, vol. 91, no. 3-4, p. 257–284, 1992.

[39] T. J. Held and F. L. Dryer, "A comprehensive mechanism for methanol oxidation," *International Journal of Chemical Kinetics*, vol. 30, no. 11, p. 805–830, 1998.

[40] J. Li, Z. Zhao, A. Kazakov, M. Chaos, F. L. Dryer, and J. J. Scire Jr, "A comprehensive kinetic mechanism for CO, CH2O, and CH3OH combustion," *International Journal of Chemical Kinetics*, vol. 39, no. 3, p. 109–136, 2007.

[41] M. Frenklach, "Systematic optimization of a detailed kinetic model using a methane ignition example," *Combustion and flame*, vol. 58, no. 1, p. 69–72, 1984.

[42] M. Frenklach, H. Wang, and M. J. Rabinowitz, "Optimization and analysis of large chemical kinetic mechanisms using the solution mapping method—combustion of methane," *Progress in Energy and Combustion Science*, vol. 18, no. 1, p. 47–73, 1992.

[43] M. Frenklach, H. Wang, C. Bowman, R. Hanson, G. Smith, D. Golden, W. Gardiner, and V. Lissianski, "An Optimized Kinetics Model for Natural Gas Combustion 25th Symp.(Int.) Comb," tech. rep., Poster WIP-3-26, 1994.

[44] C. Bowman, R. Hanson, D. Davidson, W. Gardiner, J. V. Lissianski, G. Smith, D. Golden, M. Frenklach, and M. Goldenberg, "Access: http://www.me.berkeley.edu/gri-mech/.".

[45] G. P. Smith, D. M. Golden, M. Frenklach, N. W. Moriarty, B. Eiteneer, M. Goldenberg, C. T. Bowman, R. K. Hanson, S. Song, W. C. Gardiner, J. Vitali, V. Lissianski, and Z. Qin, "Access: http://www.me.berkeley.edu/gri-mech/.".

[46] "Chemical Mechanism: Combustion Research Group at UC San Diego." `http://web.eng.ucsd.edu/mae/groups/combustion/mechanism.html`. (Accessed on 01/04/2019).

[47] J. C. Prince and F. A. Williams, "Short chemical-kinetic mechanisms for low-temperature ignition of propane and ethane," *Combustion and Flame*, vol. 159, no. 7, p. 2336–2344, 2012.

[48] H. Wang, X. You, A. V. Joshi, S. G. Davis, A. Laskin, F. Egolfopoulos, and C. K. Law, "USC Mech Version II. High-Temperature Combustion Reaction Model of H2/CO/C1-C4 Compounds.." `http://ignis.usc.edu/USC_Mech_II.htm`, `May2007`. (Accessed on 01/04/2019).

[49] H. Wang, E. Dames, B. Sirjean, D. A. Sheen, R. Tango, A. Violi, J. Y. W. Lai, F. N. Egolfopoulos, D. F. Davidson, R. K. Hanson, C. T. Bowman, C. K. Law, W. Tsang, N. P. Cernansky, D. L. Miller, and R. P. Lindstedt, "A high-temperature chemical kinetic model of n-alkane (up to n-dodecane), cyclohexane, and methyl-, ethyl-, n-propyl and n-butylcyclohexane oxidation at high temperatures, JetSurF version 2.0, September 19, 2010." `http://web.stanford.edu/group/haiwanglab/JetSurF/JetSurF2.0/index.html`. (Accessed on 01/04/2019).

[50] T. C. M. Group, "Detailed kinetic mechanisms and CFD of reacting flows." `http://creckmodeling.chem.polimi.it/`. (Accessed on 01/04/2019).

[51] W. K. Metcalfe, S. M. Burke, S. S. Ahmed, and H. J. Curran, "A hierarchical and comparative kinetic modeling study of C1- C2 hydrocarbon and oxygenated fuels," *International Journal of Chemical Kinetics*, vol. 45, no. 10, p. 638–675, 2013.

[52] Y. Li, C.-W. Zhou, K. P. Somers, K. Zhang, and H. J. Curran, "The oxidation of 2-butene: A high pressure ignition delay, kinetic modeling study and reactivity comparison with isobutene and 1-butene," *Proceedings of the Combustion Institute*, vol. 36, no. 1, p. 403–411, 2017.

[53] C.-W. Zhou, Y. Li, E. O'Connor, K. P. Somers, S. Thion, C. Keesee, O. Mathieu, E. L. Petersen, T. A. DeVerter, M. A. Oehlschlaeger, *et al.*, "A comprehensive experimental and modeling study of isobutene oxidation," *Combustion and Flame*, vol. 167, pp. 353–379, 2016.

[54] J. Gimenez-Lopez, C. T. Rasmussen, H. Hashemi, M. U. Alzueta, Y. Gao, P. Marshall, C. F. Goldsmith, and P. Glarborg, "Experimental and kinetic modeling study of C2H2 oxidation at high pressure," *International Journal of Chemical Kinetics*, vol. 48, no. 11, p. 724–738, 2016.

[55] H. Hashemi, J. M. Christensen, S. Gersen, H. Levinsky, S. J. Klippenstein, and P. Glarborg, "High-pressure oxidation of methane," *Combustion and Flame*, vol. 172, p. 349–364, 2016.

[56] S. M. Burke, *Development of a Chemical Kinetic Mechanism for Small Hydrocarbons*. PhD thesis, 2014.

[57] J. M. Simmie, "Detailed chemical kinetic models for the combustion of hydrocarbon fuels," *Progress in energy and combustion science*, vol. 29, no. 6, p. 599–634, 2003.

[58] H.-H. Carstensen and A. M. Dean, "Chapter 4 The Kinetics of Pressure-Dependent Reactions," in *Modeling of Chemical Reactions* (R. W. Carr, ed.), vol. 42 of *Comprehensive Chemical Kinetics*, p. 101–184, Elsevier, 2007.

[59] S. De Persis, A. Dollet, and F. Teyssandier, "Pressure dependence of gas-phase reaction rates," *Journal of chemical education*, vol. 81, no. 6, p. 832, 2004.

[60] R. Gilbert, K. Luther, and J. Troe, "Theory of thermal unimolecular reactions in the fall-off range. II. Weak collision rate constants," *Berichte der Bunsengesellschaft für physikalische Chemie*, vol. 87, no. 2, p. 169–177, 1983.

[61] "ANSYS Reaction Design Theory Manual." `https://www.ems.psu.edu/~radovic/ChemKin_Theory_PaSR.pdf`. (Accessed on 01/04/2019).

[62] F. Lindemann, S. Arrhenius, I. Langmuir, N. Dhar, J. Perrin, and W. M. Lewis, "Discussion on "the radiation theory of chemical action"," *Transactions of the Faraday Society*, vol. 17, p. 598–606, 1922.

[63] S. M. Burke, U. Burke, R. Mc Donagh, O. Mathieu, I. Osorio, C. Keesee, A. Morones, E. L. Petersen, W. Wang, T. A. DeVerter, *et al.*, "An experimental and modeling study of propene oxidation. Part 2: Ignition delay time and flame speed measurements," *Combustion and Flame*, vol. 162, no. 2, p. 296–314, 2015.

[64] B. J. McBride and S. Gordon, "Computer program for calculating and fitting thermodynamic functions," 1992.

[65] R. Design, *CHEMKIN theory manual*, 2007.

[66] B. Ruscic, R. E. Pinzon, G. Von Laszewski, D. Kodeboyina, A. Burcat, D. Leahy, D. Montoy, and A. F. Wagner, "Active Thermochemical Tables: thermochemistry for the 21st century," in *Journal of Physics: Conference Series*, vol. 16, p. 561, IOP Publishing, 2005.

[67] "NIST Chemical Kinetics Database."

[68] "Active Thermochemical Tables - Home." `https://atct.anl.gov/`. (Accessed on 01/04/2019).

[69] A. Burcat and B. Ruscic, *Third millenium ideal gas and condensed phase thermochemical database for combustion with updates from active thermochemical tables*. Argonne National Laboratory Argonne, IL, 2005.

[70] S. W. Benson, *Thermochemical kinetics*. Wiley, 1976.

[71] E. R. Ritter and J. W. Bozzelli, "THERM: Thermodynamic property estimation for gas phase radicals and molecules," *International Journal of Chemical Kinetics*, vol. 23, no. 9, p. 767–778, 1991.

[72] C. L. Rasmussen, J. G. Jakobsen, and P. Glarborg, "Experimental measurements and kinetic modeling of CH4/O2 and CH4/C2H6/O2 conversion at high pressure," *International Journal of Chemical Kinetics*, vol. 40, no. 12, p. 778–807, 2008.

[73] R. Janoschek and M. Rossi, "Thermochemical properties of free radicals from G3MP2B3 calculations," *International journal of chemical kinetics*, vol. 34, no. 9, p. 550–560, 2002.

[74] C. F. Goldsmith, G. R. Magoon, and W. H. Green, "Database of small molecule thermochemistry for combustion," *The Journal of Physical Chemistry A*, vol. 116, no. 36, p. 9033–9057, 2012.

[75] G. Meloni, P. Zou, S. J. Klippenstein, M. Ahmed, S. R. Leone, C. A. Taatjes, and D. L. Osborn, "Energy-resolved photoionization of alkylperoxy radicals and the stability of their cations," *Journal of the American Chemical Society*, vol. 128, no. 41, p. 13559–13567, 2006.

[76] J. Matthews, A. Sinha, and J. S. Francisco, "Unimolecular dissociation and thermochemistry of CH 3 OOH," 2005.

[77] O. Mathieu, C. R. Mulvihill, and E. L. Petersen, "Assessment of modern detailed kinetics mechanisms to predict CO formation from methane combustion using shock-tube laser-absorption measurements," *Fuel*, vol. 236, p. 1164–1180, 2019.

[78] V. P. Zhukov and A. F. Kong, "A compact reaction mechanism of methane oxidation at high pressures," *Progress in reaction kinetics and mechanism*, vol. 43, no. 1, p. 62–78, 2018.

[79] M. de Joannon, P. Sabia, and A. Cavaliere, "MILD combustion," in *Handbook of Combustion*, vol. 5, p. 237–256, WILEY, 2010.

[80] P. Sabia, M. L. Lavadera, G. Sorrentino, P. Giudicianni, R. Ragucci, and M. de Joannon, "H 2 O and CO 2 dilution in MILD combustion of simple hydrocarbons," *Flow, Turbulence and Combustion*, vol. 96, no. 2, p. 433–448, 2016.

[81] J. F. Griffiths and J. A. Barnard, *Flame and combustion*. CRC Press, 1995.

[82] E. Ranzi, A. Frassoldati, A. Stagni, M. Pelucchi, A. Cuoci, and T. Faravelli, "Reduced kinetic schemes of complex reaction systems: fossil and biomass-derived transportation fuels," *International Journal of Chemical Kinetics*, vol. 46, no. 9, p. 512–542, 2014.

[83] M. Pelucchi, E. Ranzi, A. Frassoldati, and T. Faravelli, "Alkyl radicals rule the low temperature oxidation of long chain aldehydes," *Proceedings of the Combustion Institute*, vol. 36, no. 1, p. 393–401, 2017.

[84] E. Ranzi, M. Dente, T. Faravelli, and G. Pennati, "Prediction of kinetic parameters for hydrogen abstraction reactions," *Combustion science and technology*, vol. 95, no. 1-6, p. 1–50, 1993.

[85] W. Tsang and R. Hampson, "Chemical kinetic data base for combustion chemistry. Part I. Methane and related compounds," *Journal of Physical and Chemical Reference Data*, vol. 15, no. 3, p. 1087–1279, 1986.

[86] N. Hansen, J. A. Miller, P. R. Westmoreland, T. Kasper, K. Kohse-Höinghaus, J. Wang, and T. A. Cool, "Isomer-specific combustion chemistry in allene and propyne flames," *Combustion and Flame*, vol. 156, no. 11, pp. 2153–2164, 2009.

[87] Z. Hong, D. Davidson, E. Barbour, and R. Hanson, "A new shock tube study of the h+o2=oh+o reaction rate using tunable diode laser absorption of h2o near 2.5μm," *Proceedings of the Combustion Institute*, vol. 33, no. 1, pp. 309 – 316, 2011.

[88] J. Lee, C.-J. Chen, and J. W. Bozzelli, "Thermochemical and kinetic analysis of the acetyl radical (ch3c• o)+ o2 reaction system," *The Journal of Physical Chemistry A*, vol. 106, no. 31, pp. 7155–7170, 2002.

[89] S. G. Davis, C. K. Law, and H. Wang, "Propyne pyrolysis in a flow reactor: An experimental, rrkm, and detailed kinetic modeling study," *The Journal of Physical Chemistry A*, vol. 103, no. 30, pp. 5889–5899, 1999.

[90] C. Cavallotti, "Personal communication," 2018.

[91] J. A. Miller and S. J. Klippenstein, "From the multiple-well master equation to phenomenological rate coefficients: reactions on a c3h4 potential energy surface," *The Journal of Physical Chemistry A*, vol. 107, no. 15, pp. 2680–2692, 2003.

[92] L. B. Harding, S. J. Klippenstein, and Y. Georgievskii, "On the combination reactions of hydrogen atoms with resonance-stabilized hydrocarbon radicals," *The Journal of Physical Chemistry A*, vol. 111, no. 19, pp. 3789–3801, 2007.

[93] J. A. Miller, J. P. Senosiain, S. J. Klippenstein, and Y. Georgievskii, "Reactions over multiple, interconnected potential wells: unimolecular and bimolecular reactions on a c3h5 potential," *The Journal of Physical Chemistry A*, vol. 112, no. 39, pp. 9429–9438, 2008.

[94] A. Holmen, O. Olsvik, and O. Rokstad, "Pyrolysis of natural gas: chemistry and process concepts," *Fuel Processing Technology*, vol. 42, no. 2-3, p. 249–267, 1995.

[95] T. Kovács, I. G. Zsély, r. Kramarics, and T. Turányi, "Kinetic analysis of mechanisms of complex pyrolytic reactions," *Journal of analytical and applied pyrolysis*, vol. 79, no. 1-2, p. 252–258, 2007.

[96] G. Fau, N. Gascoin, P. Gillard, and J. Steelant, "Methane pyrolysis: Literature survey and comparisons of available data for use in numerical simulations," *Journal of analytical and applied pyrolysis*, vol. 104, p. 1–9, 2013.

[97] O. Olsvik, O. A. Rokstad, and A. Holmen, "Pyrolysis of methane in the presence of hydrogen," *Chemical Engineering & Technology: Industrial Chemistry-Plant Equipment-Process Engineering-Biotechnology*, vol. 18, no. 5, p. 349–358, 1995.

[98] J. Troe and V. Ushakov, "The dissociation/recombination reaction CH4 (+ M)= CH3+ H (+ M): A case study for unimolecular rate theory," *The Journal of chemical physics*, vol. 136, no. 21, p. 214309, 2012.

[99] D. M. Golden, "What, Methane Again?!," *International Journal of Chemical Kinetics*, vol. 45, no. 4, p. 213–220, 2013.

[100] H. Wang, E. Dames, B. Sirjean, D. Sheen, R. Tangko, A. Violi, J. Lai, F. Egolfopoulos, D. Davidson, R. Hanson, *et al.*, "A high-temperature chemical kinetic model of n-alkane (up to n-dodecane), cyclohexane, and methyl-, ethyl-, n-propyl and n-butyl-cyclohexane oxidation at high temperatures," *JetSurF version*, vol. 2, no. 2, p. 19, 2010.

[101] A. W. Jasper, J. A. Miller, and S. J. Klippenstein, "Collision efficiency of water in the unimolecular reaction CH4 (+ H2O)= CH3+ H (+ H2O): One-dimensional and two-dimensional solutions of the low-pressure-limit master equation," *The Journal of Physical Chemistry A*, vol. 117, no. 47, p. 12243–12255, 2013.

[102] B. Wang, H. Hou, L. M. Yoder, J. T. Muckerman, and C. Fockenberg, "Experimental and theoretical investigations on the methyl- methyl recombination reaction," *The Journal of Physical Chemistry A*, vol. 107, no. 51, p. 11414–11426, 2003.

[103] O. Olsvik and F. Billaud, "Modelling of the decomposition of methane at 1273 K in a plug flow reactor at low conversion," *Journal of analytical and applied pyrolysis*, vol. 25, p. 395–405, 1993.

[104] S. Peukert, N. Labbe, R. Sivaramakrishnan, and J. Michael, "Direct measurements of rate constants for the reactions of CH3 radicals with C2H6, C2H4, and C2H2 at high temperatures," *The Journal of Physical Chemistry A*, vol. 117, no. 40, p. 10228–10238, 2013.

[105] W. Möller, E. Mozzhukhin, and H. Gg. Wagner, "High Temperature Reactions of CH3 2. H-Abstraction from Alkanes," *Berichte der Bunsengesellschaft für physikalische Chemie*, vol. 91, no. 6, p. 660–666, 1987.

[106] D. Baulch, C. Cobos, R. Cox, C. Esser, P. Frank, T. Just, J. Kerr, M. Pilling, J. Troe, R. Walker, *et al.*, "Evaluated kinetic data for combustion modelling," *Journal of Physical and Chemical Reference Data*, vol. 21, no. 3, p. 411–734, 1992.

[107] D. Baulch, C. Bowman, C. Cobos, R. Cox, T. Just, J. Kerr, M. Pilling, D. Stocker, J. Troe, W. Tsang, *et al.*, "Evaluated kinetic data for combustion modeling: supplement II," *Journal of physical and chemical reference data*, vol. 34, no. 3, p. 757–1397, 2005.

[108] J. A. Miller and S. J. Klippenstein, "The H+C2H2(+M)= C2H3(+ M) and H+C2H2(+ M)= C2H5(+ M) reactions: Electronic structure, variational transition-state theory, and solutions to a two-dimensional master equation," *Physical Chemistry Chemical Physics*, vol. 6, no. 6, p. 1192–1202, 2004.

[109] R. Zhu and C. Lin, "The CH3+ HO2 reaction: First-principles prediction of its rate constant and product branching probabilities," *The Journal of Physical Chemistry A*, vol. 105, no. 25, p. 6243–6248, 2001.

[110] R. X. Fernandes, K. Luther, and J. Troe, "Falloff Curves for the Reaction CH3+ O2 (+ M)= CH3O2 (+ M) in the Pressure Range 2- 1000 bar and the Temperature Range 300- 700 K," *The Journal of Physical Chemistry A*, vol. 110, no. 13, p. 4442–4449, 2006.

[111] J. Michael, S. Kumaran, and M.-C. Su, "Rate constants for CH3+ O2= CH3O+ O at high temperature and evidence for H2CO+ O2= HCO+ HO2," *The Journal of Physical Chemistry A*, vol. 103, no. 30, p. 5942–5948, 1999.

[112] R. Zhu, C.-C. Hsu, and M. Lin, "Ab initio study of the CH 3+ O 2 reaction: kinetics, mechanism and product branching probabilities," *The Journal of chemical physics*, vol. 115, no. 1, p. 195–203, 2001.

[113] J. T. Herbon, R. K. Hanson, C. T. Bowman, and D. M. Golden, "The reaction of CH3+ O2: experimental determination of the rate coefficients for the product channels at high temperatures," *Proceedings of the Combustion Institute*, vol. 30, no. 1, p. 955–963, 2005.

[114] N. Srinivasan, M.-C. Su, J. Sutherland, and J. Michael, "Reflected shock tube studies of high-temperature rate constants for CH3+ O2, H2CO+ O2, and OH+ O2," *The Journal of Physical Chemistry A*, vol. 109, no. 35, p. 7902–7914, 2005.

[115] C. J. Aul, W. K. Metcalfe, S. M. Burke, H. J. Curran, and E. L. Petersen, "Ignition and kinetic modeling of methane and ethane fuel blends with oxygen: A design of experiments approach," *Combustion and Flame*, vol. 160, no. 7, p. 1153–1167, 2013.

[116] Tiziano Faravelli, Flavio Manenti, and Eliseo Ranzi, eds., *MATHEMATICAL MODELLING OF GASPHASE COMPLEX REACTION SYSTEMS : pyrolysis and combustion, Volume 45.* ELSEVIER Science LTD, 2019.

[117] M. G. Evans and M. Polanyi, "Inertia and driving force of chemical reactions," *Trans. Faraday Soc.*, vol. 34, p. 11–24, 1938.

[118] H.-H. Carstensen and A. M. Dean, "Rate constant rules for the automated generation of gas-phase reaction mechanisms," *The Journal of Physical Chemistry A*, vol. 113, no. 2, p. 367–380, 2008.

[119] R. Sumathi, H.-H. Carstensen, and W. H. Green, "Reaction rate prediction via group additivity part 1: H abstraction from alkanes by H and CH3," *The Journal of Physical Chemistry A*, vol. 105, no. 28, p. 6910–6925, 2001.

[120] R. Sumathi, H.-H. Carstensen, and W. H. Green, "Reaction rate prediction via group additivity, part 2: H-abstraction from alkenes, alkynes, alcohols, aldehydes, and acids by H atoms," *The Journal of Physical Chemistry A*, vol. 105, no. 39, p. 8969–8984, 2001.

[121] R. Sumathi, H.-H. Carstensen, and W. H. Green, "Reaction rate predictions via group additivity. Part 3: Effect of substituents with CH2 as the mediator," *The Journal of Physical Chemistry A*, vol. 106, no. 22, p. 5474–5489, 2002.

[122] M. Saeys, M.-F. Reyniers, G. B. Marin, V. Van Speybroeck, and M. Waroquier, "Ab initio group contribution method for activation energies for radical additions," *AIChE journal*, vol. 50, no. 2, p. 426–444, 2004.

[123] M. Saeys, M.-F. Reyniers, V. Van Speybroeck, M. Waroquier, and G. B. Marin, "Ab initio group contribution method for activation energies of hydrogen abstraction reactions," *ChemPhysChem*, vol. 7, no. 1, p. 188–199, 2006.

[124] M. K. Sabbe, M.-F. Reyniers, V. Van Speybroeck, M. Waroquier, and G. B. Marin, "Carbon-centered radical addition and β-scission reactions: modeling of activation energies and pre-exponential factors," *ChemPhysChem*, vol. 9, no. 1, p. 124–140, 2008.

[125] M. K. Sabbe, A. G. Vandeputte, M.-F. Reyniers, M. Waroquier, and G. B. Marin, "Modeling the influence of resonance stabilization on the kinetics of hydrogen abstractions," *Physical Chemistry Chemical Physics*, vol. 12, no. 6, p. 1278–1298, 2010.

[126] M. K. Sabbe, K. M. Van Geem, M.-F. Reyniers, and G. B. Marin, "First principle-based simulation of ethane steam cracking," *AIChE journal*, vol. 57, no. 2, p. 482–496, 2011.

[127] T. L. Cong and P. Dagaut, "Experimental and detailed kinetic modeling of the oxidation of methane and methane/syngas mixtures and effect of carbon dioxide addition," *Combustion Science and Technology*, vol. 180, no. 10-11, p. 2046–2091, 2008.

[128] T. Le Cong, P. Dagaut, and G. Dayma, "Oxidation of natural gas, natural gas/syngas mixtures, and effect of burnt gas recirculation: Experimental and detailed kinetic modeling," *Journal of Engineering for Gas Turbines and Power*, vol. 130, no. 4, p. 041502, 2008.

[129] T. Le Cong and P. Dagaut, "Effect of water vapor on the kinetics of combustion of hydrogen and natural gas: experimental and detailed modeling study," in *ASME Turbo Expo 2008: Power for Land, Sea, and Air*, p. 319–328, American Society of Mechanical Engineers, 2008.

[130] T. Le Cong and P. Dagaut, "Oxidation of H2/CO2 mixtures and effect of hydrogen initial concentration on the combustion of CH4 and CH4/CO2 mixtures: Experiments and modeling," *Proceedings of the Combustion Institute*, vol. 32, no. 1, p. 427–435, 2009.

[131] A. El Bakali, P. Dagaut, L. Pillier, P. Desgroux, J. F. Pauwels, A. Rida, and P. Meunier, "Experimental and modeling study of the oxidation of natural gas in a premixed flame, shock tube, and jet-stirred reactor," *Combustion and Flame*, vol. 137, no. 1-2, p. 109–128, 2004.

[132] P. Dagaut and G. Dayma, "Hydrogen-enriched natural gas blend oxidation under high-pressure conditions: experimental and detailed chemical kinetic modeling," *International Journal of Hydrogen Energy*, vol. 31, no. 4, p. 505–515, 2006.

[133] G. Bagheri, M. L. Lavadera, E. Ranzi, M. Pelucchi, P. Sabia, M. de Joannon, A. Parente, and T. Faravelli, "Thermochemical oscillation of methane MILD combustion diluted with N2/CO2/H2O," *Combustion Science and Technology*, p. 1–13, 2018.

[134] M. Lubrano Lavadera, Y. Song, P. Sabia, O. Herbinet, M. Pelucchi, A. Stagni, T. Faravelli, F. Battin-Leclerc, and M. de Joannon, "Oscillatory Behavior in

Methane Combustion: Influence of the Operating Parameters," *Energy & Fuels*, p. acs.energyfuels.8b00967, jul 2018.

[135] M. S. Skjøth-Rasmussen, P. Glarborg, M. Østberg, J. Johannessen, H. Livbjerg, A. Jensen, and T. Christensen, "Formation of polycyclic aromatic hydrocarbons and soot in fuel-rich oxidation of methane in a laminar flow reactor," *Combustion and Flame*, vol. 136, no. 1-2, p. 91–128, 2004.

[136] F. Sen, B. Shu, T. Kasper, J. Herzler, O. Welz, M. Fikri, B. Atakan, and C. Schulz, "Shock-tube and plug-flow reactor study of the oxidation of fuel-rich CH4/O2 mixtures enhanced with additives," *Combustion and Flame*, vol. 169, p. 307–320, 2016.

[137] A. Cuoci, A. Frassoldati, T. Faravelli, and E. Ranzi, "OpenSMOKE++: An object-oriented framework for the numerical modeling of reactive systems with detailed kinetic mechanisms," *Computer Physics Communications*, vol. 192, p. 237–264, 2015.

[138] D. Goodwin, H. Moffat, and R. Speth, "Cantera." `https://cantera.org/`. (Accessed on 01/12/2019).

[139] H. Pitsch, "ITV -FlameMaster." `https://www.itv.rwth-aachen.de/index.php?id=flamemaster&L=1`. (Accessed on 01/12/2019).

[140] E. L. Petersen, D. F. Davidson, and R. K. Hanson, "Ignition delay times of Ram accelerator CH/O/diluent mixtures," *Journal of Propulsion and Power*, vol. 15, no. 1, p. 82–91, 1999.

[141] Y. Levy, E. Olchanski, V. Sherbaum, V. Erenburg, and A. Burcat, "Shock-Tube Ignition Study of Methane in Air and Recirculating Gases Mixture," *Journal of propulsion and power*, vol. 22, no. 3, p. 669–676, 2006.

[142] R. D. Reitz, "Directions in internal combustion engine research," *Combustion and Flame*, vol. 1, no. 160, p. 1–8, 2013.

[143] G. Rozenchan, D. Zhu, C. Law, and S. Tse, "Outward propagation, burning velocities, and chemical effects of methane flames up to 60 atm," *Proceedings of the Combustion Institute*, vol. 29, no. 2, p. 1461–1470, 2002.

[144] W. Lowry, J. de Vries, M. Krejci, E. Petersen, Z. Serinyel, W. Metcalfe, H. Curran, and G. Bourque, "Laminar flame speed measurements and modeling of pure alkanes and alkane blends at elevated pressures," in *ASME Turbo Expo 2010: Power for Land, Sea, and Air*, p. 855–873, American Society of Mechanical Engineers, 2010.

[145] I. Glassman, R. A. Yetter, and N. G. Glumac, *Combustion*. Academic press, 2014.

[146] A. Cavaliere and M. de Joannon, "Mild combustion," *Progress in Energy and Combustion science*, vol. 30, no. 4, p. 329–366, 2004.

[147] T. Hasegawa, S. Mochida, and A. Gupta, "Development of advanced industrial furnace using highly preheated combustion air," *Journal of propulsion and power*, vol. 18, no. 2, p. 233–239, 2002.

[148] S. R. Turns *et al.*, *An introduction to combustion*, vol. 499. McGraw-hill New York, 1996.

[149] T. Plessing, N. Peters, and J. G. Wünning, "Laseroptical investigation of highly preheated combustion with strong exhaust gas recirculation," in *Symposium (International) on Combustion*, vol. 27, p. 3197–3204, Elsevier, 1998.

[150] B. B. Dally, A. Karpetis, and R. Barlow, "Structure of turbulent non-premixed jet flames in a diluted hot coflow," *Proceedings of the combustion institute*, vol. 29, no. 1, p. 1147–1154, 2002.

[151] M. Oberlack, R. Arlitt, and N. Peters, "On stochastic Damkohler number variations in a homogeneous flow reactor," *Combustion Theory and Modelling*, vol. 4, no. 4, p. 495–510, 2000.

[152] Z. Chen, V. Reddy, S. Ruan, N. A. K. Doan, W. L. Roberts, and N. Swaminathan, "Simulation of MILD combustion using Perfectly Stirred Reactor model," *Proceedings of the Combustion Institute*, vol. 36, no. 3, p. 4279–4286, 2017.

[153] M. De Joannon, G. Sorrentino, and A. Cavaliere, "MILD combustion in diffusion-controlled regimes of hot diluted fuel," *Combustion and Flame*, vol. 159, no. 5, p. 1832–1839, 2012.

[154] M. De Joannon, A. Cavaliere, T. Faravelli, E. Ranzi, P. Sabia, and A. Tregrossi, "Analysis of process parameters for steady operations in methane mild combustion technology," *Proceedings of the Combustion Institute*, vol. 30, no. 2, p. 2605–2612, 2005.

[155] M. De Joannon, P. Sabia, A. Tregrossi, and A. Cavaliere, "Dynamic behavior of methane oxidation in premixed flow reactor," *Combustion science and technology*, vol. 176, no. 5-6, p. 769–783, 2004.

[156] S. M. Burke, W. Metcalfe, O. Herbinet, F. Battin-Leclerc, F. M. Haas, J. Santner, F. L. Dryer, and H. J. Curran, "An experimental and modeling study of propene oxidation. Part 1: Speciation measurements in jet-stirred and flow reactors," *Combustion and Flame*, vol. 161, no. 11, p. 2765–2784, 2014.

[157] O. Rokstad, O. Olsvik, and A. Holmen, "Thermal coupling of methane," in *Studies in Surface Science and Catalysis*, vol. 61, p. 533–539, Elsevier, 1991.

[158] M. Kumar and Y. Ando, "Chemical vapor deposition of carbon nanotubes: a review on growth mechanism and mass production," *Journal of nanoscience and nanotechnology*, vol. 10, no. 6, p. 3739–3758, 2010.

[159] F. Billaud, C. Gueret, and J. Weill, "Thermal decomposition of pure methane at 1263 K. Experiments and mechanistic modelling," *Thermochimica acta*, vol. 211, p. 303–322, 1992.

[160] A. Mazas, D. Lacoste, and T. Schuller, "Experimental and numerical investigation on the laminar flame speed of CH4/O2 mixtures diluted with CO2 and H2O," in *ASME Turbo Expo 2010: Power for Land, Sea, and Air*, p. 411–421, American Society of Mechanical Engineers, 2010.

[161] Y. Xie, J. Wang, M. Zhang, J. Gong, W. Jin, and Z. Huang, "Experimental and numerical study on laminar flame characteristics of methane oxy-fuel mixtures highly diluted with CO2," *Energy & Fuels*, vol. 27, no. 10, p. 6231–6237, 2013.

[162] B. Koroglu, O. M. Pryor, J. Lopez, L. Nash, and S. S. Vasu, "Shock tube ignition delay times and methane time-histories measurements during excess CO 2 diluted oxy-methane combustion," *Combustion and flame*, vol. 164, p. 152–163, 2016.

[163] J. W. Hargis and E. L. Petersen, "Methane ignition in a shock tube with high levels of CO2 dilution: consideration of the reflected-shock bifurcation," *Energy & Fuels*, vol. 29, no. 11, p. 7712–7726, 2015.

[164] P. Sabia, M. De Joannon, S. Fierro, A. Tregrossi, and A. Cavaliere, "Hydrogen-enriched methane mild combustion in a well stirred reactor," *Experimental Thermal and Fluid Science*, vol. 31, no. 5, p. 469–475, 2007.

[165] F. Wang, P. Li, Z. Mei, J. Zhang, and J. Mi, "Combustion of CH4/O2/N2 in a well stirred reactor," *Energy*, vol. 72, p. 242–253, 2014.

[166] F. Wang, J. Mi, and P. Li, "Combustion regimes of a jet diffusion flame in hot co-flow," *Energy & Fuels*, vol. 27, no. 6, p. 3488–3498, 2013.

[167] P. R. Medwell, M. J. Evans, Q. N. Chan, and V. R. Katta, "Laminar flame calculations for analyzing trends in autoignitive jet flames in a hot and vitiated coflow," *Energy & Fuels*, vol. 30, no. 10, p. 8680–8690, 2016.

[168] M. Evans, P. Medwell, H. Wu, A. Stagni, and M. Ihme, "Classification and lift-off height prediction of non-premixed MILD and autoignitive flames," *Proceedings of the combustion institute*, vol. 36, no. 3, p. 4297–4304, 2017.

[169] P. Li, J. Mi, B. Dally, F. Wang, L. Wang, Z. Liu, S. Chen, and C. Zheng, "Progress and recent trend in MILD combustion," *Science China Technological Sciences*, vol. 54, no. 2, p. 255–269, 2011.

[170] B. Danon, A. Swiderski, W. De Jong, W. Yang, and D. Roekaerts, "Emission and efficiency comparison of different firing modes in a furnace with four HiTAC burners," *Combustion Science and Technology*, vol. 183, no. 7, p. 686–703, 2011.

[171] N. Peters, "Principles and potential of HiCOT combustion," in *Proceedings of the Forum on High-Temperature Air Combustion Technology*, p. 109, 2001.

[172] A. A. Konnov, M. T. Javed, H. Kassman, and N. Irfan, *NOx Formation, Control and Reduction Techniques*. Wiley-VCH Verlag GmbH & Co. KGaA, 2010.

[173] M. A. Galbiati, A. Cavigiolo, A. Effuggi, D. Gelosa, and R. Rota, "Mild combustion for fuel-NOx reduction," *Combustion Science and Technology*, vol. 176, no. 7, p. 1035–1054, 2004.

[174] K. Lee and D. Choi, "Analysis of NO formation in high temperature diluted air combustion in a coaxial jet flame using an unsteady flamelet model," *International Journal of Heat and Mass Transfer*, vol. 52, no. 5-6, p. 1412–1420, 2009.

[175] M. Abian, M. U. Alzueta, and P. Glarborg, "Formation of NO from N2/O2 mixtures in a flow reactor: toward an accurate prediction of thermal NO," *International Journal of Chemical Kinetics*, vol. 47, no. 8, p. 518–532, 2015.

[176] L. Spadaccini and M. Colket Iii, "Ignition delay characteristics of methane fuels," *Progress in energy and combustion science*, vol. 20, no. 5, p. 431–460, 1994.

[177] N. Lamoureux, C.-E. Paillard, and V. Vaslier, "Low hydrocarbon mixtures ignition delay times investigation behind reflected shock waves," *Shock waves*, vol. 11, no. 4, p. 309–322, 2002.

[178] G. A. Foulds, B. F. Gray, S. A. Miller, and G. S. Walker, "Homogeneous gas-phase oxidation of methane using oxygen as oxidant in an annular reactor," *Industrial & engineering chemistry research*, vol. 32, no. 5, p. 780–787, 1993.

[179] J. Griffiths and S. Hasko, "Ignitions, extinctions and thermokinetic oscillations accompanying the oxidation of ethane in an open system (continuously stirred tank reactor)," *Proc. R. Soc. Lond. A*, vol. 396, no. 1811, p. 227–255, 1984.

[180] D. Baulch, J. Griffiths, B. Johnson, and R. Richter, "Hydroxyl radical concentrations and reactant temperature profiles during oscillatory ignition of hydrogen: experimental measurements by laser resonance absorption spectroscopy and comparisons with numerical calculations," *Proc. R. Soc. Lond. A*, vol. 430, no. 1878, p. 151–166, 1990.

[181] P. Gray, J. Griffiths, and S. Scott, "Oscillations, glow and ignition in carbon monoxide oxidation in an open system. I. Experimental studies of the ignition diagram and the effects of added hydrogen," *Proc. R. Soc. Lond. A*, vol. 397, no. 1812, p. 21–44, 1985.

[182] P. Gray, J. Griffiths, and S. Scott, "Oscillations, glow and ignition in carbon monoxide oxidation in an open system II. Theory of the oscillatory ignition limit in the cst r," *Proc. R. Soc. Lond. A*, vol. 402, no. 1823, p. 187–204, 1985.

[183] D. Baulch, J. Griffiths, and R. Richter, "Measurements of reactant temperature and free-radical concentrations during the oscillatory combustion of hydrogen and carbon monoxide in a CSTR," *Chemical engineering science*, vol. 46, no. 9, p. 2315–2322, 1991.

[184] B. F. Gray, J. F. Griffiths, G. A. Foulds, B. G. Charlton, and G. S. Walker, "The Relevance of Thermokinetic Interactions and Numerical Modeling to the Homogeneous Partial Oxidation of Methane," *Industrial and Engineering Chemistry Research*, vol. 33, no. 5, p. 1126–1135, 1994.

[185] Y. K. Park and D. G. Vlachos, "Kinetically driven instabilities and selectivities in methane oxidation," *AIChE journal*, vol. 43, no. 8, p. 2083–2095, 1997.

[186] J. Griffiths, A. Firth, and P. Gray, "The thermokinetic oscillations of hydrocarbon oxidations: A test for the role played by acetyl radicals," in *Symposium (International) on Combustion*, vol. 15, p. 1493–1501, Elsevier, 1975.

[187] C. Gibson, P. Gray, J. Griffiths, and S. Hasko, "Spontaneous ignition of hydrocarbon and related fuels: A fundamental study of thermokinetic interactions," in *Symposium (International) on Combustion*, vol. 20, p. 101–109, Elsevier, 1985.

[188] T. Wada, F. Jarmolowitz, D. Abel, and N. Peters, "An instability of diluted lean methane/air combustion: Modeling and control," *Combustion Science and Technology*, vol. 183, no. 1, p. 1–19, 2010.

[189] B. Dally and N. Peters, "Heat loss-induced oscillation of methane and ethylene in a perfectly stirred reactor," in *6th Asia-Pacific Conference on Combustion*, The Combustion Institute, 2007.

[190] P. Sabia, G. Sorrentino, A. Chinnici, A. Cavaliere, and R. Ragucci, "Dynamic behaviors in methane MILD and oxy-fuel combustion. Chemical effect of CO2," *Energy & Fuels*, vol. 29, no. 3, p. 1978–1986, 2015.

[191] Y. Park and D. Vlachos, "Isothermal Chain-Branching, Reaction Exothermicity, and Transport Interactions in the Stability of Methane/Air Mixtures*," *Combustion and Flame*, vol. 114, p. 214–230, jul 1998.

[192] F. B. Shareh, G. Silcox, and E. G. Eddings, "Calculated Impacts of Diluents on Flame Temperature, Ignition Delay, and Flame Speed of Methane–Oxygen Mixtures at High Pressure and Low to Moderate Temperatures," *Energy & Fuels*, vol. 32, no. 3, p. 3891–3899, 2018.

[193] R. Stanger, T. Wall, R. Spörl, M. Paneru, S. Grathwohl, M. Weidmann, G. Scheffknecht, D. McDonald, K. Myöhänen, J. Ritvanen, *et al.*, "Oxyfuel combustion for CO2 capture in power plants," *International Journal of Greenhouse Gas Control*, vol. 40, p. 55–125, 2015.

[194] C. E. Baukal Jr, *Oxygen-enhanced combustion*. CRC press, 2013.

[195] L. Lei and M. P. Burke, "Evaluating mixture rules and combustion implications for multi-component pressure dependence of allyl+ HO2 reactions," *Proceedings of the Combustion Institute*, 2018.

[196] O. Pryor, S. Barak, B. Koroglu, E. Ninnemann, and S. S. Vasu, "Measurements and interpretation of shock tube ignition delay times in highly CO 2 diluted mixtures using multiple diagnostics," *Combustion and Flame*, vol. 180, p. 63–76, 2017.

[197] O. Pryor, S. Barak, J. Lopez, E. Ninnemann, B. Koroglu, L. Nash, and S. Vasu, "High pressure shock tube ignition delay time measurements during oxy-methane combustion with high levels of CO2 dilution," *Journal of Energy Resources Technology*, vol. 139, no. 4, p. 042208, 2017.

[198] B. Koroglu, O. Pryor, J. Lopez, L. Nash, and S. Vasu, "Methane ignition delay times in CO2 diluted mixtures in a shock tube," in *51st AIAA/SAE/ASEE Joint Propulsion Conference*, p. 4088, 2015.

[199] A. W. Jasper, R. Sivaramakrishnan, and S. J. Klippenstein, "Are Termolecular Reactions Facile in Radical Recombinations?," *11th U. S. National Combustion Meeting*, 2019.

[200] M. R. Wright, *Introduction to chemical kinetics*. John Wiley & Sons, 2005.

[201] A. W. Jasper, C. M. Oana, and J. A. Miller, ""Third-body" collision efficiencies for combustion modeling: Hydrocarbons in atomic and diatomic baths," *Proceedings of the Combustion Institute*, vol. 35, no. 1, p. 197–204, 2015.

[202] S. J. Klippenstein, "From theoretical reaction dynamics to chemical modeling of combustion," *Proceedings of the Combustion Institute*, vol. 36, no. 1, p. 77–111, 2017.

[203] M. P. Burke and R. Song, "Evaluating mixture rules for multi-component pressure dependence: H+ O2 (+ M)= HO2 (+ M)," *Proceedings of the Combustion Institute*, vol. 36, no. 1, p. 245–253, 2017.

[204] G. H. Abd-Alla, "Using exhaust gas recirculation in internal combustion engines: a review," *Energy Conversion and Management*, vol. 43, no. 8, p. 1027–1042, 2002.

[205] M. Zheng, G. T. Reader, and J. G. Hawley, "Diesel engine exhaust gas recirculation—-a review on advanced and novel concepts," *Energy conversion and management*, vol. 45, no. 6, p. 883–900, 2004.

[206] M. B. Toftegaard, J. Brix, P. A. Jensen, P. Glarborg, and A. D. Jensen, "Oxy-fuel combustion of solid fuels," *Progress in energy and combustion science*, vol. 36, no. 5, p. 581–625, 2010.

[207] S. Jahangirian, A. Engeda, and I. S. Wichman, "Thermal and chemical structure of biogas counterflow diffusion flames," *Energy & Fuels*, vol. 23, no. 11, p. 5312–5321, 2009.

[208] S. Chen and C. Zheng, "Counterflow diffusion flame of hydrogen-enriched biogas under MILD oxy-fuel condition," *International journal of hydrogen energy*, vol. 36, no. 23, p. 15403–15413, 2011.

[209] M. De Joannon, P. Sabia, G. Cozzolino, G. Sorrentino, and A. Cavaliere, "Pyrolitic and oxidative structures in hot oxidant diluted oxidant (HODO) MILD combustion," *Combustion Science and Technology*, vol. 184, no. 7-8, p. 1207–1218, 2012.

[210] P. Glarborg and L. L. Bentzen, "Chemical effects of a high CO2 concentration in oxy-fuel combustion of methane," *Energy & Fuels*, vol. 22, no. 1, p. 291–296, 2007.

[211] P. Heil, D. Toporov, M. Förster, and R. Kneer, "Experimental investigation on the effect of O2 and CO2 on burning rates during oxyfuel combustion of methane," *Proceedings of the Combustion Institute*, vol. 33, no. 2, p. 3407–3413, 2011.

[212] A. Mazas, B. Fiorina, D. Lacoste, and T. Schuller, "Effects of water vapor addition on the laminar burning velocity of oxygen-enriched methane flames," *Combustion and Flame*, vol. 158, no. 12, p. 2428–2440, 2011.

[213] M. Abián, J. Giménez-López, R. Bilbao, and M. U. Alzueta, "Effect of different concentration levels of CO2 and H2O on the oxidation of CO: Experiments and modeling," *Proceedings of the Combustion Institute*, vol. 33, no. 1, p. 317–323, 2011.

[214] R. Getzinger and L. Blair, "Recombination in the hydrogen-oxygen reaction: A shock tube study with nitrogen and water vapour as third bodies," *Combustion and Flame*, vol. 13, no. 3, p. 271–284, 1969.

[215] D. Davidson, E. Petersen, M. Röhrig, R. Hanson, and C. Bowman, "Measurement of the rate coefficient of H+ O2+ M= HO2+ M for M= Ar and N2 at high pressures," in *Symposium (International) on Combustion*, vol. 26, p. 481–488, Elsevier, 1996.

[216] P. Ashman and B. Haynes, "Rate coefficient of H þ O2 þ M $1/4$ HO2 þ M (M $1/4$ H2O, N2, Ar, and CO2)," in *Proc Combust Inst*, vol. 27, p. 185–91, 1998.

[217] R. W. Bates, D. M. Golden, R. K. Hanson, and C. T. Bowman, "Experimental study and modeling of the reaction H+ O 2+ M=HO 2+ M (M= Ar, N 2, H2O) at elevated pressures and temperatures between 1050 and 1250 K," *Physical Chemistry Chemical Physics*, vol. 3, no. 12, p. 2337–2342, 2001.

[218] W. Wong and D. Davis, "A flash photolysis-resonance fluorescence study of the reaction of atomic hydrogen with molecular oxygen H+ O2+ M=HO2+ M," *International Journal of Chemical Kinetics*, vol. 6, no. 3, p. 401–416, 1974.

[219] J. Michael, M.-C. Su, J. Sutherland, J. Carroll, and A. Wagner, "Rate constants for H+ O2+ M=HO2+ M in seven bath gases," *The Journal of Physical Chemistry A*, vol. 106, no. 21, p. 5297–5313, 2002.

[220] R. Fernandes, K. Luther, J. Troe, and V. Ushakov, "Experimental and modelling study of the recombination reaction H+ O 2 (+ M)=HO 2 (+ M) between 300 and 900 K, 1.5 and 950 bar, and in the bath gases M= He, Ar, and N 2," *Physical Chemistry Chemical Physics*, vol. 10, no. 29, p. 4313–4321, 2008.

[221] N. J. Labbe, R. Sivaramakrishnan, C. F. Goldsmith, Y. Georgievskii, J. A. Miller, and S. J. Klippenstein, "Ramifications of including non-equilibrium effects for HCO in flame chemistry," *Proceedings of the Combustion Institute*, vol. 36, no. 1, p. 525–532, 2017.

[222] H. N. Najm, P. H. Paul, C. J. Mueller, and P. S. Wyckoff, "On the adequacy of certain experimental observables as measurements of flame burning rate," *Combustion and flame*, vol. 113, no. 3, p. 312–332, 1998.

[223] Z. M. Nikolaou and N. Swaminathan, "Heat release rate markers for premixed combustion," *Combustion and Flame*, vol. 161, no. 12, p. 3073–3084, 2014.

[224] L. L. N. Laboratory, "DEtailed Kinetic Mechanisms." `https://combustion.llnl.gov/mechanisms`. (Accessed on 06/16/2019).

[225] "Chemical Mechanism: Combustion Research Group at UC San Diego." `https://web.eng.ucsd.edu/mae/groups/combustion/mechanism.html`. (Accessed on 06/16/2019).

[226] T. Varga, C. Olm, T. Nagy, I. G. Zsély, v. Valkó, R. Pálvölgyi, H. J. Curran, and T. Turányi, "Development of a joint hydrogen and syngas combustion mechanism based on an optimization approach," *International journal of chemical kinetics*, vol. 48, no. 8, p. 407–422, 2016.

[227] G. Blanquart, P. Pepiot-Desjardins, and H. Pitsch, "Chemical mechanism for high temperature combustion of engine relevant fuels with emphasis on soot precursors," *Combustion and Flame*, vol. 156, no. 3, p. 588–607, 2009.

[228] J. Troe, "Predictive possibilities of unimolecular rate theory," *Journal of Physical Chemistry*, vol. 83, no. 1, p. 114–126, 1979.

[229] J. A. Miller and S. J. Klippenstein, "Dissociation of propyl radicals and other reactions on a C3H7 potential," *The Journal of Physical Chemistry A*, vol. 117, no. 13, p. 2718–2727, 2013.

[230] G. E. Box and N. R. Draper, *Empirical model-building and response surfaces.* John Wiley & Sons, 1987.

[231] H. Wang and D. A. Sheen, "Combustion kinetic model uncertainty quantification, propagation and minimization," *Progress in Energy and Combustion Science*, vol. 47, p. 1–31, 2015.

[232] R. K. Hanson, "Applications of quantitative laser sensors to kinetics, propulsion and practical energy systems," *Proceedings of the Combustion Institute*, vol. 33, no. 1, pp. 1–40, 2011.

Glossary

A

A	Pre-exponential factor. 16

B

β	Temperature exponent. 16

C

$\mathring{C}_P$	Standard heat capacitiy. 10
CFD	Computational fluid dynamic. 5
$[X]$	Concentration of given species X. 10
C_p	Heat capacity at constant pressure. 13
C_v	Heat capacity at constant volume. 13

E

E_a	Activation energy. 16

G

G	Gibbs free energy. 9

H

H	Enthalpy. 9
$\mathring{H}_f$	Standard enthalpy of formation. 10

J

JSR	Jet stirred reactor. 3, 24, 26, 27

K

K_c	Equilibrium constant. 10
k_f	Forward rate constant. 16
K_p	Equilibrium constant. 10, 11
k_r	Reverse rate constant. 16

M

MILD	Moderate or intense low-oxygen dilution. 2–4, 17, 19, 23–25, 28, 36, 40

Glossary

O

1-D flame	One dimension flame. 3

P

PFR	Plug flow reactor. 3
p_X	Partial presseure of given species X. 10

Q

q_i	Rate of progress variable. 15

R

R	Gas constant. 10

S

S	Entropy. 9
$\mathring{S}$	Standard entropy. 10

T

T	Temerature [K]. 10

V

υ'_{ni}	Forward stoichiometric coefficients. 15
υ''_{ni}	Reverse stoichiometric coefficients. 15

W

$\dot{\omega}_n$	Formation rate. 15

Part I

Appendix

Supplementary Materials

Contents

1. Jet-Stirred Reactor (JSR)

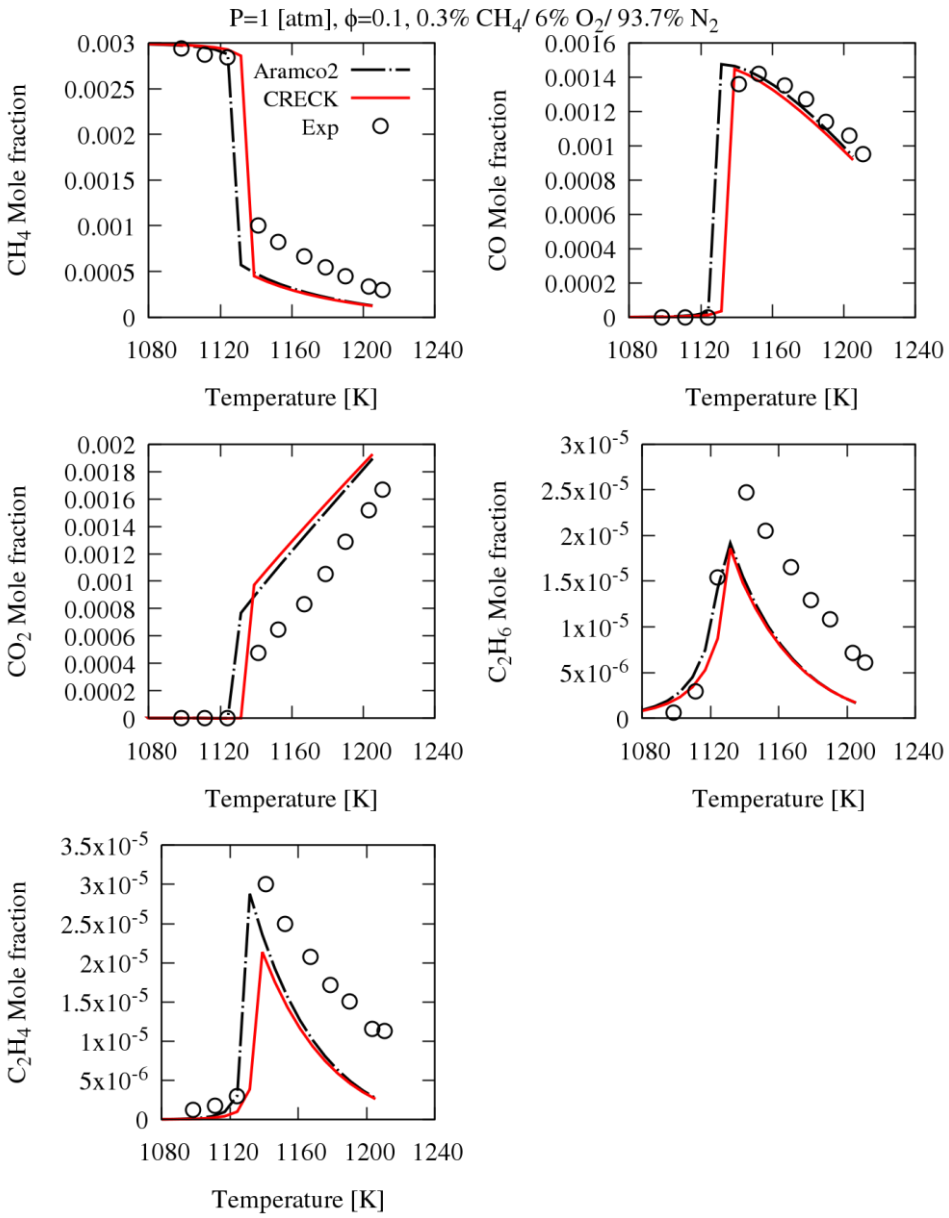

Figure 1 Jet-stirred reactor species profiles of methane oxidation. Exp refers to [1].

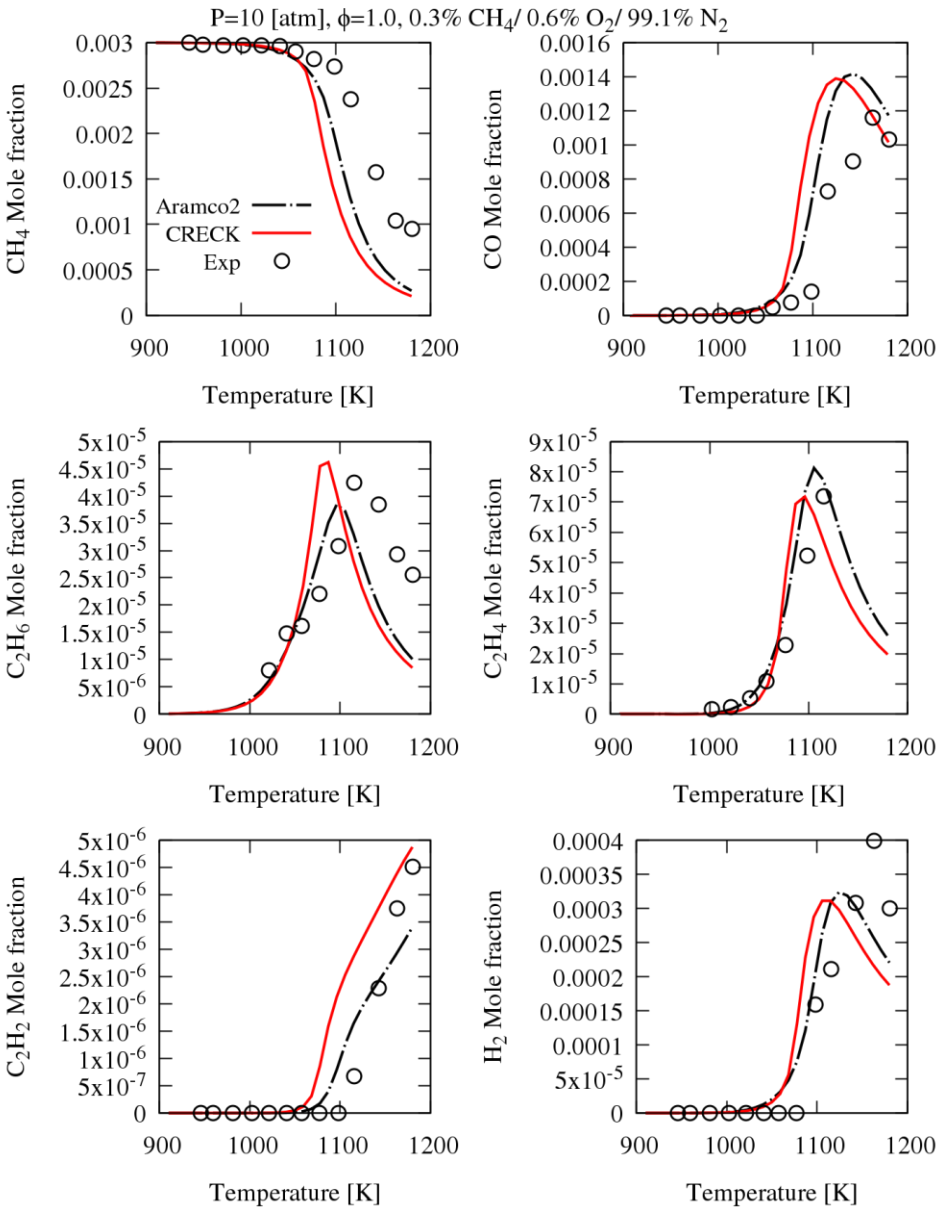

Figure 2 Jet-stirred reactor species profiles of methane oxidation. Exp refers to [1].

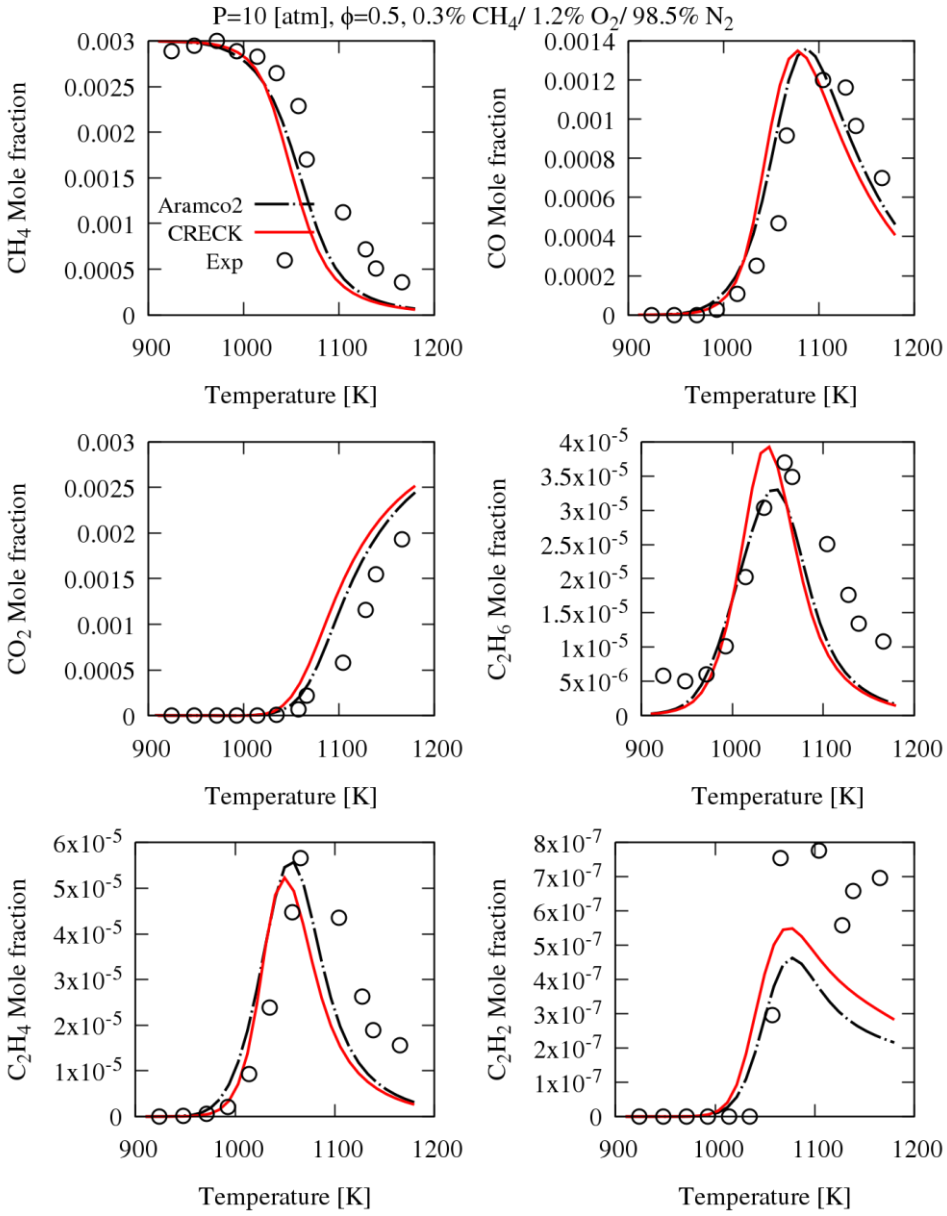

Figure 3 Jet-stirred reactor species profiles of methane oxidation. Exp refers to [1].

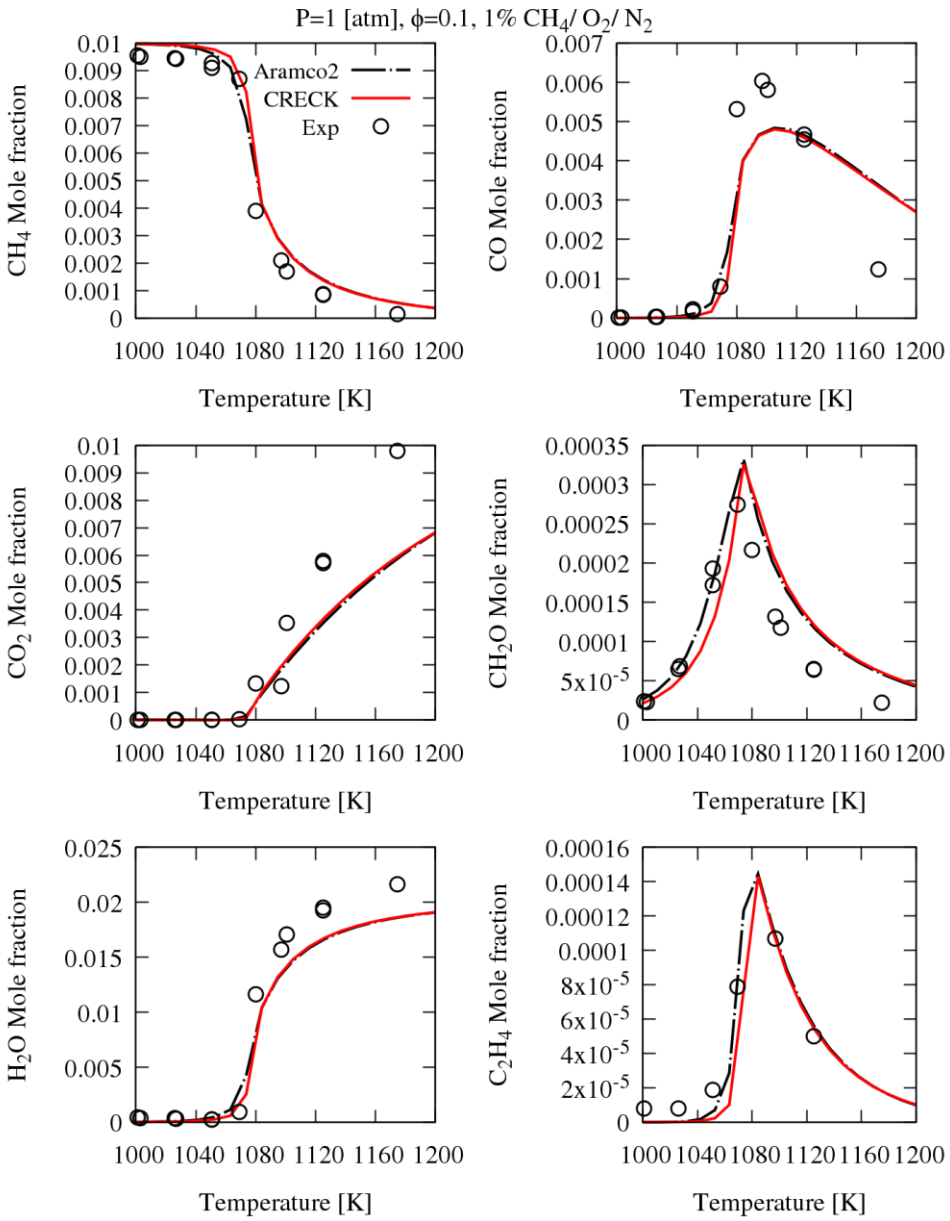

Figure 4 Jet-stirred reactor species profiles of methane oxidation. Exp refers to [2].

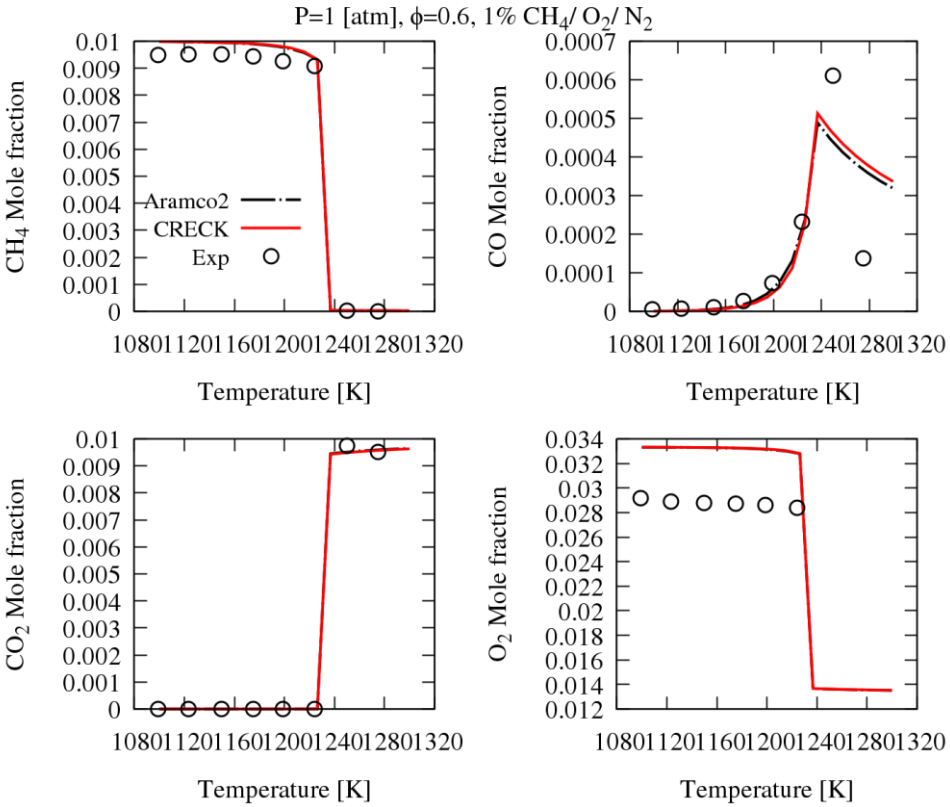

Figure 5 Jet-stirred reactor species profiles of methane oxidation. Exp refers to [2].

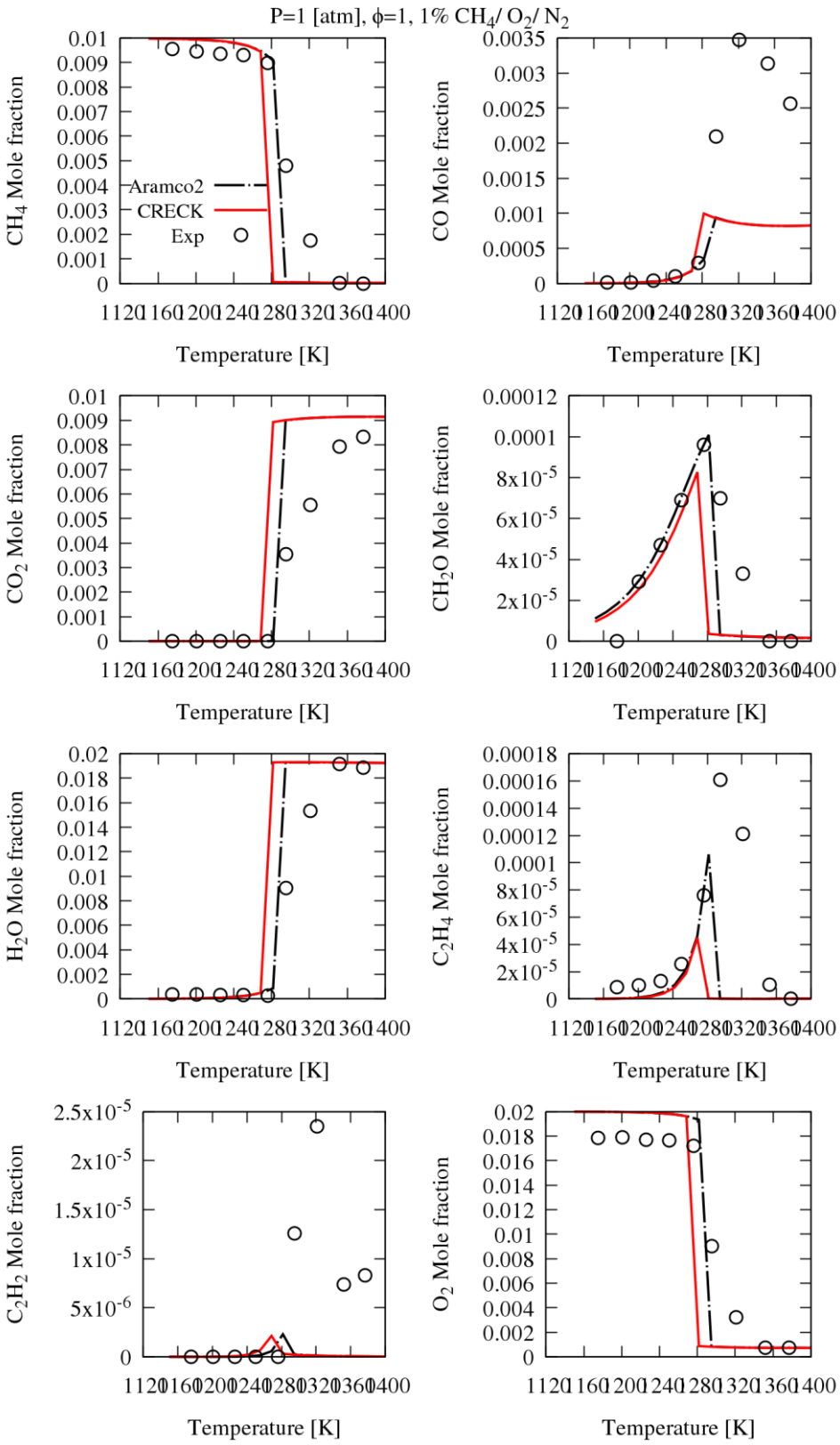

Figure 6 Jet-stirred reactor species profiles of methane oxidation. Exp refers to [2].

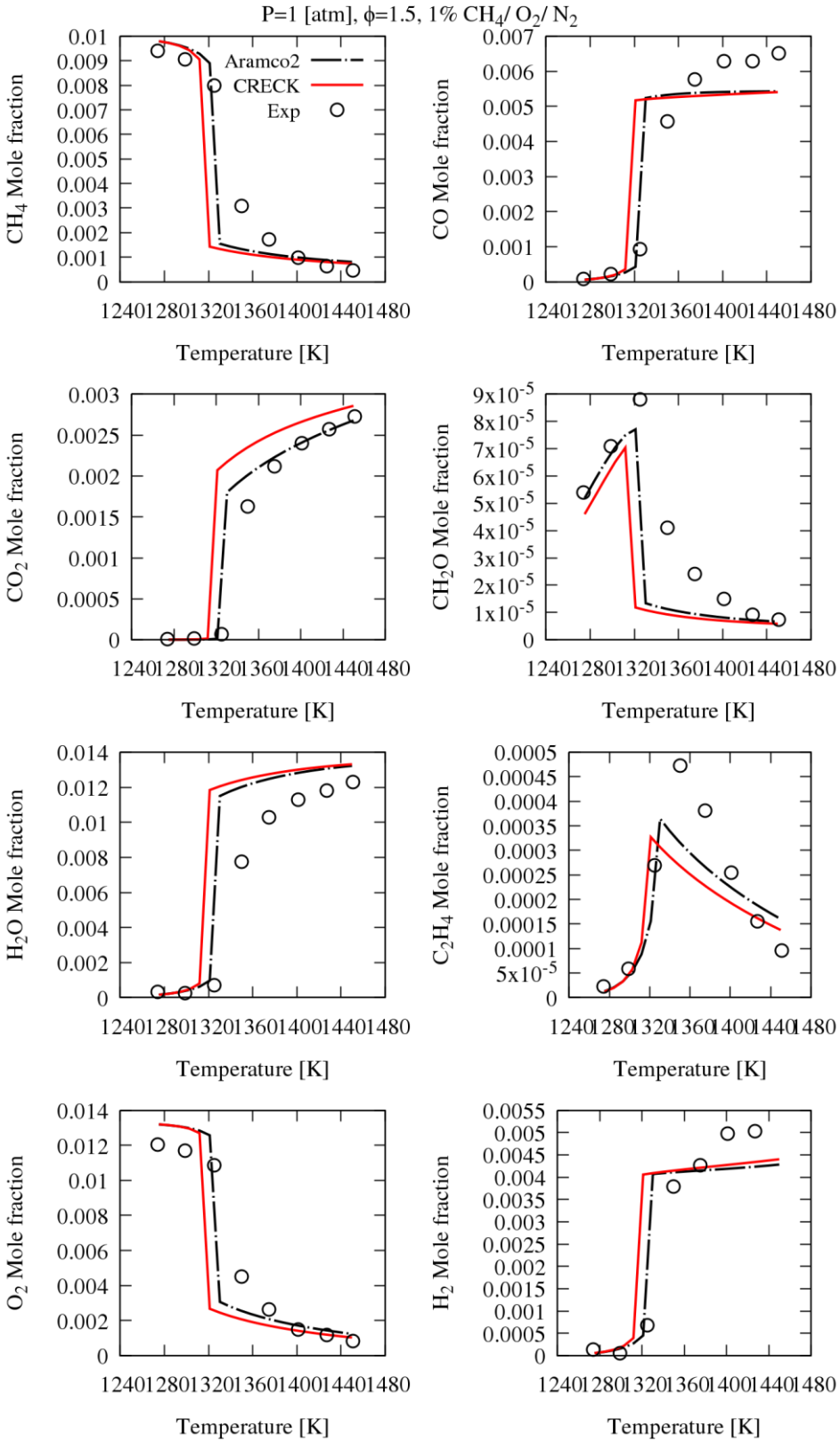

Figure 7 Jet-stirred reactor species profiles of methane oxidation. Exp refers to [2].

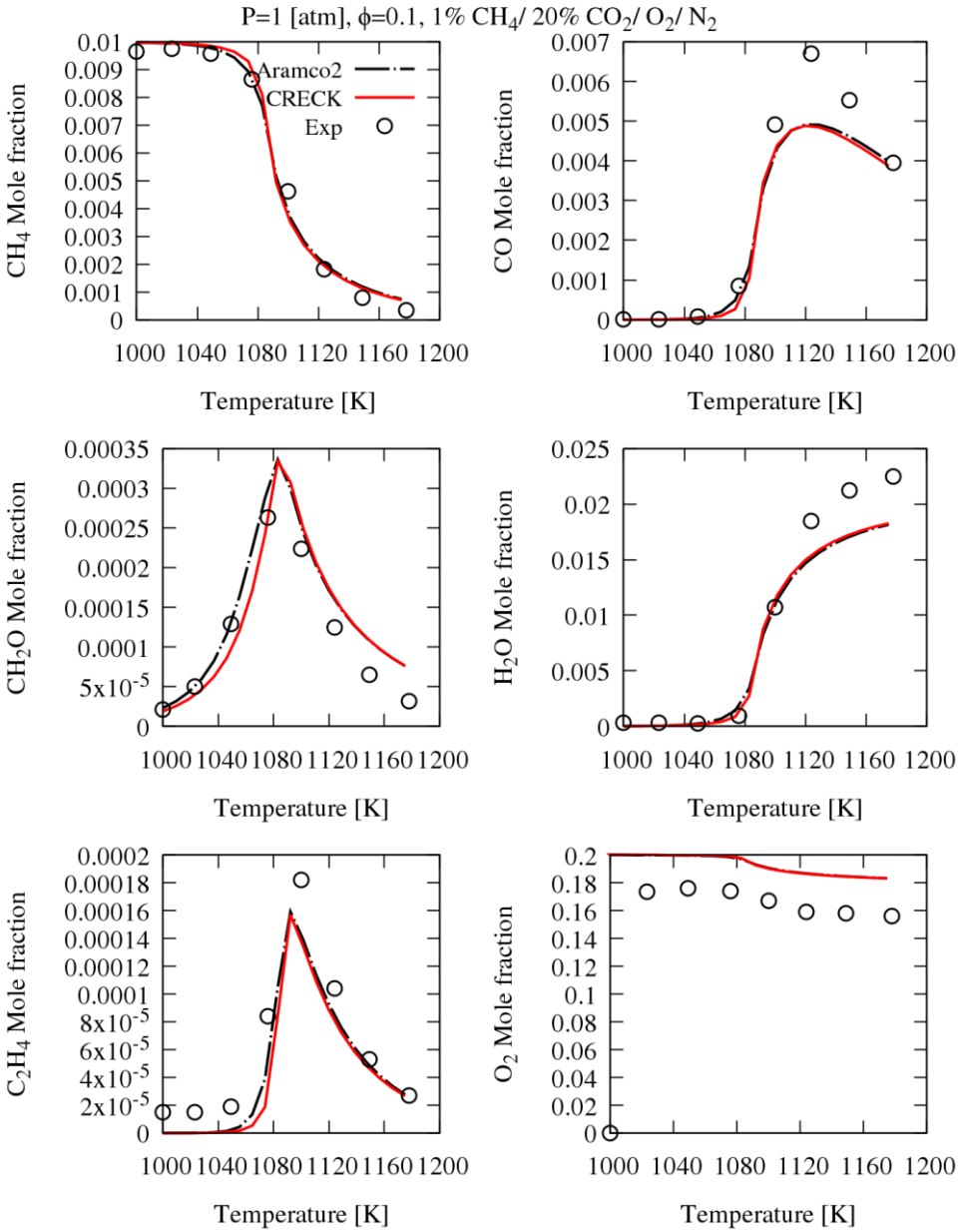

Figure 8 Jet-stirred reactor species profiles of methane oxidation. Exp refers to [2].

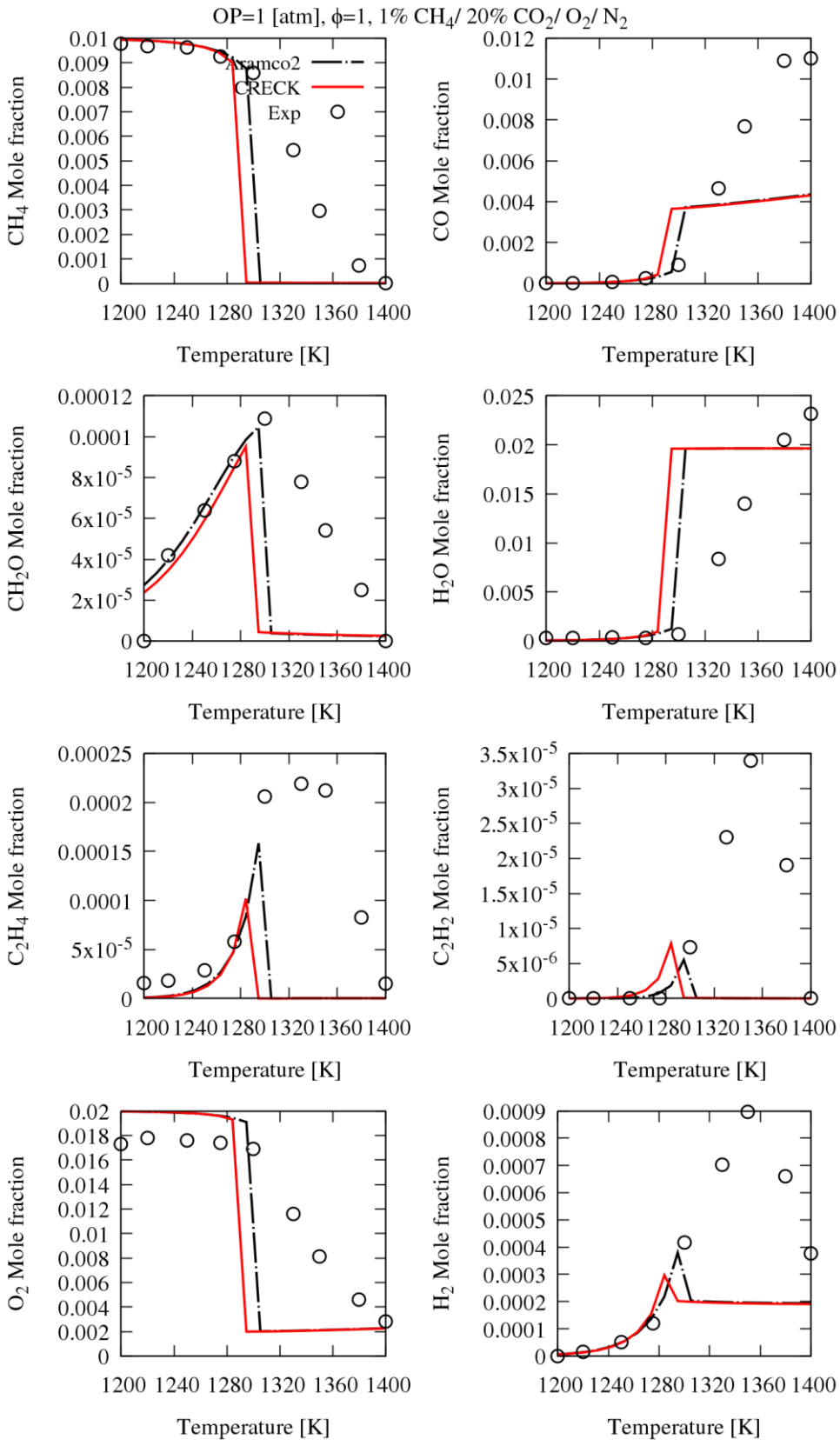

Figure 9 Jet-stirred reactor species profiles of methane oxidation. Exp refers to [2].

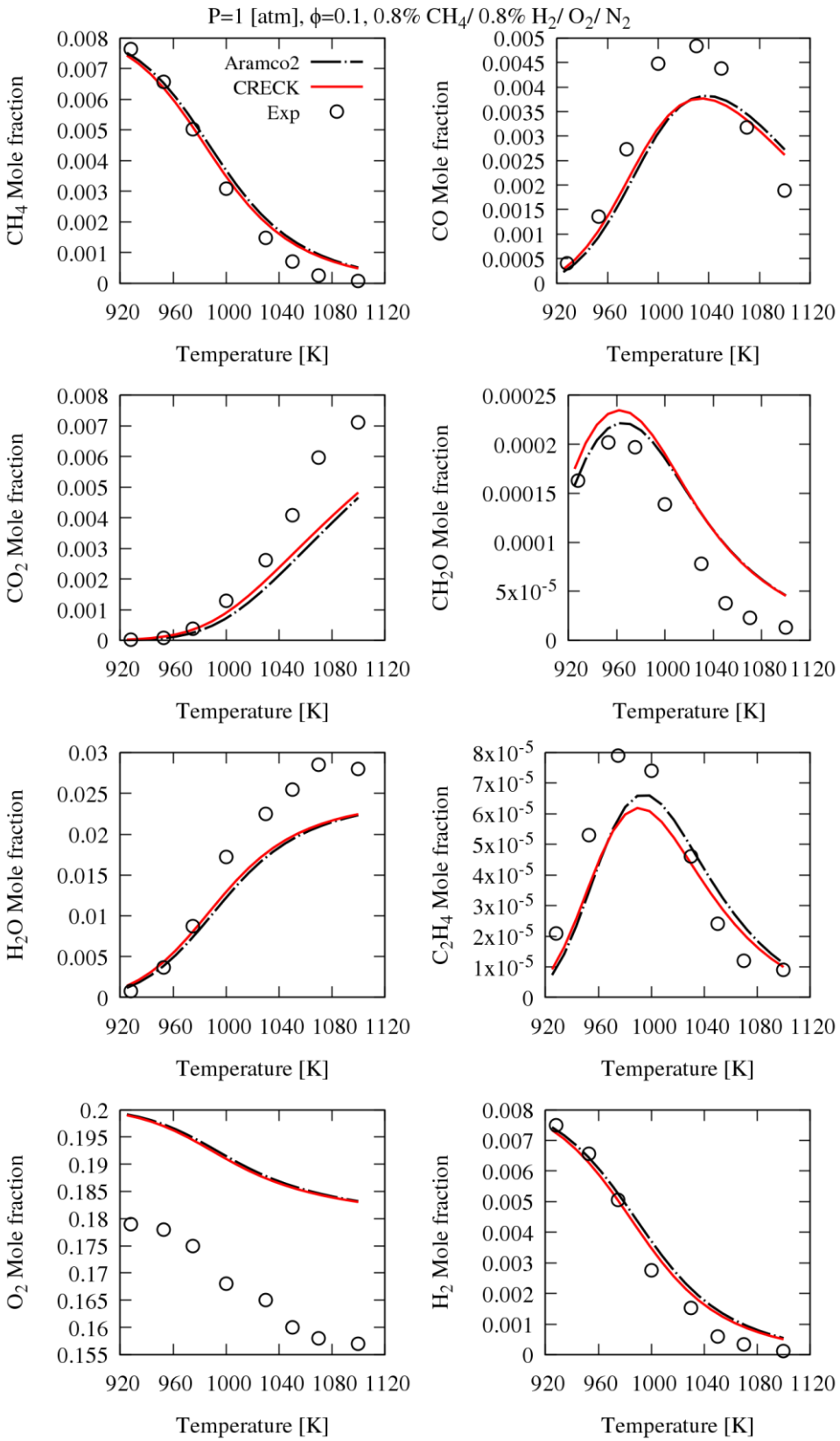

Figure 10 Jet-stirred reactor species profiles of methane oxidation doped by hydrogen. Exp refers to [2].

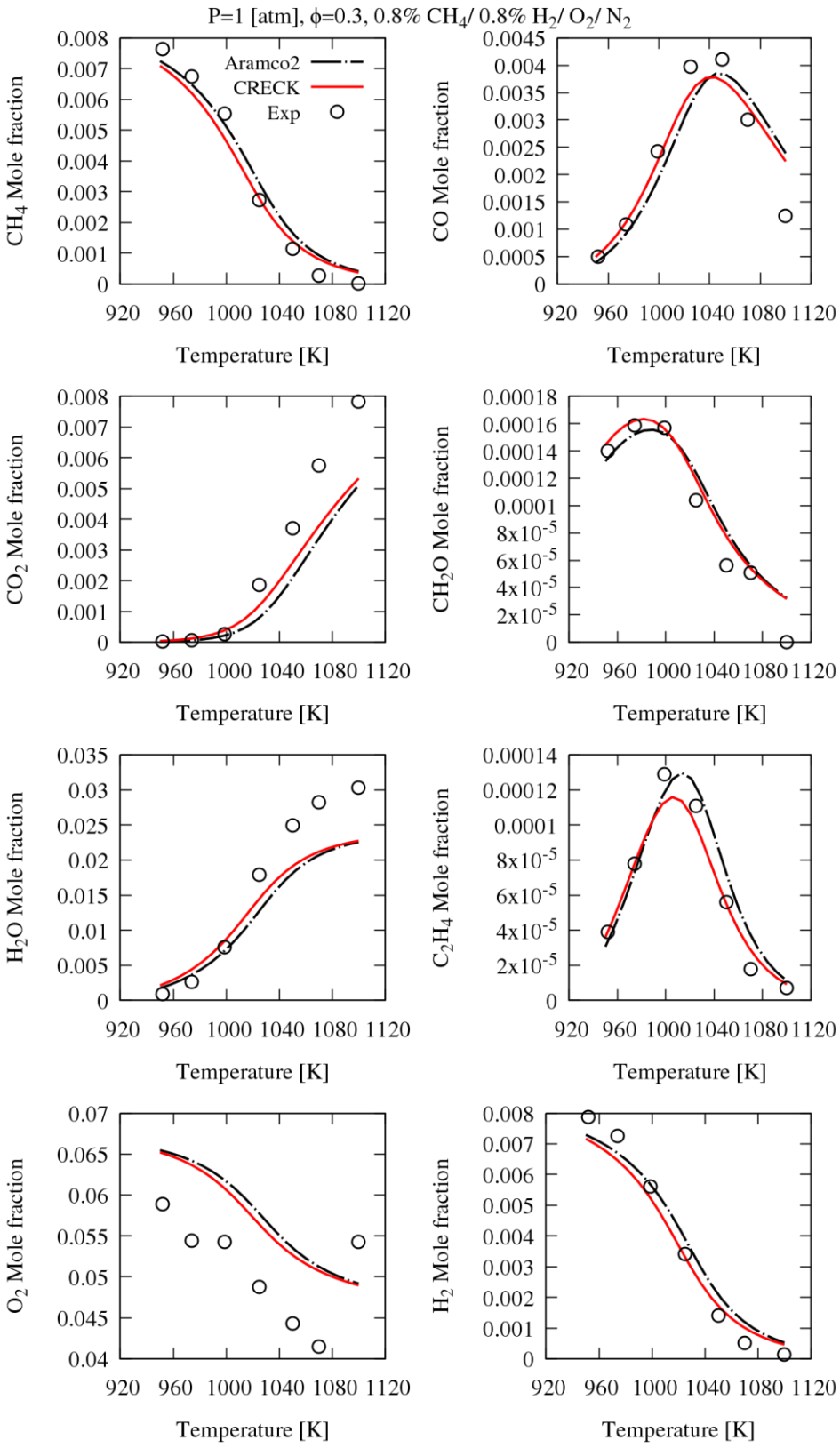

Figure 11 Jet-stirred reactor species profiles of methane oxidation doped by hydrogen. Exp refers to [2].

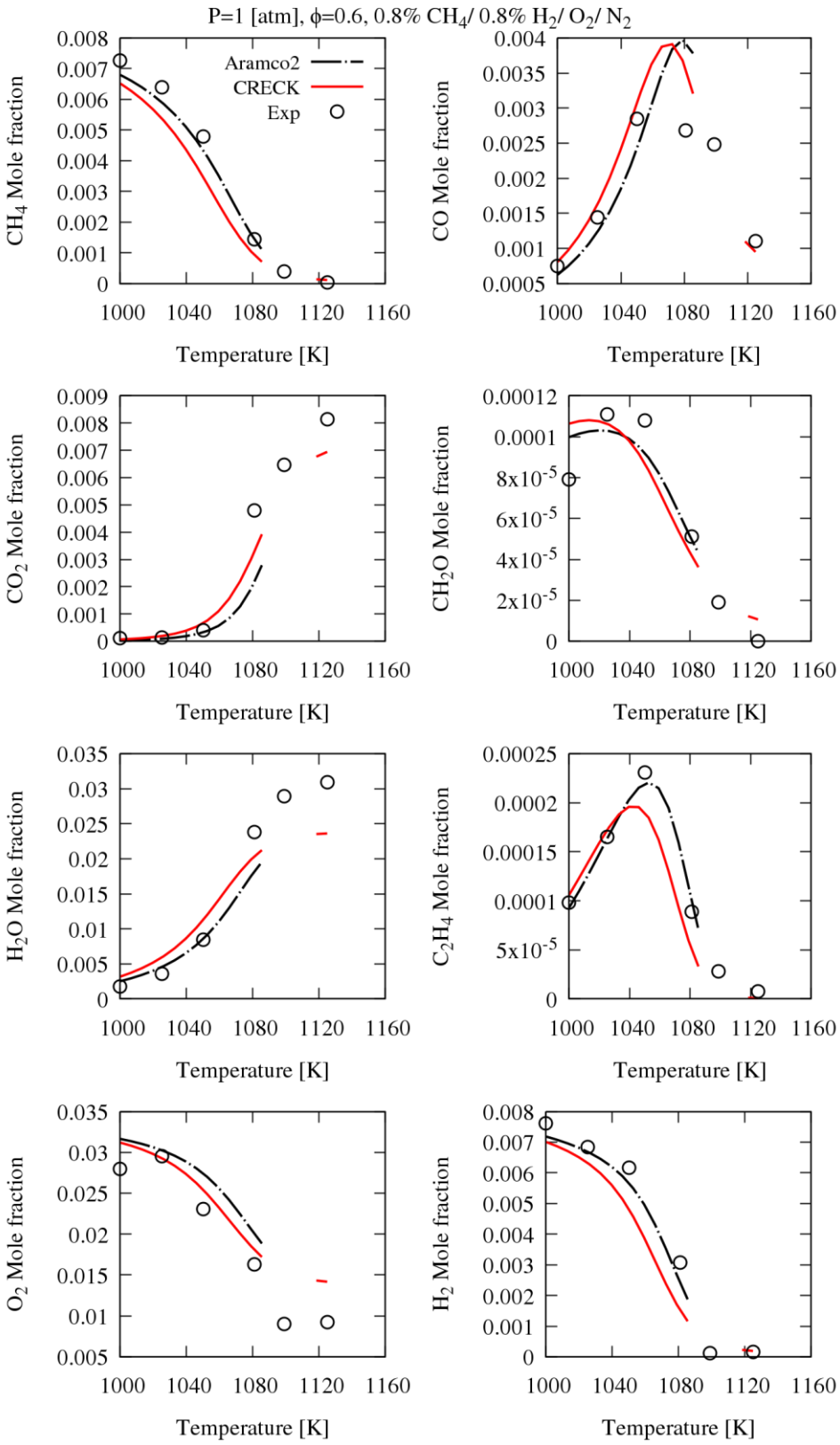

Figure 12 Jet-stirred reactor species profiles of methane oxidation doped by hydrogen. Exp refers to [2].

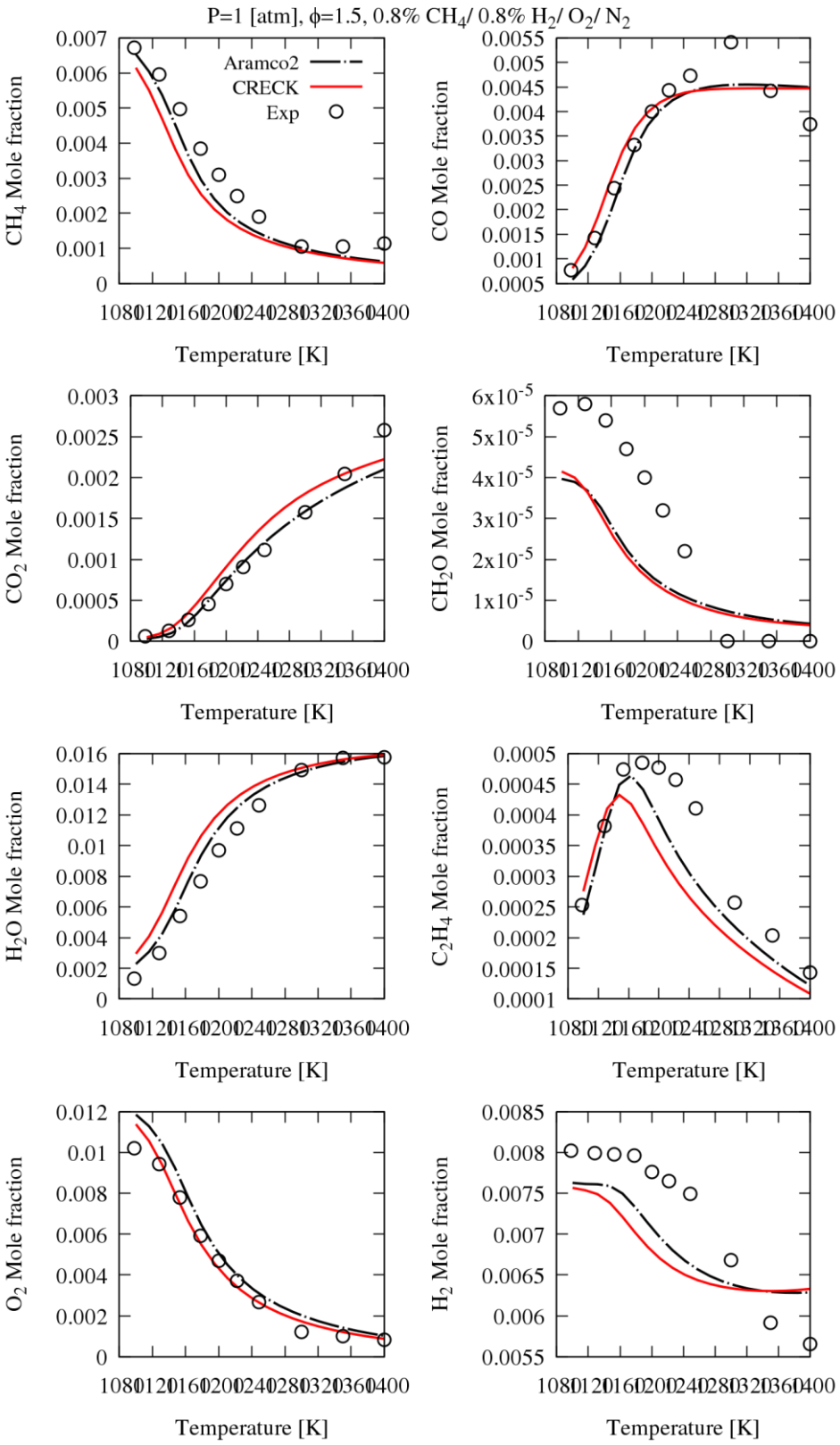

Figure 13 Jet-stirred reactor species profiles of methane oxidation doped by hydrogen. Exp refers to [2].

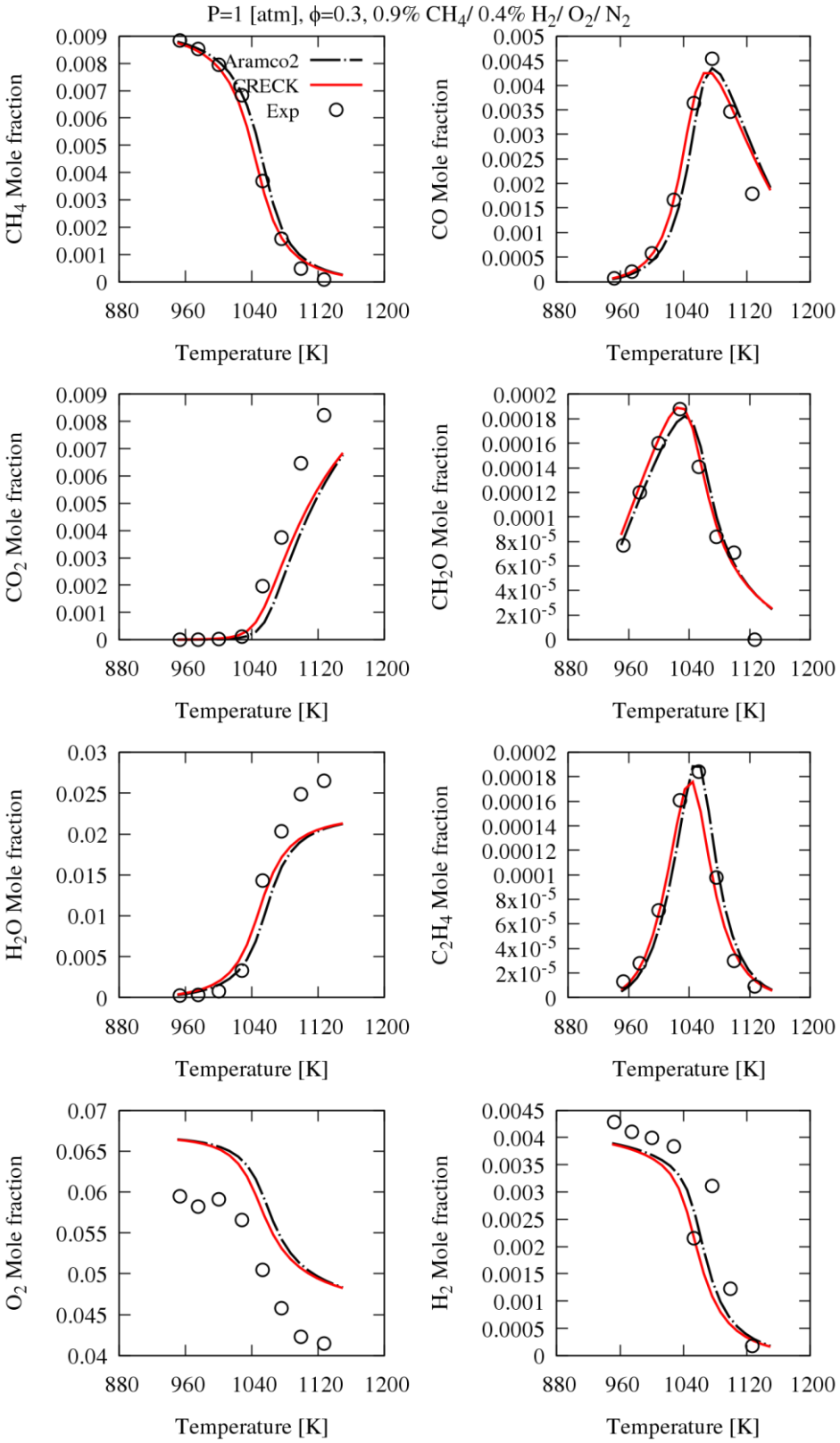

Figure 14 Jet-stirred reactor species profiles of methane oxidation doped by hydrogen. Exp refers to [2].

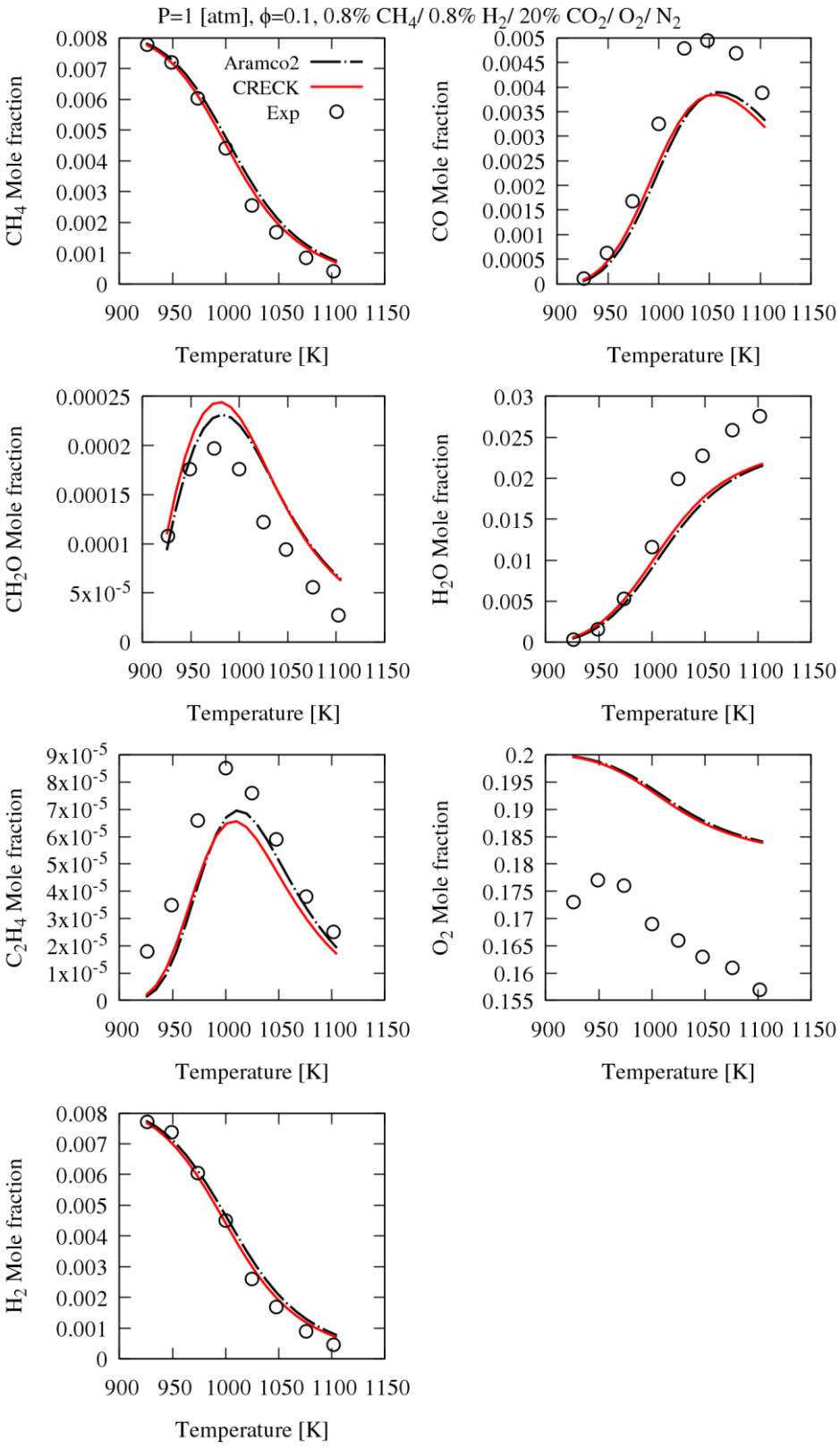

Figure 15 Jet-stirred reactor species profiles of methane oxidation doped by hydrogen. Exp refers to [2].

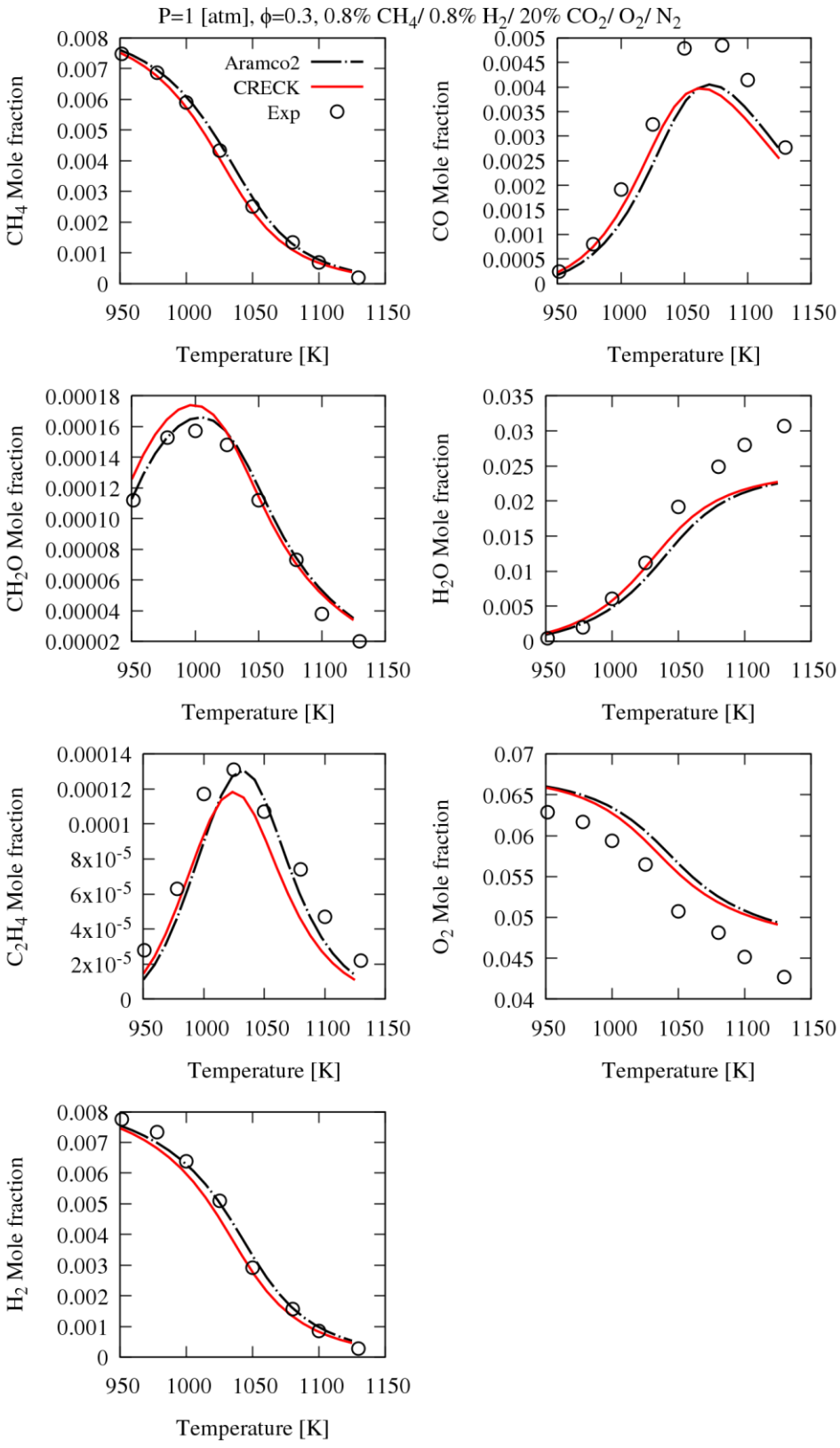

Figure 16 Jet-stirred reactor species profiles of methane oxidation doped by hydrogen. Exp refers to [2].

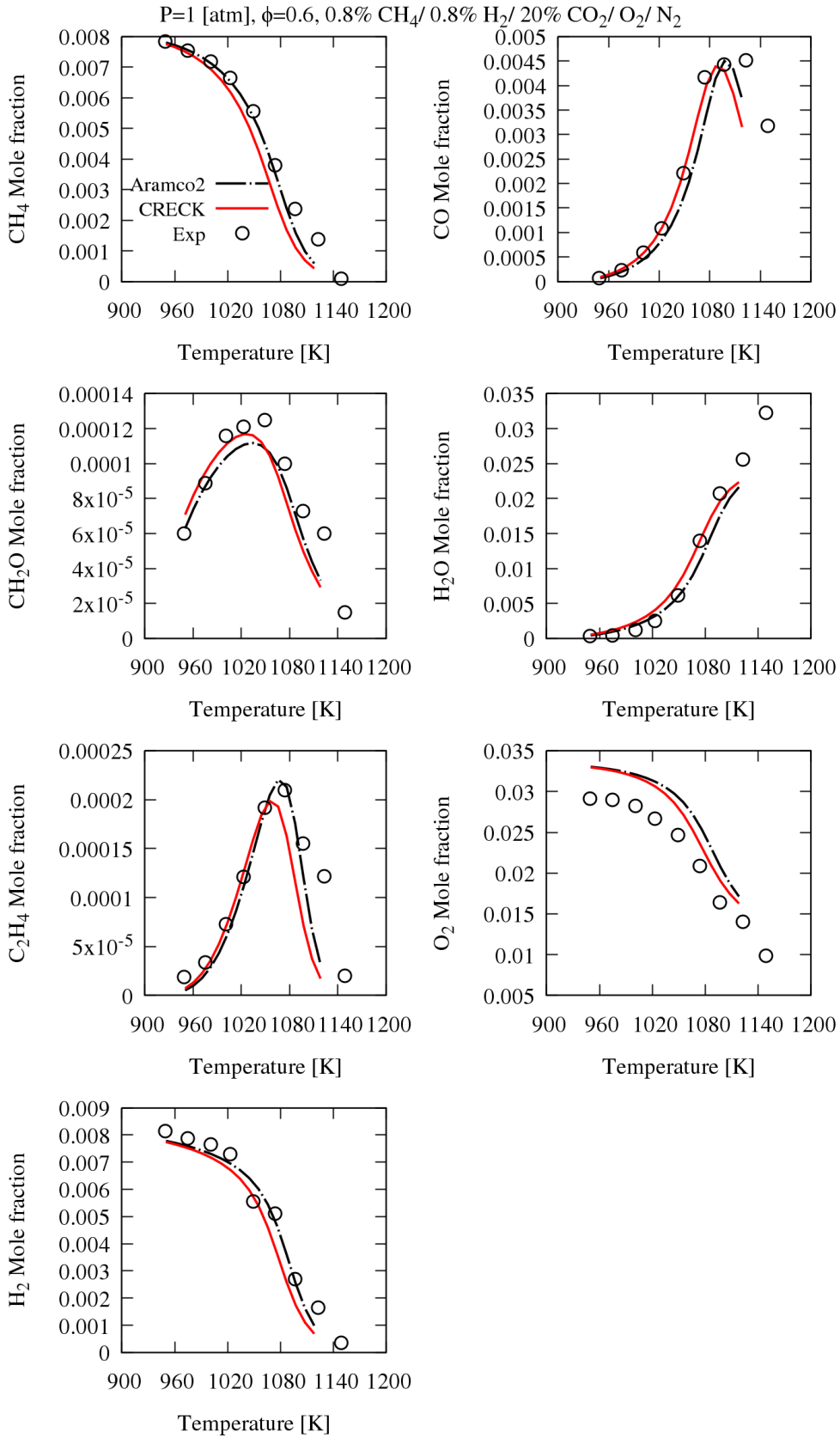

Figure 17 Jet-stirred reactor species profiles of methane oxidation doped by hydrogen. Exp refers to [2].

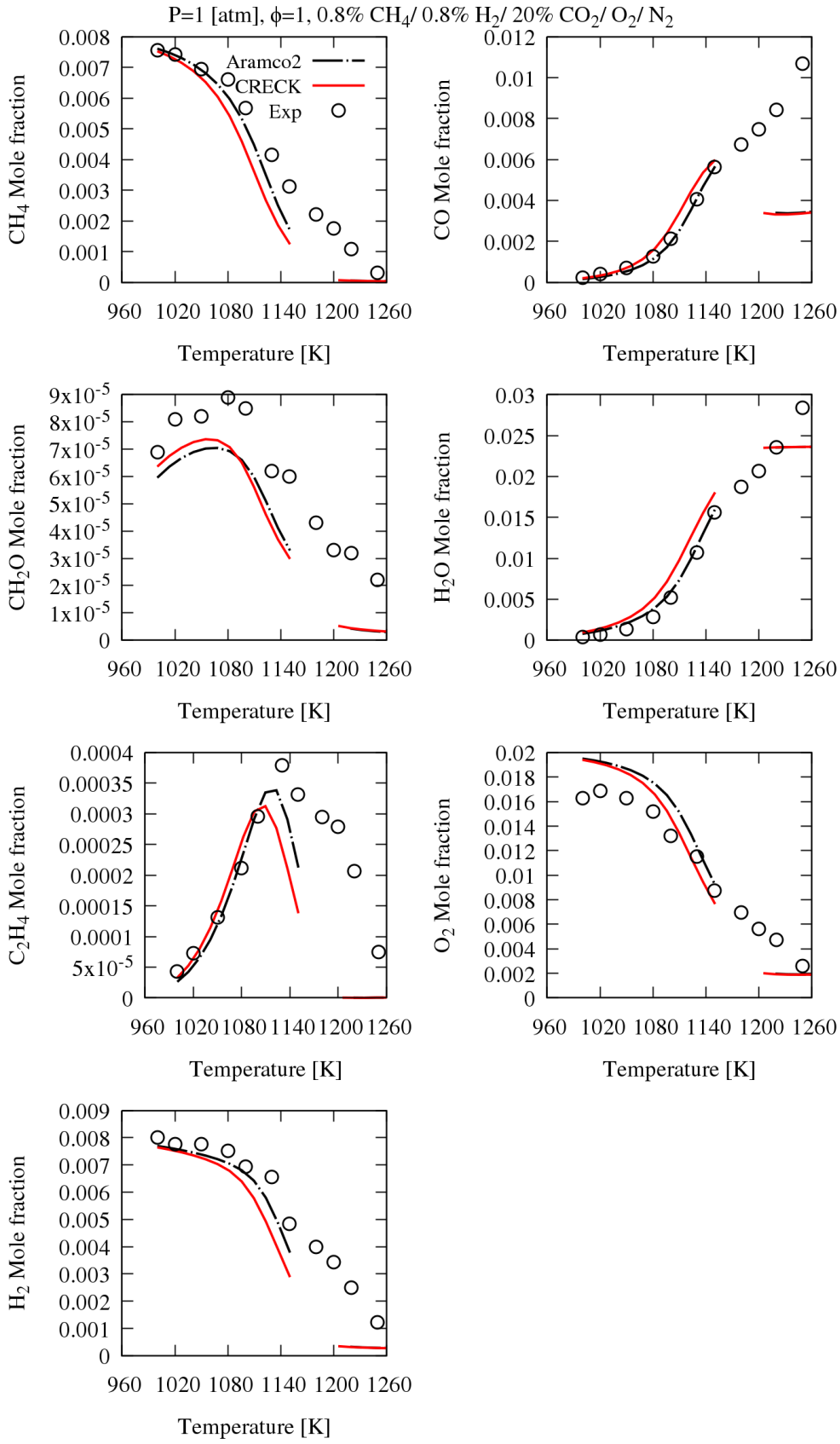

Figure 18 Jet-stirred reactor species profiles of methane oxidation doped by hydrogen. Exp refers to [2].

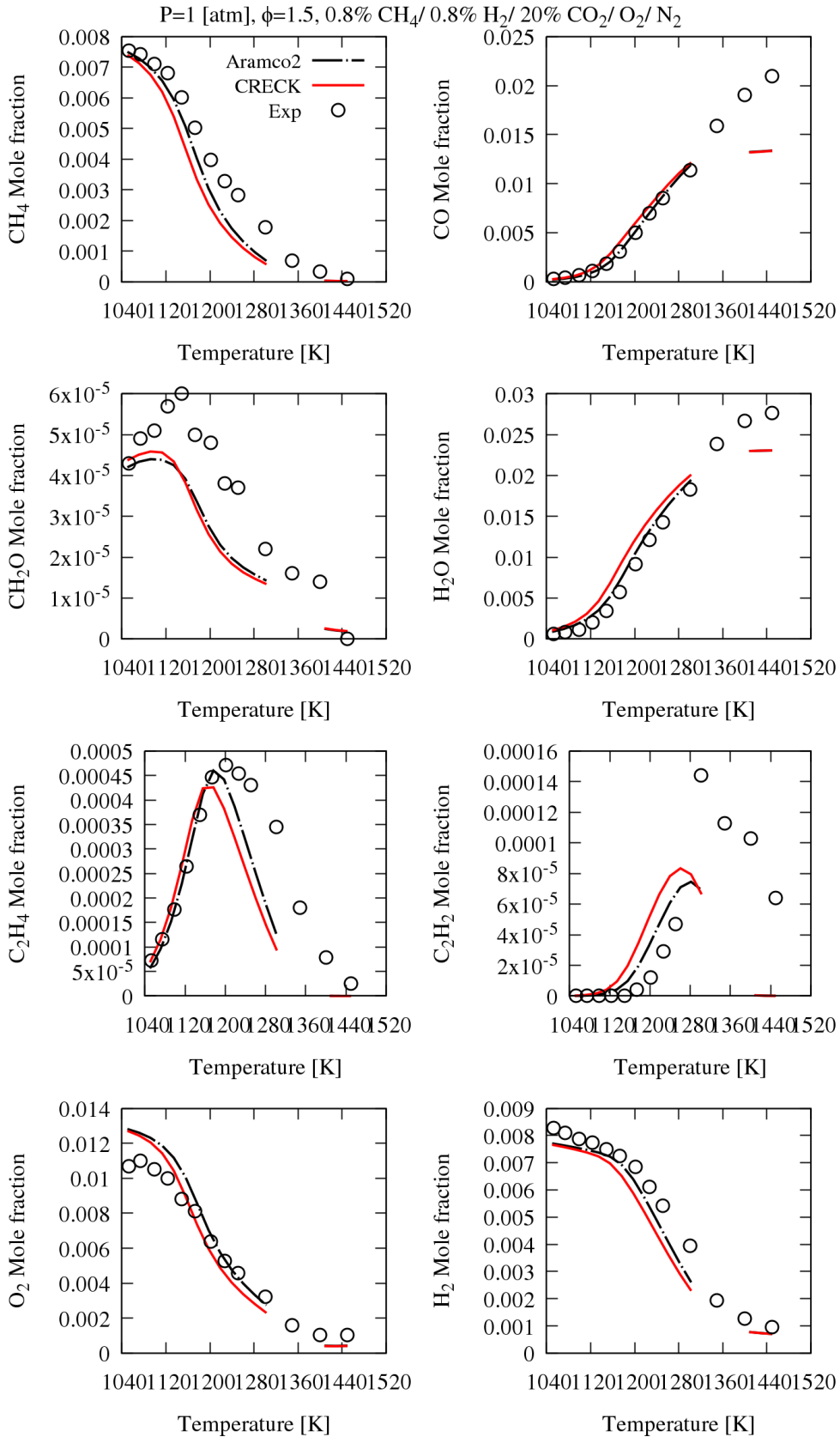

Figure 19 Jet-stirred reactor species profiles of methane oxidation doped by hydrogen. Exp refers to [2].

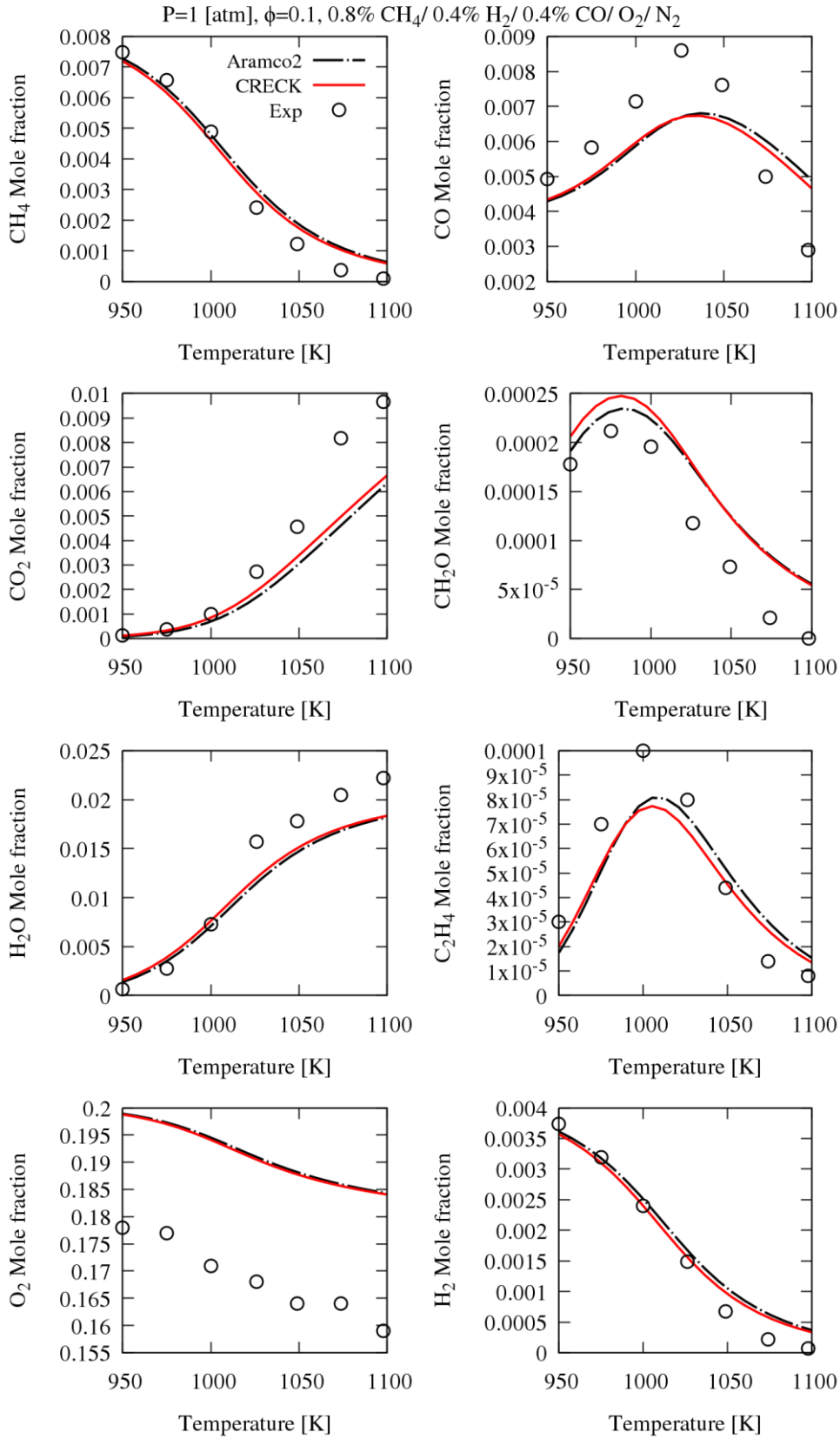

Figure 20 Jet-stirred reactor species profiles of methane oxidation doped by hydrogen and CO. Exp refers to [2].

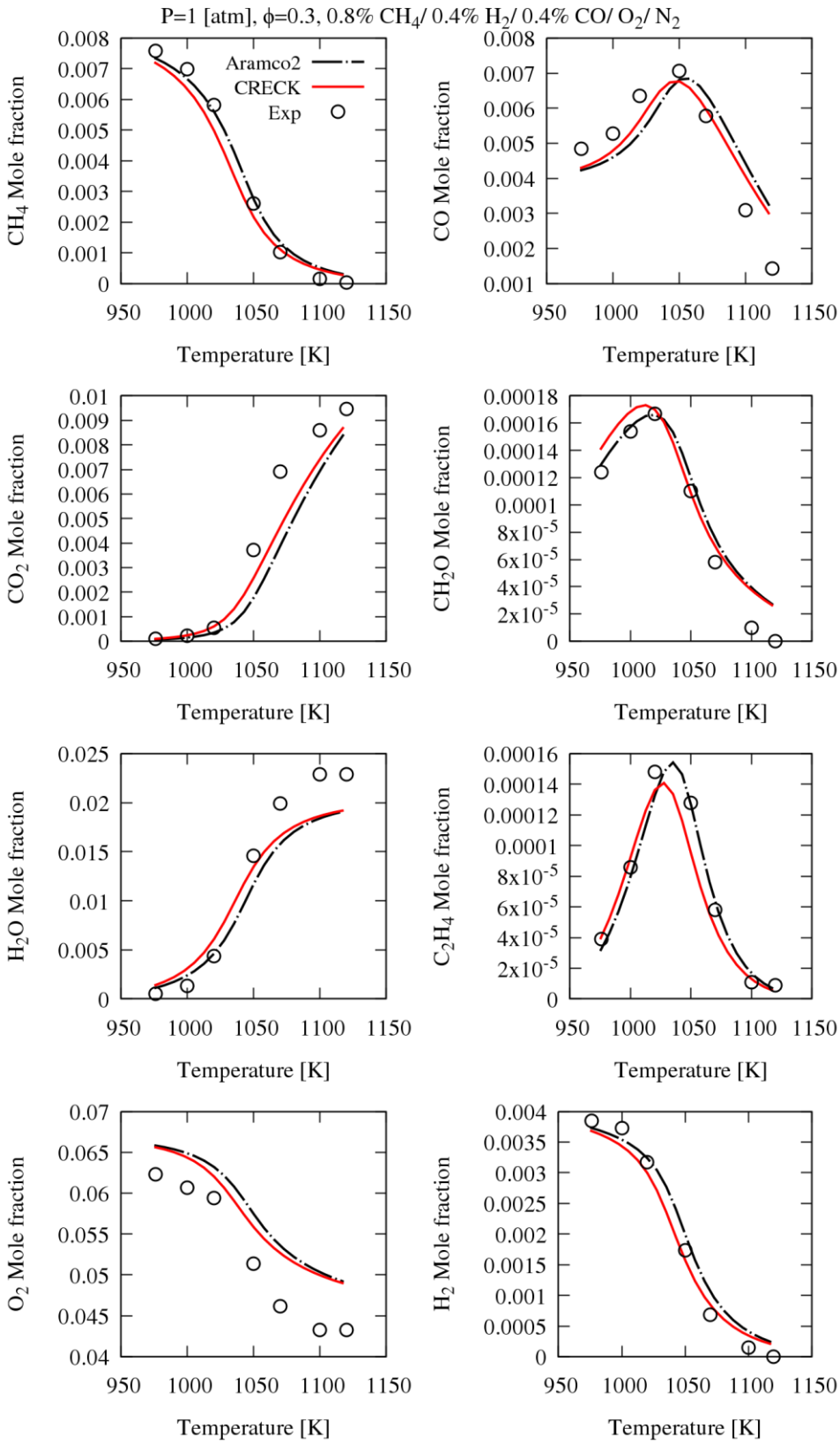

Figure 21 Jet-stirred reactor species profiles of methane oxidation doped by hydrogen and CO. Exp refers to [2].

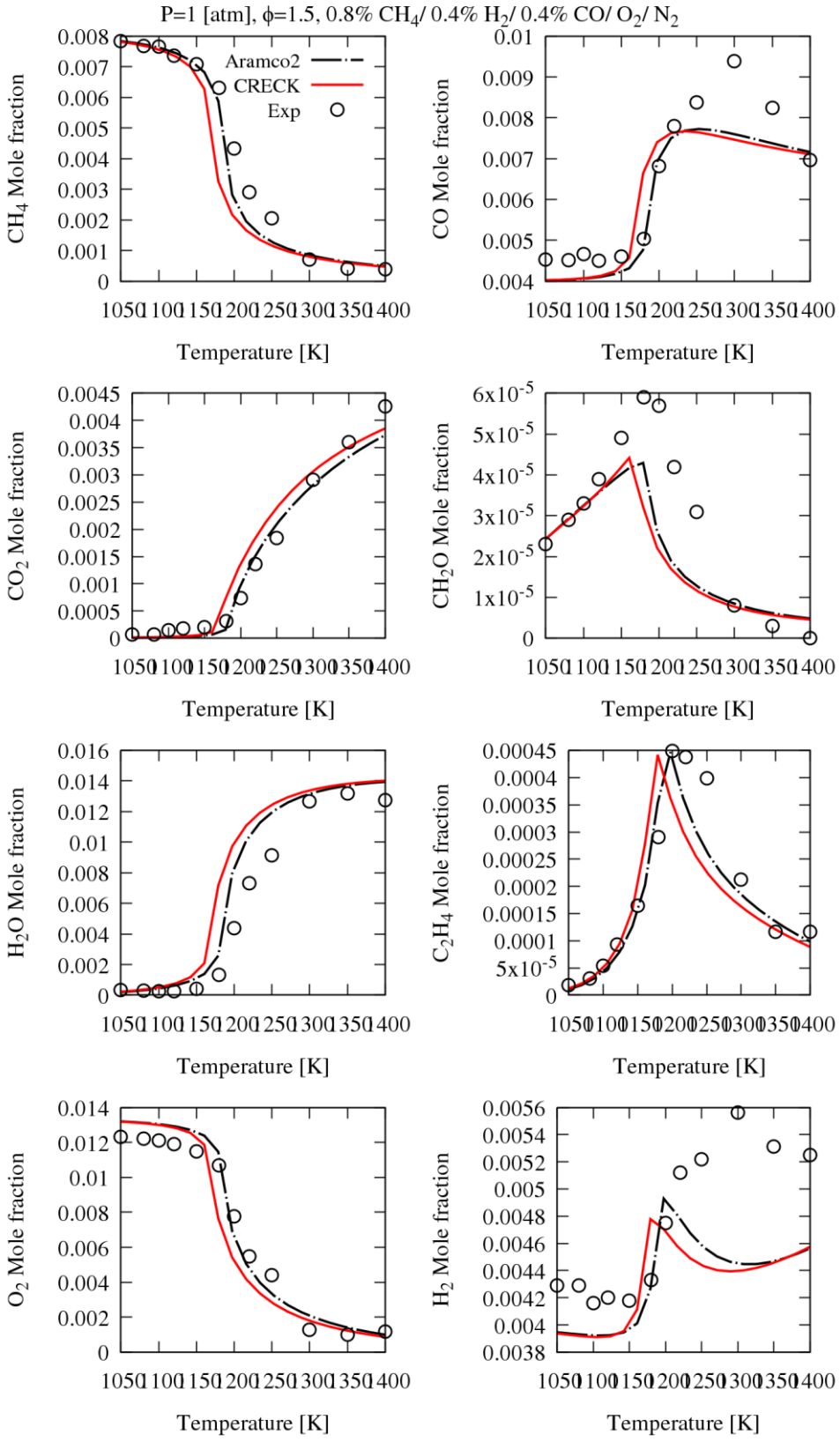

Figure 22 Jet-stirred reactor species profiles of methane oxidation doped by hydrogen and CO. Exp refers to [2].

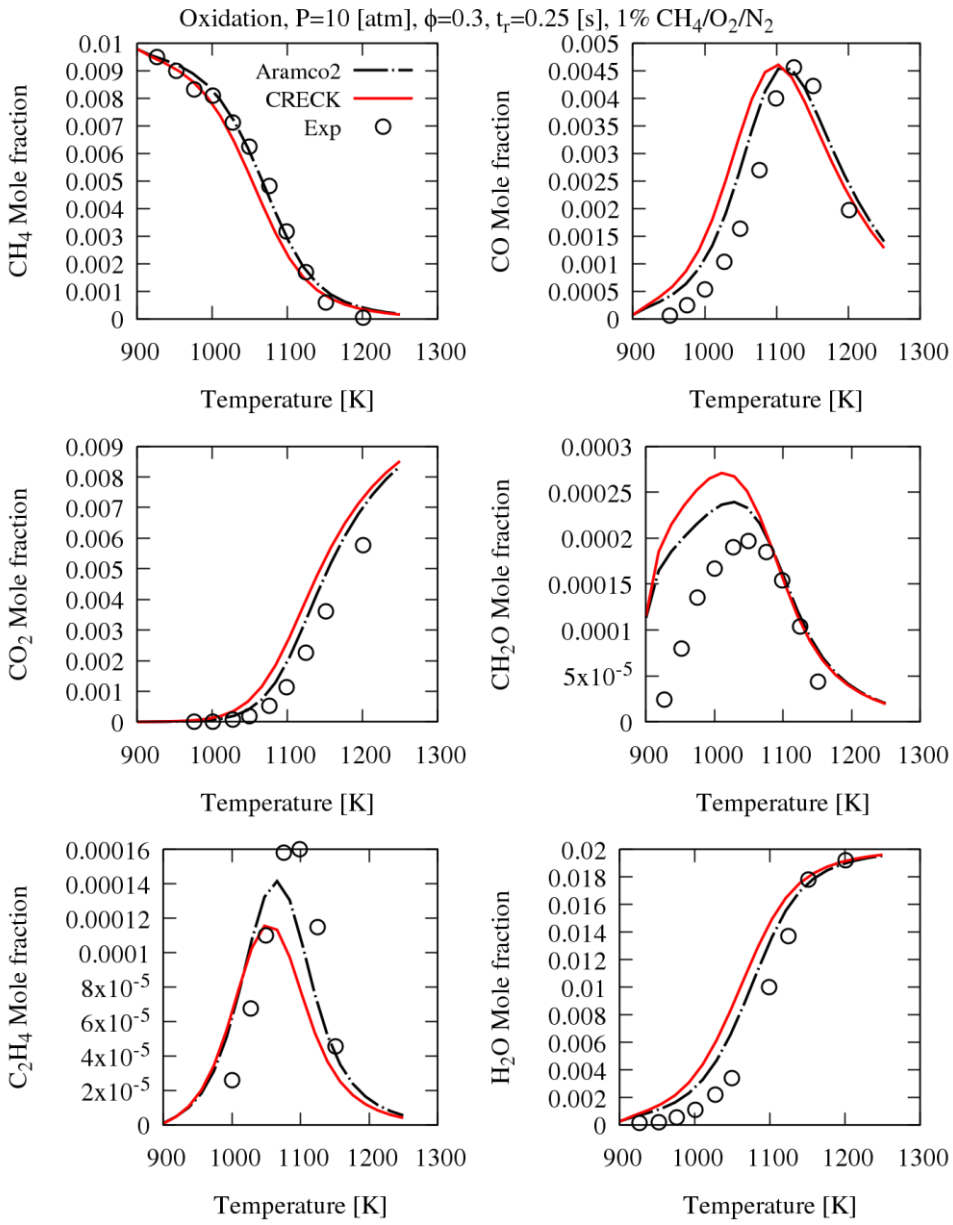

Figure 23 Jet-stirred reactor species profiles of methane oxidation. Exp refers to [3].

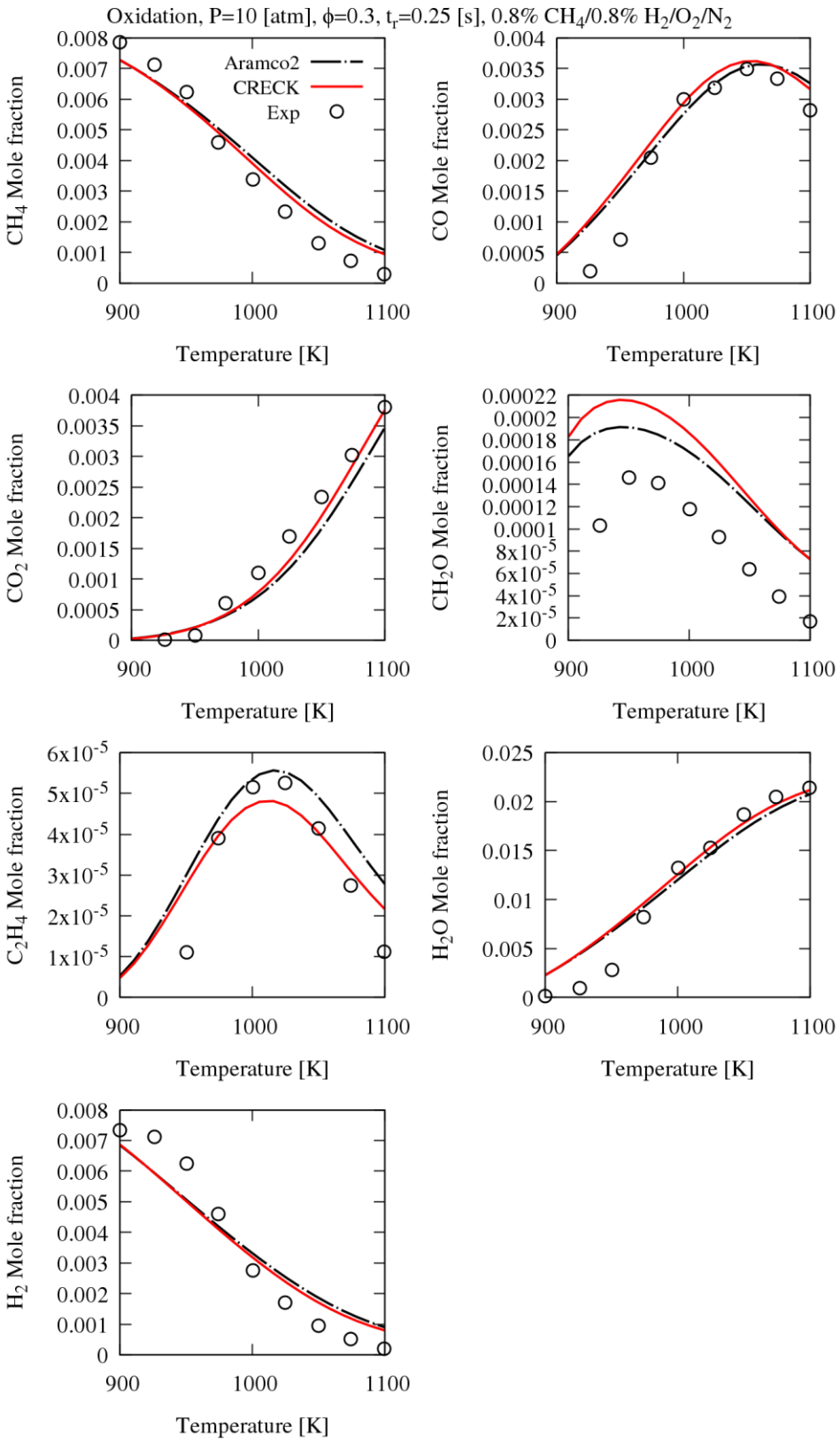

Figure 24 Jet-stirred reactor species profiles of methane oxidation. Exp refers to [3].

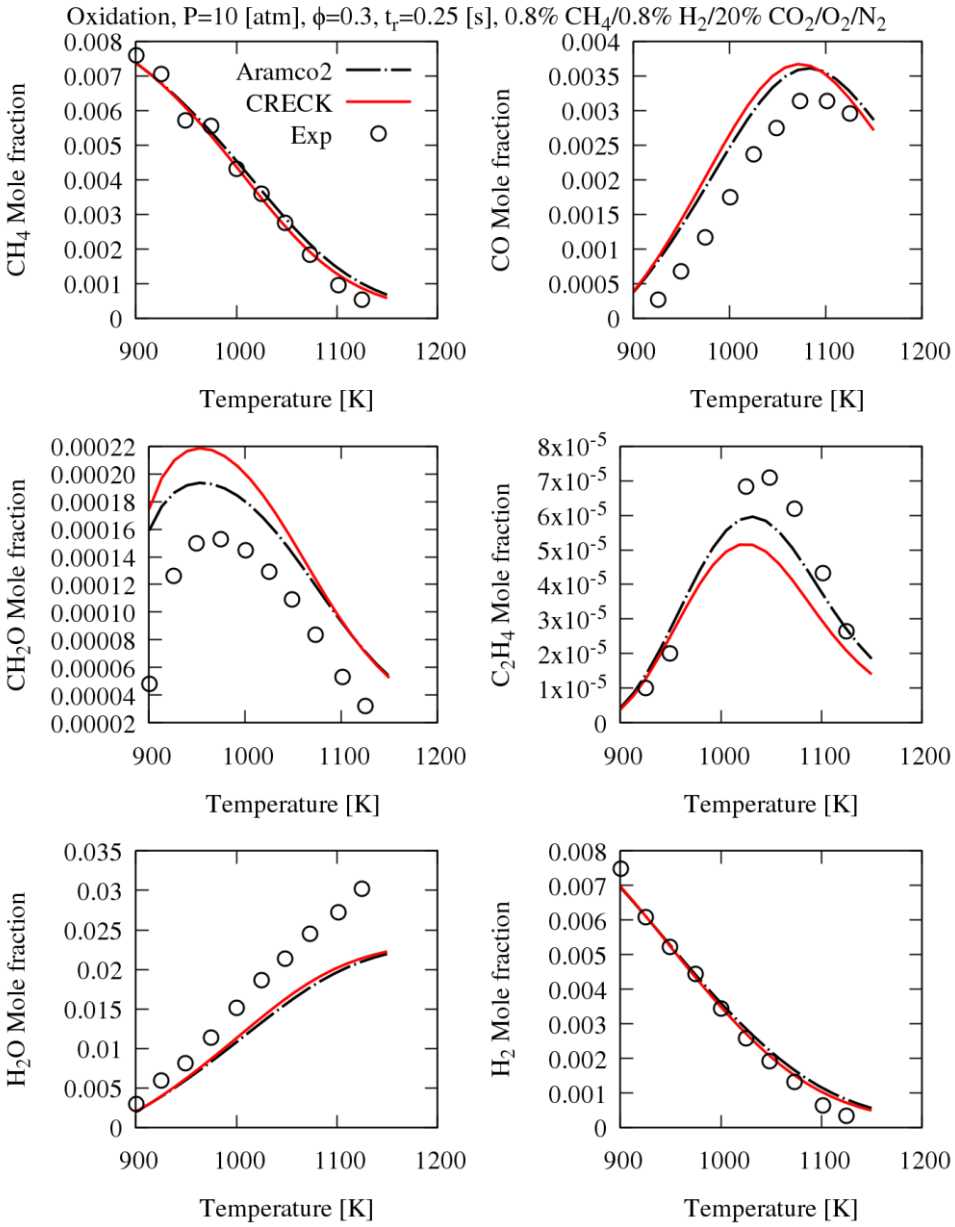

Figure 25 Jet-stirred reactor species profiles of methane oxidation. Exp refers to [3].

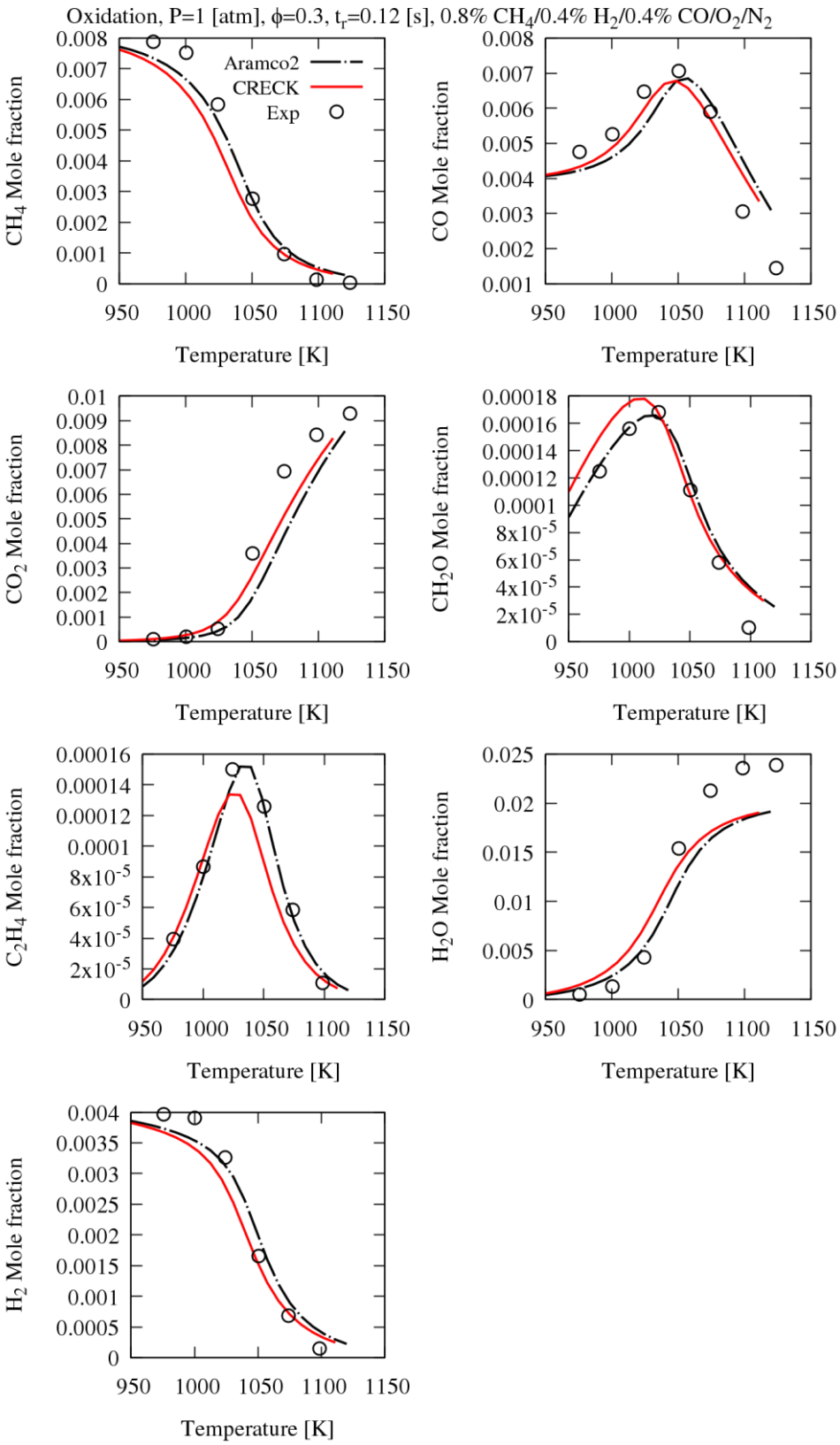

Figure 26 Jet-stirred reactor species profiles of methane oxidation. Exp refers to [3].

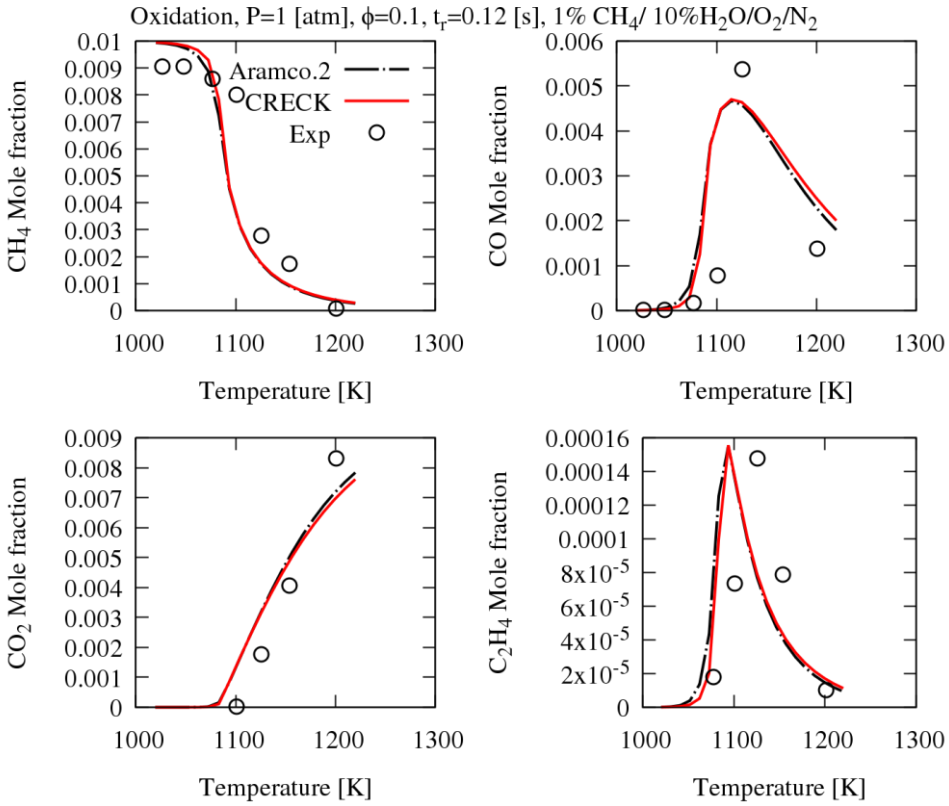

Figure 27 Jet-stirred reactor species profiles of methane oxidation. Exp refers to [4].

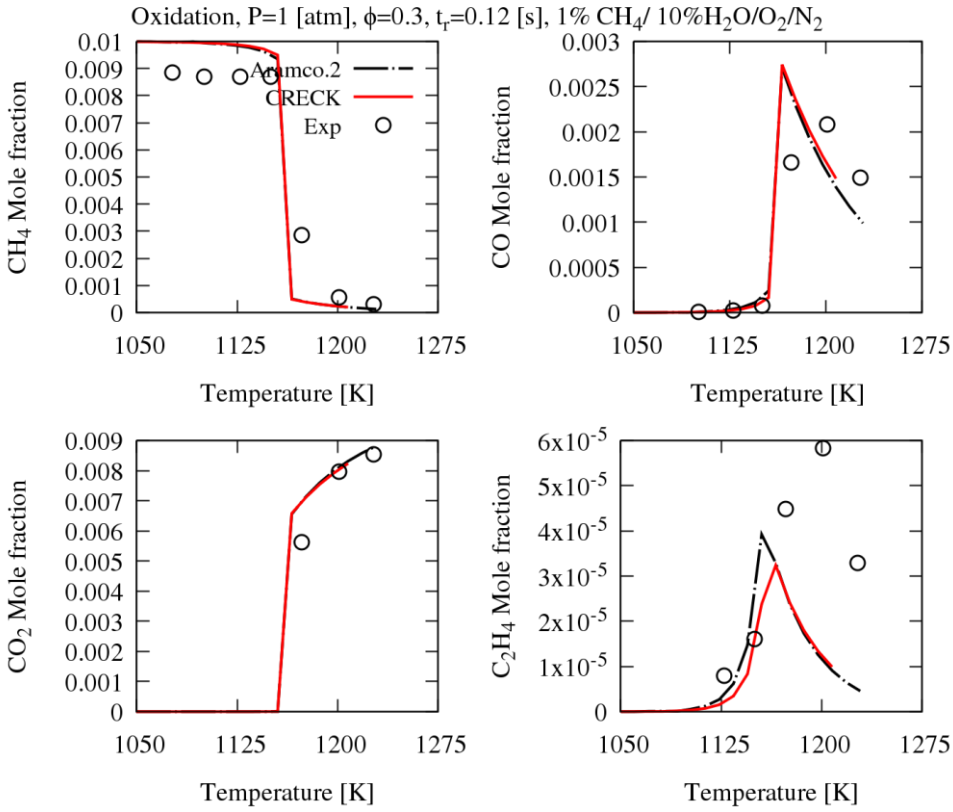

Figure 28 Jet-stirred reactor species profiles of methane oxidation. Exp refers to [4].

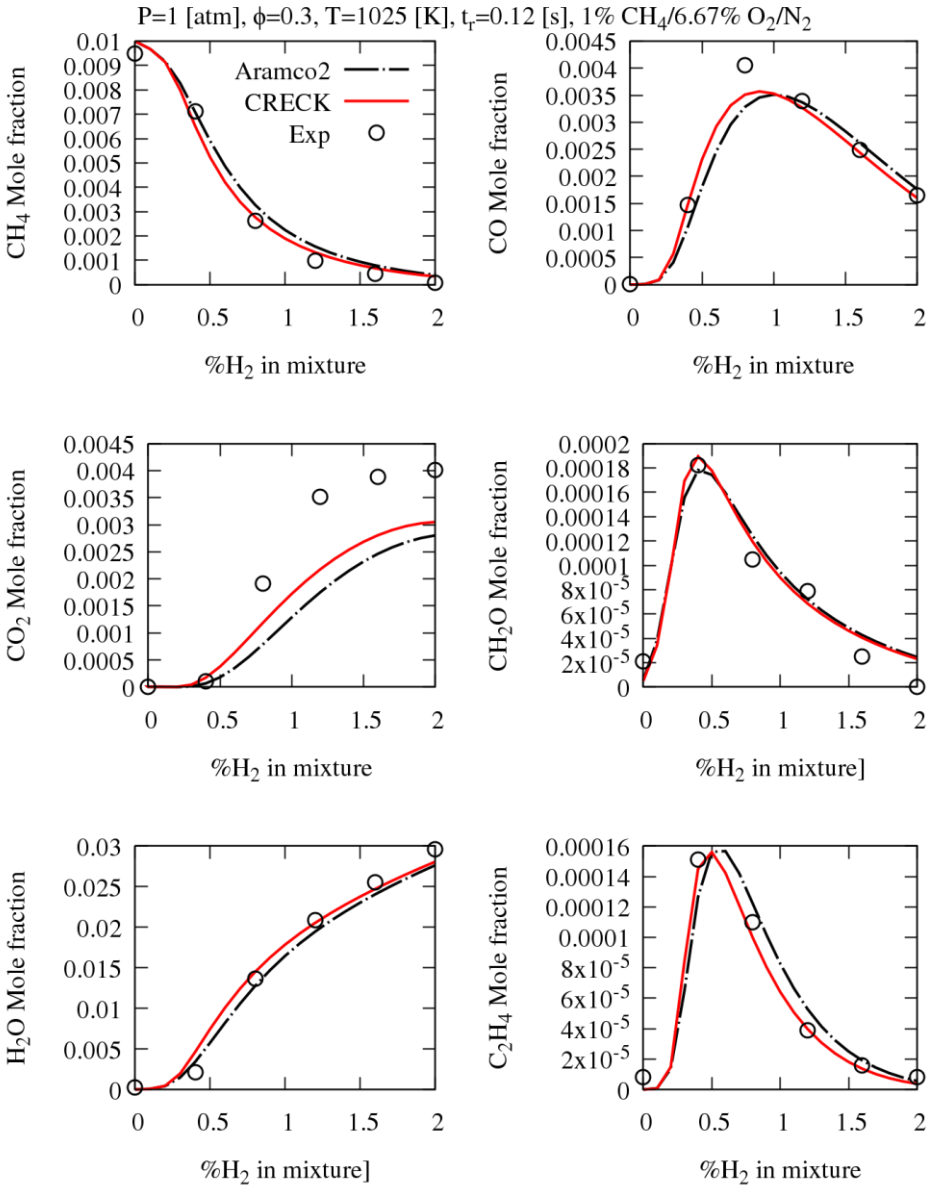

Figure 29 Jet-stirred reactor species profiles of methane oxidation doped by hydrogen. Exp refers to [5].

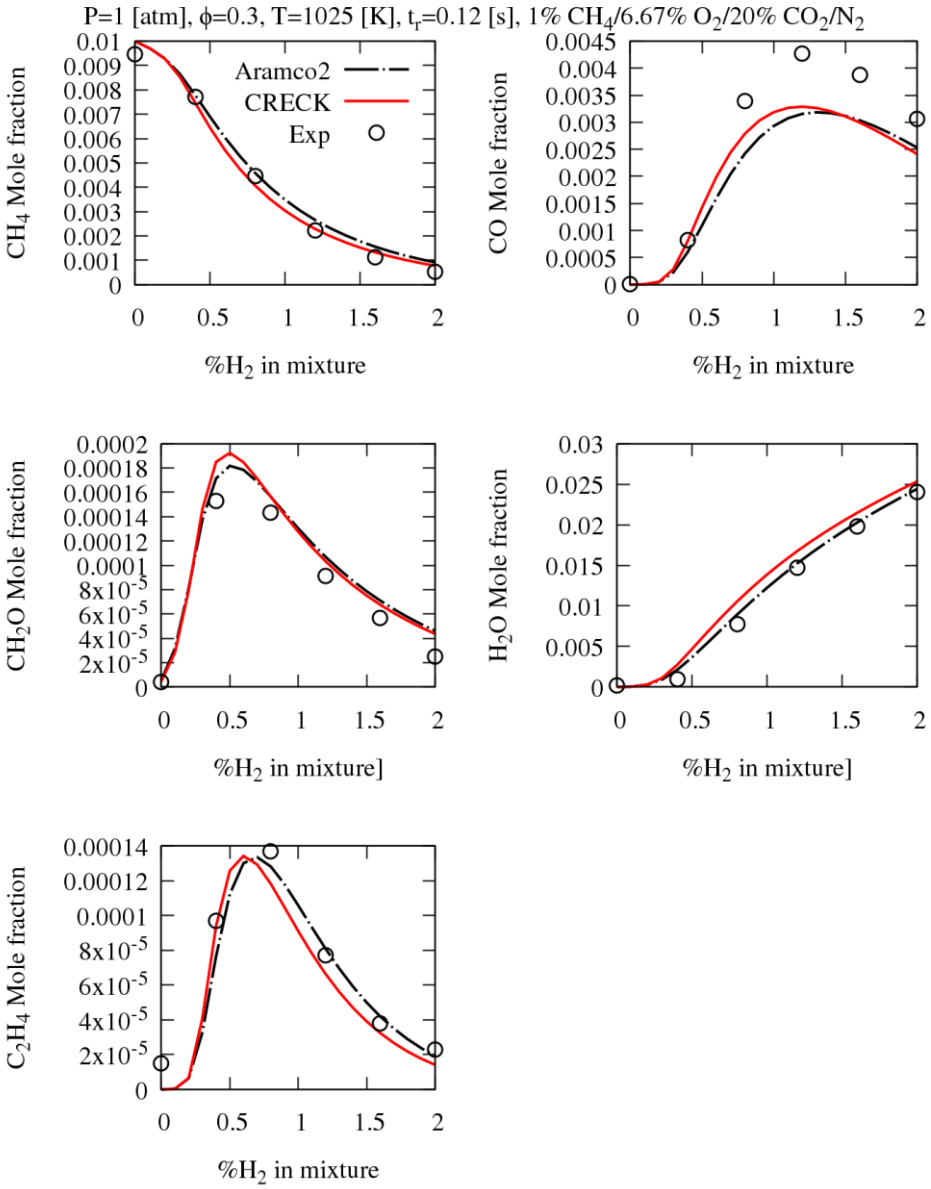

Figure 30 Jet-stirred reactor species profiles of methane oxidation doped by hydrogen. Exp refers to [5].

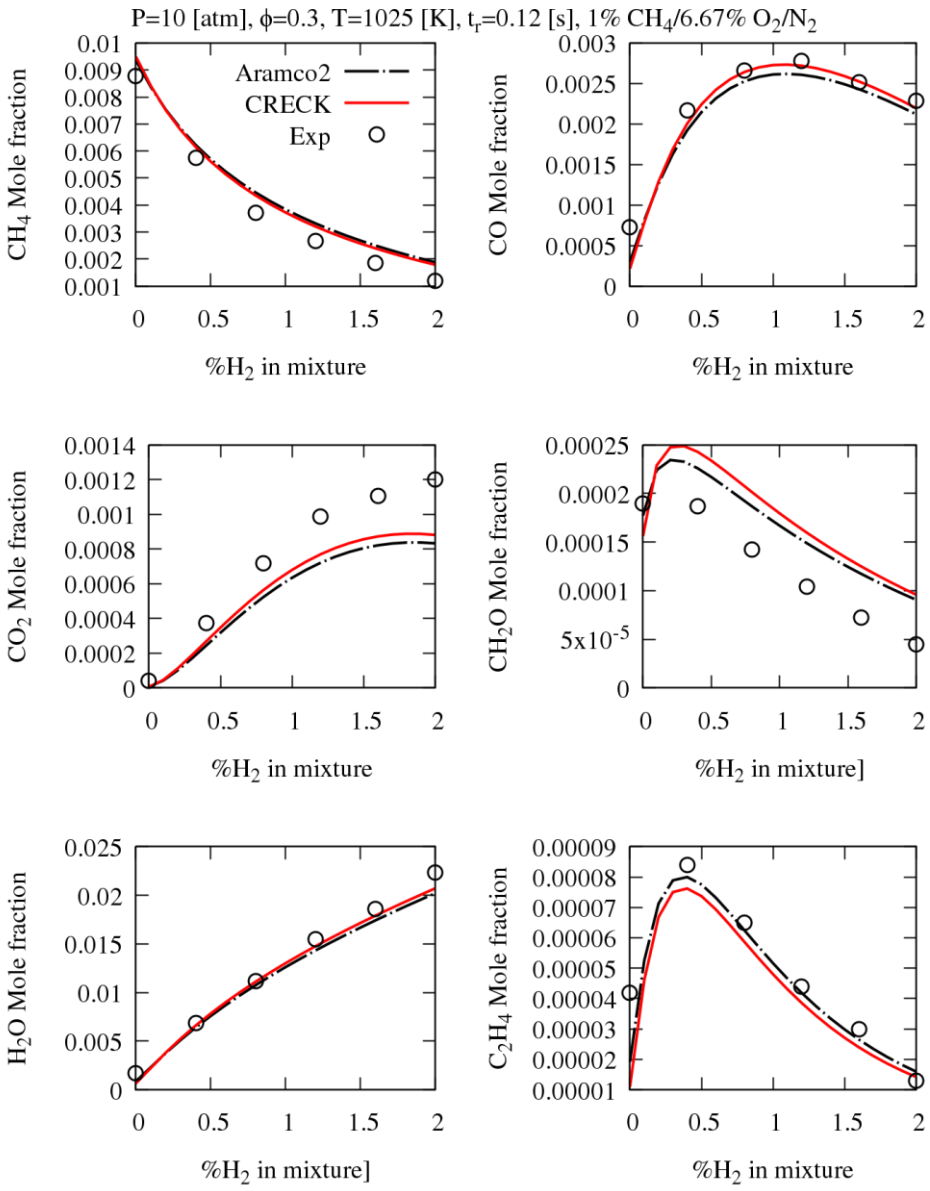

Figure 31 Jet-stirred reactor species profiles of methane oxidation doped by hydrogen. Exp refers to [5].

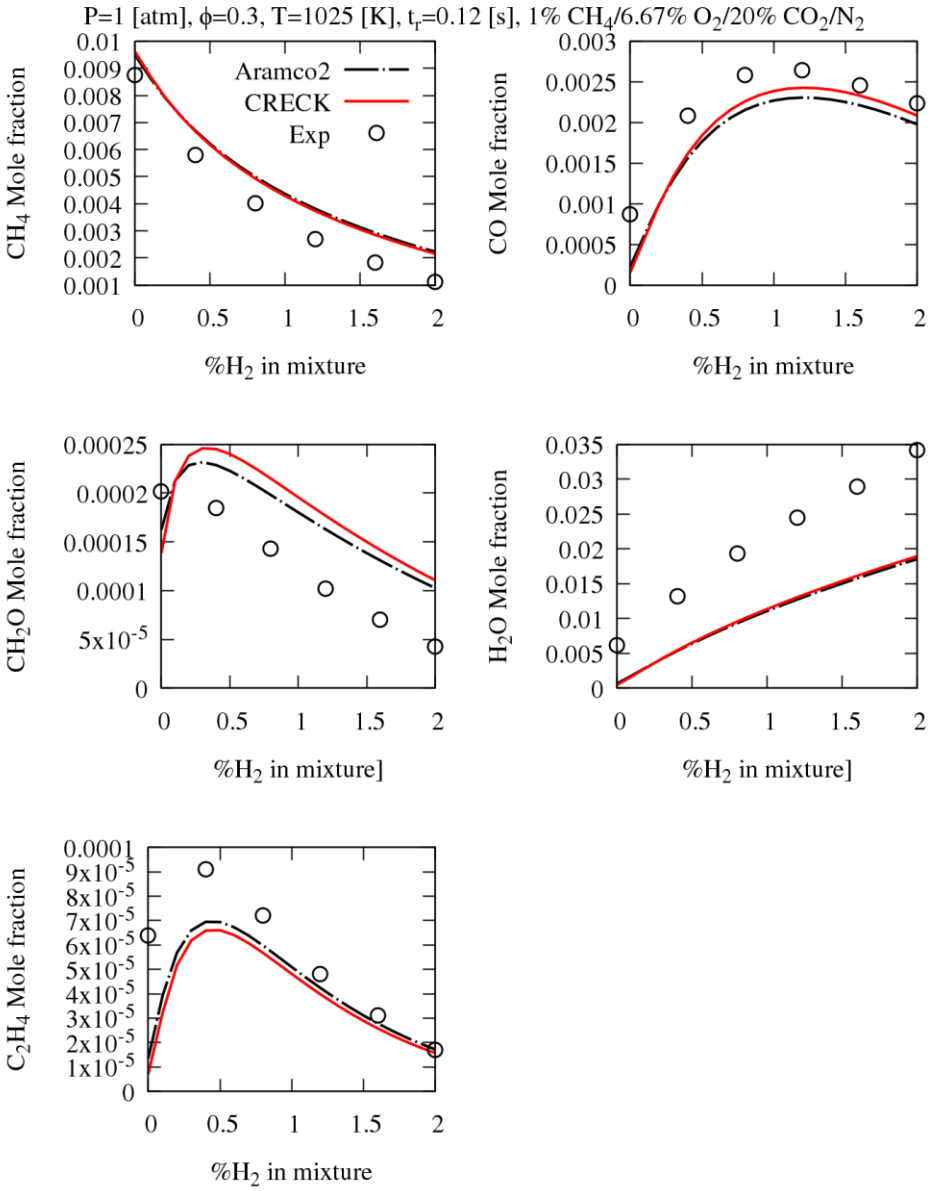

Figure 32 Jet-stirred reactor species profiles of methane oxidation doped by hydrogen. Exp refers to [5].

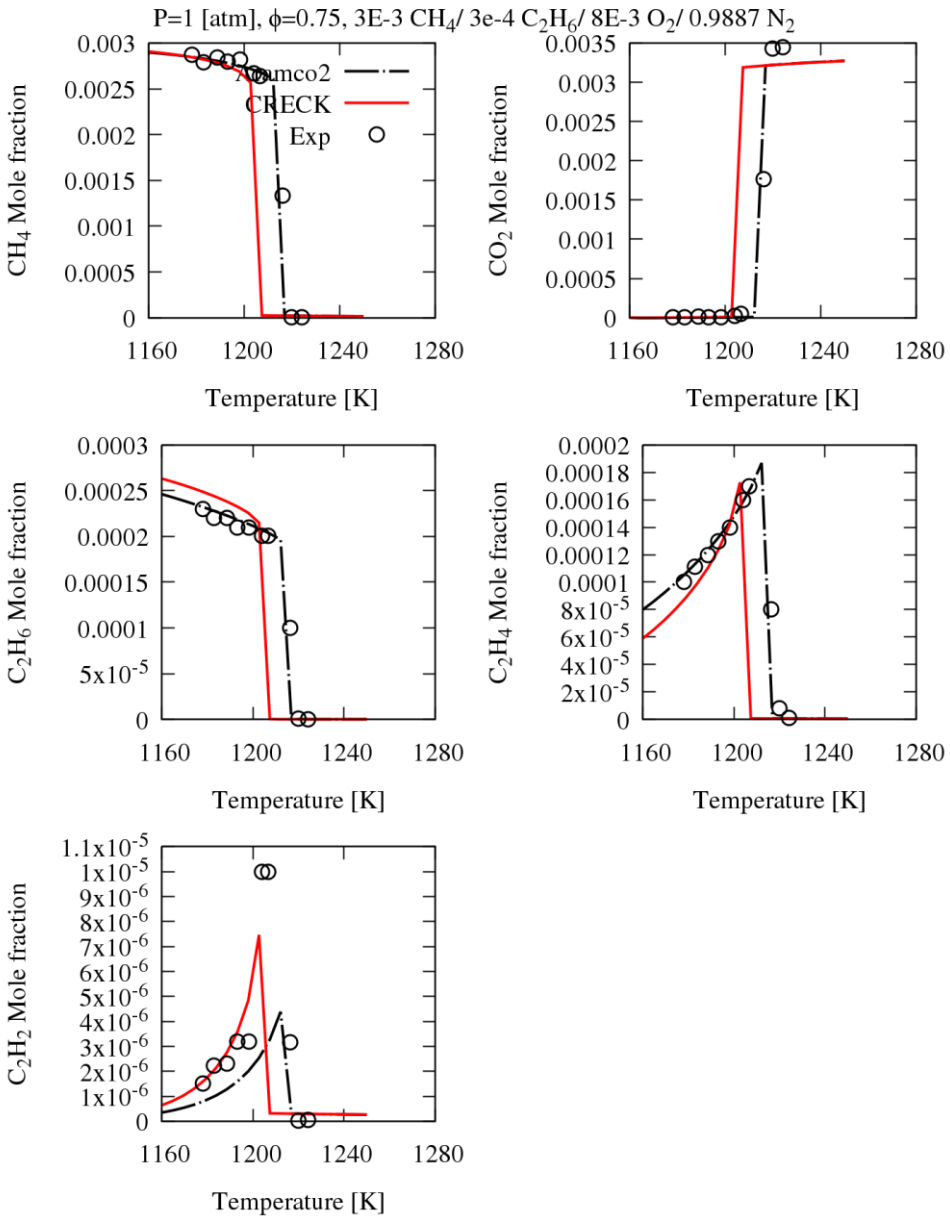

Figure 33 Jet-stirred reactor species profiles of methane oxidation doped by ethane. Exp refers to [6].

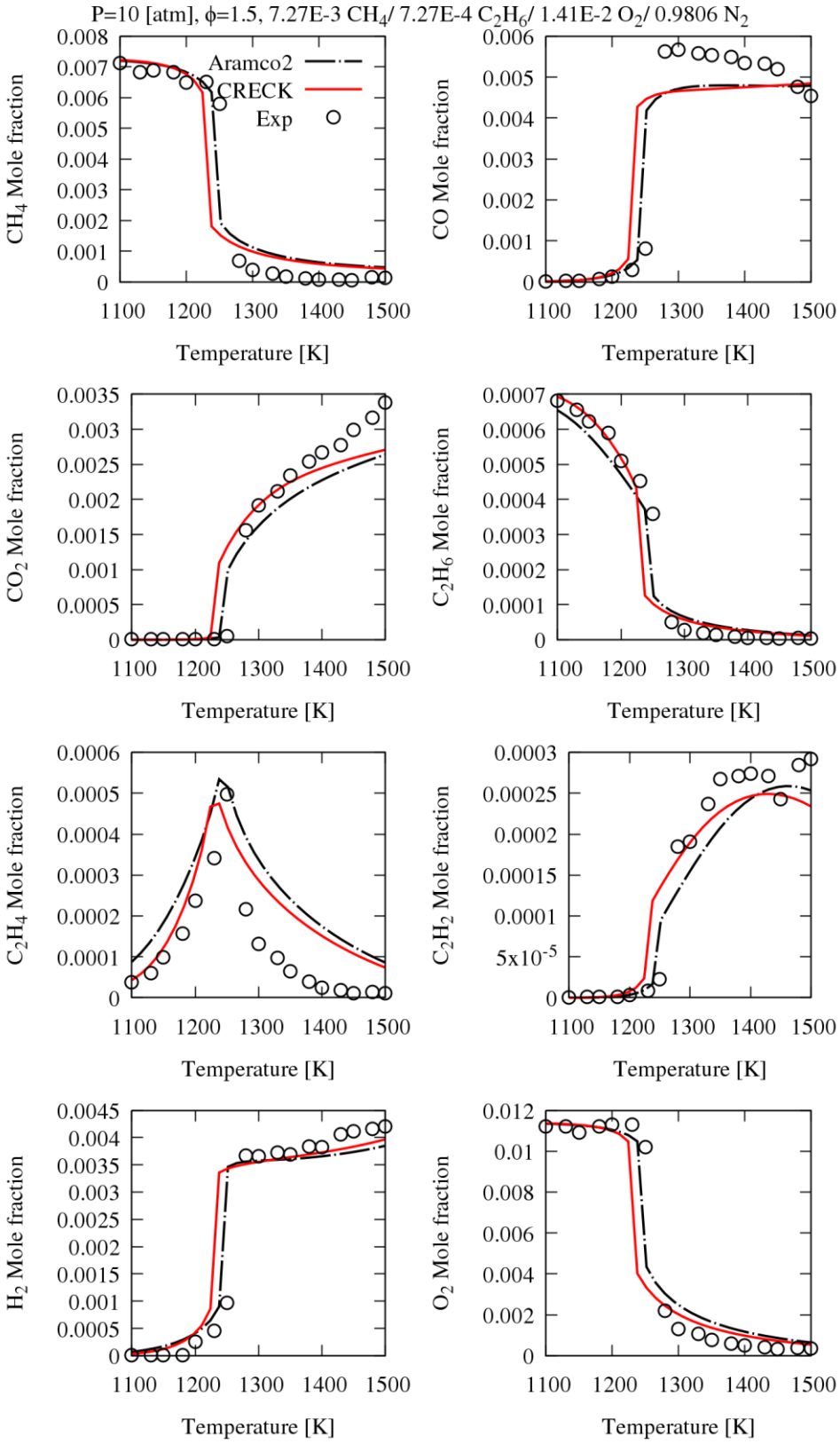

Figure 34 Jet-stirred reactor species profiles of methane oxidation doped by ethane. Exp refers to [6].

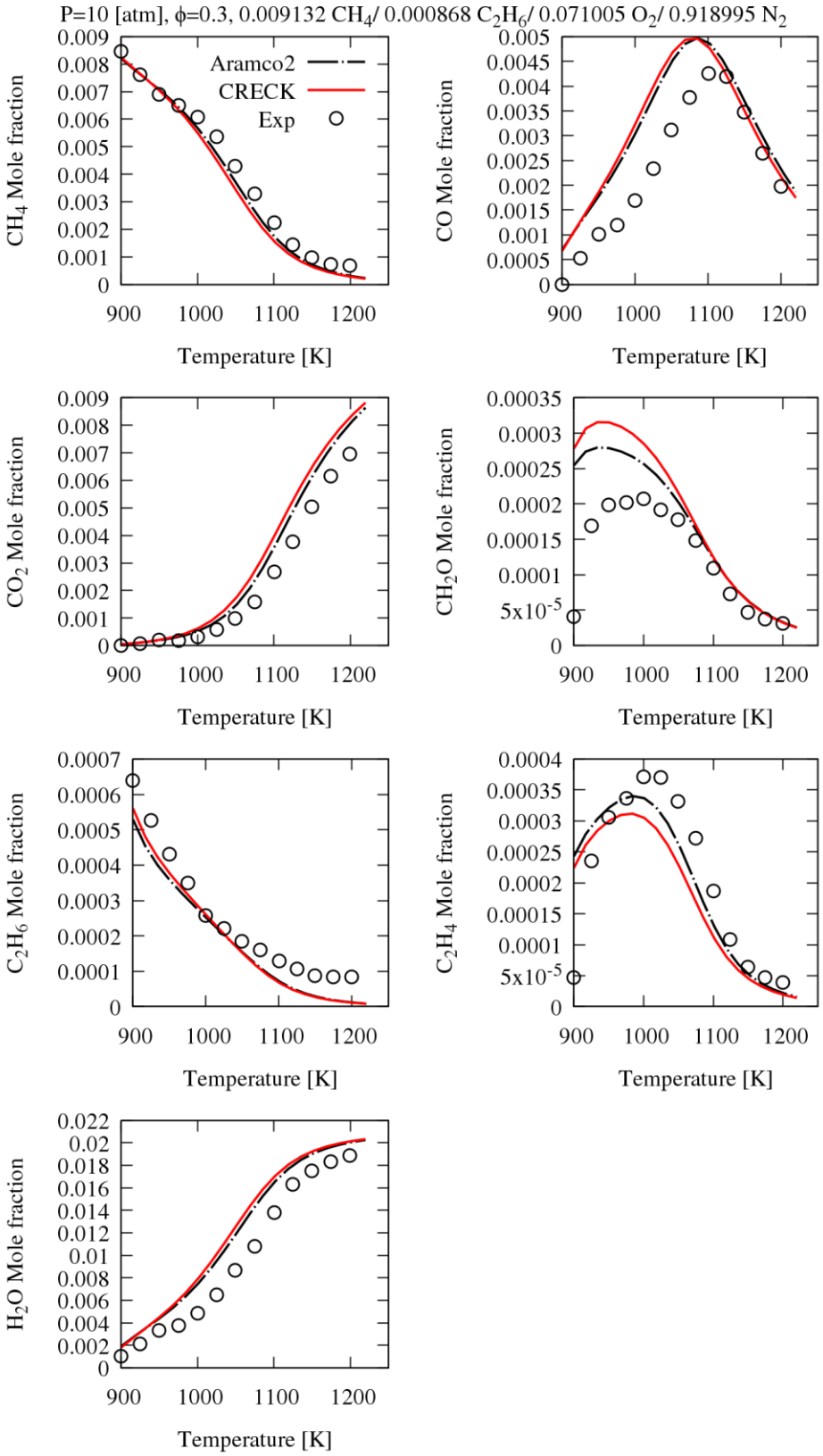

Figure 35 Jet-stirred reactor species profiles of methane oxidation doped by ethane. Exp refers to [7].

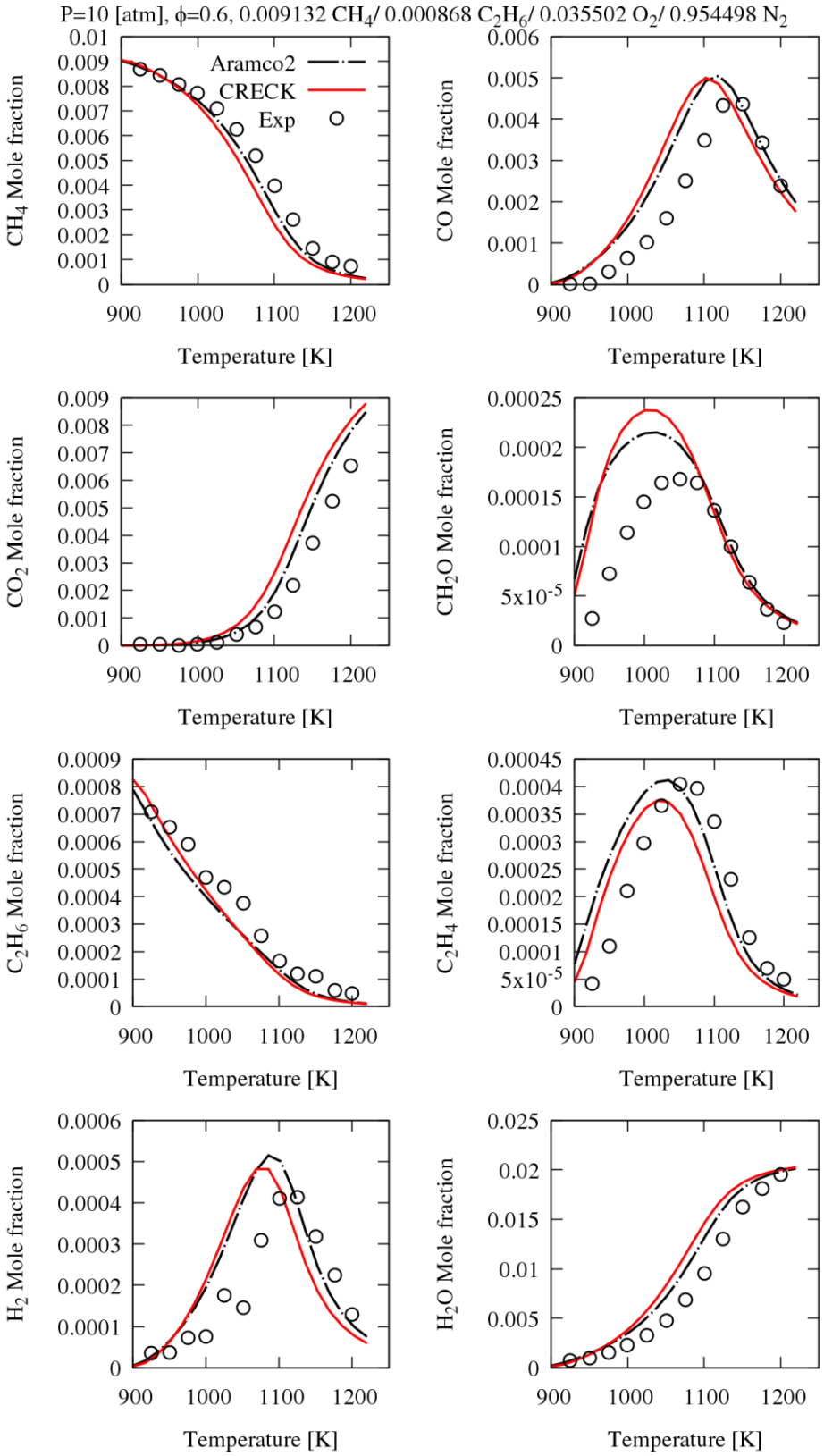

Figure 36 Jet-stirred reactor species profiles of methane oxidation doped by ethane. Exp refers to [7].

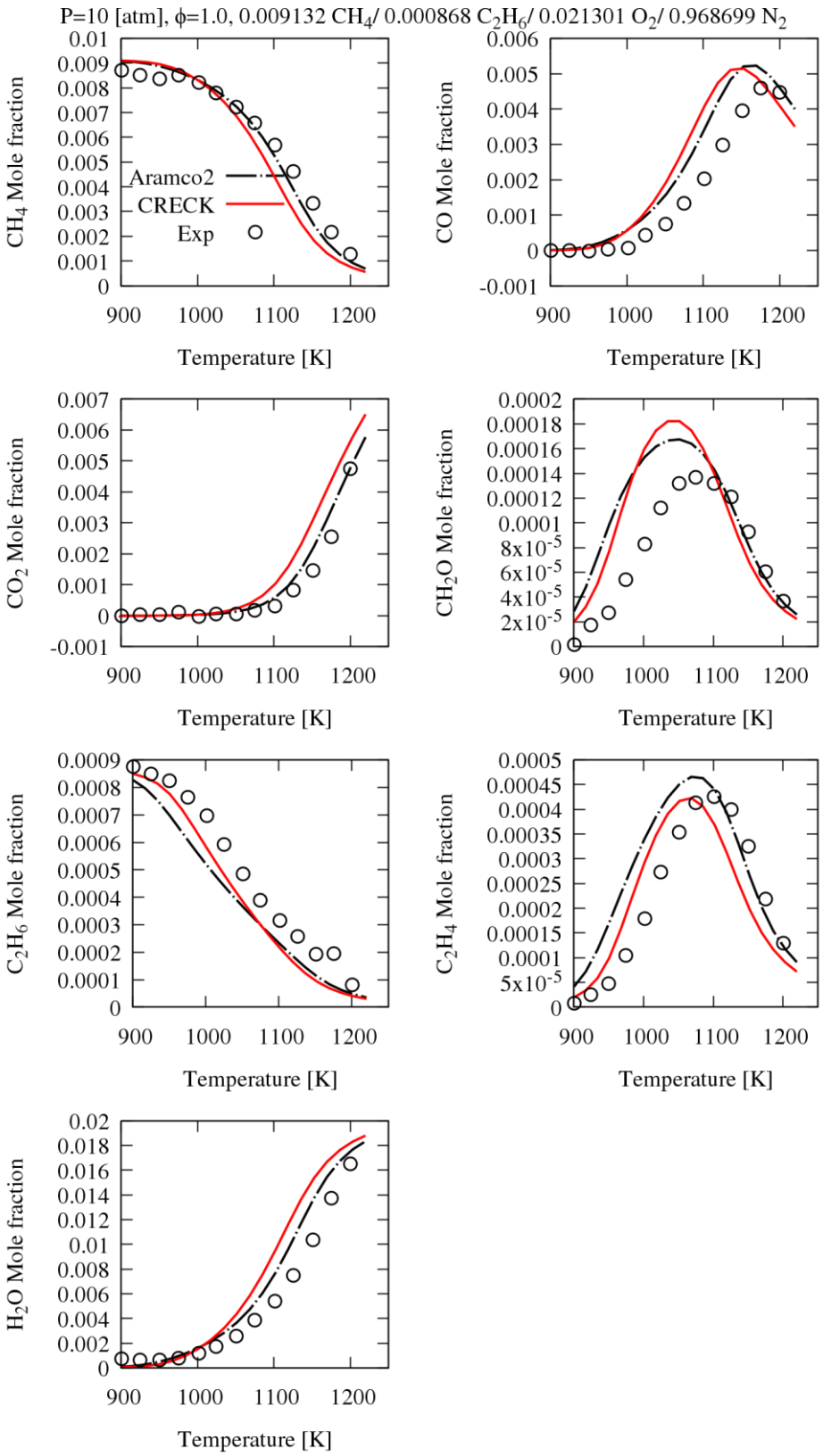

Figure 37 Jet-stirred reactor species profiles of methane oxidation doped by ethane. Exp refers to [7].

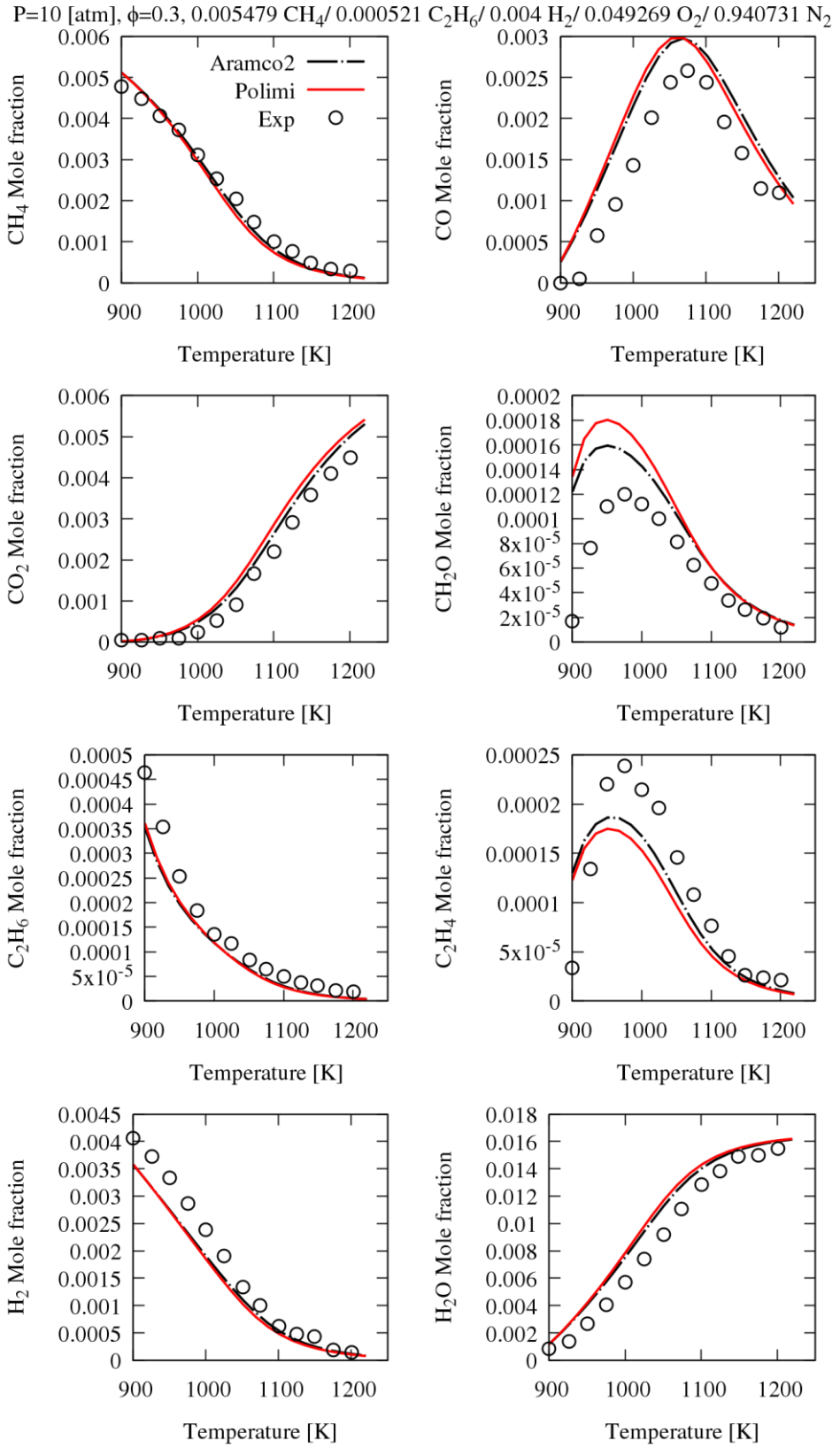

Figure 38 Jet-stirred reactor species profiles of methane oxidation doped by ethane and hydrogen. Exp refers to [7].

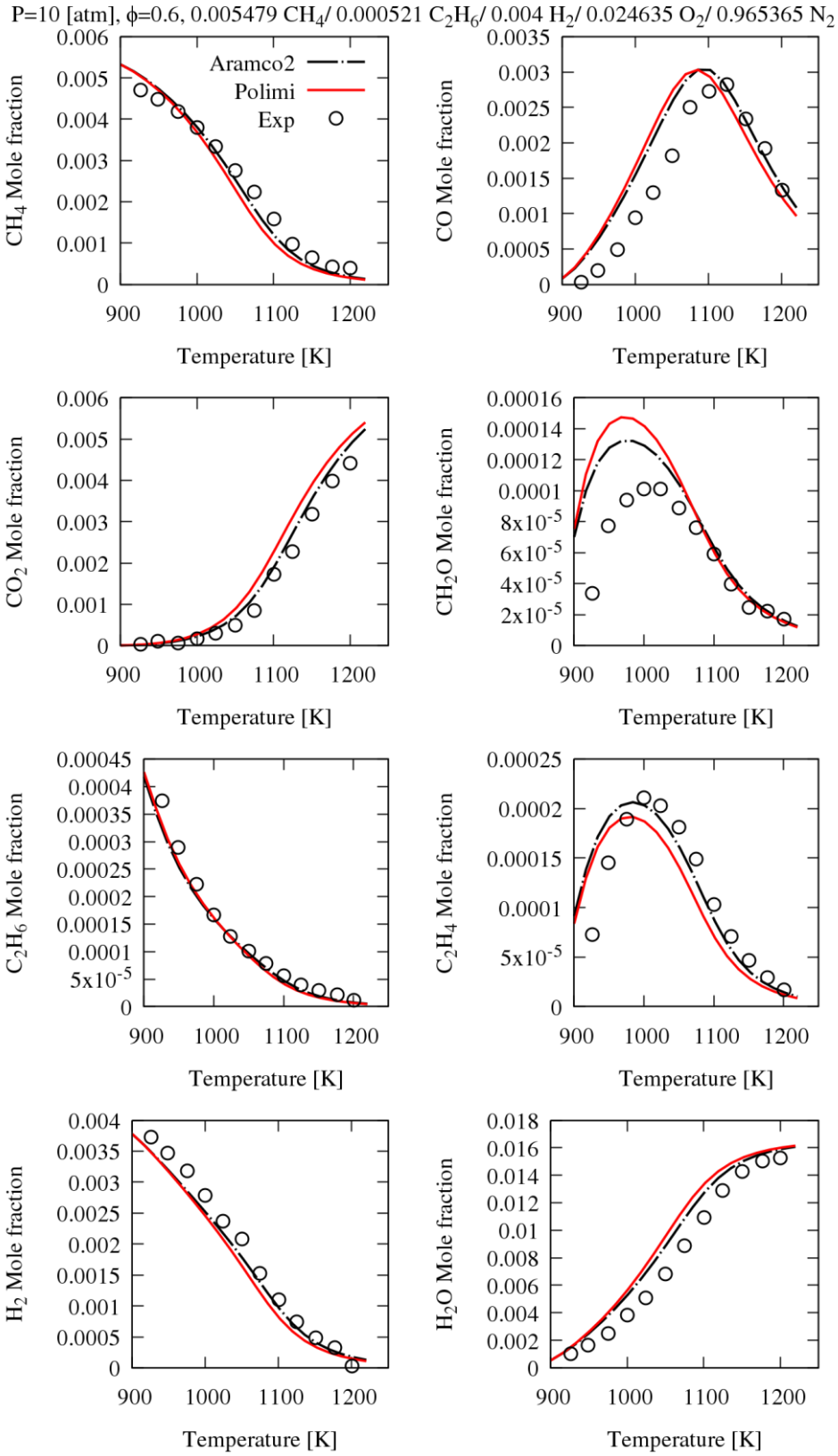

Figure 39 Jet-stirred reactor species profiles of methane oxidation doped by ethane and hydrogen. Exp refers to [7].

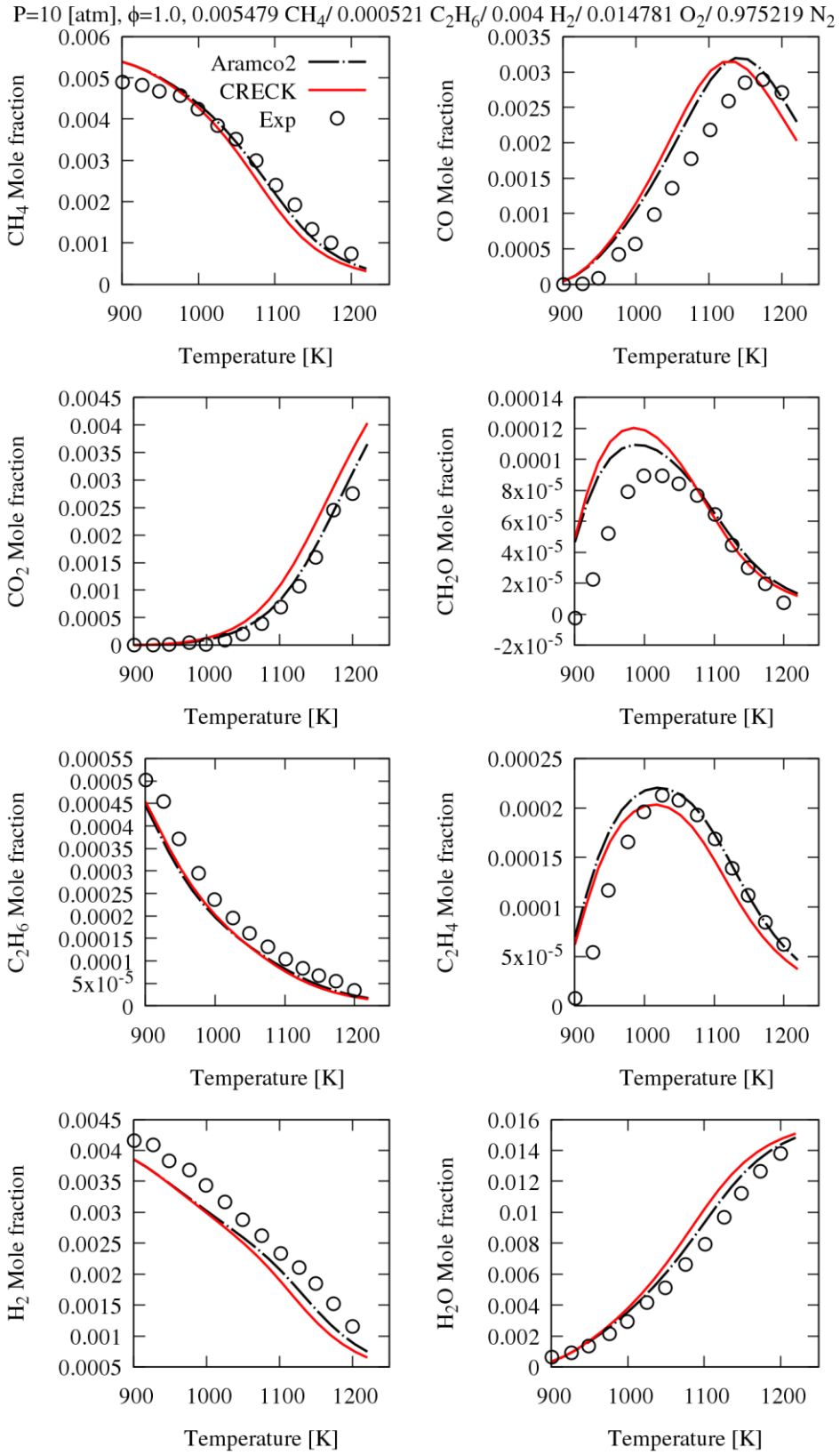

Figure 40 Jet-stirred reactor species profiles of methane oxidation doped by ethane and hydrogen. Exp refers to [7].

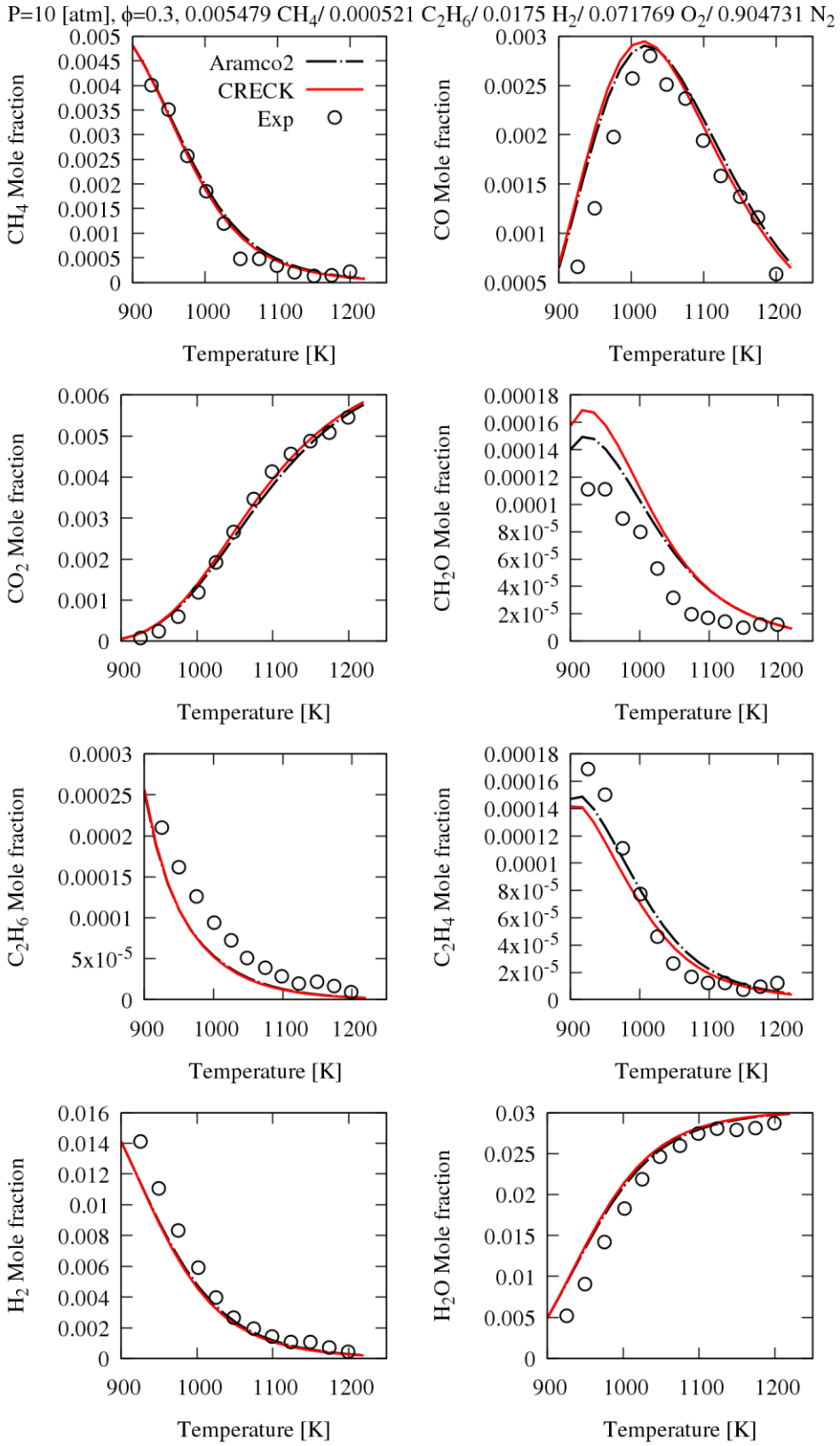

Figure 41 Jet-stirred reactor species profiles of methane oxidation doped by ethane and hydrogen. Exp refers to [7].

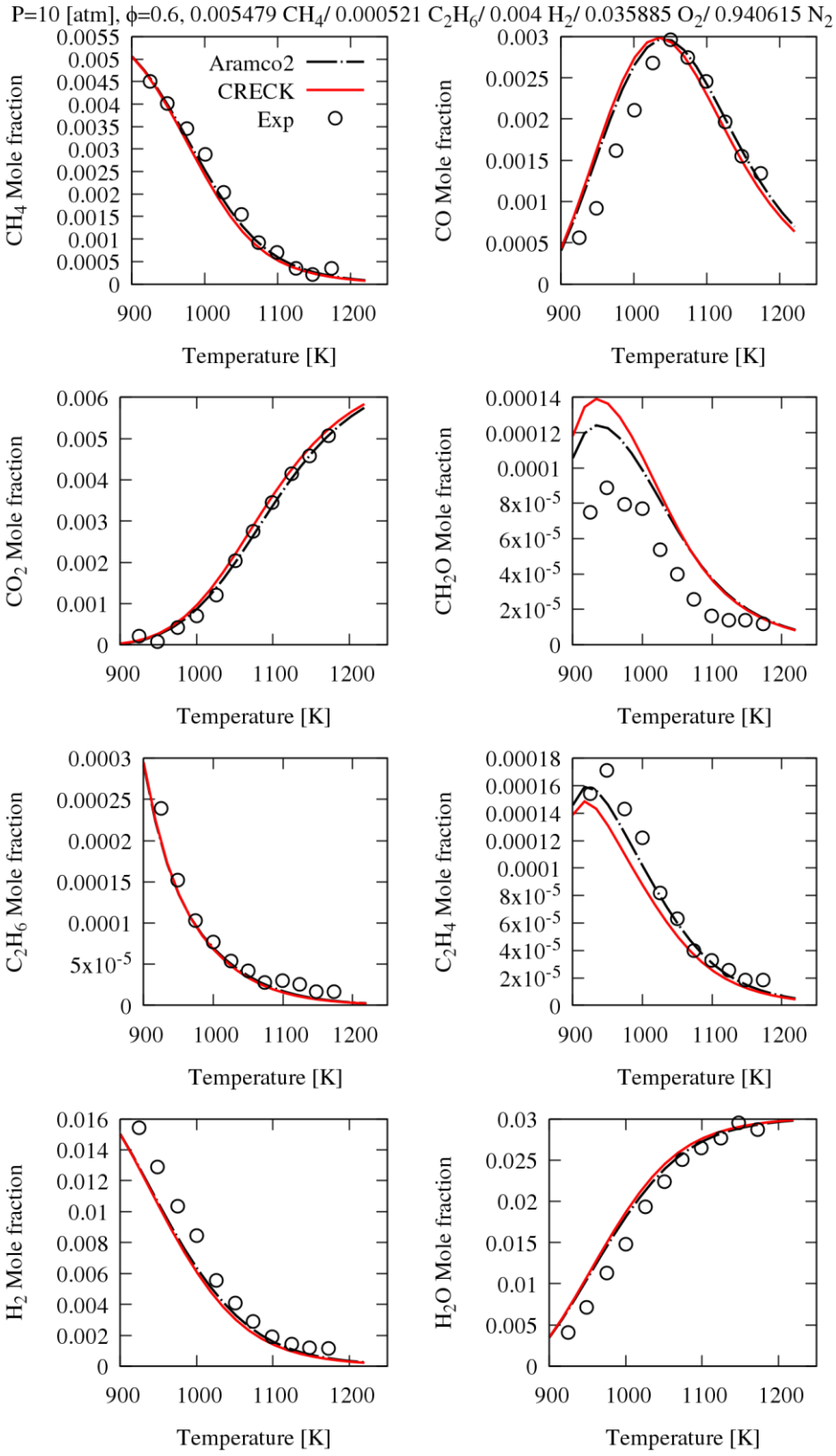

Figure 42 Jet-stirred reactor species profiles of methane oxidation doped by ethane and hydrogen. Exp refers to [7].

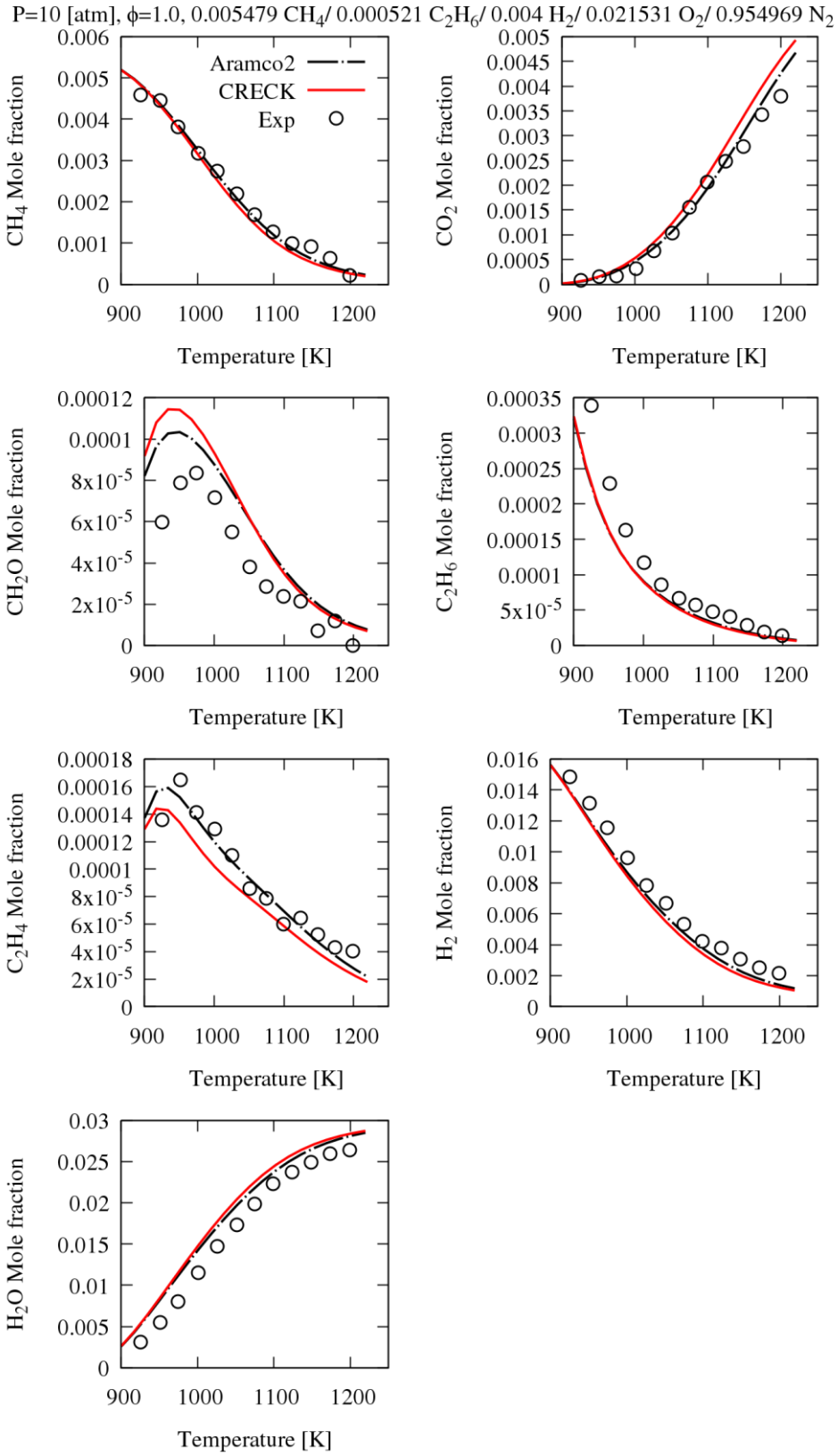

Figure 43 Jet-stirred reactor species profiles of methane oxidation doped by ethane and hydrogen. Exp refers to [7].

Oscillation in MILD (Jest Stirred reactor)

The symbols show experimental results, blue lines show the steady-state solution, and shadow areas present the region and amplitude of oscillations.

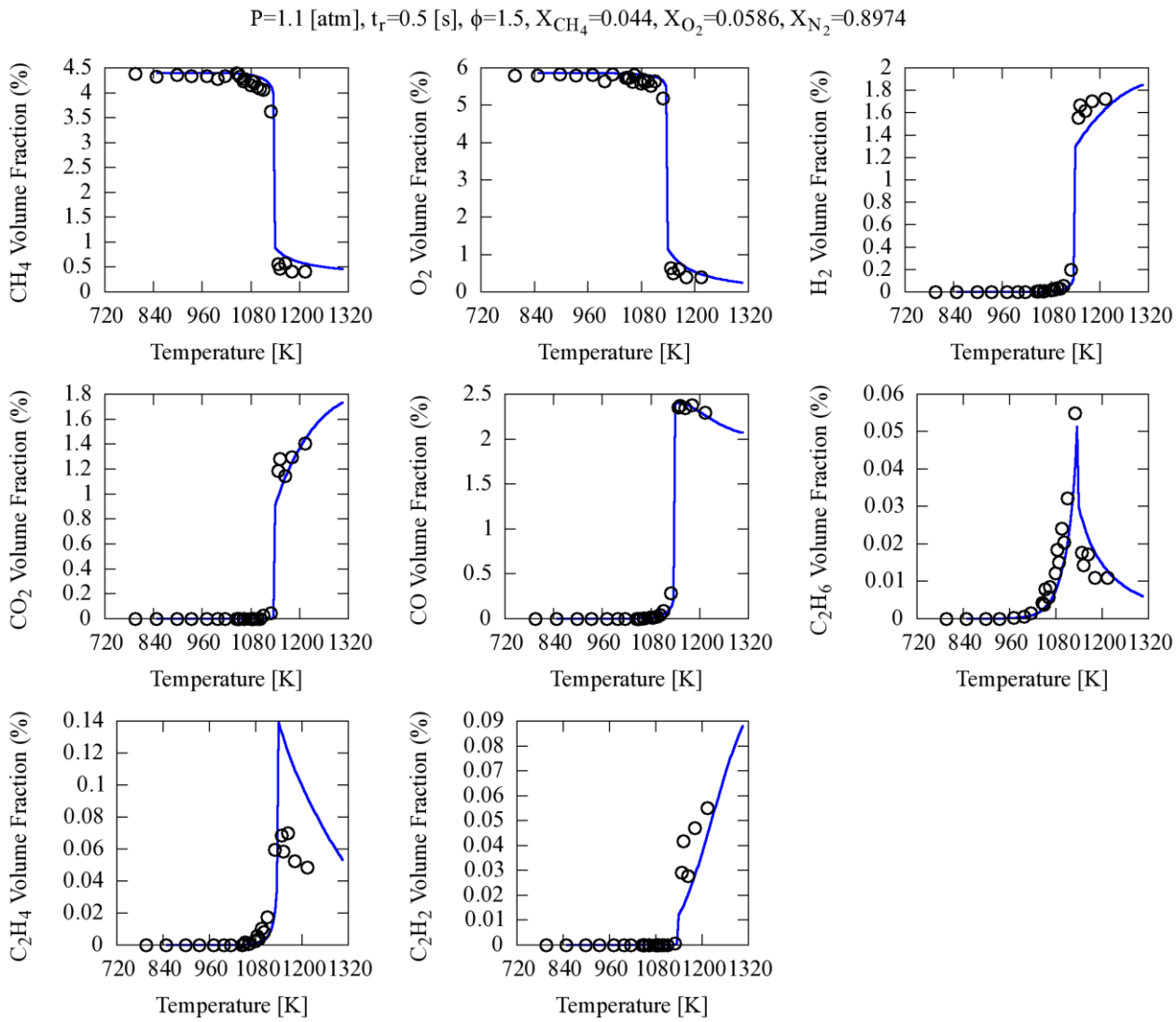

Figure 44. N_2 diluted system in the rich condition φ=1.5. symbols refers to [8].

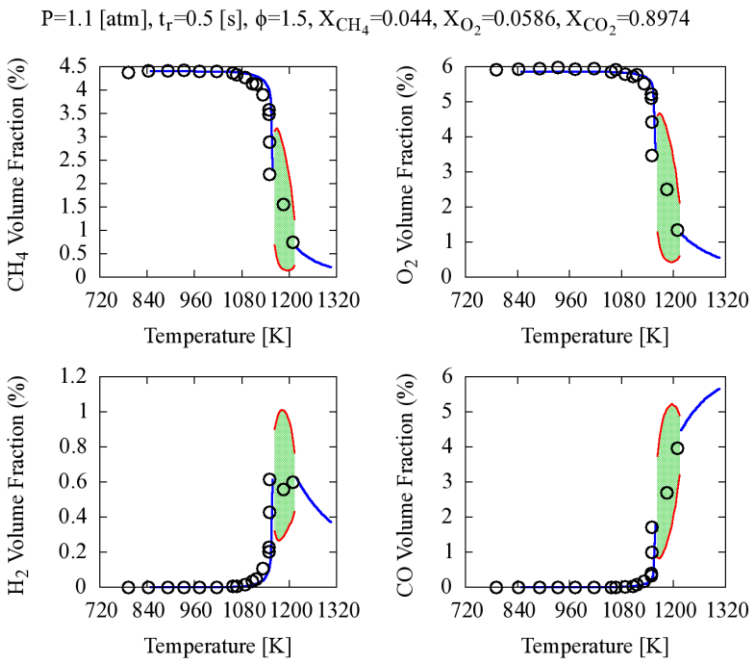

Figure 45. CO_2 diluted system in the rich condition φ=1.5. symbols refers to [8]

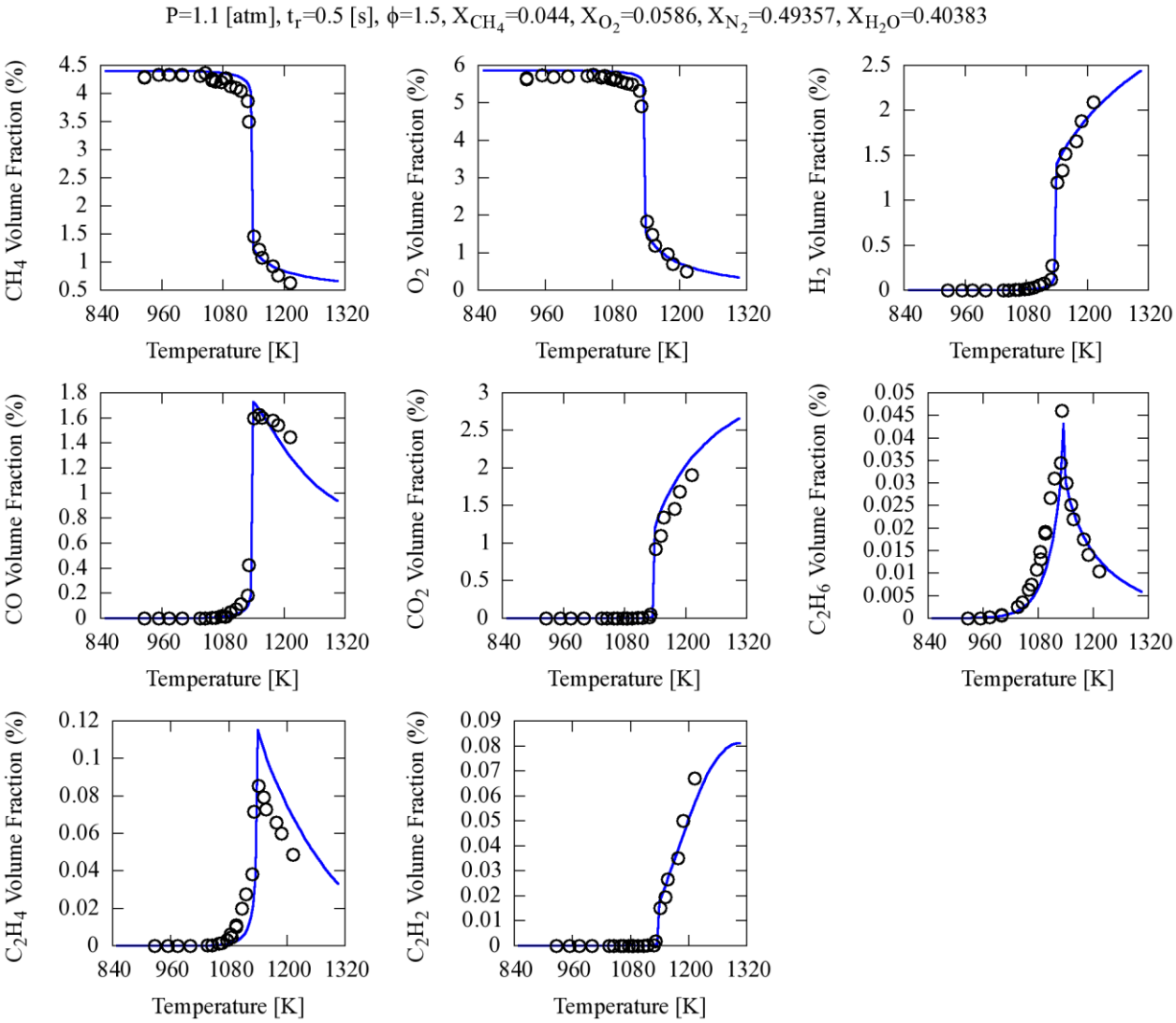

Figure 46 N_2/H_2O diluted system in the rich condition φ=1.5. symbols refers to [8].

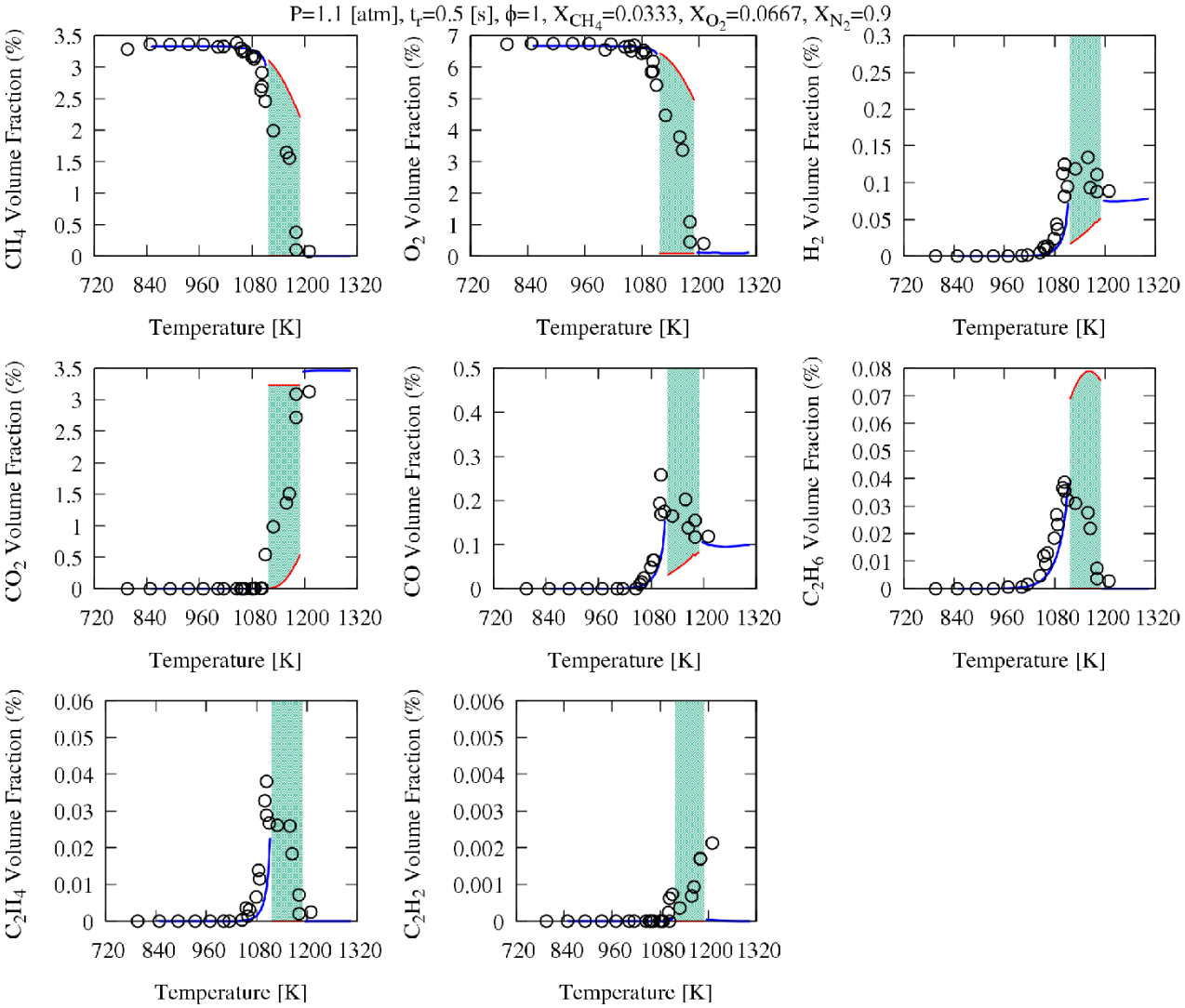

Figure 47 N_2 diluted system in the stoichiometric condition φ=1. symbols refers to [9].

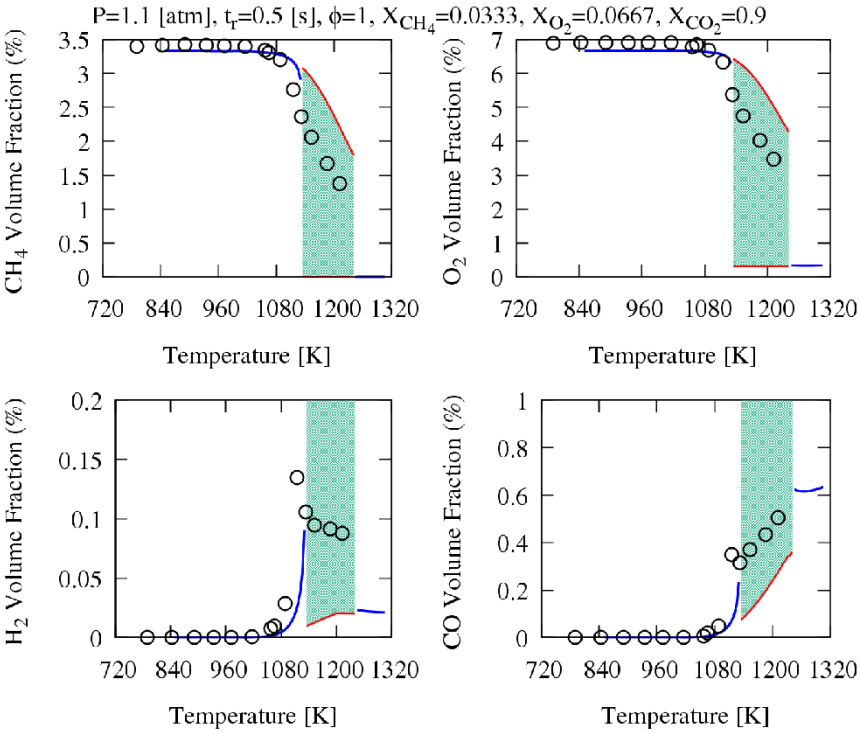

Figure 48 CO_2 diluted system in the stoichiometric condition φ=1. symbols refers to [9].

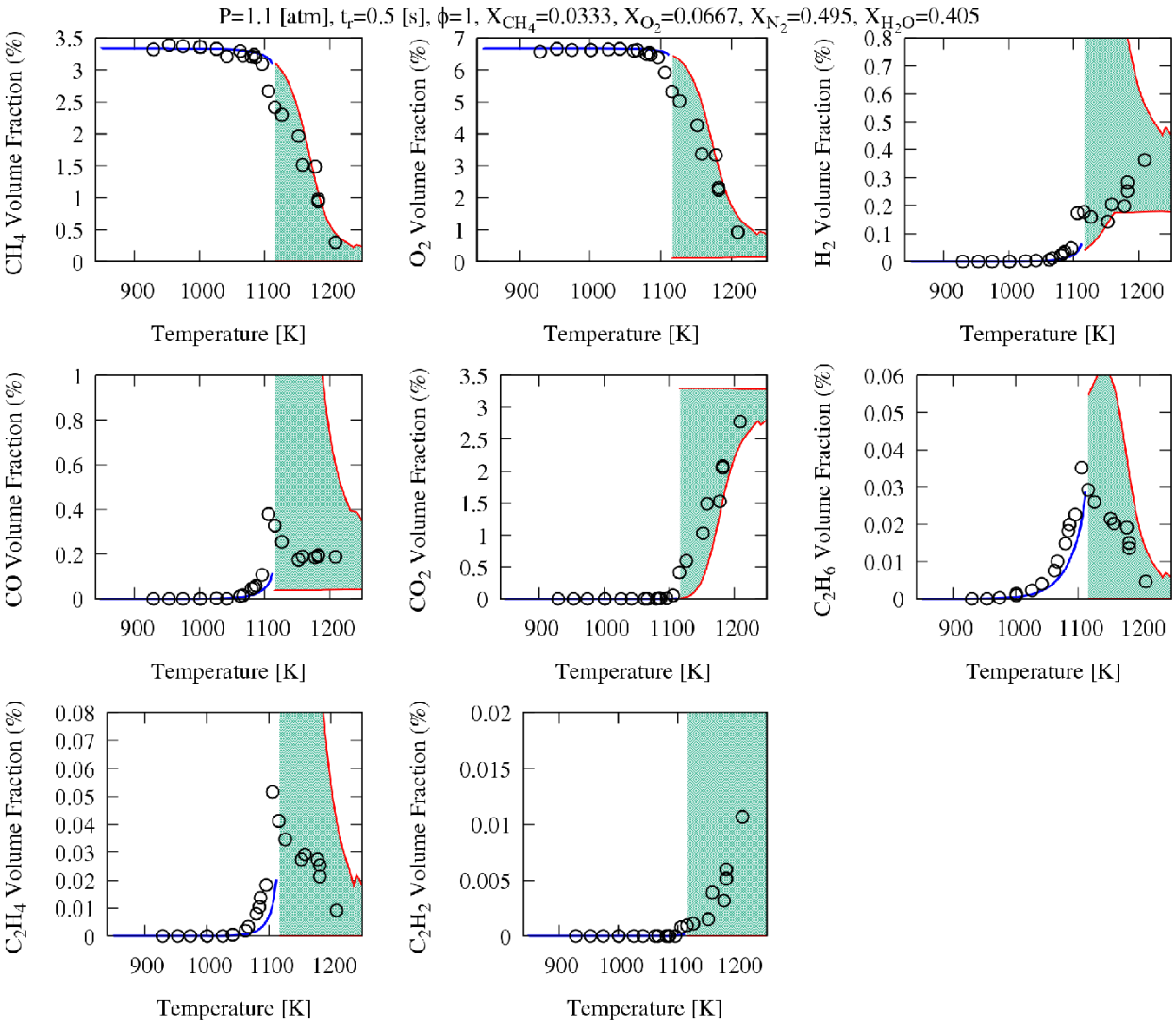

Figure 49 N_2/H_2O diluted system in the stoichiometric condition φ=1. symbols refers to [9].

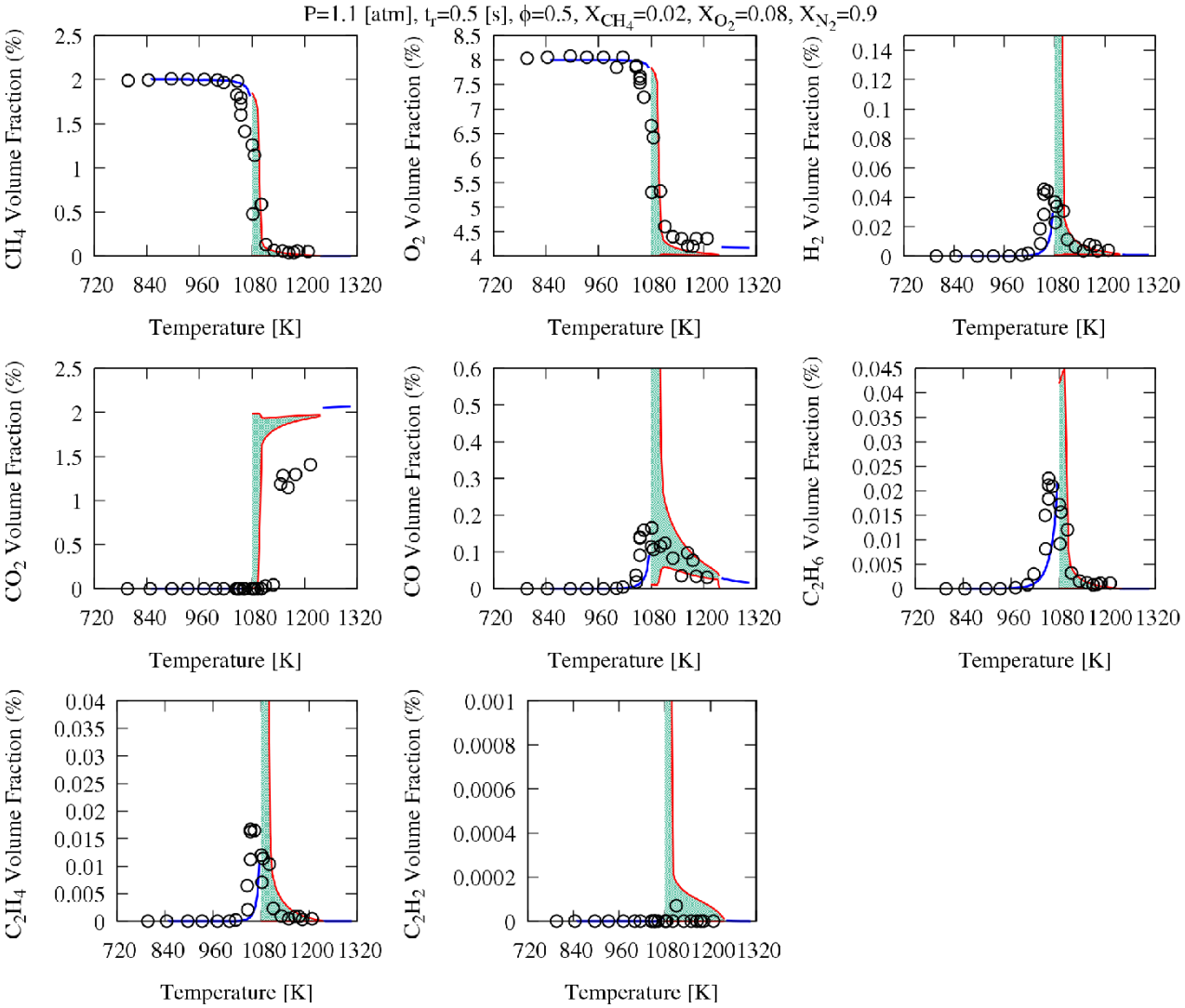

Figure 50 N_2 diluted system in the lean condition φ=0.5. symbols refers to [8].

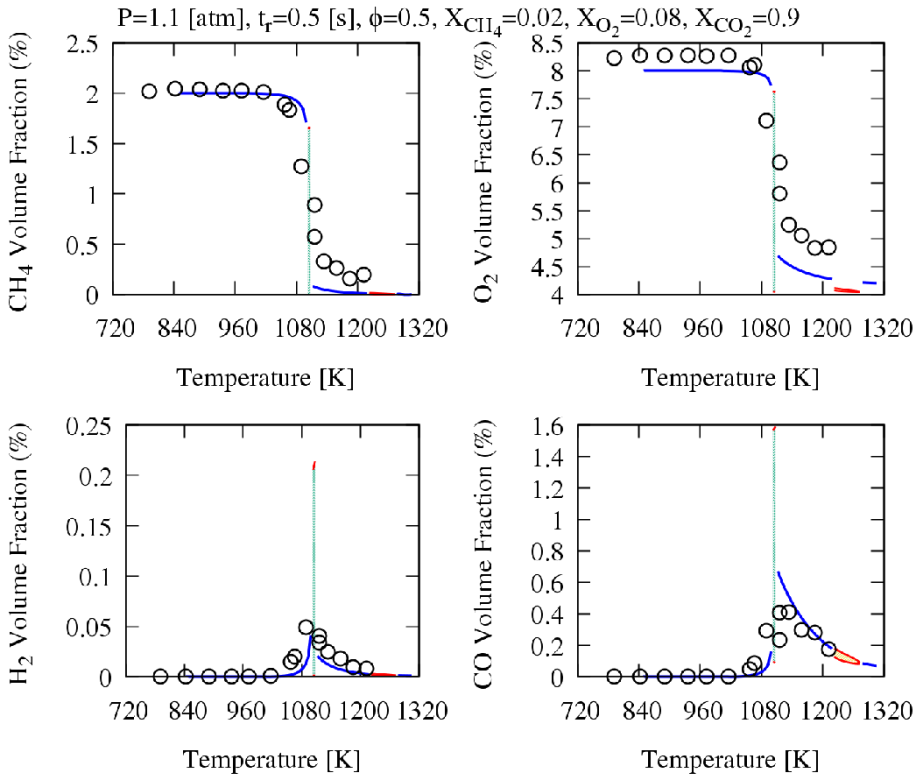

Figure 51 CO_2 diluted system in the lean condition φ=0.5. symbols refers to [8].

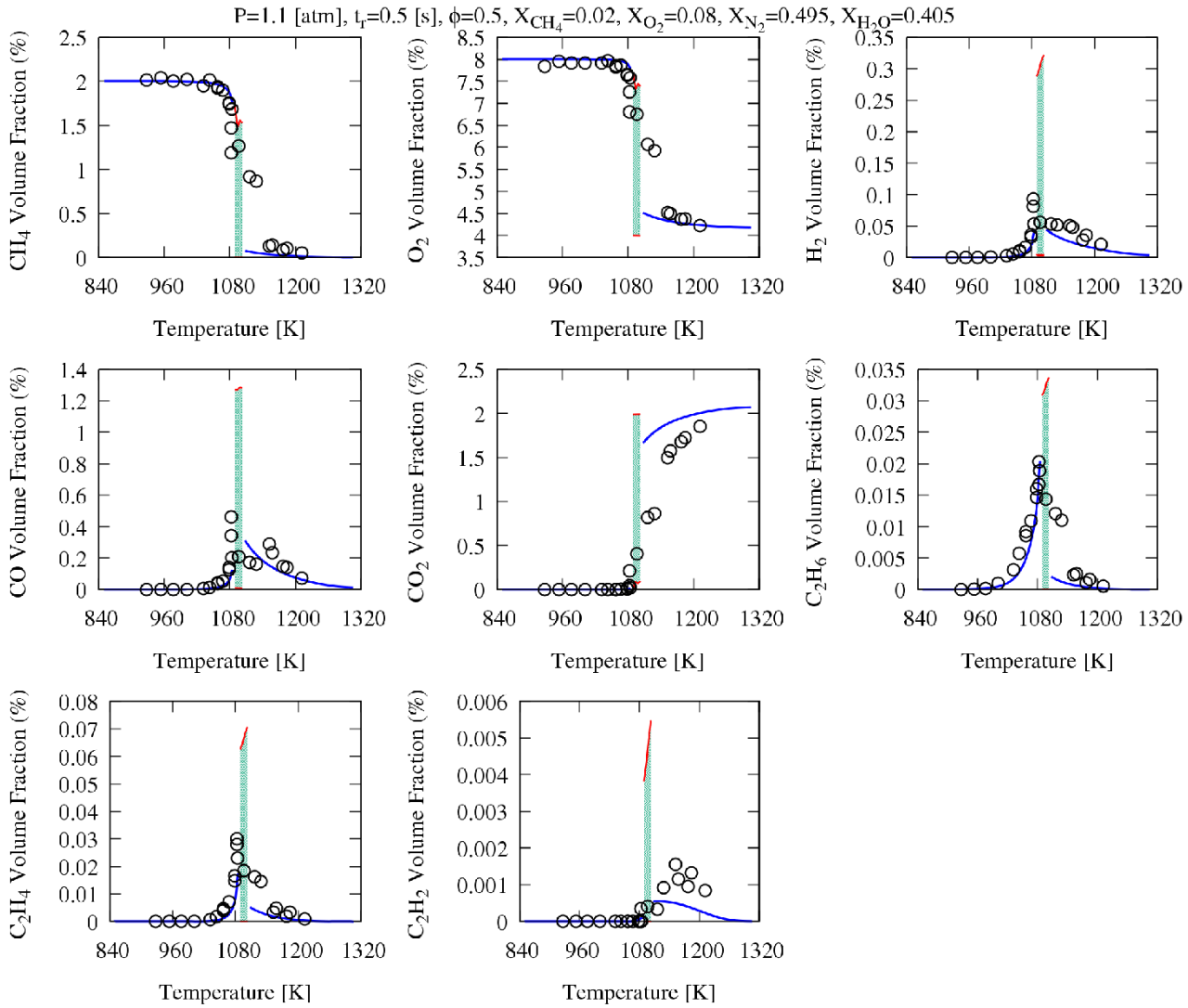

Figure 52 N_2/H_2O diluted system in the lean condition φ=0.5. symbols refers to [8].

2. Plug Flow Reactor (PFR)

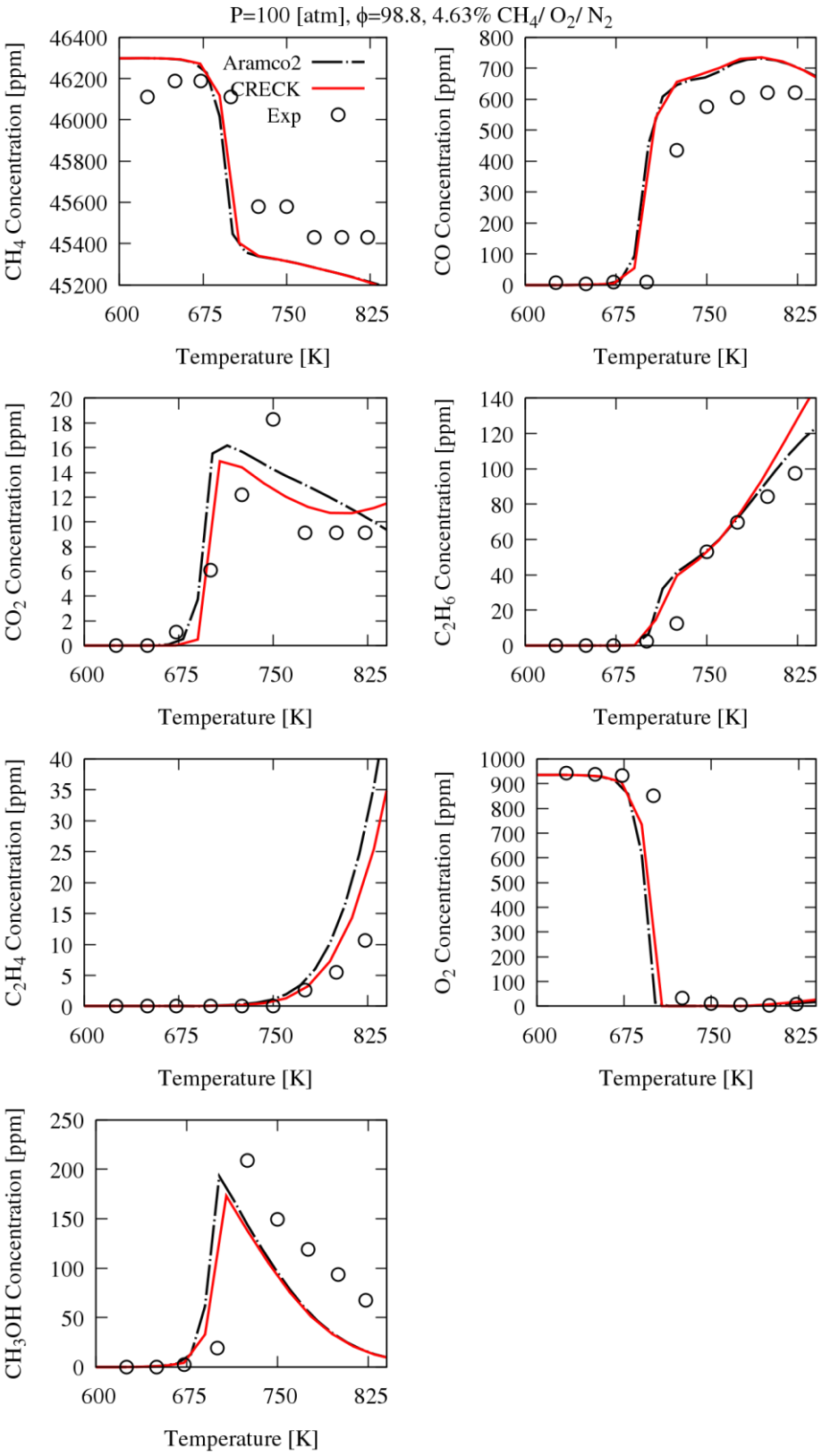

Figure 53 Plug flow reactor species profiles of methane oxidation. Exp refers to [10].

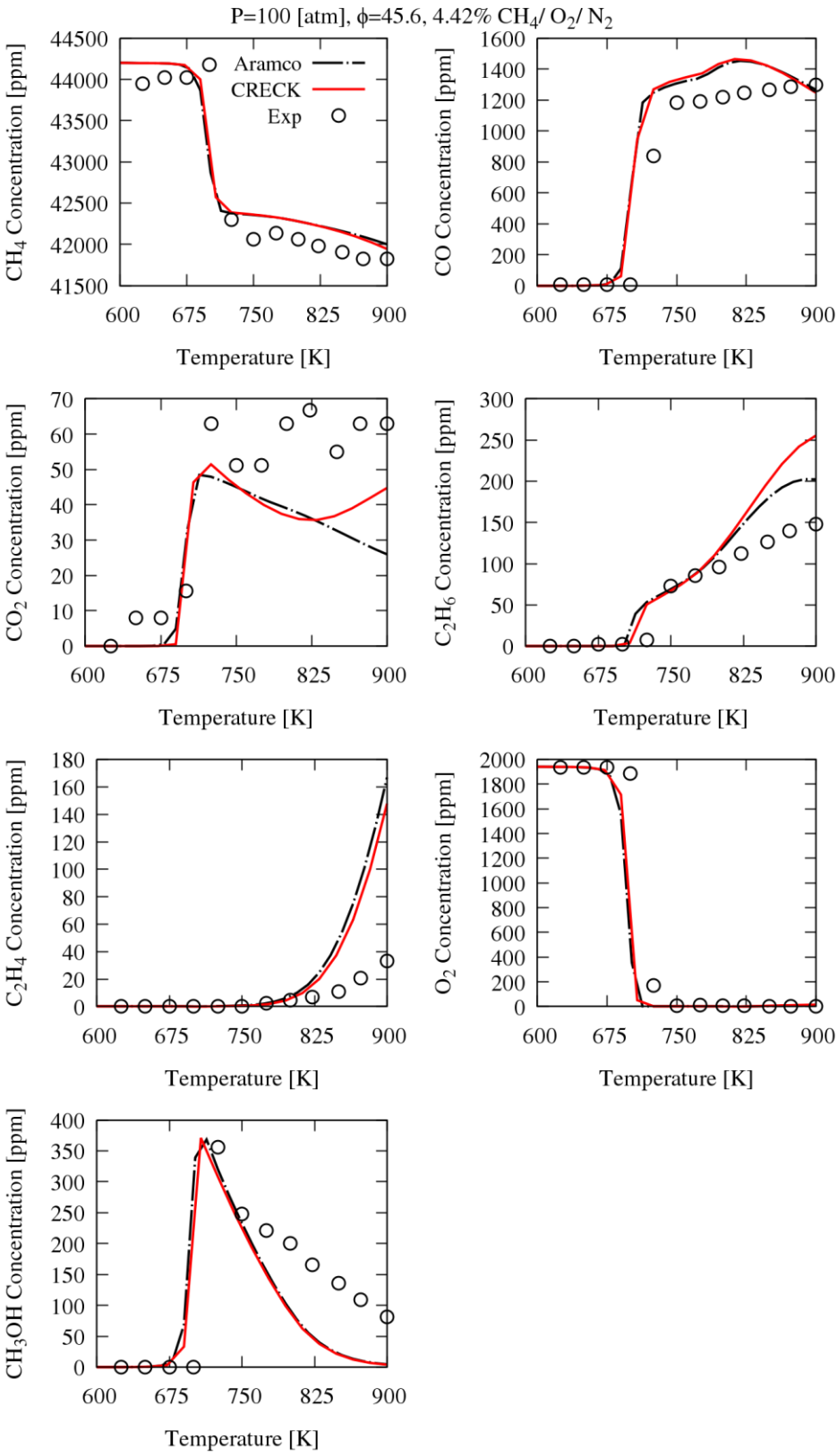

Figure 54 Plug flow reactor species profiles of methane oxidation. Exp refers to [10].

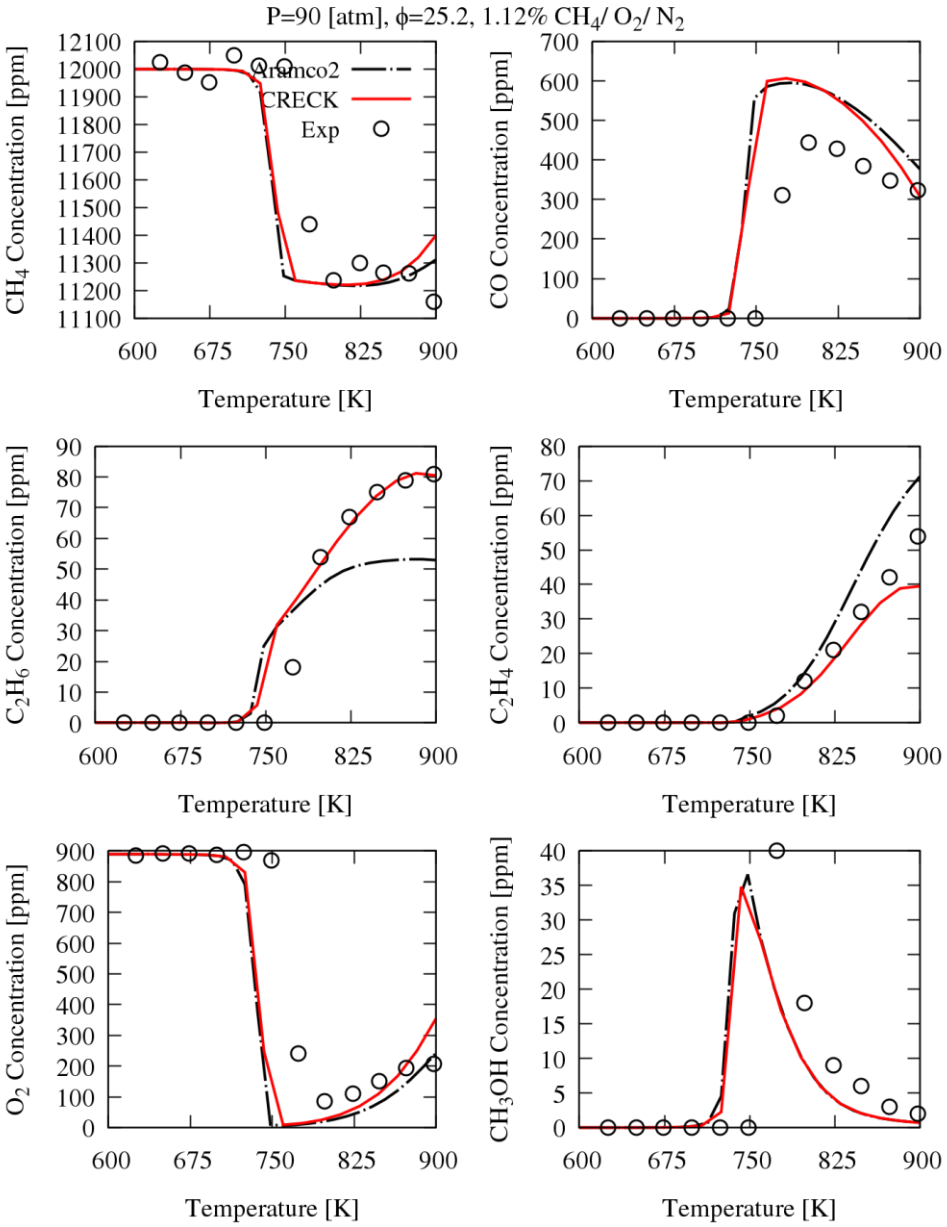

Figure 55 Plug flow reactor species profiles of methane oxidation. Exp refers to [10].

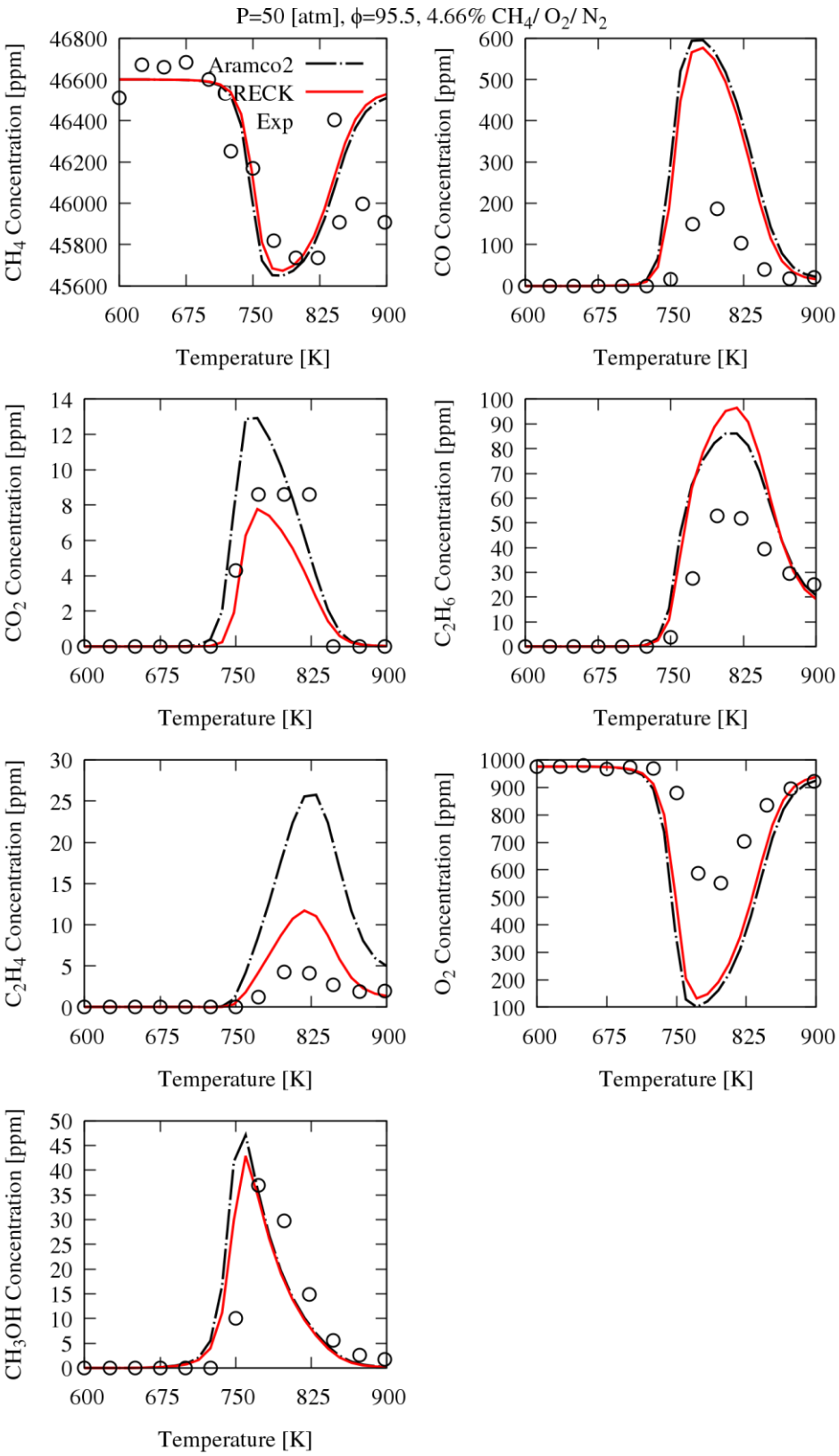

Figure 56 Plug flow reactor species profiles of methane oxidation. Exp refers to [10].

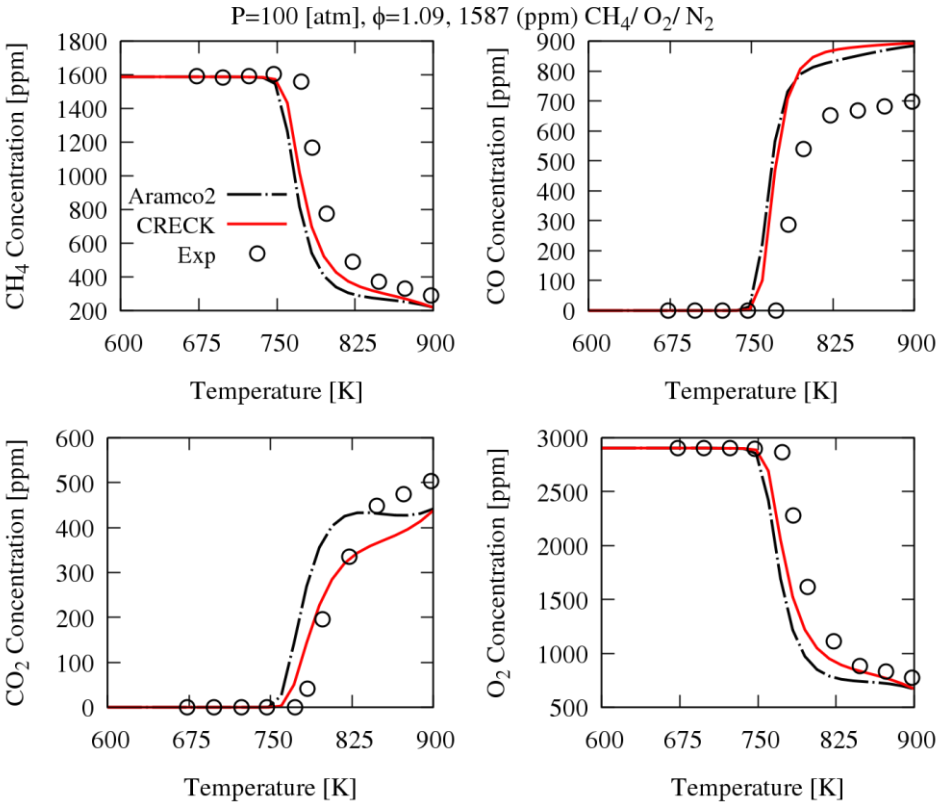

Figure 57 Plug flow reactor species profiles of methane oxidation. Exp refers to [10].

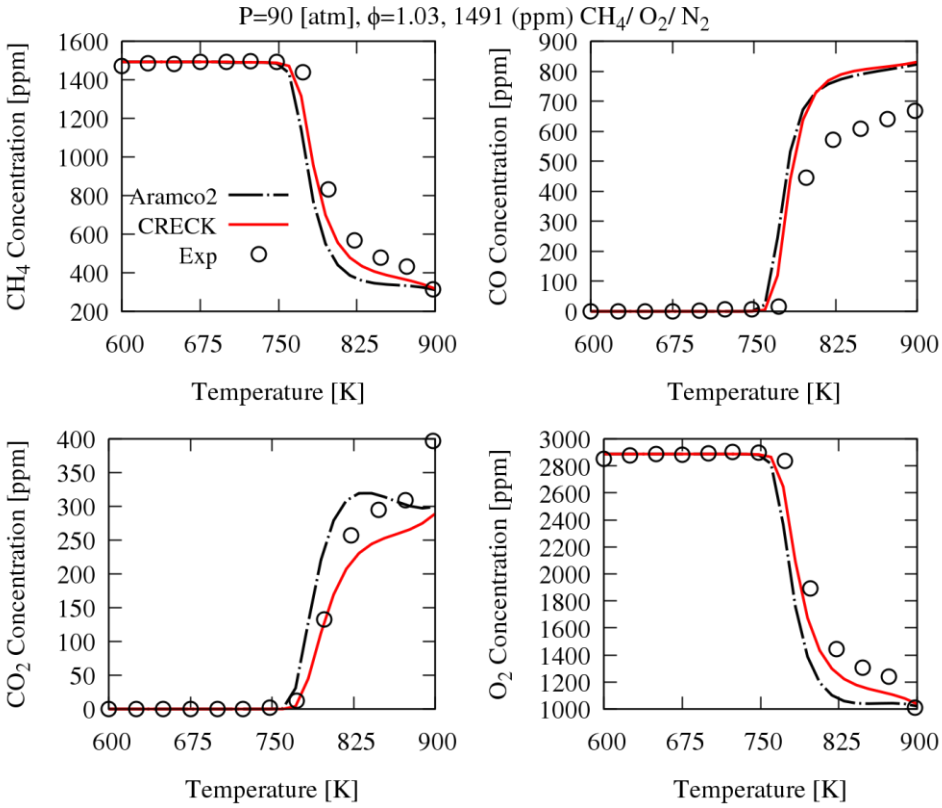

Figure 58 Plug flow reactor species profiles of methane oxidation. Exp refers to [10].

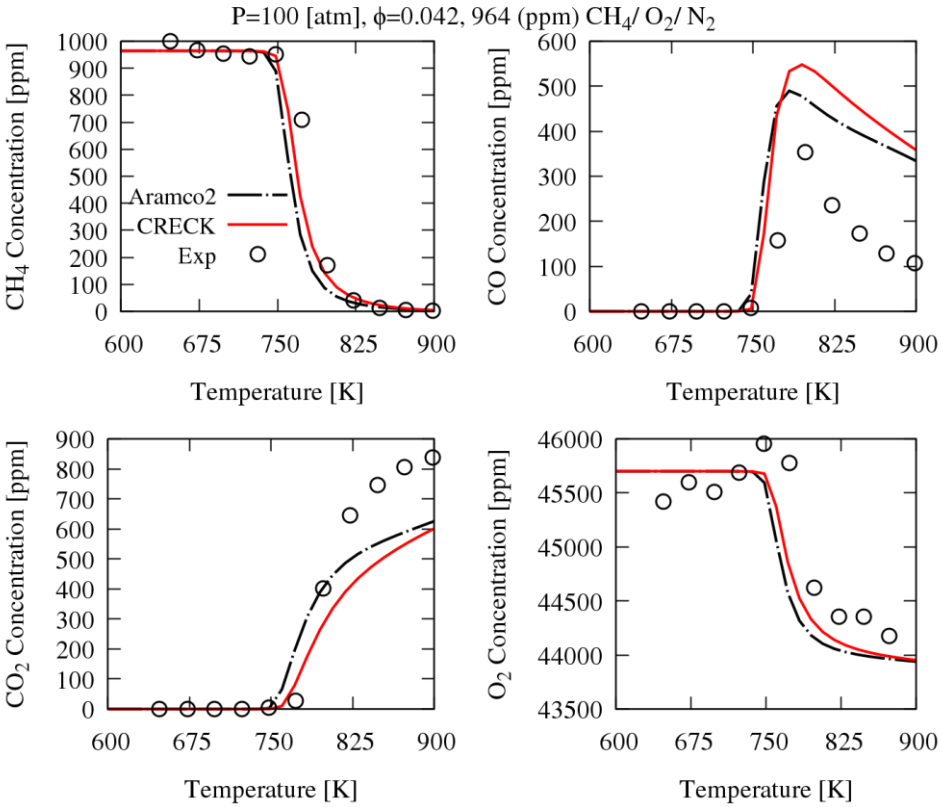

Figure 59 Plug flow reactor species profiles of methane oxidation. Exp refers to [10].

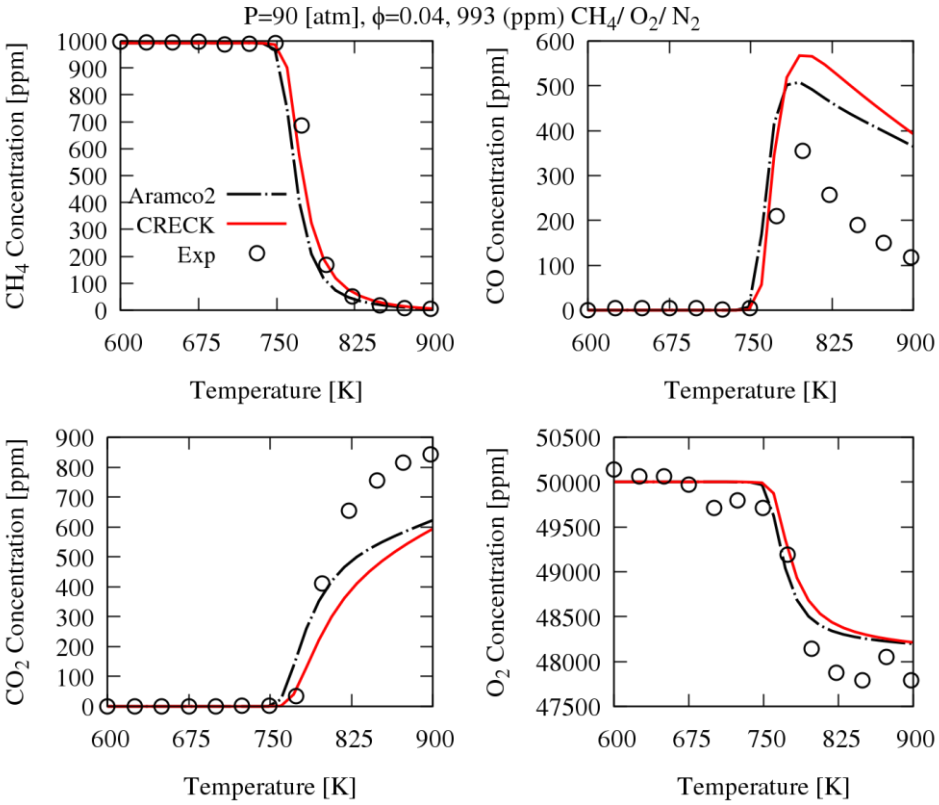

Figure 60 Plug flow reactor species profiles of methane oxidation. Exp refers to [10].

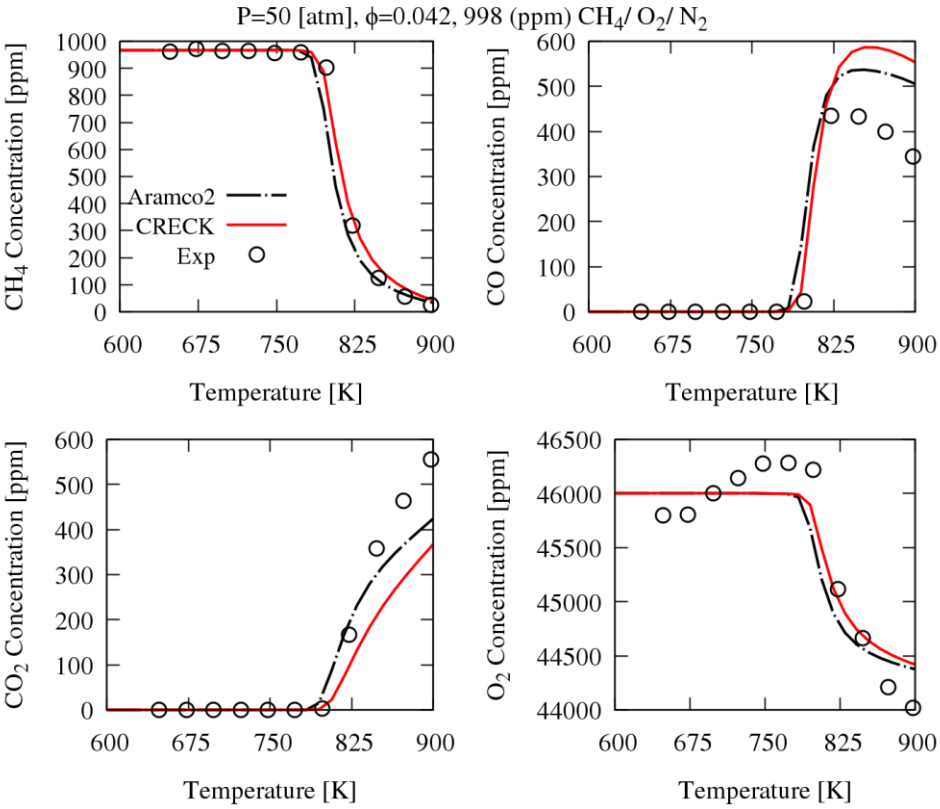

Figure 61 Plug flow reactor species profiles of methane oxidation. Exp refers to [10].

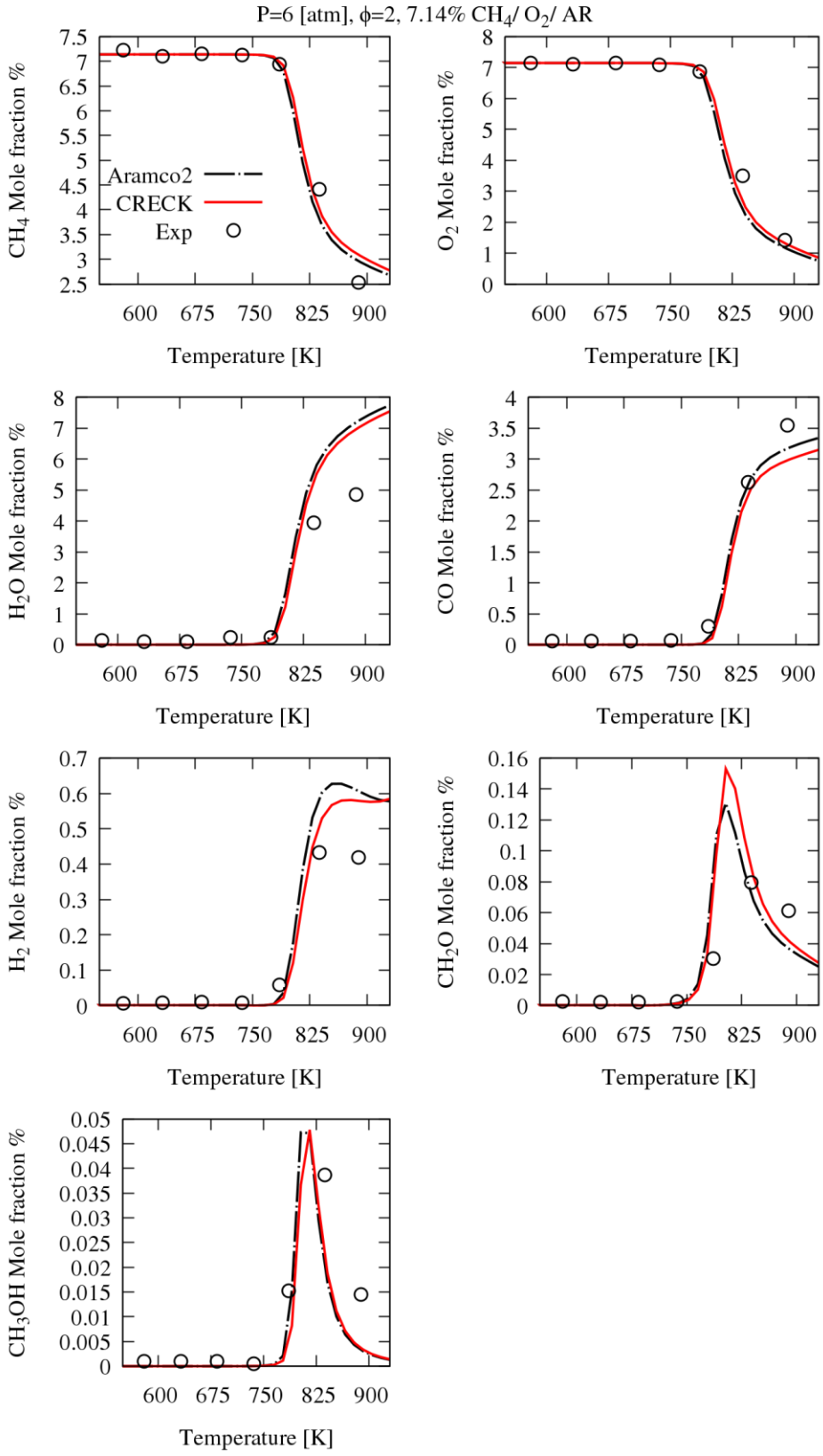

Figure 62 Plug flow reactor species profiles of methane oxidation. Exp refers to [11].

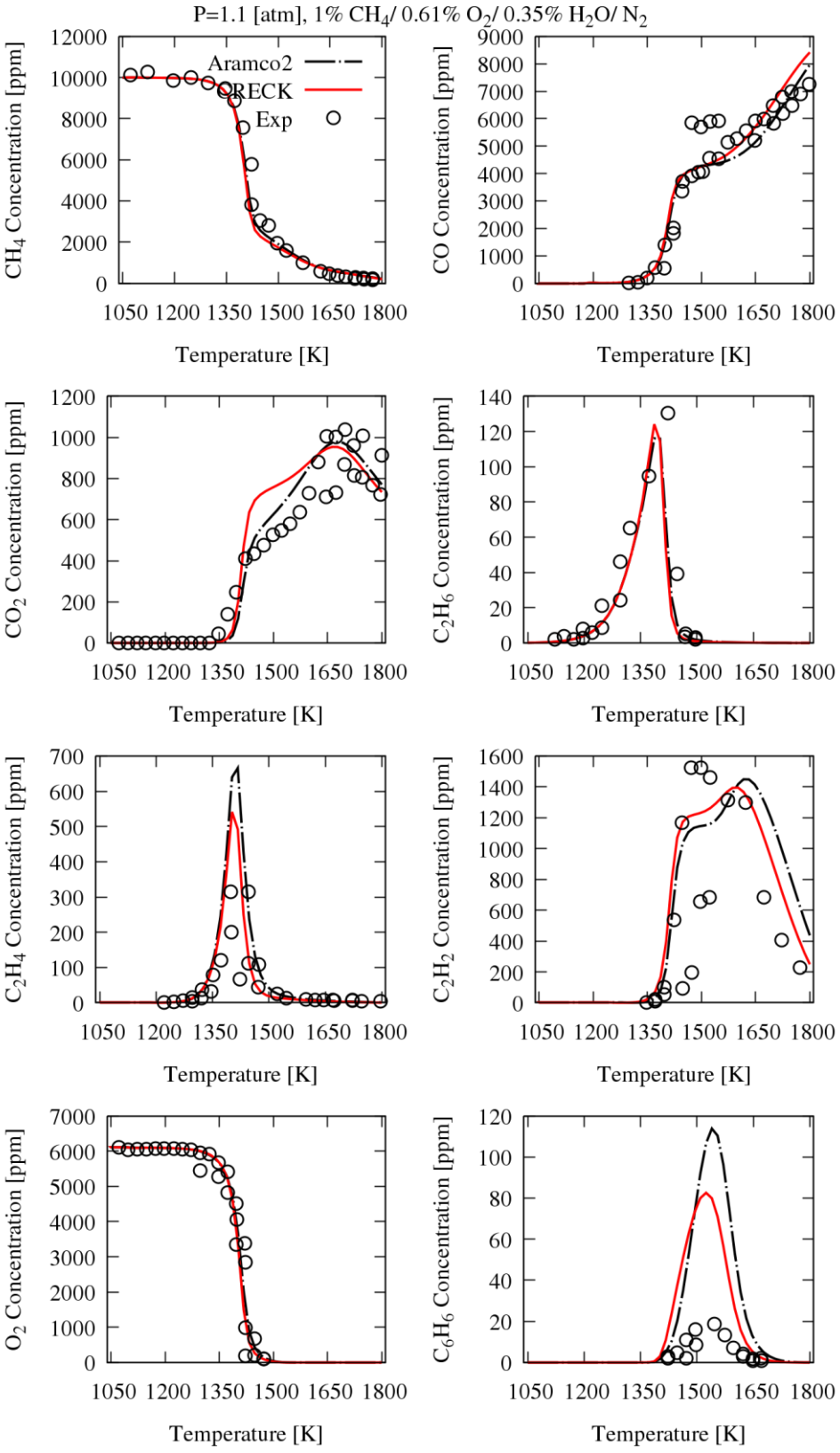

Figure 63 Plug flow reactor species profiles of methane oxidation. Exp refers to [12].

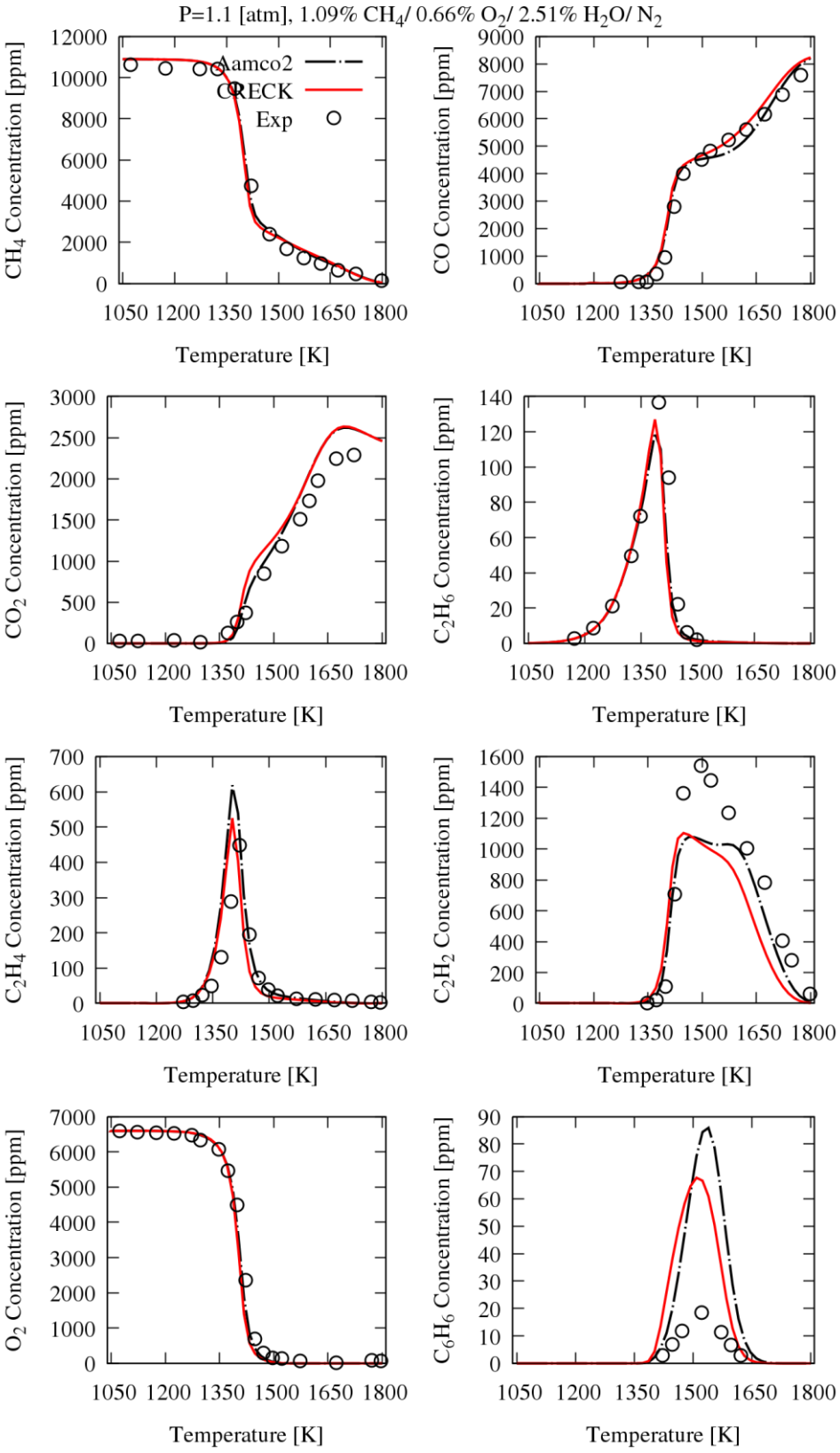

Figure 64 Figure 65 Plug flow reactor species profiles of methane oxidation. Exp refers to [12].

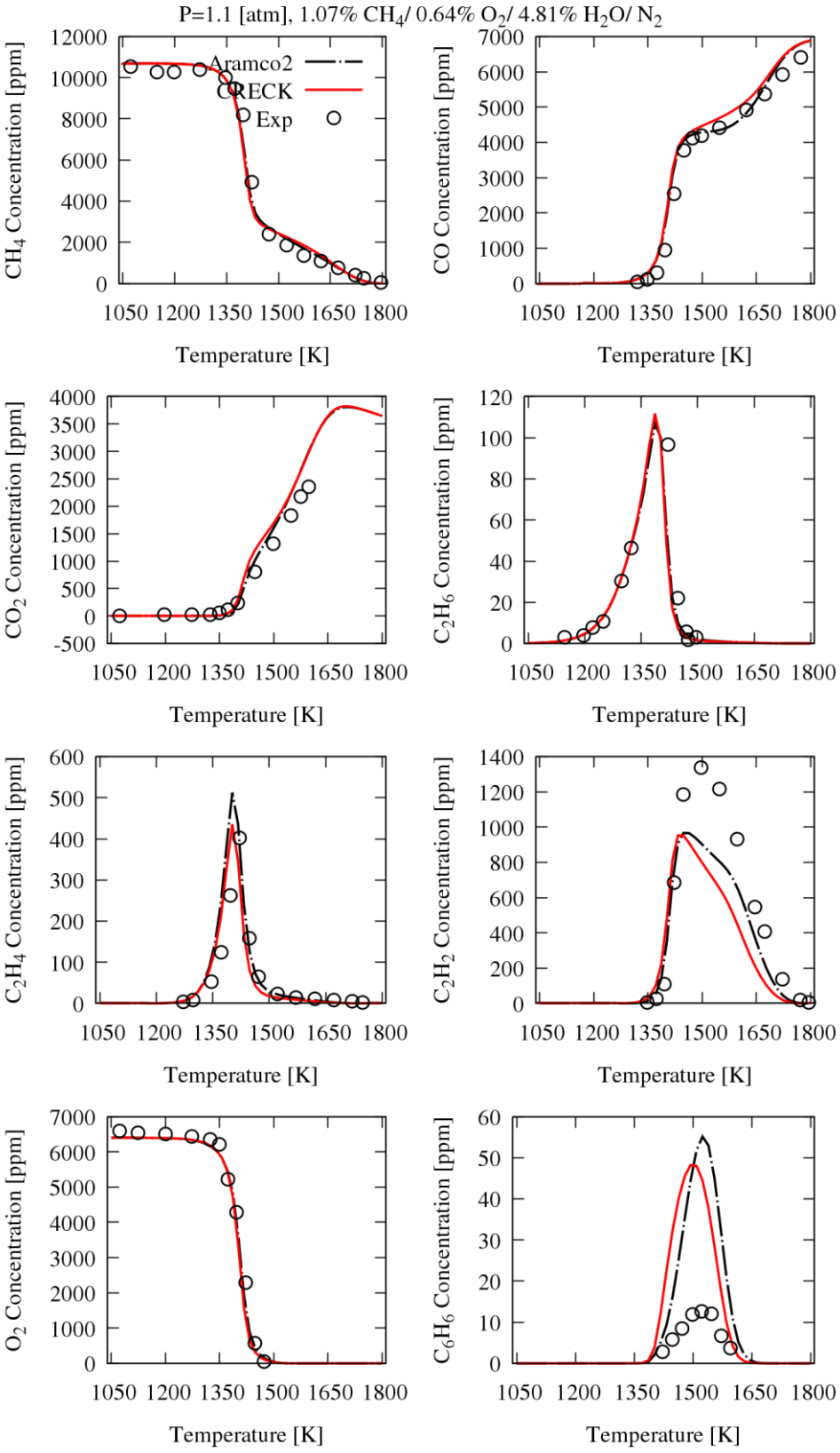

Figure 66 Figure 67 Plug flow reactor species profiles of methane oxidation. Exp refers to [12].

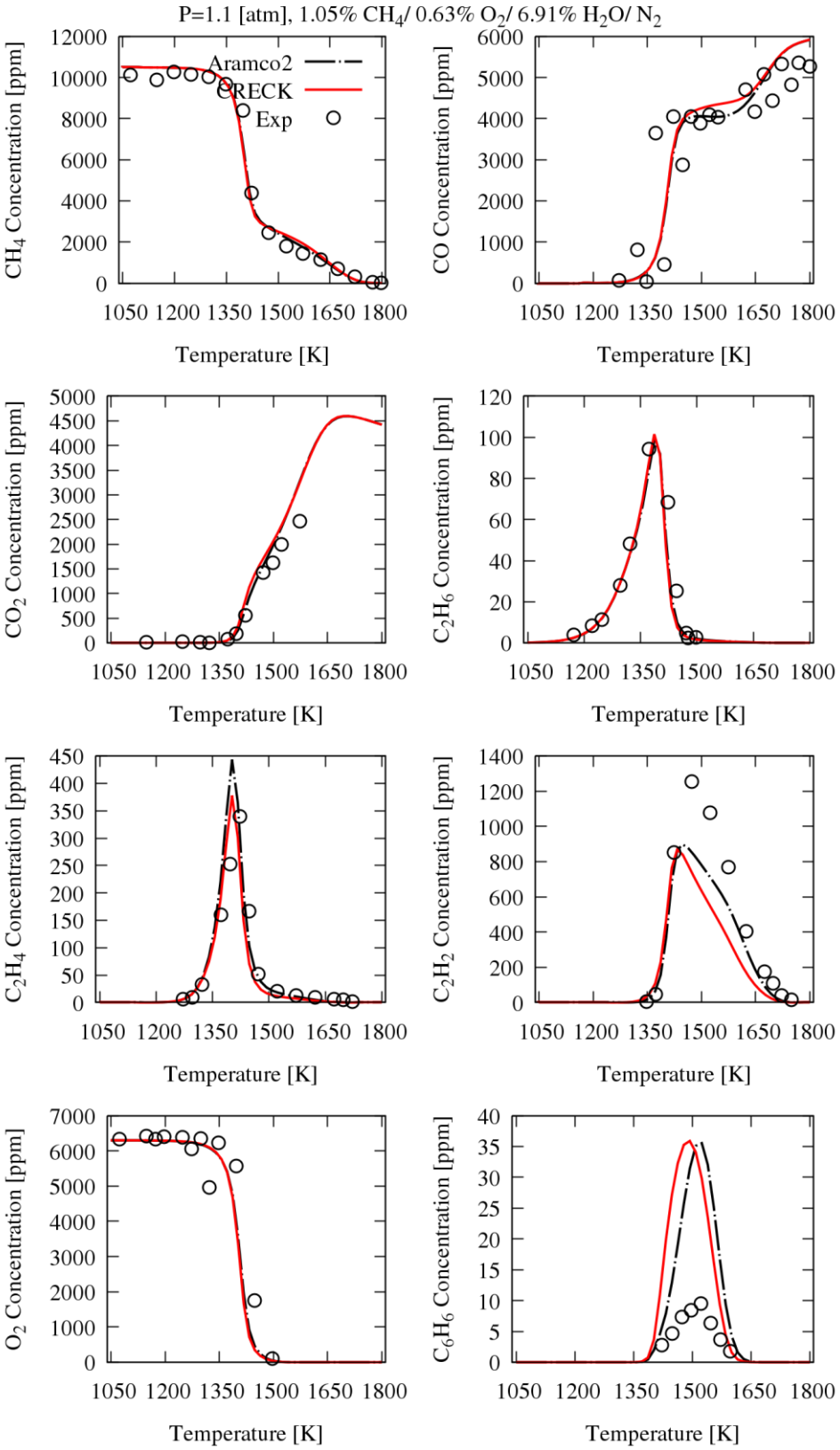

Figure 68 Figure 69 Plug flow reactor species profiles of methane oxidation. Exp refers to [12].

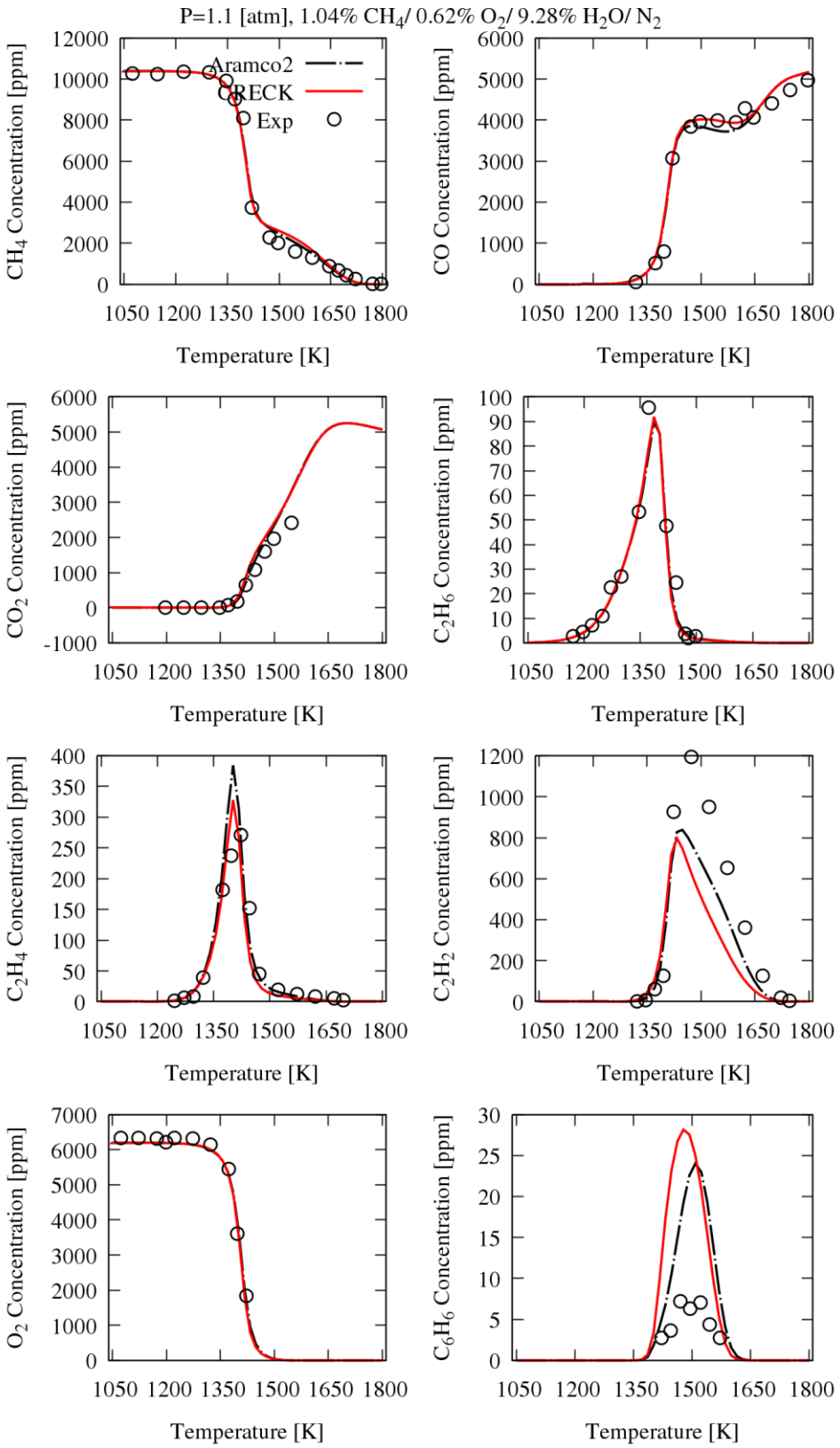

Figure 70 Figure 71 Plug flow reactor species profiles of methane oxidation. Exp refers to [12].

3. Ignition Delay Time

Shock Tube

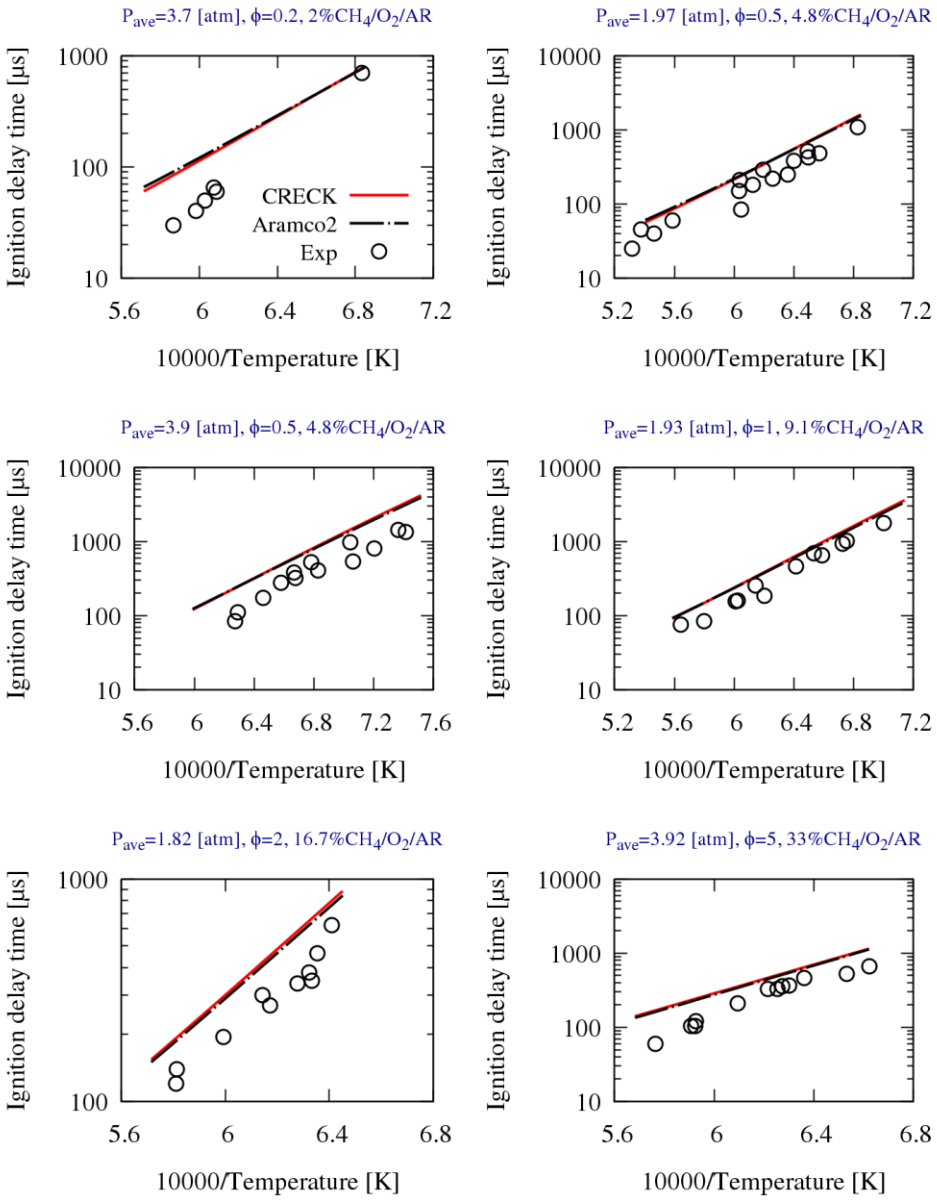

Figure 72 Shock tube ignition delay times of methane oxidation. Exp refers to [13].

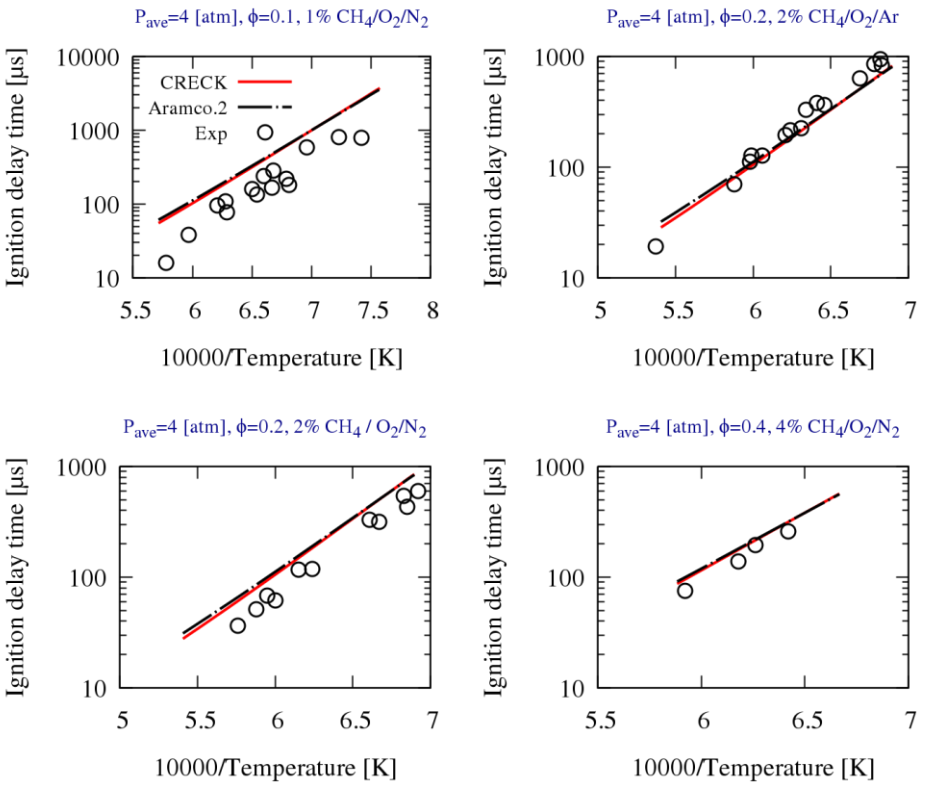

Figure 73 Shock tube ignition delay times of methane oxidation. Exp refers to [14].

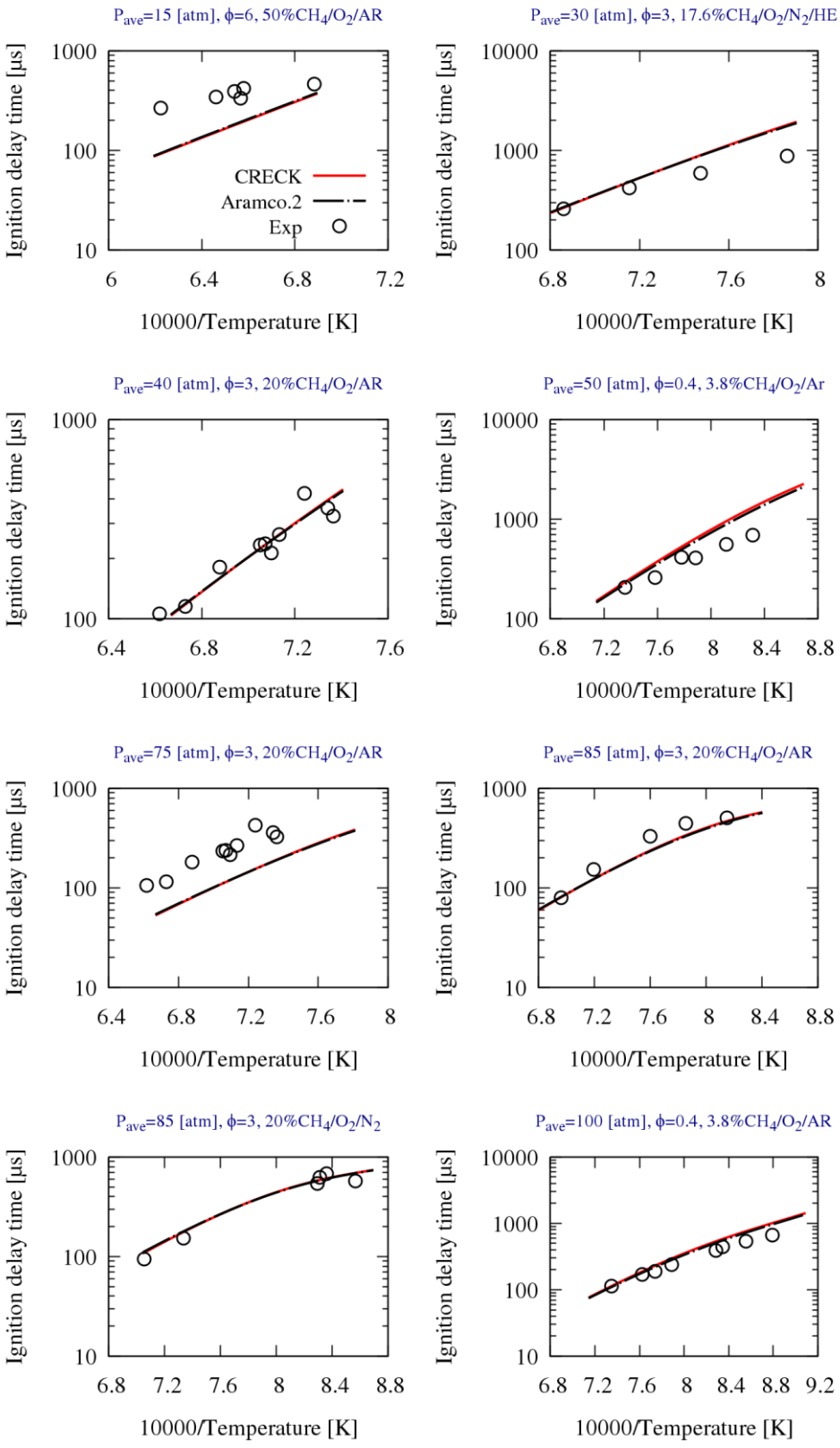

Figure 74 Shock tube ignition delay times of methane oxidation. Exp refers to [15].

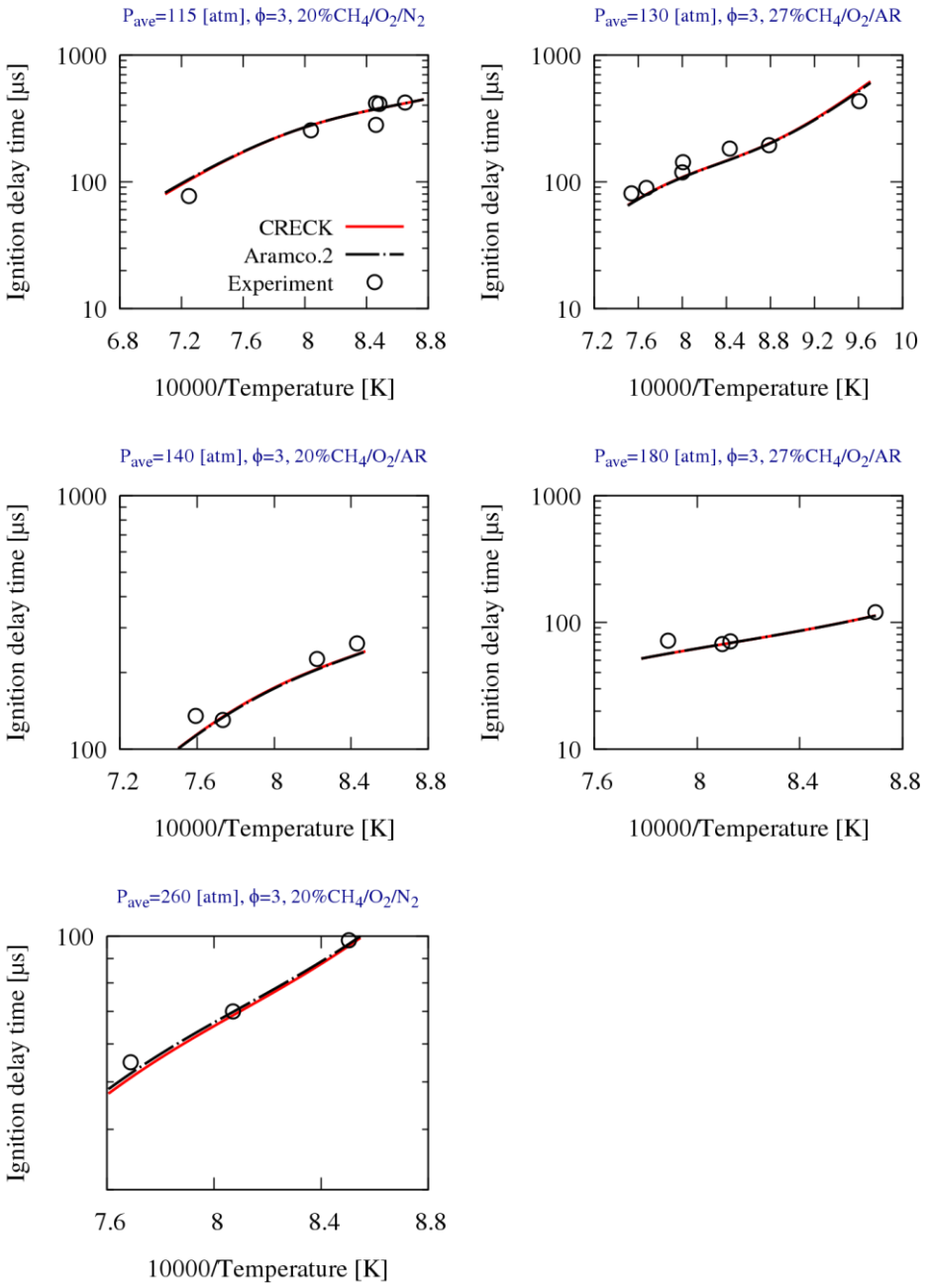

Figure 75 Shock tube ignition delay times of methane oxidation. Exp refers to [15].

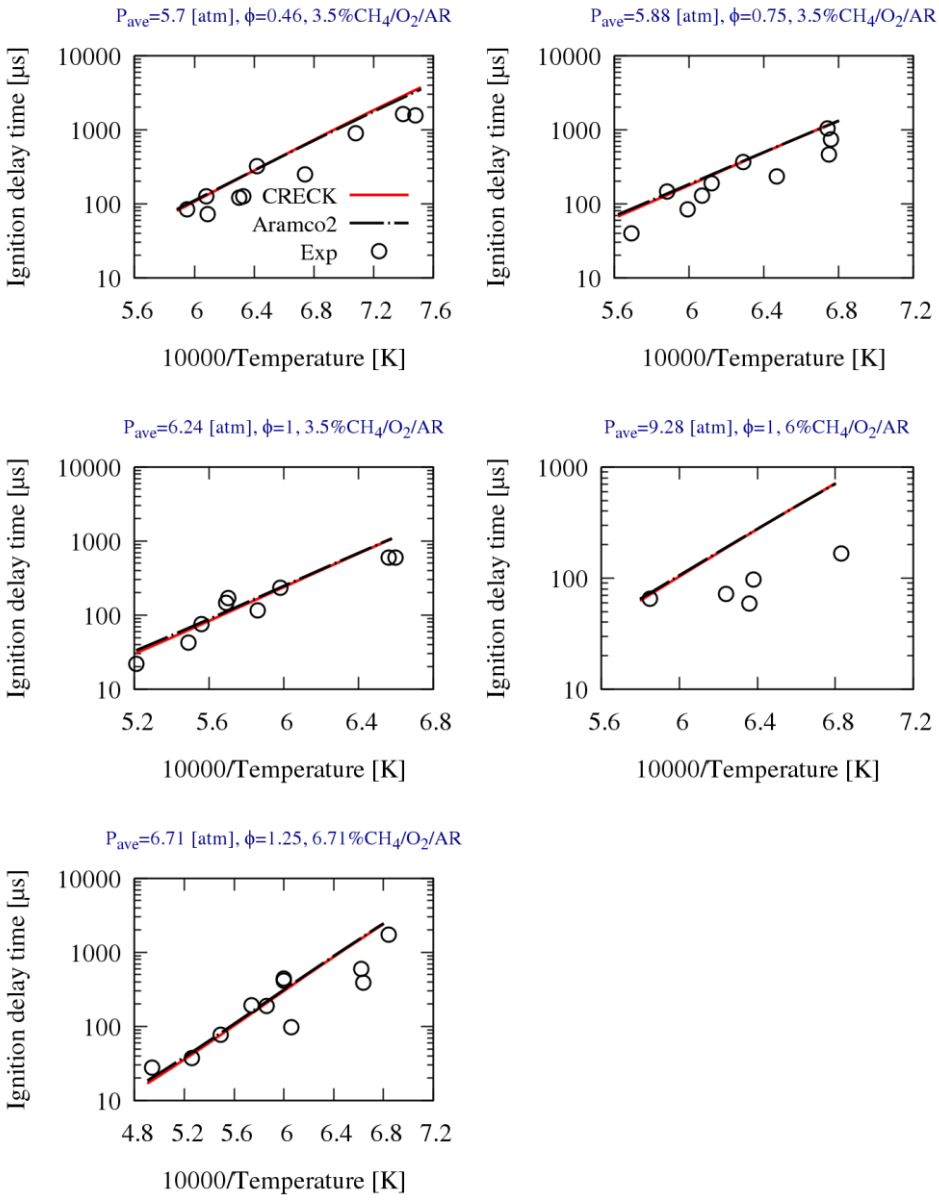

Figure 76 Shock tube ignition delay times of methane oxidation. Exp refers to [16].

MILD Ignition Delay Time (Plug Flow Reactor)

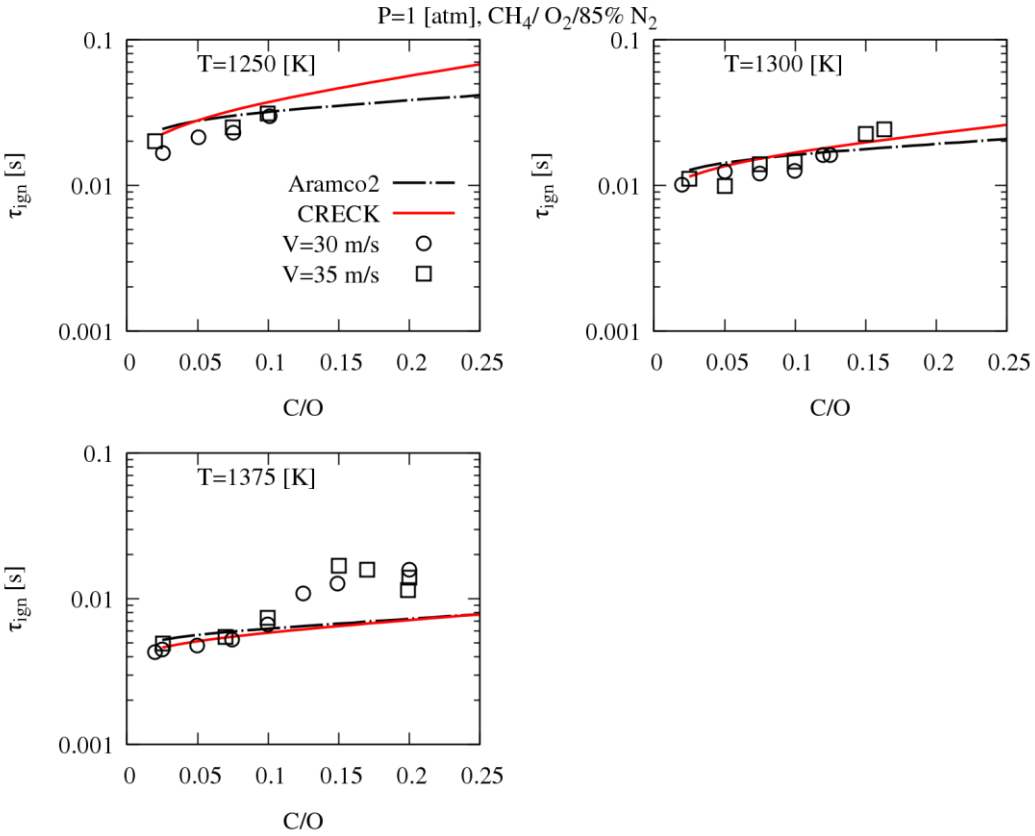

Figure 77 Plug flow reactor ignition delay times of methane at constant temperature and various C/O ratios. Exp refers to [17].

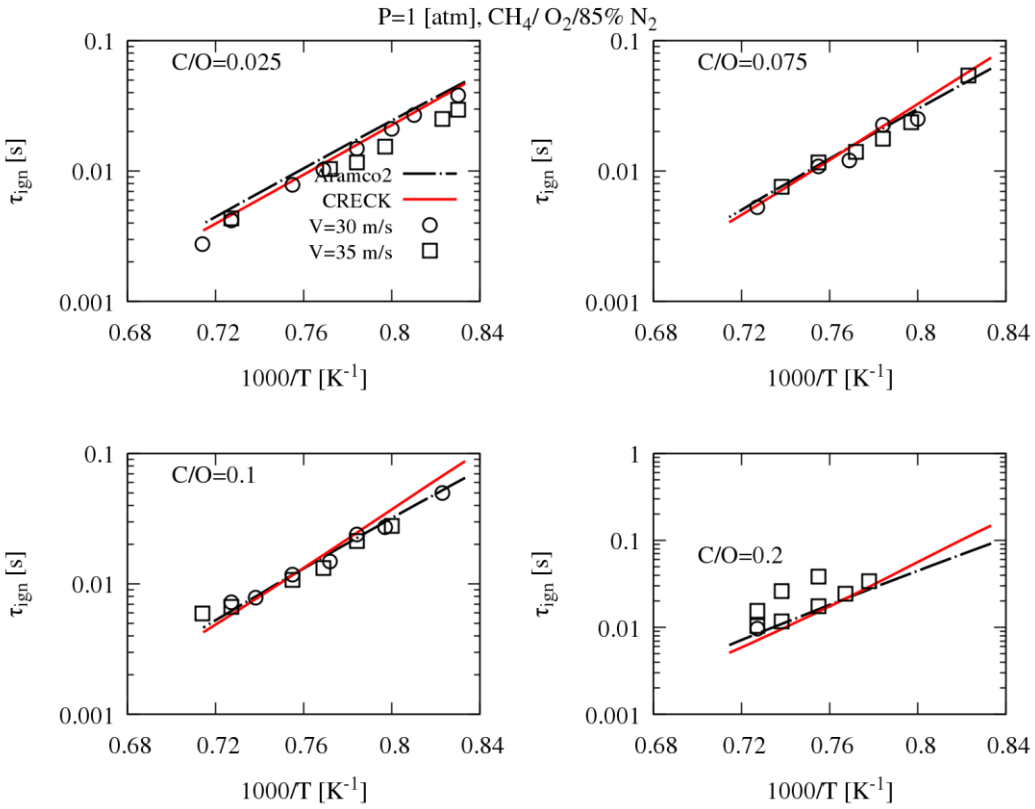

Figure 78 Plug flow reactor ignition delay times of methane at constant equivalence ratio. Exp refers to [17].

Oxy-Fuel Ignition Delay Time (Shock Tube)

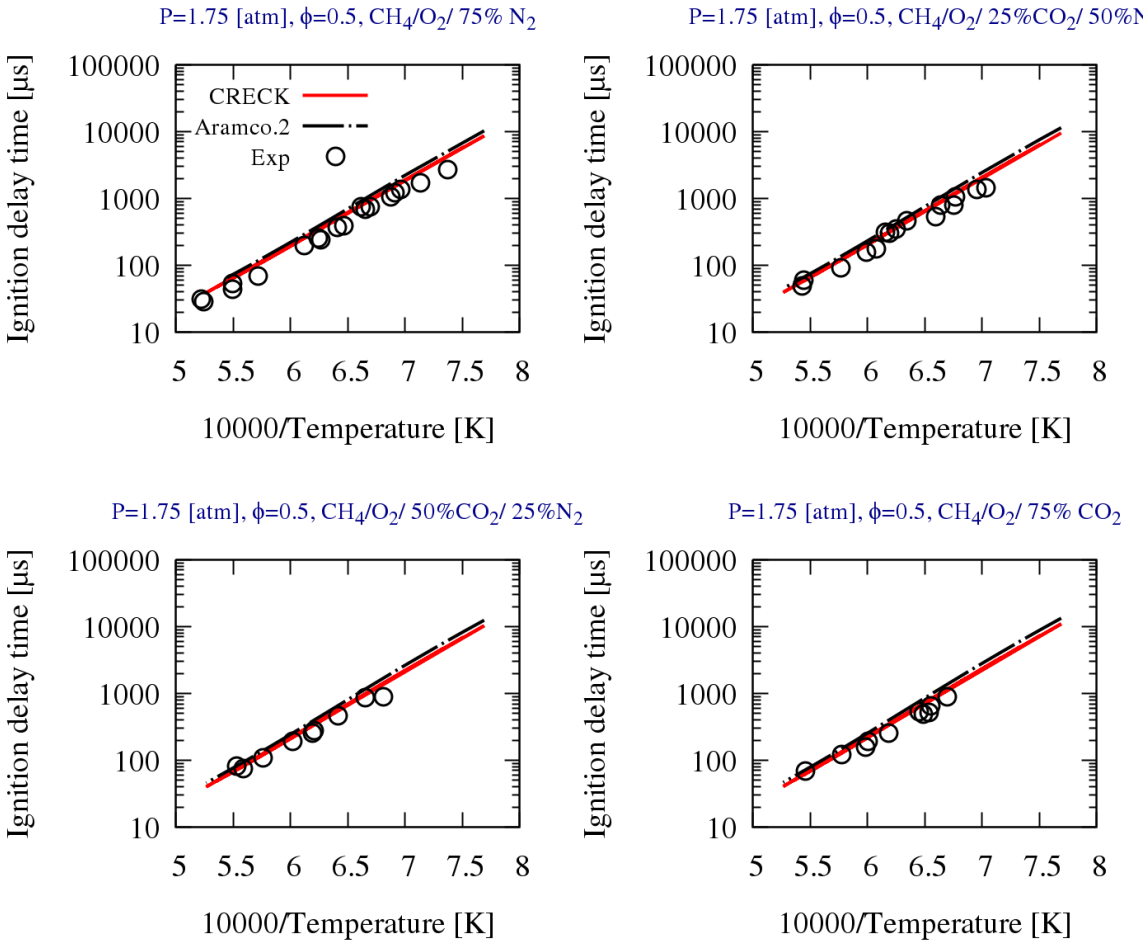

Figure 79 Ignition delay times of methane Oxy-fuel condition measured in shock tube. Exp refers to [18].

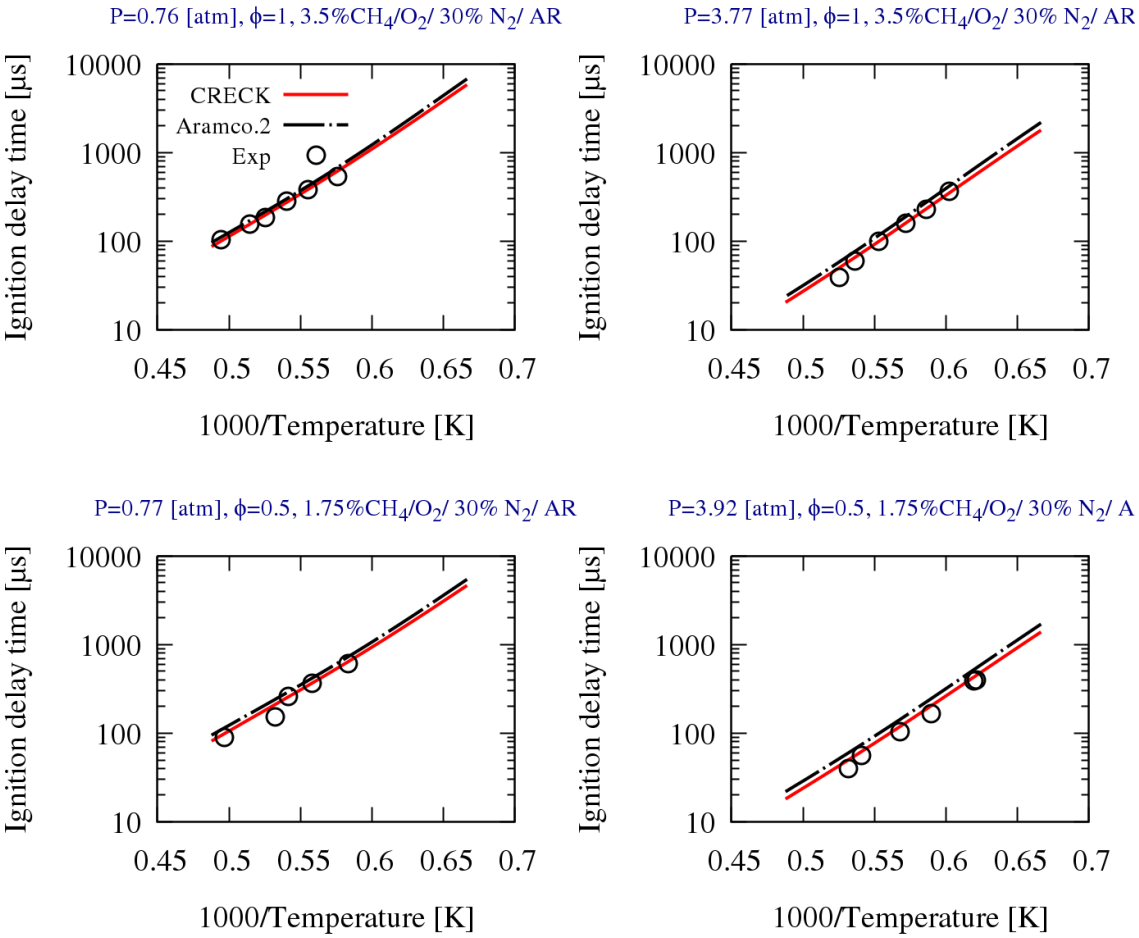

Figure 80 Ignition delay times of methane Oxy-fuel condition measured in shock tube. Exp refers [19].

4. Flame speed

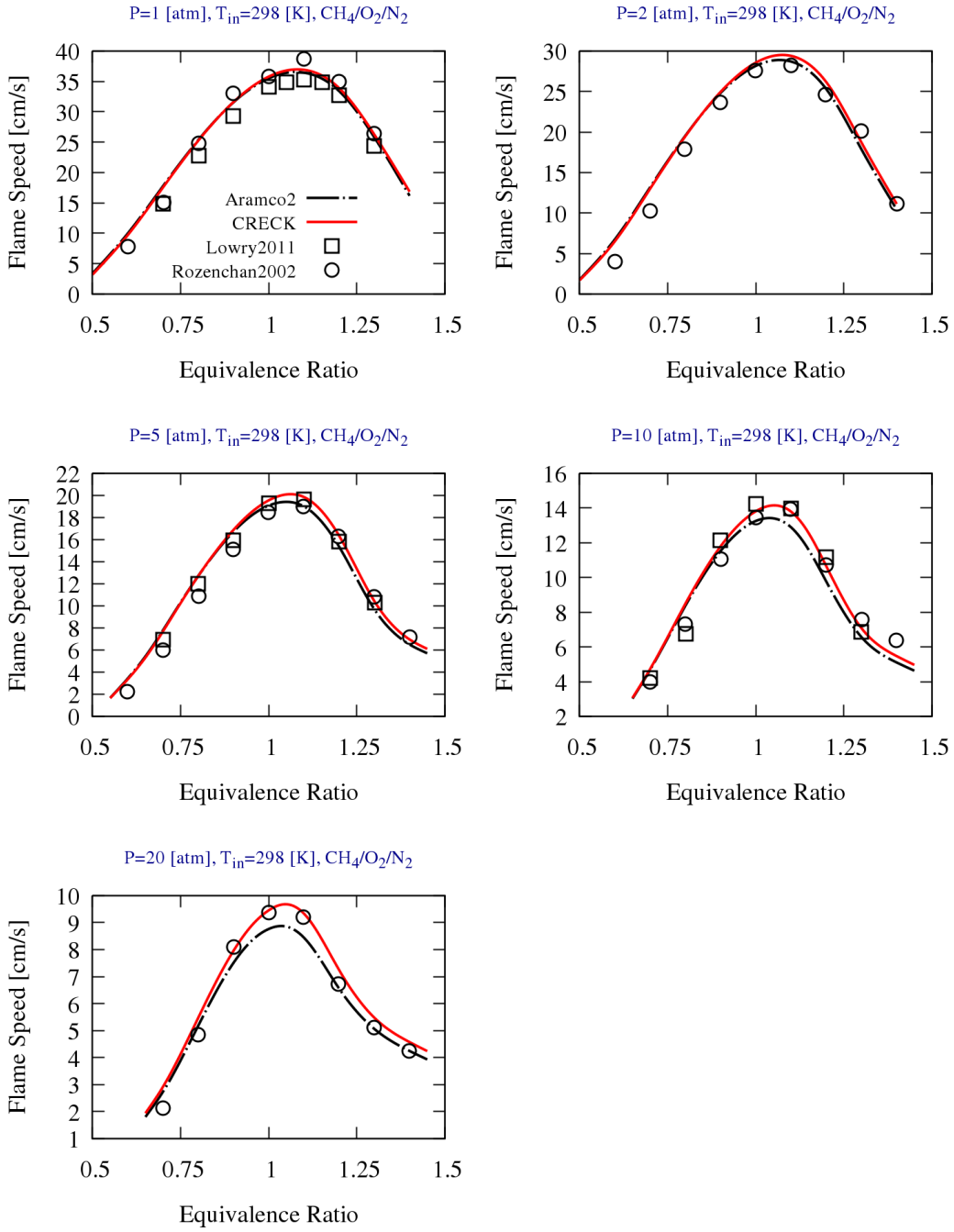

Figure 81 Laminar flame speed measurements methane/air mixture. Rozenchan2002 refers to [20] *and Lowry2011 refers to* [21].

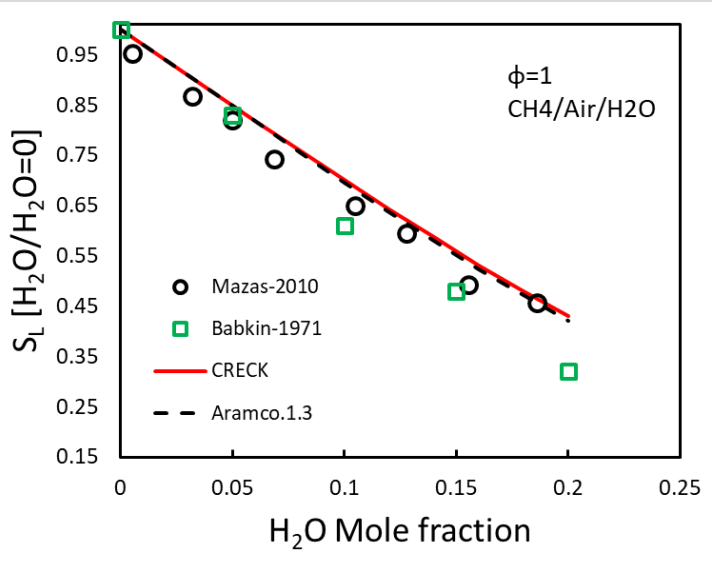

Figure 82 Laminar flame speed ratios of various H_2O dilution level over zero H_2O dilution (S_L(XH2O)/S_L(XH2O = 0) of stoichiometric CH_4/Air/H_2O mixtures, at T_{in}= 473 K and atmospheric pressure. Babkin-1971 and Mazas-2010 refer to [22] *and* [23]*, respectively.*

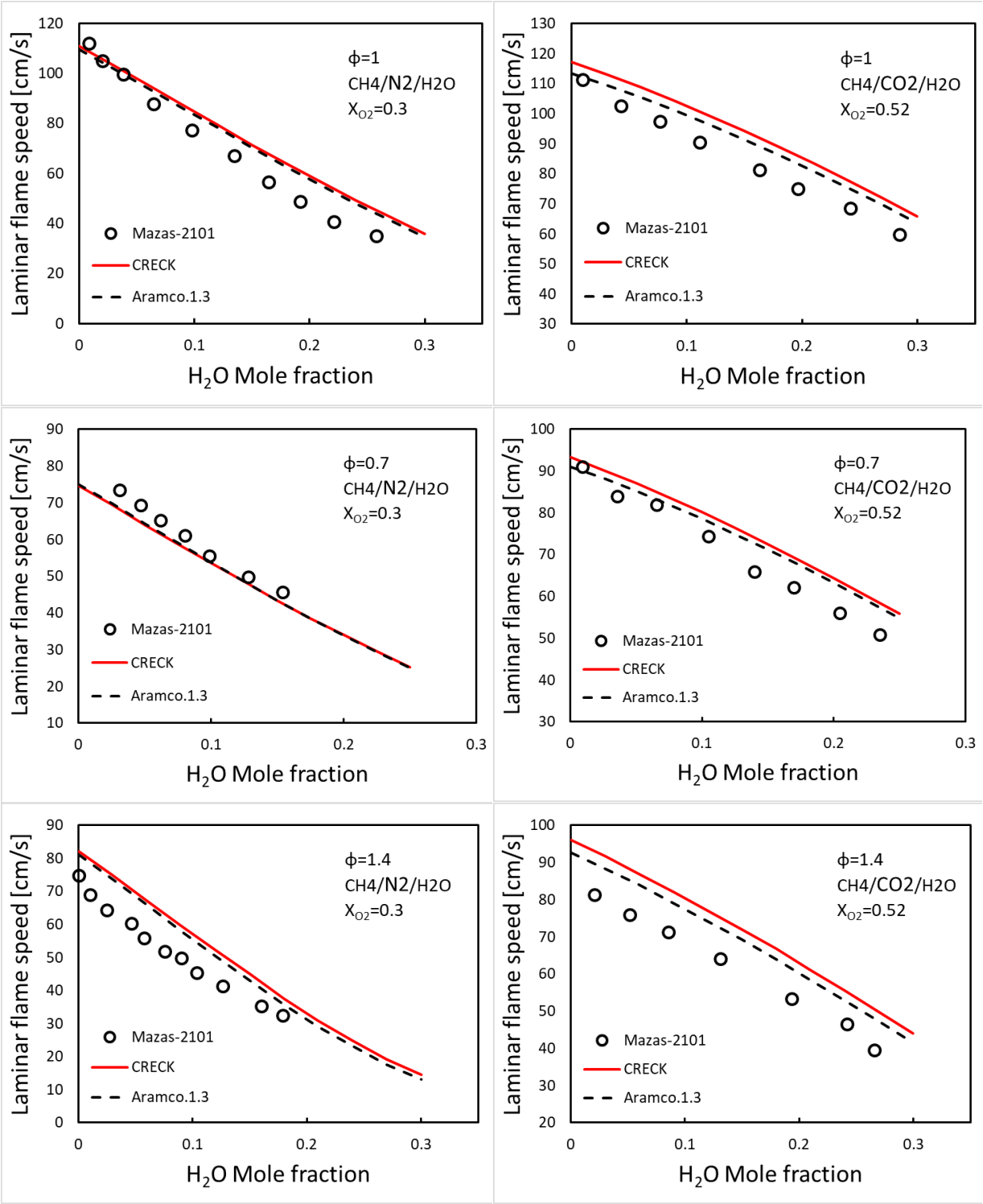

Figure 83 Laminar flame speeds of CH4/O2/N2/H2O and CH4/O2/CO2/H2O mixtures, for XO2=O2/(O2+(N2 or CO2)), at T_{in} = 373 K and atmospheric pressure. Mazas-2101 refer to [23].

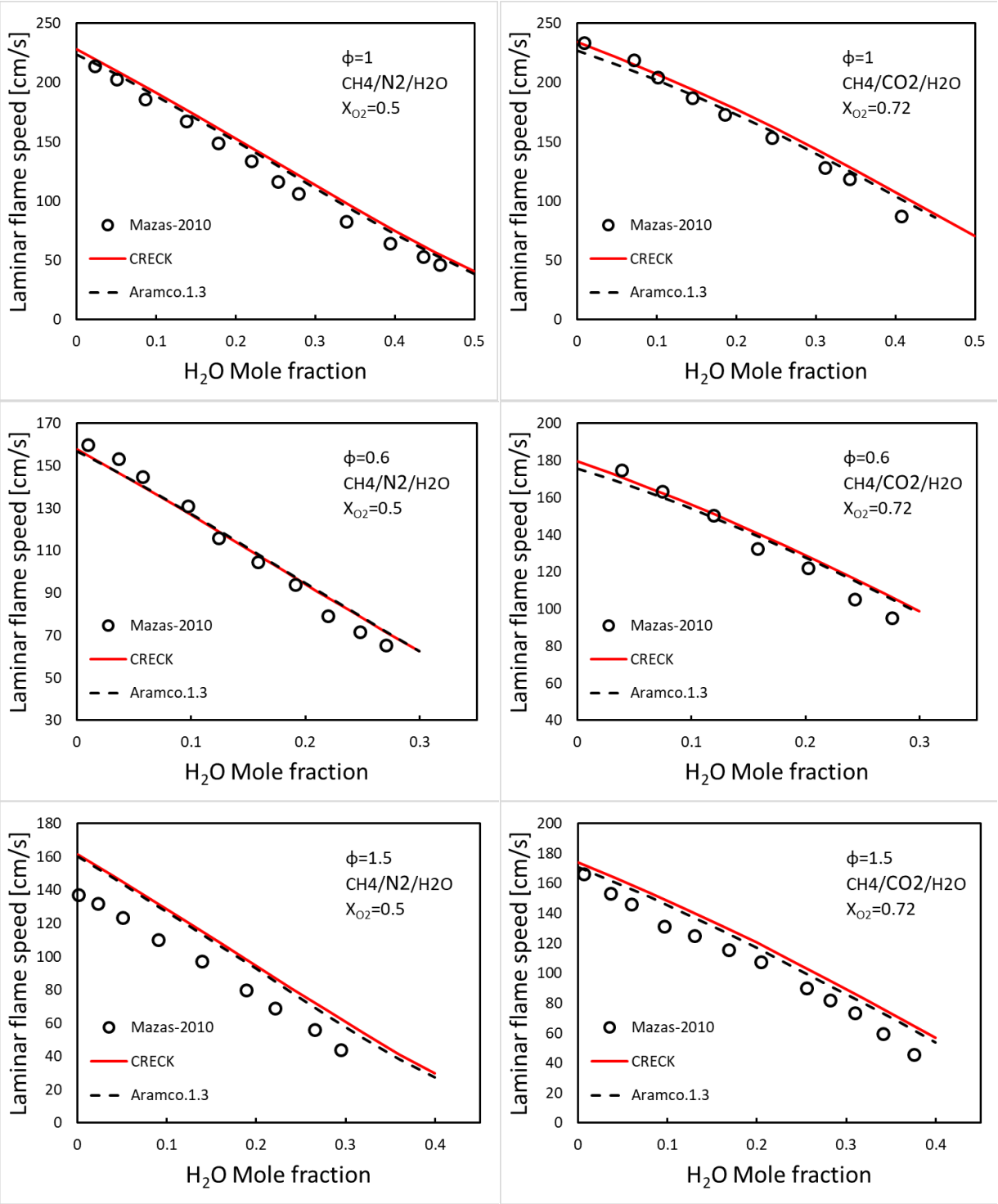

Figure 84 Laminar flame speeds of CH4/O2/N2/H2O and CH4/O2/CO2/H2O mixtures, for XO2=O2/(O2+(N2 or CO2)), at T_{in} = 373 K and atmospheric pressure. Mazas-2101 refer to [23].

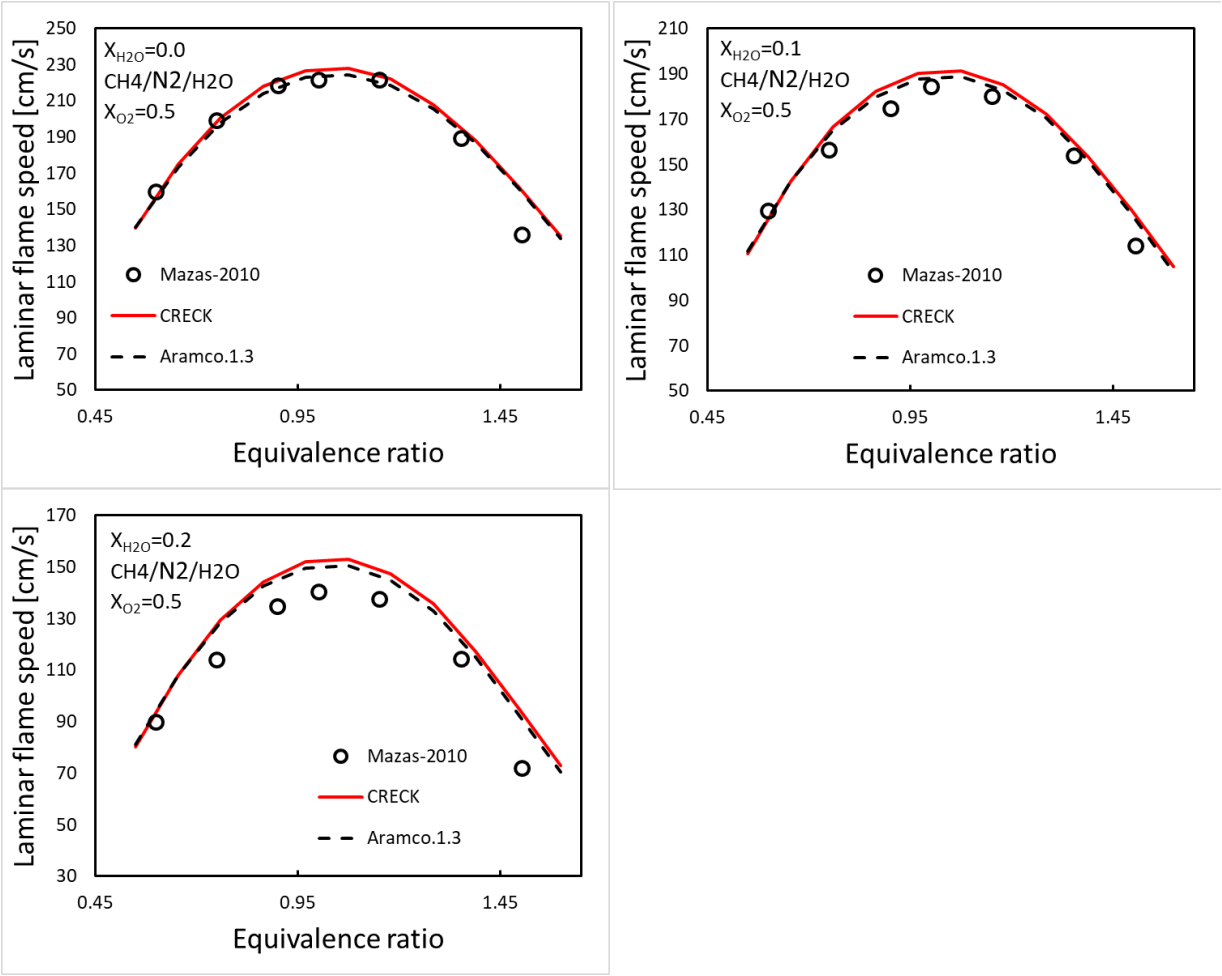

Figure 85 Laminar flame speeds of CH4/O2/N2/H2O mixtures as a function of the equivalence ratio, for XO_2=O2/(O2 +N2)=0.50 and XH2O = 0, 0.10 and 0.20, at T_{in}=373 K and atmospheric pressure. Mazas-2010 refers to [23].

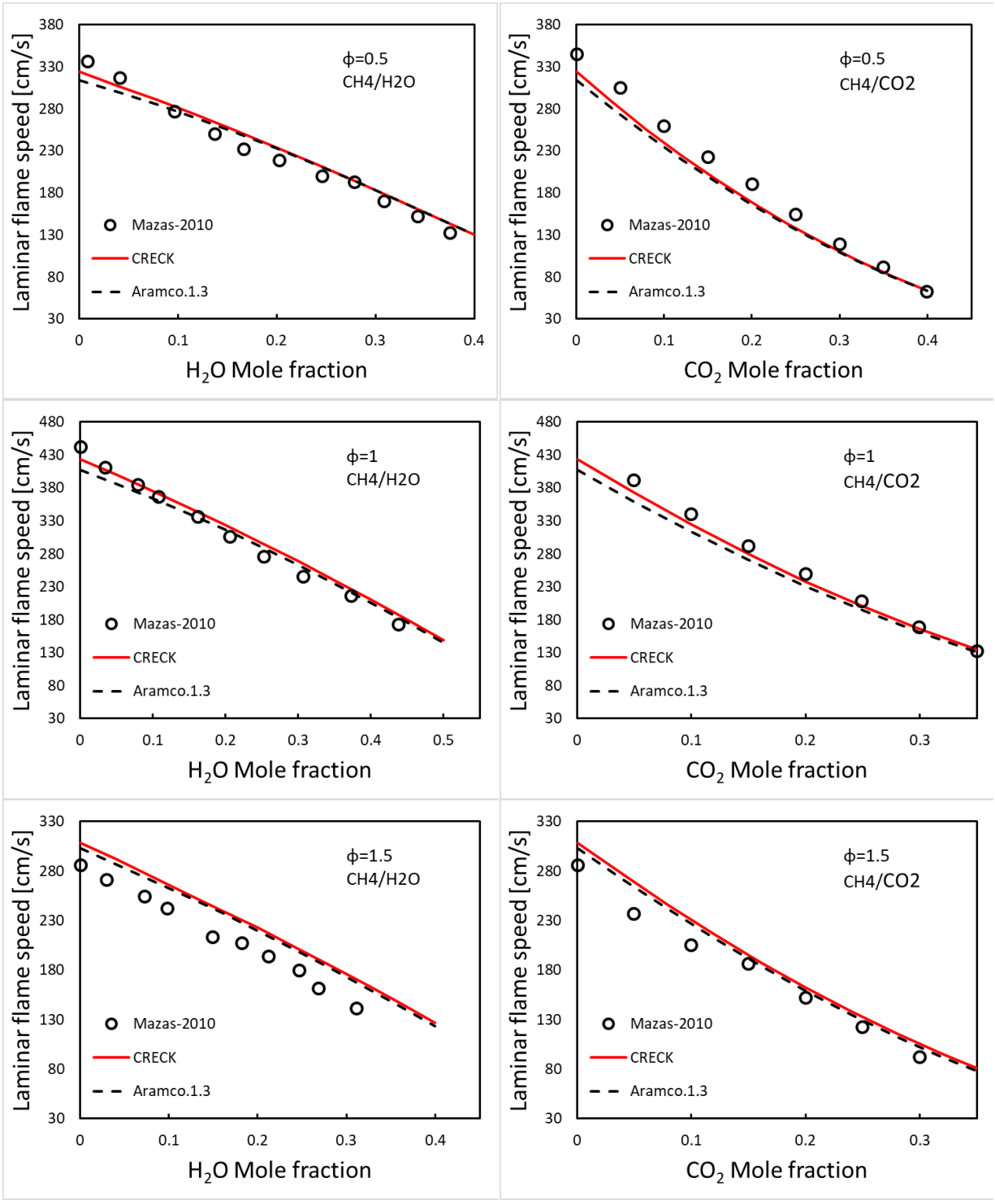

Figure 86 Laminar flame speeds of CH4/O2/H2O and CH4/O2/CO2 mixtures, for φ = 0.5, 1 and 1.5, at T_{in}= 373 K and atmospheric pressure. Mazas-2010 refers to [23].

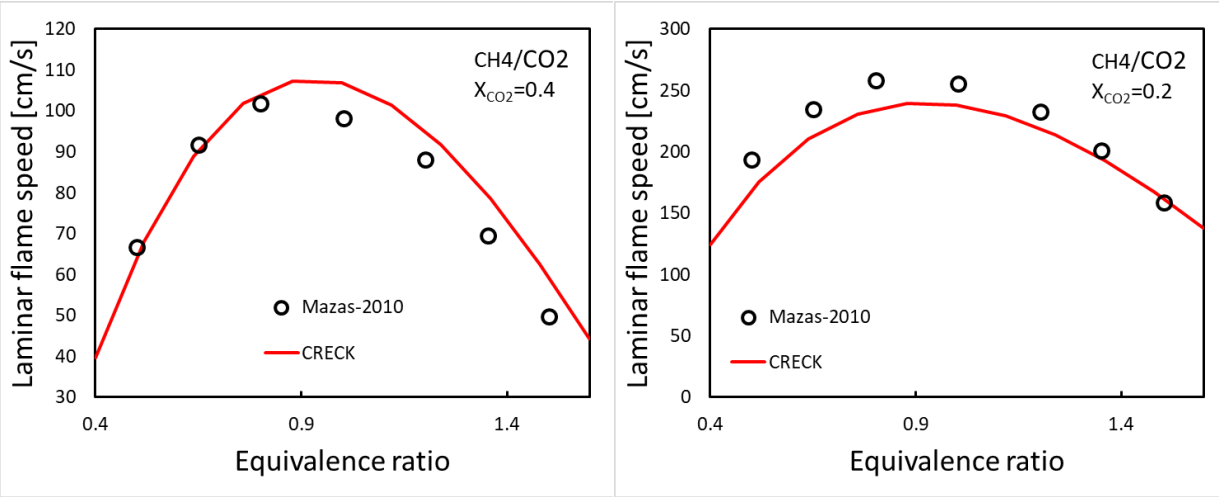

Figure 87 Laminar flame speeds of CH4/O2/CO2 mixtures as a function of the equivalence ratio for XCO2=0.20 and 0.40, at T_{in}= 373 K and atmospheric pressure. Mazas-2010 refers to [23].

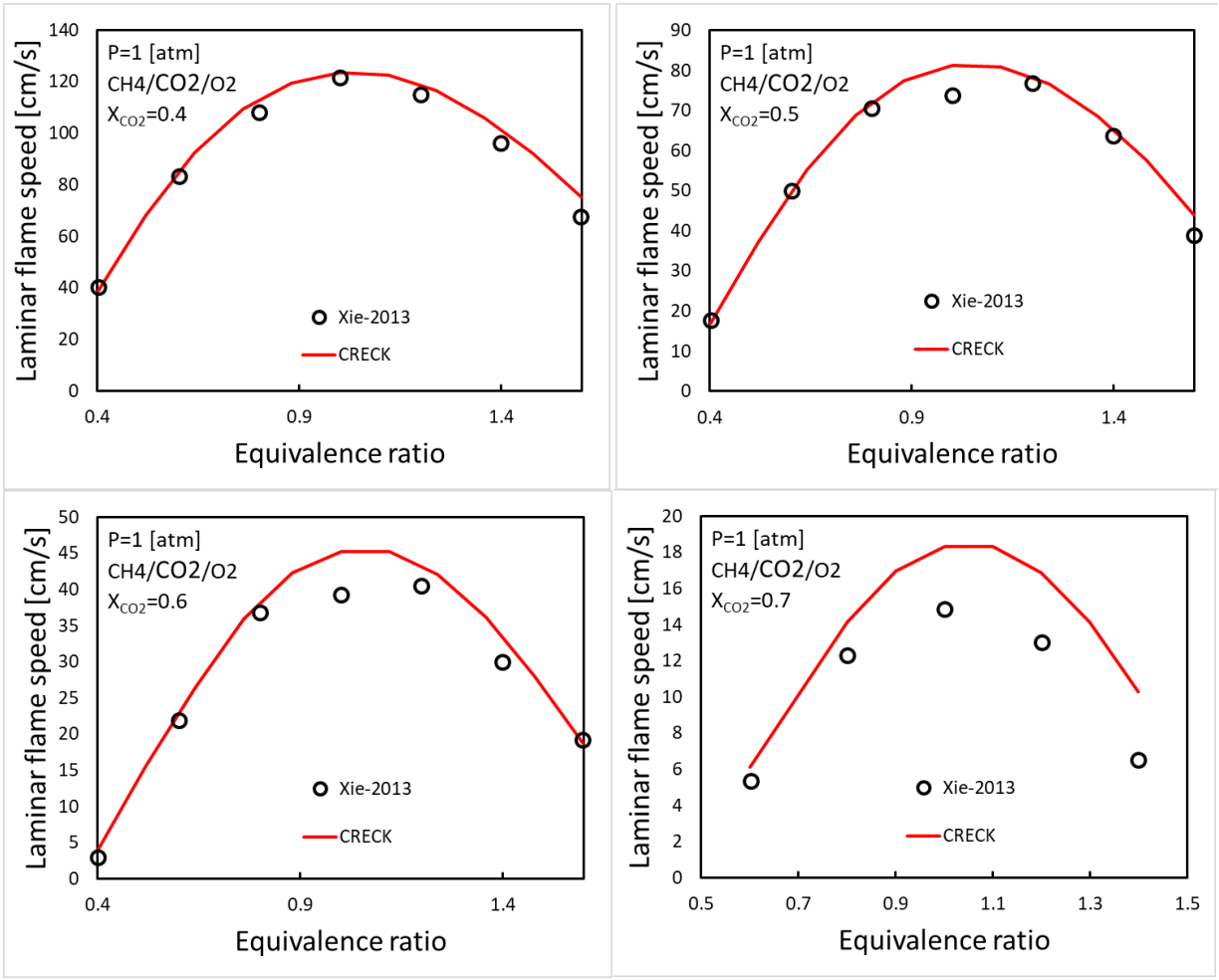

Figure 88 Laminar burning velocities of the CH4/CO2/O2 mixture at P=1 [atm]. X_{CO2}=CO2/(CO2 +O2). Xie-2013 refers to [24].

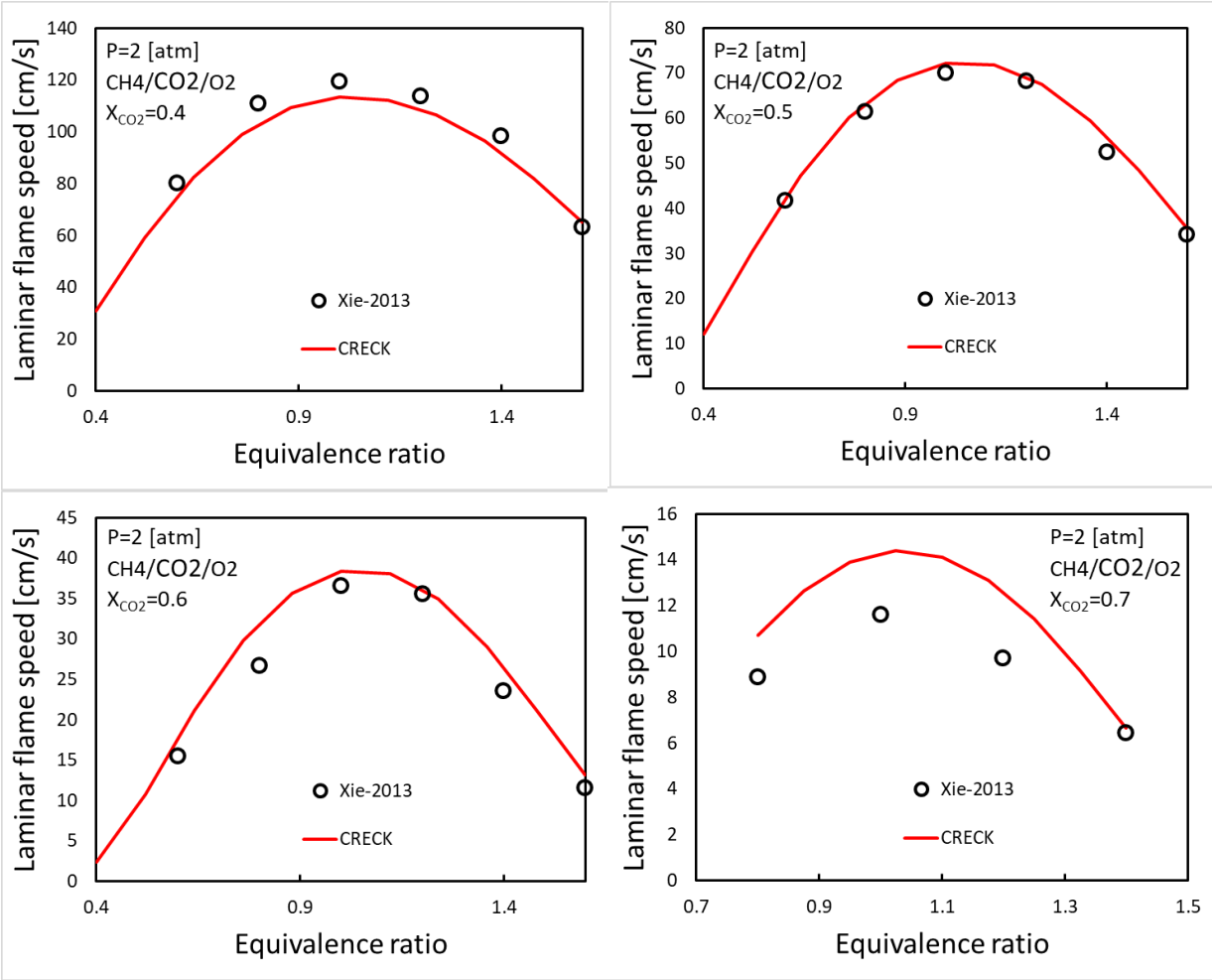

Figure 89 Laminar burning velocities of the CH4/CO2/O2 mixture at P=2 [atm]. X_{CO2}=CO2/(CO2 +O2). Xie-2013 refers to [24].

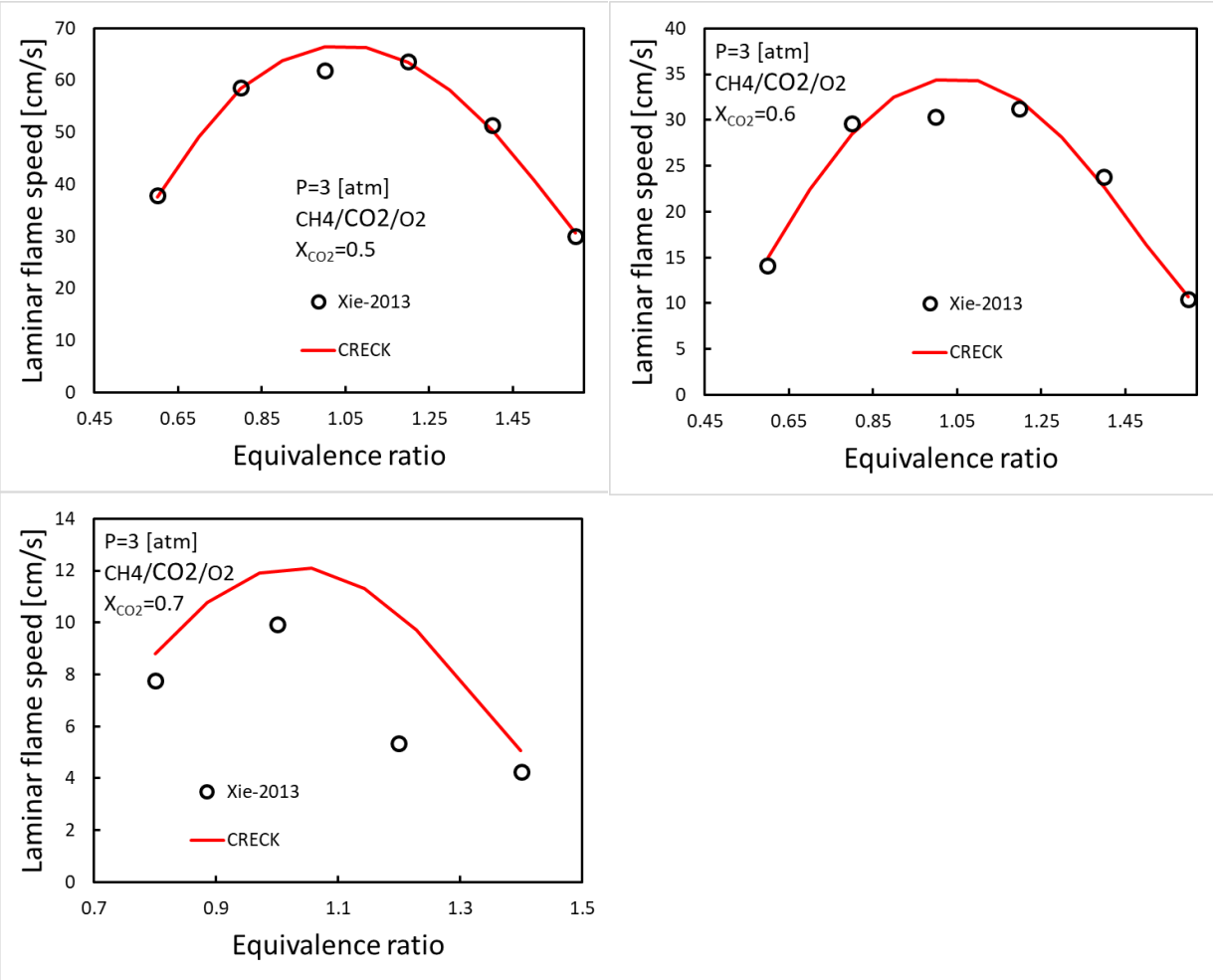

Figure 90 Laminar burning velocities of the CH4/CO2/O2 mixture at P=3 [atm]. X_{CO2}=CO2/(CO2 +O2). Xie-2013 refers to [24].

5. References:

[1] P. DAGAUT, J.-C. BOETTNER, and M. CATHONNET, “Methane Oxidation: Experimental and Kinetic Modeling Study,” *Combustion Science and Technology*, vol. 77, no. 1–3, pp. 127–148, 1991.

[2] T. Le Cong and P. Dagaut, “Experimental and detailed kinetic modeling of the oxidation of methane and methane/syngas mixtures and effect of carbon dioxide addition,” *Combustion Science and Technology*, vol. 180, no. 10–11, pp. 2046–2091, 2008.

[3] T. Le Cong, P. Dagaut, and G. Dayma, “Oxidation of Natural Gas, Natural Gas/Syngas Mixtures, and Effect of Burnt Gas Recirculation: Experimental and Detailed Kinetic Modeling,” *Journal of Engineering for Gas Turbines and Power*, vol. 130, no. 4, p. 041502, 2008.

[4] T. Le Cong and P. Dagaut, “Effect of Water Vapor on the Kinetics of Combustion of Hydrogen and Natural Gas: Experimental and Detailed Modeling Study,” *Energy & Fuels*, vol. 23, no. x, pp. 725–734, 2009.

[5] T. Le Cong and P. Dagaut, “Oxidation of H2/CO2mixtures and effect of hydrogen initial concentration on the combustion of CH4and CH4/CO2mixtures: Experiments and modeling,” *Proceedings of the Combustion Institute*, vol. 32 I, no. 1, pp. 427–435, 2009.

[6] A. El Bakali *et al.*, “Experimental and modeling study of the oxidation of natural gas in a premixed flame, shock tube, and jet-stirred reactor,” *Combustion and Flame*, vol. 137, no. 1–2, pp. 109–128, 2004.

[7] P. Dagaut and G. Dayma, “Hydrogen-enriched natural gas blend oxidation under high-pressure conditions: Experimental and detailed chemical kinetic modeling,” *International Journal of Hydrogen Energy*, vol. 31, no. 4, pp. 505–515, 2006.

[8] M. Lubrano Lavadera *et al.*, “Oscillatory Behavior in Methane Combustion: Influence of the Operating Parameters,” *Energy & Fuels*, p. acs.energyfuels.8b00967, Jul. 2018.

[9] G. Bagheri *et al.*, “Thermochemical oscillation of methane MILD combustion diluted with N 2 /CO 2 /H 2 O,” *Combustion Science and Technology*, pp. 1–13, Apr. 2018.

[10] C. L. Rasmussen, J. G. Jakobsen, and P. Glarborg, “Experimental measurements and kinetic modeling of CH 4 /O 2 and CH 4 /C 2 H 6 /O 2 conversion at high pressure,” *International Journal of Chemical Kinetics*, vol. 40, no. 12, pp. 778–807, Dec. 2008.

[11] F. Sen *et al.*, “Shock-tube and plug-flow reactor study of the oxidation of fuel-rich CH4/O2mixtures enhanced with additives,” *Combustion and Flame*, vol. 169, pp. 307–320, 2016.

[12] M. S. Skjoth-Rasmussen *et al.*, “Formation of polycyclic aromatic hydrocarbons and soot in fuel-rich oxidation of methane in a laminar flow reactor,” *Combustion and Flame*, vol. 136, no. 1–2, pp. 91–128, 2004.

[13] D. J. Seery and C. T. Bowman, “An experimental and analytical study of methane oxidation behind shock waves,” *Combustion and Flame*, vol. 14, no. 1, pp. 37–47, Feb. 1970.

[14] C. S. Eubank, M. J. Rabinowitz, W. C. Gardiner, and R. E. Zellner, “Shock-initiated

ignition of natural gas—Air mixtures," *Symposium (International) on Combustion*, vol. 18, no. 1, pp. 1767–1774, Jan. 1981.

[15] E. L. Petersen, D. F. Davidson, and R. K. Hanson, "Ignition Delay Times of Ram Accelerator CH/O/Diluent Mixtures," *Journal of Propulsion and Power*, vol. 15, no. 1, pp. 82–91, 1999.

[16] L. J. Spadaccini and M. B. Colket, "Ignition delay characteristics of methane fuels," *Progress in Energy and Combustion Science*, vol. 20, no. 5, pp. 431–460, Jan. 1994.

[17] P. Sabia, M. de Joannon, A. Picarelli, and R. Ragucci, "Methane auto-ignition delay times and oxidation regimes in MILD combustion at atmospheric pressure," *Combustion and Flame*, vol. 160, no. 1, pp. 47–55, 2013.

[18] J. W. Hargis and E. L. Petersen, "Methane Ignition in a Shock Tube with High Levels of CO 2 Dilution: Consideration of the Reflected-Shock Bifurcation," *Energy & Fuels*, vol. 29, no. 11, pp. 7712–7726, Nov. 2015.

[19] B. Koroglu, O. M. Pryor, J. Lopez, L. Nash, and S. S. Vasu, "Shock tube ignition delay times and methane time-histories measurements during excess CO2diluted oxy-methane combustion," *Combustion and Flame*, vol. 164, pp. 152–163, 2016.

[20] G. Rozenchan, D. L. Zhu, C. K. Law, and S. D. Tse, "Outward propagation, burning velocities, and chemical effects of methane flames up to 60 ATM," *Proceedings of the Combustion Institute*, vol. 29, no. 2, pp. 1461–1470, Jan. 2002.

[21] W. Lowry *et al.*, "Laminar Flame Speed Measurements and Modeling of Pure Alkanes and Alkane Blends at Elevated Pressures," *Journal of Engineering for Gas Turbines and Power*, vol. 133, no. 9, p. 091501, 2011.

[22] V. Babkin, A. V.- Combustion, undefined Explosion, and S. Waves, and undefined 1971, "Effect of water vapor on the normal burning velocity of a methane-air mixture at high pressures," *Springer*.

[23] A. N. Mazas, D. A. Lacoste, and T. Schuller, "Experimental and Numerical Investigation on the Laminar Flame SPEED OF CH4/O2 MIXTURES DILUTED WITH CO2 AND H2O," *Asme*, 2010.

[24] Y. Xie, J. Wang, M. Zhang, J. Gong, W. Jin, and Z. Huang, "Experimental and Numerical Study on Laminar Flame Characteristics of Methane Oxy-fuel Mixtures Highly Diluted with CO 2," *Energy & Fuels*, vol. 27, no. 10, pp. 6231–6237, Oct. 2013.